Alma Mater Studiorum - Università di Bologna
DEIS - Dipartimento di Elettronica Informatica e Sistemistica

XXI Ciclo del Dottorato di Ricerca in Ingegneria Elettronica,
Informatica e delle Telecomunicazioni
Settore scientifico disciplinare: ING-INF 03

Wireless Ambient Networks

(Reti Radio per Comunicazioni Ambientali)

Tesi di:
Ing. Chiara Buratti

Coordinatore:
Chiar.mo Prof. Ing. Paola Mello

Relatori:
Chiar.mo Prof. Ing. Oreste Andrisano

Chiar.mo Prof. Ing. Roberto Verdone

Esame finale anno 2009

To those who believe in me

Table of Contents

Abstract

Wireless Sensor Networks (WSNs) are commonly recognized as one of the technological cornerstones for Wireless Ambient Networks. Low-cost, low-power networks of sensors can collect a huge amount of information from the environment. This thesis investigates different aspects of these networks, for providing some design guidelines, with particular attention to: connectivity, topology design and medium access control (MAC) protocols. The starting point is represented by a mathematical framework for studying mono-sink WSNs, enabling environmental monitoring through the estimate of a scalar field. Signal processing, connectivity, channel randomness and MAC are jointly considered, but the scenario and the communication protocols applied are quite simple. To account for more useful scenarios and protocols, the following models have been provided: a connectivity model for multi-sink multi-hop WSNs and an analytical model for the IEEE 802.15.4 MAC protocol. The latter model differs from the ones present in the literature, since it precisely captures the essence of the protocol, in a typical WSN application scenario. Finally, these two models have been integrated to realise a framework able to study multi-sink 802.15.4 WSNs, under different perspectives. The model provides some guidelines for designing the network, that is, for example, for setting MAC parameters, nodes density or transmit power, to achieve target performance.

Introduction

Wireless Ambient Networks (WANs) represent a novel research field. Over recent years the concept of *Ambient Intelligence* has emerged to describe interactions between a multitude of network-enabled devices and services [1], [2]. In this ambient intelligence world technology will be almost invisible, embedded in all kinds of objects and everyday environments, such as the home, office, car and train. The term *Ambient Intelligence* has been defined by the ISTAG (Advisory Group to the EU Information Society Technology Program) as the convergence of three major key technologies: ubiquitous computing, ubiquitous communication, and interfaces adapting to the user. WSNs are commonly recognized as one of the technological cornerstones of WANs. Agile, low-cost, ultra-low power networks of sensors can collect a huge amount of critical information from the environment. Using a biological analogy, a sensor network can be seen as the sensory system of the intelligent environment *organism* [3]. Sensor networks are irregular aggregations of communicating sensor nodes, which collect and process information coming from on-board sensors, and they exchange part of this information with neighboring nodes or with nearby collection stations.

Design, implementation, and deployment of a WSN involves a wide range of disciplines and considerations for numerous application-specific constraints. In the last

five years, significant progress has been made in the development of WSNs, and some WSN-based commercial products have already appeared on the market.

In this thesis this kind of networks are investigated under different perspective, with the purpose of providing guidelines for network design. The mainly investigated aspects are: connectivity problems, topology design and MAC protocols.

The reference air interface considered in almost all the work, is the IEEE 802.15.4, that is one of the most suitable standard for WSNs, thanks to its characteristics of low-cost, low-complexity, low-power consumption and low-rate. In particular, the MAC protocol defined by the 802.15.4 Task Group and the tree-based topology defined by the Zigbee Alliance are largely used and investigated.

Finally, note that most of the results achieved have been obtained through mathematical analysis, since this methodology allows rapid investigation of the sensitivity of performance to the different scenario, network and system parameters.

The work performed has been developed in three different phases, shown in Figure 1.

Some previous papers have been published before the beginning of the PhD. These works were devoted to the study of energy-efficient carrier sensing multiple access (CSMA)-based MAC protocols for clustered WSNs [4], and to the application of some cross layer approaches to this kind of networks [5]. Also a paper related to modelling in WSNs has been published [6].

The first phase was related to the study of a self-organising single-sink WSN,

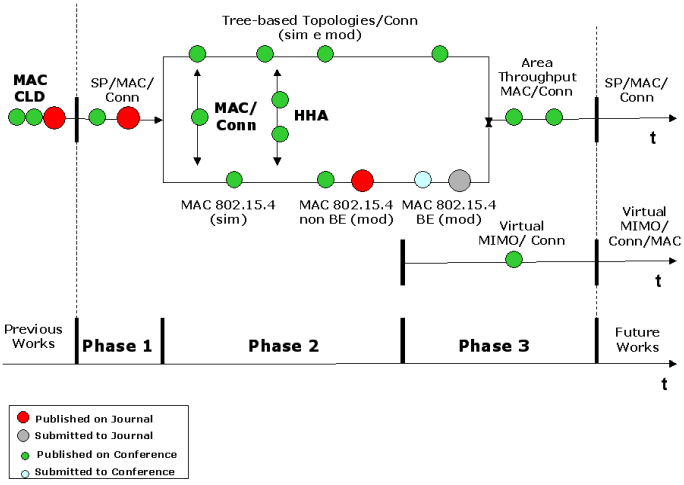

Figure 1: The different phases of the work.

enabling environmental monitoring through the estimate of a scalar field over a bi-dimensional scenario. Connectivity issues, randomness of the channel, MAC issues and the role of distributed digital signal processing (DDSP) techniques, are jointly accounted for, in the mathematical framework developed. This work has led up to the publication of a Journal paper [7] and of a Conference paper [8]. Despite its completeness this framework has some limits: (i) a single-sink scenario and not the more general multi-sink scenario, is accounted for; (ii) border effects are not considered and nodes are assumed to be deployed over an infinite plane; (iii) the model is valid only for cluster-based topologies, therefore nodes have to reach the sink through a two-hop communication, whereas the more general case of multi-hop is not treated; (iv) the MAC protocol is very simple, and no reference to any specific standard air interface, is provided.

The following phases of the thesis were mainly devoted to overcome these limits.

In particular, the second phase has seen the development of two separate models:

one related to connectivity studies and topology design of multi-sink WSNs organised in trees, and another one devoted to the analytical modeling of the IEEE 802.15.4 MAC protocol. These studies were published in the following Conference papers: [9], [10], [11], [12], [13]. Moreover, to analytically evaluate performance of a real air interface suitable for WSNs, the non beacon- and beacon-enabled modes of the IEEE 802.15.4 standard, have been modelled. The non beacon-enabled model has been published in a Journal and a Conference papers [14], [15]. Two papers devoted to the beacon-enabled mode, instead, have been submitted to a Journal and to a Conference [16], [17] (this work, in fact, has been performed in the last year).

In conclusion, multi-sink scenarios, multiple hops communication, border effects and the MAC protocol of a real air interface, have been envisaged in this phase.

The two separate works have been integrated in the third phase of the thesis. In this phase, in fact, a mathematical framework for the evaluation of the throughput (namely, the *area throughput*, defined in the following) of a multi-sink two-hop WSN, has been developed. In this model connectivity, channel randomness, MAC issues, different distributions of nodes and sinks in the area, and also, border effects, are accounted for. This work has led up to the publication of the following Conference papers: [18], [19], [20], [21]. Note that in this final work almost all the limits of the model developed in the first phase have been overcome. However, here signal processing issues, are not accounted for. The application of these issues to the new mathematical framework is an open issue, and is left for possible future works.

In parallel to this last work in the third phase of the thesis, a study related to a new research topic, has also started. This study is devoted to the application of Multiple Input Multiple Output (MIMO) systems to WSNs. Being sensor devices

very tiny, they cannot be equipped with multiple antenna elements, therefore, the concept of Virtual MIMO (V-MIMO) must be applied. V-MIMO systems, in fact, exploit MIMO capability, by using devices having a single antenna element, thanks to cooperation between nodes. Connectivity issues in Poisson fields of nodes are applied to the study of the capacity of a two-hop V-MIMO system [22]. Since this work started in the last year of the PhD, the results shown here are very preliminary.

It is, finally, important to underline that, as it will be clear in the following, the energy consumption issue has been addressed in the thesis, being one of the fundamental issues of WSNs. This performance metric is, in fact, evaluated in almost all mathematical models developed in the thesis.

I would like, also, to precise that the models for the beacon- and non beacon-enabled 802.15.4 networks, described in Chapter 4, have been completely developed by myself, under the supervision of Prof. Verdone. Instead, the models described in Chapters 2, 3 and 5 derive from the collaboration with other researchers and PhD students, therefore, my own contribution was mainly focused on parts, and not on the whole, models themselves.

This thesis has been performed mainly in four frameworks: the three Networks of Excellence (NoE) funded by the European Commission (EC) through the Sixth and the Seventh Framework Programmes, NEWCOM (2005-2007), CRUISE (2006-2007) and NEWCOM++ (2008-2010), and a collaboration with an Italian SME, Sadel. In the framework of NEWCOM two collaborations with researchers at Bilkent and Manchester Universities have been carried out. These collaborations have produced the following publications to European Conferences: [23], [9], [10], and the

results of these works are reported in Chapter 3. CRUISE (CReating Ubiquitous Intelligent Sensing Environments) is a NoE mainly devoted to the planning and coordination of research on communication and application aspects of wireless sensor networking in Europe. In this framework a collaboration with University of Roma "La Sapienza" has been established. Thanks to this collaboration the paper [24], has been published. The reference scenario selected by this project consists of a Wireless Hybrid Network (WHN), namely the Hybrid Hierarchical Architecture (HHA), which puts together the two paradigm of the infrastructure-based (e.g., Universal Mobile Telecommunications System (UMTS)) and infrastructure-less networks (e.g., IEEE 802.15.4). In this framework a study related to the characterisation of the statistics of the traffic generated by a 802.15.4 network transmitting data to a sink, acting as gateway toward the UMTS network, has been carried out [25], [26]. Since this work is related to the topic of this thesis, being focused on IEEE 802.15.4 traffic statistics characterisation, it is reported in the Appendix. However, being this part a minor contribution with respect to the rest of the thesis, in the Appendix the paper accepted for publication at the European Wireless Conference [26] is directly reported, since its integration with the rest of the contents of this thesis is out of the scope. In the framework of NEWCOM++, the follow up of NEWCOM, a collaboration with Aachen University has led up to the following publications: [21], [20], and these results are reported in Chapter 5. Finally, for what concerns the collaboration with Sadel, the supervision of some experimental measurements performed with 802.15.4 standard-compliant devices, produced by Freescale, has been done.

According to the different phases of the work, the thesis is outlined as follows. Chapter 1 provides an overview of the main issues related to WSNs, like applications,

technologies, etc.., and then introduces all the basic concepts needed to understand the rest of the thesis, that are mainly, the IEEE 802.15.4 MAC protocol, the Zigbee-compliant tree-based topology, the link and channel models used here. Chapter 2 describes the mathematical model developed in the first phase. Chapter 3 and 4 are devoted to the second phase, dealing with connectivity issues in multi-sink WSNs organised in trees, and to the modeling of the 802.15.4 MAC protocol, respectively. Chapter 5 deals with the model for deriving the area throughput, a performance metric accounting for connectivity and MAC issues. In Chapter 6 the studies of V-MIMO systems are introduced and then conclusions and open issues are discussed. Finally, in the Appendix the paper [26] is reported.

All the work described above has led up to the following publications (in one case it is only submitted) to Journals:

- C. Buratti, A. Giorgetti and R. Verdone. Cross Layer Design of an Energy Efficient Cluster Formation Algorithm with Carrier Sensing Multiple Access for Wireless Sensor Networks. *EURASIP Journal*, vol. 5, pp. 672-685, Dec. 2005;

- D. Dardari, A.Conti, C. Buratti and R. Verdone. Mathematical evaluation of environmental monitoring estimation error through energy-efficient Wireless Sensor Networks. *IEEE Trans. on Mobile Computing*, vol. 6, n. 7, pp. 790-803, July 2007;

- C. Buratti and R. Verdone. Performance Analysis of IEEE 802.15.4 Non-Beacon Enabled Mode. To appear in *IEEE Trans. on Vehicular Technologies*, 2009;

- C. Buratti. Performance Analysis of IEEE 802.15.4 Beacon-Enabled Mode.

Submitted to *IEEE Transaction on Vehicular Technologies*;

and to the following publications (in one case it is only submitted) to International Conferences:

- C. Buratti, A. Giorgetti and R. Verdone. Simulations of Energy Efficient Carrier Sensing Multiple Access Protocol for Clustered Wireless Sensor Network. *Proc. of IEEE IWWAN 2004*, June 2004, Oulu;

- A. Conti, D. Dardari, C. Buratti, D. Sangiorgi and R. Verdone. Simulation of Energy Efficient Carrier Sensing Multiple Access Protocol for Clustered Wireless Sensor Network. *Proc. of European Conference on Wireless Sensor Networks, EWSN 2005*, Jan. 2005, Instanbul, Turchy;

- R. Verdone and C. Buratti. Modelling for Wireless Sensor Network Protocol Design. *Proc. of IEEE IWWAN 2005*, May 2005, London, England;

- R. Verdone, C. Buratti and J. Orriss. On the Design of Tree-Based Topologies for Wireless Sensor Networks. *Proc. IEEE MedHocNet 2006*, June 2006, Lipari Island, Italy;

- C. Buratti, J. Orriss and R. Verdone. On the design of tree-based topologies for multi-sink wireless sensor networks. *Proc. of IEEE NEWCOM/ACORN Workshop 2006*, Sept. 2006, Vienna, Austria;

- C. Buratti and R. Verdone. On the Number of Cluster Heads Minimizing the Error Rate for a Wireless Sensor Network using a Hierarchical Topology Over

IEEE 802.15.4. *Proc. of IEEE Int. Symp. on Personal, Indoor and MoRadio Communications, PIMRC 2006*, Sept. 2006, pp. 1-6, Helsinky, Finland;

- C. Buratti, F. Cuomo, S. D. Luna and U. Monaco and J. Orriss and R. Verdone. Optimum Tree-Based Topologies for Multi-Sink Wireless Sensor Networks Using IEEE 802.15.4. *Proc. of IEEE 65th Vehicular Technology Conference, VTC07*, Apr. 2007, pp. 130-134, Dublin, Ireland;

- C. Buratti and R. Verdone. Tree-Based Topology Design for Multi-Sink Wireless Sensor Networks. *Proc. of IEEE Int. Symp. on Personal, Indoor and MoRadio Communications, PIMRC 2007*, Sept. 2007, Atene, Greece;

- C. Buratti and R. Verdone. A Hybrid Hierarchical Multi-Hop Wireless Network: From Wireless Sensors to the Fixed Infrastructure. *Proc. of LOCAN 2007*, Oct. 2007, Pisa, Italy;

- C. Buratti, I. Korpeoglu, E. Karasan and R. Verdone, Bluetooth or 802.15.4 Technologies to Optimise Lifetime of Wireless Sensor Networks: Numerical Comparison Under a Common Framework. *Proc. of* WNC^3, March 2008, Berlin, Germany;

- C. Buratti and R. Verdone. A Hybrid Hierarchical Architecture: From a Wireless Sensor Network to the Fixed Infrastructure. *Proc. of IEEE European Wireless, EW2008*, June 2008, Prague, Czech Republic.

- C. Buratti and R. Verdone. A Mathematical Model for Performance Analysis of IEEE 802.15.4 Non-Beacon Enabled Mode. *Proc. of IEEE European Wireless, EW2008*, June 2008, Prague, Czech Republic;

- R. Verdone, F. Fabbri and C. Buratti. Area Throughput for CSMA Based Wireless Sensor Networks. *Proc. of IEEE Int. Symp. on Personal, Indoor and MoRadio Communications, PIMRC 2008*, Sept. 2008, Cannes, France;

- F. Fabbri, C. Buratti and R. Verdone. A multi-sink multi hop Wireless Sensor Network Over a Bounded Region: Connectivity and Energy Consumption Issues. *Proc. of IEEE Wireless Mesh and Sensor Networks, WMSN 08*, Nov. 2008, New Orleans, LA, USA;

- C. Buratti, F. Fabbri and R. Verdone. Area Throughput of an IEEE 802.15.4 Based Wireless Sensor Network. *Proc. of European Conference on Wireless Sensor Networks, EWSN 2009*, Feb. 2009, Cork, Ireland;

- J. Riihijärvi, F. Fabbri, C. Buratti, P. Mähönen and R. Verdone. Area Throughput and Energy Efficiency for Clustered Wireless Sensor Networks Deployed in Bounded Regions. *Proc. of IEEE NEWCOM/ACORN Workshop 2009*, March 2009, Barcelona, Spain;

- C. Buratti and Alberto Zanella. Capacity Analysis of Two-Hop Virtual MIMO Systems in a Poisson Field of nodes. *Proc. of IEEE Vehicular Technologies, VTC fall 2009*, Apr. 2009, Barcelona, Spain;

- F. Fabbri, C. Buratti, R. Verdone, J. Riihijärvi and P. Mähönen. Area Throughput and Energy Consumption for Clustered Wireless Sensor Networks. *Proc. of IEEE WCNC 2009*, Apr. 2009, Budapest, Hungary;

- C. Buratti. A Mathematical Model for Performance of IEEE 802.15.4 Beacon-Enabled Mode. Submitted to *IEEE IWCMC 2009*.

The list of Deliverables of the projects NEWCOM, CRUISE and NEWCOM++, edited follows:

- DRA.5: C. Buratti, R. Verdone, R. Narcisi, S. Palazzo, *Recommendations for the reference scenarios to be defined in E-MORANS and for the Data Base for Knowledge Networking*, NEWCOM, WPR.A;

- DRA.6: C. Buratti, *Second report on common frameworks/models matching Project A needs*, NEWCOM, WPR.A;

- DRA.8: C. Buratti, C. F. Chiasserini, F. Chiti, D. Dardari, J. Haerri, A. Leonardi, R. Narcisi, S. Palazzo, D. Tarchi, *Second report on software libraries*, NEWCOM, WPR.A;

- DR10.1: *State of the art of research on fundamental performance limits of wireless network*, NEWCOM++, WPR.10.

Finally, I have contributed to the following Deliverables: DRA.1, DRA.2, DRA.3 of NEWCOM, D210.1, D210.2, D220.1, D220.2, D112.1, D112.2 and D113.3 of CRUISE.

Chapter 1

Wireless Sensor Networks

This Chapter introduces the topic of WSNs, providing a definition and the main characteristics and issues of this kind of networks. A brief overview of the state of the art of the research in this field, with particular attention toward the main European projects, is also provided. The main technologies available for the realisation of such networks (e.g., IEEE 802.15.4, UltraWideBand and Bluetooth) are briefly described, with particular emphasis to the IEEE 802.15.4 standard, that will be the reference technology in this thesis. Finally, the channel and link models used are introduced, including some connectivity proprieties for Poisson Point Process (PPP) fields of nodes, useful for the connectivity models developed in this thesis.

1.1 What is a Wireless Sensor Network?

A Wireless Sensor Network (WSN) [27–34], can be defined as a network of devices, denoted as *nodes*, which can sense the environment and communicate the information gathered from the monitored field (e.g., an area or volume) through wireless links [35]. The data is forwarded, possibly via multiple hops, to a *sink* (sometimes denoted as *controller* or *monitor*) that can use it locally or is connected to other networks (e.g.,

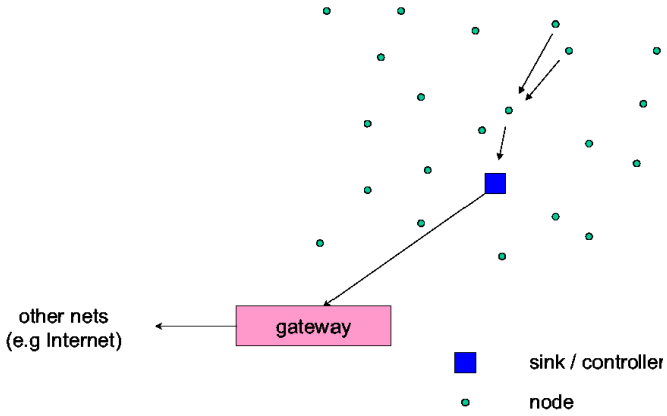

Figure 1.1: Traditional single-sink WSN.

the Internet) through a *gateway*. The nodes can be stationary or moving. They can be aware of their location or not. They can be homogeneous or not.

This is a traditional single-sink WSN (see Fig. 1.1). Almost all scientific papers in the literature deal with such a definition. This single-sink scenario suffers from the lack of scalability: by increasing the number of nodes, the amount of data gathered by the sink increases and once its capacity is reached, the network size can not be augmented. Moreover, for reasons related to MAC and routing aspects, network performance cannot be considered independent from the network size.

A more general scenario includes multiple sinks in the network (see Fig. 1.2) [36]. Given a level of node density, a larger number of sinks will decrease the probability of isolated clusters of nodes that cannot deliver their data owing to unfortunate signal propagation conditions. In principle, a multiple-sink WSN can be scalable (i.e., the same performance can be achieved even by increasing the number of nodes), while

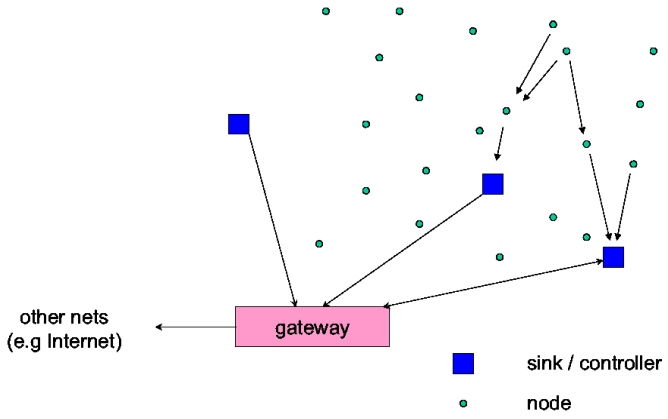

Figure 1.2: Multi-sink WSN.

this is clearly not true for a single-sink network. However, a multi-sink WSN does not represent a trivial extension of a single-sink case for the network engineer. There might be mainly two different cases: i) all sinks are connected through a separate network (either wired or wireless), or ii) the sinks are disconnected. In the former case, a node needs to forward the data collected to any element in the set of sinks. From the protocol viewpoint, this means that a selection can be done, based on a suitable criterium (e.g., minimum delay, maximum throughput, minimum number of hops, etc). The presence of multiple sinks in this case ensures better network performance with respect to the single-sink case (assuming the same number of nodes is deployed over the same area), but the communication protocols must be more complex and should be designed according to suitable criteria. In the second case, when the sinks are not connected, the presence of multiple sinks tends to partition the monitored field into smaller areas; however from the communication protocols

viewpoint no significant changes must be included, apart from simple sink discovery mechanisms. Clearly, the most general and interesting case (because of the better potential performance) is the first one, with the sinks connected through any type of mesh network, or via direct links with a common gateway.

1.1.1 The nodes' architecture

The basic elements of a WSN are the nodes (i.e., the sensors), the sinks and the gateways. Sinks and gateways, are usually more complex devices than the sensor nodes, because of the functionalities they need to provide. The sensor node is the simplest device in the network, and in most applications the number of sensor nodes is much larger than the number of sinks. Therefore, their cost and size must be kept as low as possible. Also, in most applications the use of battery-powered devices is very convenient, to make the deployment of such nodes easier. To let the network work under specified performance requirements for a sufficient time, denoted as *network lifetime*, the nodes must be capable of playing their role for a sufficiently long period, using the energy provided by their battery, which in many applications should be not renewed for years. Thus, energy efficiency of all tasks performed by a node is a must for the WSN design [37, 38].

The traditional architecture of a sensor node is reported in Fig. 1.3 [27]. A microprocessor manages all tasks; one or more sensors are used to take data from the environment; a memory is included over the board which is used to store temporary data, or during its processing; a radio transceiver (with the antenna) is also present. All these devices are powered by a battery. Traditional batteries can provide initial charges in the order of 10,000 Joules and they should be parsimoniously used for the

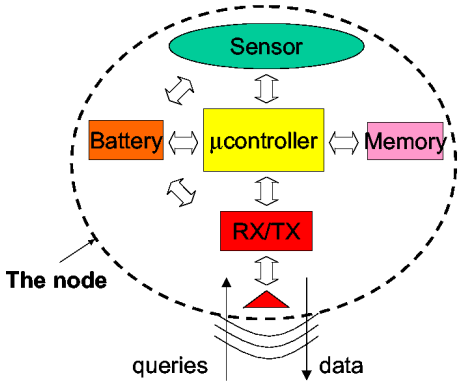

Figure 1.3: Architecture of a sensor node.

whole duration of the network lifetime by all these devices. In some cases, energy scavenging techniques can be introduced to enlarge lifetime of nodes, but in few applications this can be really considered as a viable technique.

As a result of this need to have energy efficient techniques implemented over the board, all data processing tasks are normally distributed over the network; therefore, the nodes cooperate to provide the data to the sinks. This is also because of the low complexity that is accepted for the architecture of such nodes.

In conclusion, a WSN can be generally described as a network of nodes that cooperatively sense the environment and may control it, enabling interaction between people or computers and the surrounding environment.

The density of nodes and sinks is a very relevant parameter for WSNs: the density of sensor nodes defines the level of coverage of the monitored space (i.e., what percentage is such that if an event happens inside, it is detected by at least one node); however, it also defines the degree of connectivity, or reachability, that is a relevant

issue described as in Chapter 3. On the other hand the density of sinks plays a significant role in defining the performance of the network in terms of success rate of data transmissions, etc.. (see Chapter 4).

1.1.2 Main Features of WSNs

The main features of WSNs, as could be deduced by the general description given in the previous sections, are: scalability with respect to the number of nodes in the network, self-organisation, self-healing, energy efficiency, a sufficient degree of connectivity among nodes, low-complexity, low cost and size of nodes. Those protocol architectures and technical solutions providing such features can be considered as a potential framework for the creation of these networks, but, unfortunately, the definition of such a protocol architecture and technical solution is not simple, and the research still needs to work on it [31].

The massive research on WSNs started after the year 2000. However, it took advantage of the outcome of the research on wireless networks performed since the second half of the previous century. In particular, the study of ad hoc networks attracted a lot of attention for several decades, and some researchers tried to report their skills acquired in the field of ad hoc networks, to the study of WSNs.

According to some general definitions, wireless ad hoc networks are formed dynamically by an autonomous system of nodes connected via wireless links without using an existing network infrastructure or centralised administration. Nodes are connected through "ad hoc" topologies, set up and cleared according to user needs and temporary conditions. Apparently, this definition can include WSNs. However,

this is not true. This is the list of main features for wireless ad hoc networks: unplanned and highly dynamical; nodes are "smart" terminals (laptops, etc); typical applications include real-time or non real-time data, multimedia, voice; every node can be either source or destination of information; every node can be a router toward other nodes; energy is not the most relevant matter; capacity is the most relevant matter.

Apart from the very first item, which is common to WSNs, in all other cases there is a clear distinction between WSNs and wireless ad hoc networks. In WSNs, nodes are simple and low-complexity devices; the typical applications require few bytes sent periodically or upon request or according to some external event; every node can be either source or destination of information, not both; some nodes do not play the role of routers; energy efficiency is a very relevant matter, while capacity is not for most applications. Therefore, WSNs are not a special case of wireless ad hoc networks. Thus, a lot of care must be used when taking protocols and algorithms which are good for ad hoc networks, and using them in the context of WSNs.

1.1.3 Issues Related to Energy Management

As stated above, energy efficiency is a key issue for most WSN applications. Network lifetime must be kept as long as possible. Clearly, it depends on how long can be the period of time starting with network deployment, and ending when the battery of sensor nodes is no more able to provide the energy needed for communication, sensing or processing. The energy consumption issue is taken into account in all this thesis. However, here a brief discussion about some important aspects of the energy management, is introduced.

As shown in Fig. 1.3, a node is basically composed of a battery, a microprocessor, a memory, the sensors and the transceiver. Normally, when in transmit mode, the transceiver drains much more current from the battery than the microprocessor in active state, or the sensors and the memory chip. As a conclusion, the transceiver is the part responsible for the consumption of most energy. This justifies the energy consumption model adopted in almost all the thesis. Moreover, the ratio between the energy needed for transmitting and for processing a bit of information is usually assumed to be much larger than one, and this is the reason why the communication protocols need to be designed according to energy efficient paradigms, while processing tasks are not, usually. On the other hand, sometimes data processing techniques implemented in WSNs require long processing tasks to be performed at the microprocessor. This can cause significant energy consumption by the microprocessor, even comparable to the energy consumed during transmission, or reception, by the transceiver. This is the reason why in Chapter 2 the energy consumed for performing signal processing is accounted for. Thus, the general rule that communication protocol design is much more important than a careful design of the processing task scheduling, can not be considered always true.

Intuitively, the transceiver state is the state that requires more current drain from the battery is the transmit state, as both the baseband and radio frequency (RF) part of the transceiver are active. However, the same is true for the receive state. Therefore, the receive state can consume as much energy as the transmit does. Owing to the hardware design principles, sometimes in the receive state the transceiver can consume even more energy than in the transmit state. For this reason the energy consumed for receiving packets and for doing carrier sensing is accounted

for in almost all the thesis. Therefore, receive and transmit states are both very energy consuming, and the transceiver must be kept in those two states for the shortest possible percentage of time.

Clearly, permanence in the transmit state is needed only when a data burst needs to be transmitted. The lesser are the data burst to be transmitted, the longer is node life. This suggests to avoid using protocols based on complex handshakes. As an example, in some cases it could be better to avoid acknowledge mechanisms. However, a transceiver might need to stay in receive mode for longer periods of time, if proper scheduling of transmit times is not performed. Protocols should avoid a phenomenon, called *overhearing*, such that nodes need to stay in receive time for long periods waiting for a packet while listening to many data bursts sent to other nodes. However, this is not enough. In fact, many MAC protocols consider channel sensing mechanisms: the transceiver senses the wireless channel for some periods of time in order to determine whether it is busy or free. Depending on the specific hardware platform, channel sensing can be very energy consuming, almost as the transmit and receive states. Thus, protocols must not abuse of the channel sensing mechanism and when using a CSMA protocol, long (in the order of 95%-99% of time) intervals of time with the transceiver in sleep state, are required. During such periods, a data burst sent to the node can not be detected. Therefore, the management of sleep mode is a very relevant issue for WSNs.

A final consideration regards the use of power control. This technique, setting the transmit power at the minimum level needed to allow signal correct detection at the receiver, is often used in wireless networks to reduce the interference impact of transmissions, and the useless emission of radiowaves with large power. However,

setting a proper power level requires information on the channel gain, which might be difficult to achieve in applications with very bursty data transmissions. Therefore it is worthwhile wandering whether power control is a useful technique for WSNs. Moreover, looking at the data reported on the datasheet of a sample transceiver used in many commercial platforms, such as CHIPCON CC2420 [39], one can derive an interesting conclusion. When transmitting at the largest power level (0 [dBm]), about 17 [mA] are drained from the battery. At minimum transmit power (-25 [dBm]), the current drained is 8.5 [mA]. Therefore there is no relevant energy saving, when decreasing the power level of transmission by 25 [dB]. Even if this example is given with reference to a specific chip, there are reasons to state that the conclusion is general. The energy consumed in transmission state is not proportional to the transmit power level used, and therefore power control is not an efficient technique to reduce energy consumption. For this reason power control is not used in this thesis.

1.2 Current and Future Research on WSNs

Many technical topics of WSNs are still considered by research, as the current solutions are known to be non optimised, or too much constrained.

From the physical layer viewpoint, standardisation is a key issue for success of WSN markets. Currently the basic options for building HW/SW platforms for WSNs are Bluetooth, IEEE 802.15.4 and 802.15.4a (all these technologies are briefly treated in sections 1.4 and 1.5). At least, most commercially available platforms use these three standards for the air interface. For low data rate applications (250 [kbit/s] on the air), IEEE 802.15.4 seems to be the most flexible technology currently available. Clearly, the need to have low-complexity and low-cost devices does not push research

in the direction of advanced transmission techniques.

MAC and network layer have attracted a lot of attention in the past years and still deserve investigation. In particular, combined approaches that jointly consider MAC and routing seem to be very successful.

Topology creation, control and maintenance are very hot topics. Especially with IEEE 802.15.4, which allows creation of several types of topologies (stars, mesh, trees, cluster-trees), these issues play a very significant role.

Being WSNs a very hot topic in the recent years many works dealing with MAC and routing protocols [34, 40, 41] have been published. For the sake of conciseness, an overview of the literature related to these topics is not reported in this thesis. Examples of overviews for these protocols could be found in [27, 29–31, 42].

Basically, the research in the field of WSNs started very recently with respect to other areas of the wireless communication society, as examples like broadcasting or cellular networks. The first IEEE papers on WSNs were published after the turn of the Millennium.

The first European projects on WSNs were financed after year 2001. In the US the research on WSNs was boosted few years before. Many theoretical issues still need a lot of investments. Europe will finance projects having WSNs as core technologies for at least the next seven years, within the Seventh Framework Programme.

In Europe, during the sixth and seventh Framework Programmes, four Projects were financed by the EC, with explicit activities dedicated to communication protocols, architectural and technological solutions for embedded systems: WISENTS [43],

e-SENSE [44], CRUISE [45] and CONET [46]. Embedded WISENTS was a Coordinated Action funded by the EC, aiming at increasing the awareness and to find out a vision as well as a roadmap towards wireless sensor networks and cooperating embedded systems within the academic community and, most importantly, within the manufacturers of proper technologies as well as potential users community. e-SENSE project, was focused on capturing ambient intelligence for beyond 3G mobile communication systems through wireless sensor networks. e-SENSE has proposed a context capturing framework that enabled the convergence of many input modalities, mainly focusing on energy efficient wireless sensor networks that are multi-sensory in their composition, heterogeneous in their networking, and either mobile or integrated in the environment. CRUISE (CReating Ubiquitous Intelligent Sensing Environments) was a Network of Excellence mainly devoted to the planning and coordination of research on communication and application aspects of wireless sensor networking in Europe. The reference scenario of this project consists of a WHNs, namely the HHA (described and studied in the Appendix of this thesis) which puts together the two paradigms of the infrastructure based and infrastructure less networks. In this architecture wireless sensor, actuators and very tiny devices, like smart tags, have to transmit their data to the infrastructure, through mobile gateways, carried usually by people. Finally, CONET (Cooperating Objetcs NETwork on Excellence) aims at creating a visible community of researchers in the area of cooperating objects capable of driving the domain in the coming years. *Cooperation* is defined as the ability of individual entities or objects (that could be sensors, controllers or actuators) to use communication as well as dynamic and loose federation to jointly strive to reach common goal while taking care not to overtax their available resources.

Then, it is also relevant to mention that there exist two European Technology Platforms, gathering all stakeholders in the field, related to the area of WSNs: e-Mobility and ARTEMIS. They have drawn research agendas that will drive the selection of large cooperative projects in the next years in Europe.

1.3 Applications

This section provides an overview of the major applications for WSNs. The application areas considered are the following [35]:

- Environmental monitoring
- Health Care
- Mood based services
- Positioning and tracking
- Tourism
- Logistics
- Transportation
- Home and office

A brief description of those applications which are strictly related to WANs, is provided: environmental monitoring, health care, positioning and tracking and home and office.

Finally, another classification for WSN applications, is introduced. This classification divides applications between: Event Detection and Spatial and Time Random Process.

Environmental Monitoring

These applications may monitor indoor or outdoor environments, where the supervised area may be thousands of square kilometers and the duration of the supervision may last years. One of the main issue could be to determine the location of the events. Such systems are to be infrastructure-less and very robust, because of the inevitable challenges in the nature, like living things or atmospheric events. Natural disasters such as floods, forest fire, earthquakes may be perceived earlier by installing networked embedded systems closer to places where these phenomena may occur. The system should respond to the changes of the environment as quick as possible. The environment to be observed will mostly be inaccessible by the human all the time. Hence, robustness plays an important role. Also security and surveillance applications have the most number of challenging requirements: real-time monitoring technologies with high security requirements, are required.

Health Care

Applications in this category include telemonitoring of human physiological data, tracking and monitoring of doctors and patients inside a hospital, drug administrator in hospitals etc. Merging wireless sensor technology into health and medicine applications will make life much easier for doctors, disables people and patients. They

will also make diagnosis and consultancy processes regardless of location and transition automatically from one network in a clinic to the other installed in patient's home. As a result, high quality healthcare services will get closer to the patients. Health applications are critical, since vital events of humans will be monitored and automatically interfered. The main issues are reliability and limited delays.

Positioning and animals tracking

Also the localisation of people, objects and animals are important applications of WSNs. Technologies using global positioning systems have emerged from some time now but most of the solutions only work in outdoor scenarios. Localization indoors involves much more difficulties and represents an unsolved problem in many cases, especially when relative positioning to others and to objects is required, while in movement.

Homes and Office

It is a wonderful idea for home automation using the ability to turn lights on and off remotely, monitor a sleeping baby without being in the room and having a fresh hot coffee cup in the kitchen for breakfast. Smart homes have the ability to acquire and apply knowledge about human surroundings and also adapt in order to improve human experience. It is saturated with computing and communication capabilities to make intelligent decisions in an automated manner. Its intelligent assistants provide interaction with the information web. Its advance electronics is also used to enable early detection of possible problems and emergency situations. Also the development of smart offices, could provide employers scanning the environment to get the

information on the localisation of movable objects in the office.

1.3.1 Event Detection and Spatial and Time Random Process Estimation

According to the type of data that must be gathered in the network, the different applications could be classified into two categories: Event Detection and Spatial and Time Random Process Estimation.

In the first case sensors must detect an event, for example a fire in a forest, a quake, etc.., therefore, sensors simply aim at comparing the scalar field with given thresholds [47, 48]. The signal processing within devices is very simple, owing to the fact that each device has to compare measurement results to a given threshold and send the binary information to the final sink(s). The density of nodes must ensure that the event is detected with given probability and that the report can be received by the sink(s) with given probability. The sampling frequency, that is the frequency with which nodes take samples from the environment must ensure that the event is detected with given probability and that the report timely reaches the sink(s).

In the spatial and time random process estimation application the WSN aims at estimating a given physical phenomenon (e.g., the atmospheric pressure in a wide area, or the ground temperature variations in a small volcanic site), which can be modelled as a bi-dimensional random process (generally non stationary). Therefore, in this case the estimation of the entire behavior of the scalar field is needed [49, 50]. Considering a typical application related to data gathering from an area and forwarding data to final sink(s), when sensors receive a service request, coming from the sink(s), they take a sample from the environment and transmit it, by following an appropriate

communication protocol, to it, which is in charge of collecting all information detected by nodes and estimating the process realisation. The sampling frequency must ensure that the process evolution is tracked.

1.4 IEEE 802.15.4 Technology

IEEE 802.15.4 wireless technology is a short-range communication system intended to provide applications with relaxed throughput and latency requirements in wireless personal area networks (WPANs). The key features of 802.15.4 wireless technology are low complexity, low cost, low power consumption, low data rate transmissions, to be supported by cheap either fixed or moving devices. The main field of application of this technology is the implementation of WSNs.

The IEEE 802.15.4 Working Group[1] focuses on the standardization of the bottom two layers of ISO/OSI protocol stack. The other layers are normally specified by industrial consortia such as the ZigBee Alliance[2].

In the following some technical details related to the physical layer and the MAC sublayer as defined in the standard, are reported. Moreover, some characteristics related to higher layers will be presented, with particular attention to Zigbee tree-based topology, largely used in this thesis.

1.4.1 IEEE 802.15.4 Physical Layer

The 802.15.4 core system consists of an RF transceiver and the protocol stack, depicted in Fig. 1.4. The system offers low rate services that enable the connection of

[1]See also the IEEE 802.15.4 web site: http://www.ieee802.org/15/pub/TG4.html
[2]See also the ZigBee Alliance web site: http://www.zigbee.org/en/index.asp

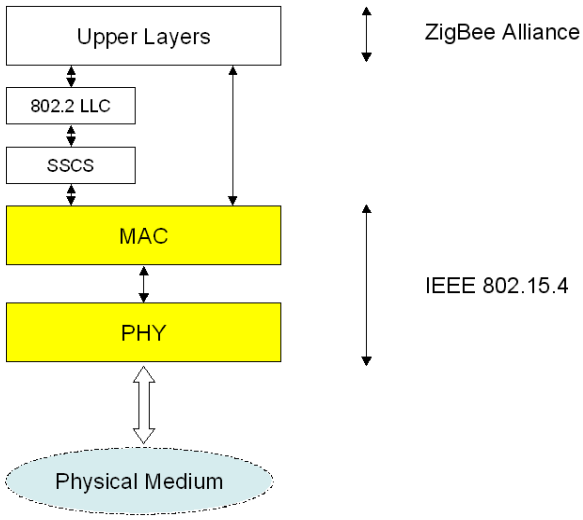

Figure 1.4: ZigBee protocol stack.

possibly mobile low-complexity devices based on the carrier sensing multiple access with collision avoidance (CSMA/CA) channel access technique.

The 802.15.4 physical layer operates in three different unlicensed bands (and with different modalities) according to the geographical area where the system is deployed. However, direct sequence spread spectrum (DS-SS) is wherever mandatory to reduce the interference level in shared unlicensed bands.

The physical (PHY) provides the interface with the physical medium. It is in charge of radio transceiver activation and deactivation, energy detection, link quality, clear channel assessment, channel selection, and transmission and reception of the message packets. Moreover, it is responsible for establishment of the RF link

between two devices, bit modulation and demodulation, synchronization between the transmitter and the receiver, and, finally, for packet level synchronization.

IEEE 802.15.4 specifies a total of 27 half-duplex channels across the three frequency bands, whose channelization is depicted in Fig. 1.5 and is organized as follows:

- the 868 [MHz] band, ranging from 868.0 and 868.6 [MHz] and used in the European area, implements a -cosine-shaped binary phase shift keying (BPSK) modulation format, with DS-SS at chip-rate 300 [kchip/s] (a pseudo-random sequence of 15 chips transmitted in a 25 [μs] symbol period). Only a single channel with data rate 20 [kbps] is available and, with a required minimum -92 [dBm] RF sensitivity, the ideal transmission range (i.e., without considering wave reflection, diffraction and scattering) is approximatively 1 [km];

- the 915 [MHz] band, ranging between 902 and 928 [MHz] and used in the North American and Pacific area, implements a raised-cosine-shaped BPSK modulation format, with DS-SS at chip-rate 600 [kchip/s] (a pseudo-random sequence of 15 chips is transmitted in a 50 [μs] symbol period). Ten channels with rate 40 [kbps] are available and, with a required minimum -92 [dBm] RF sensitivity, the ideal transmission range is approximatively 1 [km];

- the 2.4 [GHz] industrial scientific medical (ISM) band, which extends from 2400 to 2483.5 [MHz] and is used worldwide, implements a half-sine-shaped Offset Quadrature Shift Keying (O-QPSK) modulation format, with DS-SS at 2 [Mchip/s] (a pseudo-random sequence of 32 chips is transmitted in a 16 [μs] symbol period). Sixteen channels with data rate 250 [kbps] are available and,

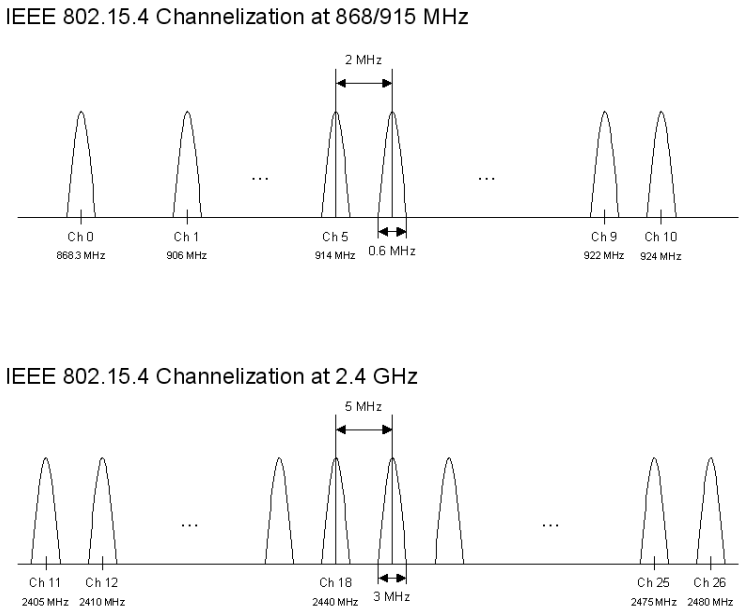

Figure 1.5: Channelization at the 868/915 [MHz] bands and at the 2.4 [GHz] band.

with minimum -85 [dBm] RF sensitivity required, the ideal transmission range is approximatively 220 [m].

The ideal transmission range is computed considering that, although any legally acceptable power is permitted, IEEE 802.15.4-compliant devices should be capable of transmitting at -3 [dBm].

Since the 2.4 [GHz] band is shared with many other services, the other two available bands can be used as an alternative.

Power consumption is a primary concern, so, to achieve long battery life the energy must be taken continuously at an extremely low rate, or in small amounts at a low power duty cycle: this means that IEEE 802.15.4-compliant devices are active only

during a short time. The standard allows some devices to operate with both the transmitter and the receiver inactive for over 99% of time. So, the instantaneous link data rates supported (i.e., 20 [kbps], 40 [kbps], and 250 [kbps]) are high with respect to the data throughput in order to minimize device duty cycle.

According to the IEEE 802.15.4 standard, transmission is organized in frames, which can differ according to the relevant purpose. In particular, there are four frame structures, each designated as a Physical Protocol Data Unit (PPDU): a beacon frame, a data frame, an acknowledgement frame and a MAC command frame. They are all structured with a Synchronization Header (SHR), a Physical Header (PHR), and a Physical Service Data Unit (PSDU), which is composed of a MAC Payload Data Unit (MPDU), which in turn is constructed with a MAC Header (MHR), a MAC Footer (MFR), and a MAC Service Data Unit (MSDU), excepting the acknowledgement frame, which does not contain an MSDU. The structure of each possible frame is depicted in Fig. 1.6-1.9. To detect that a message has been received correctly, a cyclic redundancy check (CRC) is used. The meaning of the four possible frame structures will be clear in the following, after introducing the possible network topologies and the possible MAC channel access strategies.

1.4.2 IEEE 802.15.4 Network Topologies and Operational Modes

To overcome the limited transmission range, multihop self-organizing network topologies are required. These can be realized taking into account that IEEE 802.15.4 defines two type of devices: the full function device (FFD) and the reduced function

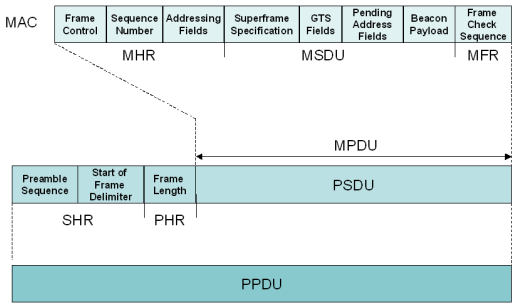

Figure 1.6: Beacon frame structure.

device (RFD). The FFD contains the complete set of MAC services and can operate as either a network coordinator (from this point in time also denoted as WPAN *coordinator*) or as a simple network device. The RFD contains a reduced set of MAC services and can operate only as a network device.

Two basic topologies are allowed, but not completely described by the standard since definition of higher layers functionalities are out of the scope of 802.15.4: the star topology, formed around an FFD acting as a WPAN coordinator, which is the only node allowed to form links with more than one device, and the peer-to-peer topology, where each device is able to form multiple direct links to other devices so that redundant paths are available. An example of both the IEEE 802.15.4-compliant network topologies is shown in Fig. 1.10.

Star topology is preferable in case coverage area is small and low latency is required

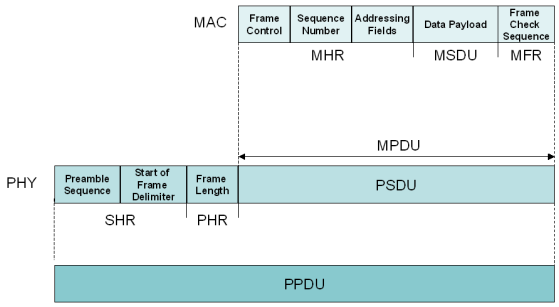

Figure 1.7: Data frame structure.

by the application. In this topology, communication is controlled by the WPAN coordinator that acts as network master, sending packets, named *beacons* for synchronization and managing device association. Network devices are allowed to communicate only with the WPAN coordinator and any FFD may establish its own network by becoming a WPAN coordinator according to a predefined policy. A network device wishing to join a star network listen for a beacon message and, after receiving it, the network device can send an association request back to the WPAN coordinator, which allows the association or not. Star networks support also a non beacon-enabled mode. In this case, beacons are used for association purpose only, whereas synchronization is achieved by polling the WPAN coordinator for data on a periodic basis. Star networks operate independently from their neighboring networks.

Peer-to-peer topology is preferable in case a large area should be covered and latency is not a critical issue. This topology allows the formation of more complex networks and permits any FFD to communicate with any other FFD behind its

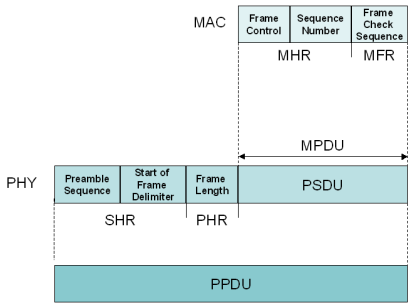

Figure 1.8: Acknowledgement frame structure.

transmission range via multi-hop. Each device in a peer-to-peer structure needs to proactively search for other network devices. Once a device is found, the two devices can exchange parameters to recognize the type of services and features each supports. However, the introduction of multihop requires additional device memory for routing tables.

IEEE 802.15.4 can also support other network topologies, such as cluster, mesh, and tree. These last network topology options are not part of the IEEE 802.15.4 standard, but the tree topology is described in the ZigBee Alliance specifications [51]. This topology, which is depicted in Fig. 1.11 as an example, can be interpreted as a hierarchical tree of network devices where all the devices in the network must be FFDs with the exception of the leaves which, since they must do no message relaying, may be either FFDs or RFDs. Exactly one device in the network assumes the special role of the WPAN coordinator. Surrounding each coordinator, a hierarchical tree may be formed in a typical parent-child relationship, but only one single device

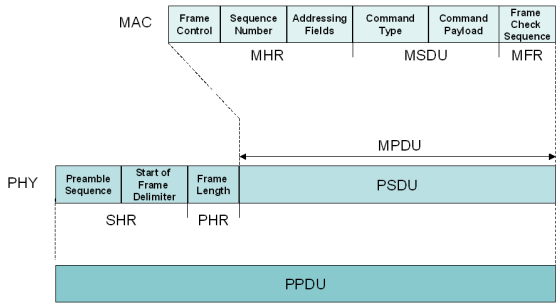

Figure 1.9: MAC command frame structure.

in the entire network functions as the WPAN coordinator. In case more WPAN coordinators are present, a forest of disjoint trees, rooted at the WPAN coordinators is established. In this case the coordinators and the nodes belonging to the different WPANs will use different channel frequencies (that is the channel selected by the WPAN coordinator during the topology formation phase, see section 1.4.5) and nodes belonging to different WPANs do not interfere.

All devices, regardless of the type of topology, belonging to a particular network use their unique IEEE 64-bit addresses and a short 16-bit address is allocated by the WPAN coordinator to uniquely identify the network.

Finally, the WPAN coordinator election can be performed in different ways according to the application. In particular, for the applications in which only one device can be the coordinator (e.g., a gateway) it is preferable to have a dedicated WPAN coordinator, or in other applications it could be significant several eligible FFDs and to have an event-determined WPAN coordinator, or finally there can be applications

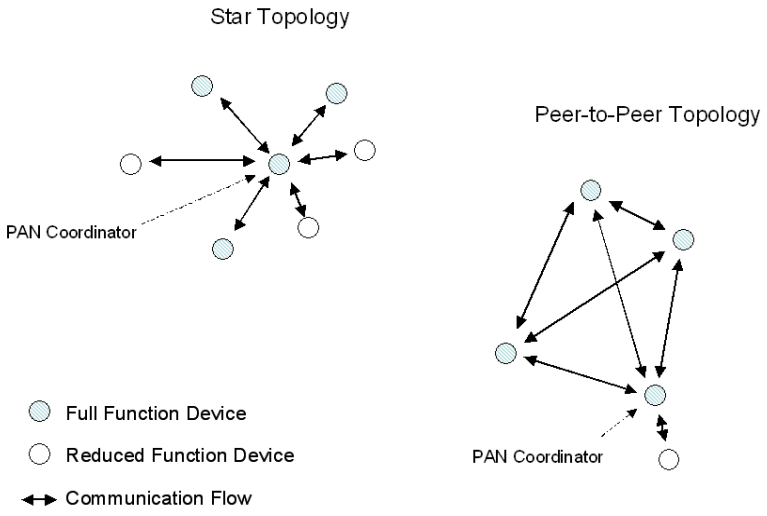

Figure 1.10: The two IEEE 802.15.4-compliant network topologies: star and peer-to-peer topology.

where it is not relevant which particular device is the WPAN coordinator, in this case it can be self-determined. Moreover, the WPAN coordinator may be selected because it has special computation capability, a bridging capability to other network protocols, or simply because it was among the first participants in the formation of the network.

1.4.3 IEEE 802.15.4 MAC Sublayer

The MAC sublayer, together with the Logical Link Control (LLC) sublayer, comprises the data link layer in the ISO/OSI model. The MAC layer provides access control to

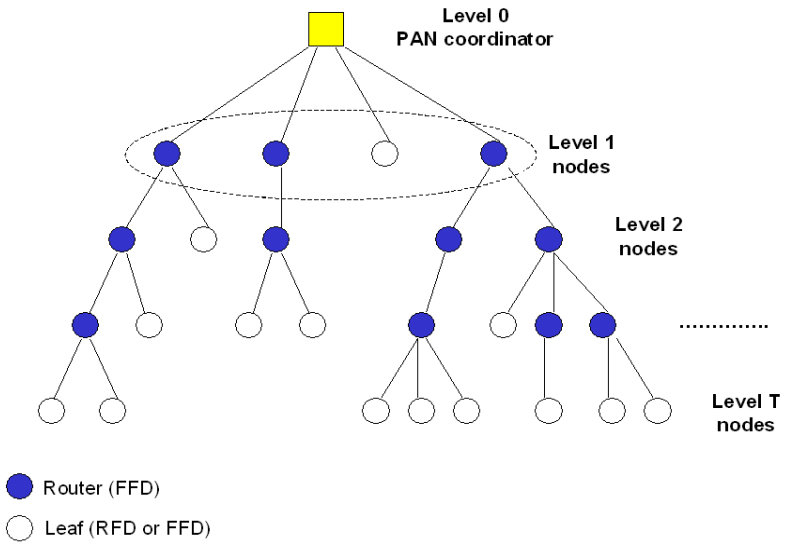

Figure 1.11: ZigBee-compliant tree network topology.

a shared channel and reliable data delivery.

IEEE 802.15.4 uses a protocol based on the CSMA/CA algorithm, which requires listening to the channel before transmitting to reduce the probability of collisions with other ongoing transmissions. The main functions performed by the MAC sublayer are: association and disassociation, security control, optional star network topology functions (such as beacon generation and Guaranteed Time Slots (GTSs) management), generation of acknowledge (ACK) frames (if used), and finally to provide application support for the two possible network topologies described in the standard.

IEEE 802.15.4 defines two different operational modes, namely the *beacon-enabled*

and the *non beacon-enabled*, which correspond to two different channel access mechanisms.

In the non beacon-enabled mode nodes use an unslotted CSMA/CA protocol to access the channel and transmit their packets [52]. The algorithm is implemented using units of time called backoff periods.

Each node maintains two variables for each transmission attempt: NB and BE. NB is the number of times the CSMA/CA algorithm was required to backoff while attempting the current transmission; this value will be initialized to 0 before each new transmission attempt and cannot assume values larger than NB_{max}, equal to 4. BE is the backoff exponent related to the maximum number of backoff periods a node will wait before attempting to assess the channel. BE will be initialized to the value of BE_{min}, equal to 3, and cannot assume values larger than BE_{max}, equal to 5. Figure 1.12 illustrates the steps of the CSMA/CA algorithm, starting from when the node has data to be transmitted. First, NB and BE are initialized and then the MAC layer will delay any activities for a random number of backoff periods in the range (0, 2^{BE}-1) [step (1)]. After this delay, channel sensing is performed for one unit of time [step (2)]. If the channel is assessed to be busy [step (3)], the MAC sublayer will increase both NB and BE by one, ensuring that BE is not larger than BE_{max}. If the value of NB is less than or equal to NB_{max}, the CSMA/CA algorithm will return to step (1). If the value of NB is larger than NB_{max}, the CSMA/CA algorithm will terminate with a "Failure," meaning that the node does not succeed in accessing the channel. If the channel is assessed to be idle [step (4)], the MAC layer will begin transmission of data immediately ("Success" in accessing the channel).

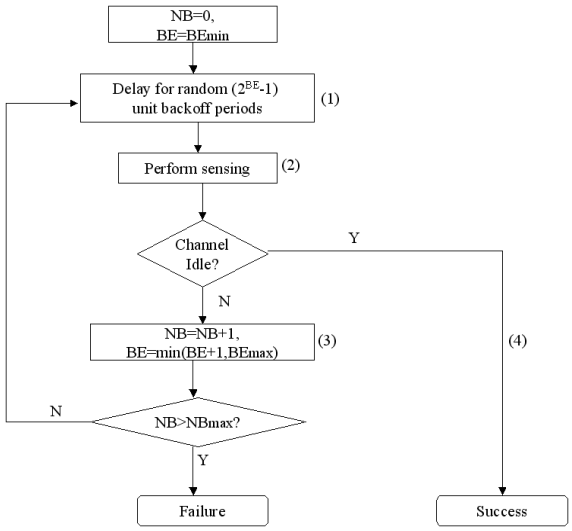

Figure 1.12: The IEEE 802.15.4 CSMA/CA algorithm in the non beacon-enabled case.

In the beacon-enabled mode [52], instead, the access to the channel is managed through a superframe, starting with a packet, called *beacon*, transmitted by WPAN coordinator. The superframe may contain an inactive part, allowing nodes to go in sleeping mode, whereas the active part is divided into two parts: the Contention Access Period (CAP) and the Contention Free Period (CFP), composed by GTSs, that can be allocated by the sink to specific nodes (see Figure 1.14). The use of GTSs is optional.

The duration of the active part and of the whole superframe, depend on the value of two integer parameters ranging from 0 to 14, that are, respectively, the superframe order (SO), and the beacon order (BO), with $BO \geq SO$. BO defines the interval of time between two successive beacons, namely the beacon interval, BI, is equal to

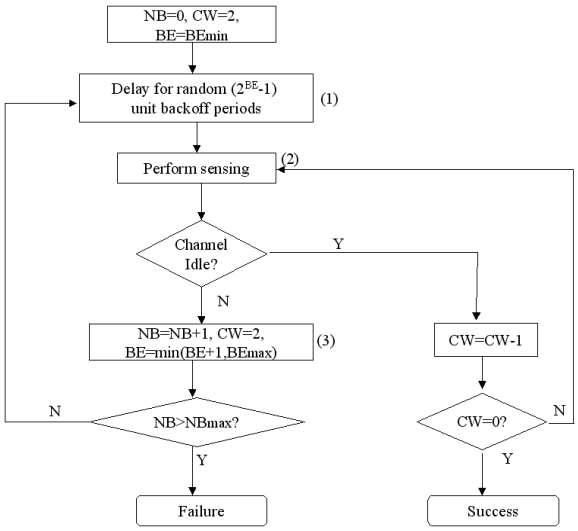

Figure 1.13: The IEEE 802.15.4 CSMA/CA algorithm in the beacon-enabled case.

$$BI = 16 \cdot 60 \cdot 2^{BO} \cdot T_s \,, \tag{1.4.1}$$

where $T_s = 16$ $[\mu s]$ is the symbol time.

The duration of the active part of the superframe, containing CAP and CFP, namely the superframe duration, SD, is equal to

$$SD = 16 \cdot 60 \cdot 2^{SO} \cdot T_s \,. \tag{1.4.2}$$

According to the standard each GTS must have a duration multiple of $60 \cdot 2^{SO} \cdot T_s$ and must contain the packet to be transmitted by the node to which the GTS is allocated to and also an inter-frame space, equal to $40\,T_s$. This is, in fact, the minimum interval of time that must be guaranteed between the reception of two subsequent packets. The WPAN coordinator may allocate up to seven GTSs, but a

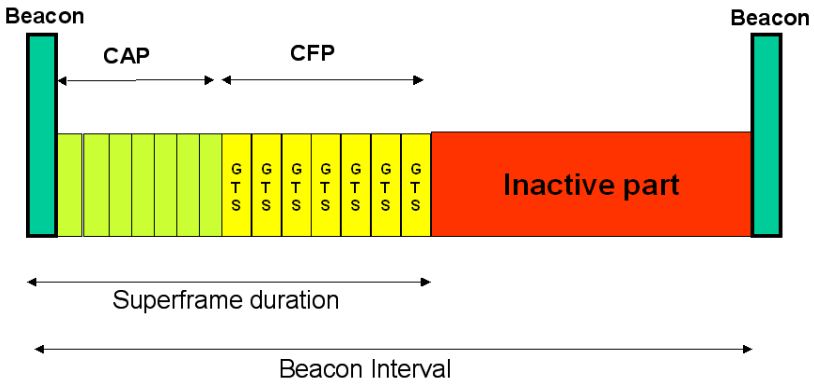

Figure 1.14: Superframe Structure.

sufficient portion of the CAP must remain for contention-based access. The minimum CAP duration is equal to 440 T_s.

For what concerns the CSMA/CA algorithm used in the CAP portion of the superframe the only difference with the non beacon-enabled mode is that nodes have to find the channel free for two subsequent backoff periods before transmitting the packet (see Figure 1.13). To this aim, each node maintains another variable, called CW, denoting the number of backoff periods that need to be clear of channel activity before the transmission can start. First, CW is initialized to 2. When channel sensing is performed for one backoff period [step (2)], if the channel is assessed to be busy, CW is set to 2 and if $NB < NB_{max}$ the algorithm returns to step (1);

otherwise the algorithm will unsuccessfully terminate, meaning that the node does not succeed in accessing the channel. If the channel is assessed to be idle, instead, CW is decremented by 1 and compared with 0. If $CW > 0$, the algorithm returns to step (2); otherwise a transmission may start.

The other difference with the non beacon-enabled case is that backoff period boundaries of every node in the WPAN must be aligned with the superframe slot boundaries of the coordinator, therefore, the beginning of the first backoff period of each node is aligned with the beginning of the beacon transmission. Moreover, all transmissions may start on the boundary of a backoff period.

1.4.4 Data transfer Protocol and MAC Frames

As a consequence of the different type of topologies and the possibility of implementing the beacon-enable mode, three different MAC data transfer protocols are defined by IEEE 802.15.4:

- in case of beacon-enabled star topology, a network device wishing to send data to the WPAN coordinator needs to listen for a beacon. If it does not have a GTS assigned, the device transmits its data frame in the contention access period with CSMA/CA. If the device has a GTS assigned, it waits for the appropriate one to transmit its data frame. Afterwards, the WPAN coordinator sends back an acknowledgement to the network device, as shown in Fig. 1.15. When the WPAN coordinator has data for a network device, it sets a special flag in its beacon. Once the appropriate network device detects that the WPAN coordinator has pending data for it, it sends back a "Data Request" message. The WPAN coordinator responds with an acknowledgment followed by the data

frame, and, finally, an acknowledgement is sent from the network device, as depicted in Fig. 1.16;

- in case of non-beacon-enabled star topology, a network device wishing to transfer data sends a data frame to the WPAN coordinator using CSMA/CA. The WPAN coordinator responds to the network device, sending an acknowledgement message, as shown in Fig. 1.17. When a WPAN coordinator requires making a data transfer to a network device, it shall keep the data until the network device sends a data request message. The acknowledgement message from the WPAN coordinator will contain information indicating the network device if there are data pending, in which case, the data will be sent immediately after the acknowledgement. Finally, the network device acknowledges reception of the data frame, as depicted in Fig. 1.18;

- in case of peer-to-peer topology, the strategy is governed by the specific network layer managing the wireless network. A given network device may stay in reception mode scanning the radio channel for on-going communications or can send periodic "hello" messages to achieve synchronization with other potential listening devices.

The case of tree topology, specified by the ZigBee Alliance [51] is described in details in the following sections, since this topology is largely used in the rest of the thesis.

Finally, as far as the MAC frame structure is concerned, a MAC frame consists of three parts: header, variable length payload, and footer. The MAC header contains

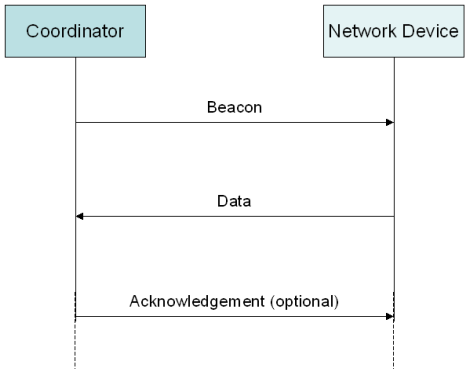

Figure 1.15: Communication from a network device to the PAN in a beacon-enabled network.

a frame control field and an addressing field. The MAC payload contains information specific to the type of transaction being handled by the MAC. The MAC footer consists of a 16-bit CRC algorithm. When the three components of the MAC frame are assembled into the PHY packet, it is called the MPDU. Four types of MAC frames are defined: beacon, data, acknowledgment, and MAC command.

1.4.5 The IEEE 802.15.4 Topology Formation Procedure

The IEEE 802.15.4 Group defined a mechanism to support a WPAN coordinator in channel selection when starting a new WPAN, and a procedure, called *association procedure*, which allows other devices to join the WPAN. A WPAN coordinator wishing to establish a new WPAN needs to find a channel which is free from interference

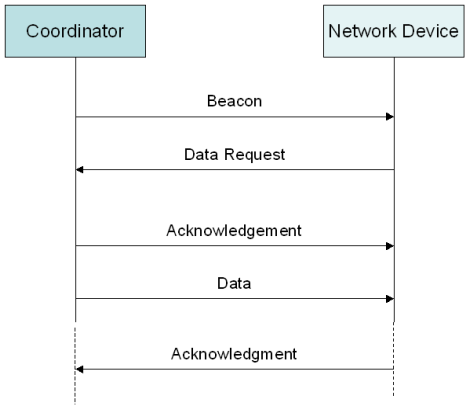

Figure 1.16: Communication from the PAN to a network device in a beacon-enabled network.

that would render the channel unsuitable (e.g., in a multi-sink network, a channel may be already occupied by other WPANs). The channel selection is performed by the WPAN coordinator through the energy detection (ED) scan which returns the measure of the peak energy in each channel. It must be noticed that the standard only provides the ED mechanism but it does not specify the channel-selection logic. The operations accomplished by a device to discover an existing WPAN and to join it can be summarised as follows: i) search for available WPANs; ii) select the WPAN to join; iii) start the association procedure with the WPAN coordinator or with another FFD device, which has already joined the WPAN. The discovery of available WPANs is performed by scanning beacon frames broadcasted by the coordinators. Two different types of scan that can be used in the association phase are proposed:

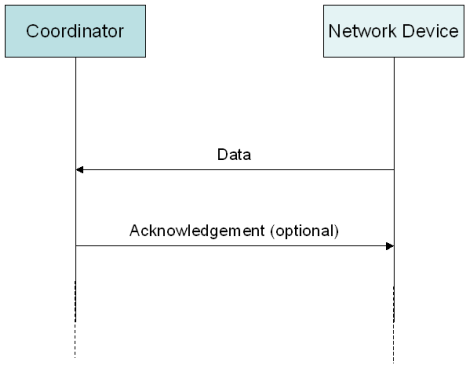

Figure 1.17: Communication from a network device to the PAN in a non-beacon-enabled network.

1. passive scan: in beacon-enabled networks the associated devices periodically transmit beacon frames hence the information on the available WPAN can be derived by eavesdropping the wireless channels;

2. active scan: in non-beacon-enabled networks the beacon frames are not periodically transmitted but shall be explicitly requested by the device by means of beacon request command frame.

After the scan of the channels, a list of available WPANs is used by the device to choose the network to try to connect with. In the standard, no specific procedure to select a WPAN is provided and so, this selection among potential parents is open for different implementations. Hence, the device sends an association request frame to the coordinator device by means of which the selected network was discovered.

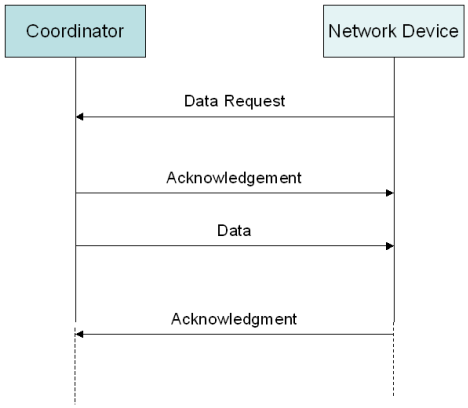

Figure 1.18: Communication from the PAN to a network device in a non-beacon-enabled network.

The association phase ends with a successful association response command frame to the requesting device. This procedure basically results in a set of MAC association relationships between devices, named in the following parent-child relationship.

1.4.6 The Zigbee Tree-Based Topology

The Zigbee specifications [51] define a beacon-enabled tree-based topology, as a particular case of the IEEE 802.15.4 peer-to-peer networks (shown in Figure 1.11). A tree, rooted at the WPAN coordinator, is formed, and nodes at a given level transmit data to nodes at a lower level, to reach the WPAN coordinator, which is a level zero, in the example shown in the Figure. Two different types of nodes are present in the tree: the routers, that must be FFDs, which receive data from their children,

aggregate them, and transmit the packet obtained to their parents; and the leafs, that could be FFDs or RFD, which have no routing functionalities and have only to transmit their packets to the parent.

The topology formation procedure is started by the WPAN coordinator, which broadcasts beacon packets to neighbour nodes. A candidate node receiving the beacon may request to join the network at the WPAN coordinator. If the WPAN coordinator allows the node to join, it will begin transmitting periodic beacons so that other candidate nodes may join the network.

As stated above, nodes must be in beacon-enabled mode: each child node tracks the beacon of its parent (see Figure 1.19, where the tracking period is outlined as a dashed rectangle). A core concept of this tree topology is that the child node may transmit its own beacon at a predefined offset with respect to the beginning of its parent beacon: the offset must always be larger than the parent superframe duration and smaller than beacon interval (see Figure 1.19). This implies that the beacon and the active part of child superframe reside in the inactive period of the parent superframe; therefore, there is no overlap at all between the active portions of the superframes of child and parent. This concept can be expanded to cover more than two nodes: the selected offset must not result in beacon collisions with neighbouring nodes. This implies that the node must record the time stamp of all neighbouring nodes and selects a free time slot for its own beacon. Obviously a child will transmit a beacon packet only in case it is a router in the tree; if the child is a leaf it has only to transmit the packet to its parent. Each child will transmit its packet to the parent in the active part (CAP or CFP) of the parent superframe.

Therefore, each router in the tree, after the reception of the beacon coming from

the parent, will select the instant in which transmits its beacon (see Figure 1.20). Beacon scheduling is necessary to prevent the beacon frames of one device from colliding with either the beacon frames or data transmissions of its neighboring devices.

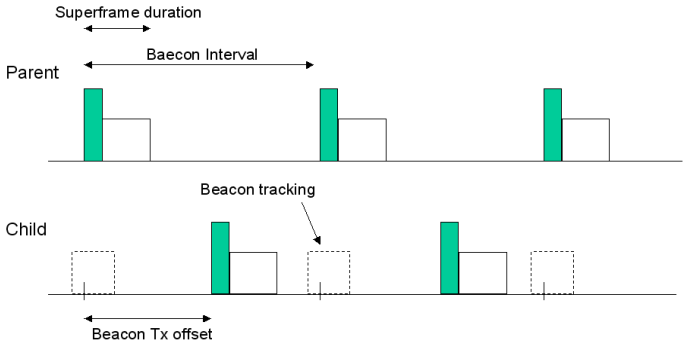

Figure 1.19: The tracking of the beacon's parent, performed by a generic child.

ZigBee Higher Levels Overview

The purpose of the ZigBee Alliance is to univocally describe the ZigBee protocol standard in such a way that interoperability is guaranteed also among devices produced by different companies, provided that each device implements the ZigBee protocol stack.

The ZigBee stack architecture is composed of a set of blocks called layers. Each layer performs a specific set of services for the layer above.

The ZigBee stack architecture is depicted in detail in Fig. 1.21. Given the IEEE

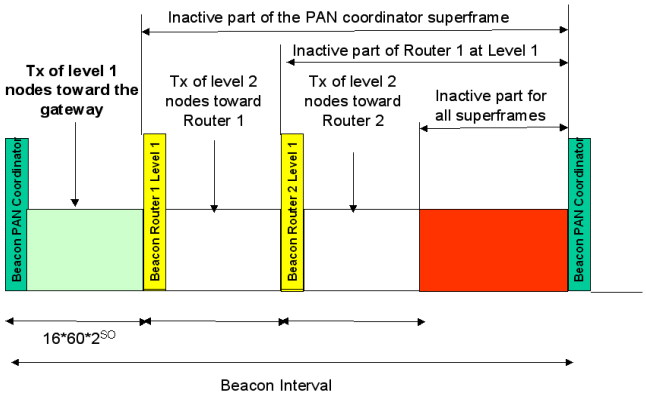

Figure 1.20: The superframe structure used in the tree-based topology.

802.15.4 specifications on PHY and MAC layer, the ZigBee Alliance provides the network layer and the framework for the application layer.

The responsibilities of the ZigBee network layer include: mechanisms to join and leave a network, frame security, routing, path discovery, one-hop neighbours discovery, neighbour information storage.

The ZigBee application layer consists of the application support sublayer, the application framework, the ZigBee device objects and the manufacturer-defined application objects. The responsibilities of the application support sublayer include: maintaining tables for binding (defined as the ability to match two devices together based on their services and their needs), and forwarding messages between bound devices. The responsibilities of the ZigBee device objects include: defining the role of the device within the network (e.g., WPAN coordinator or end device), initiating

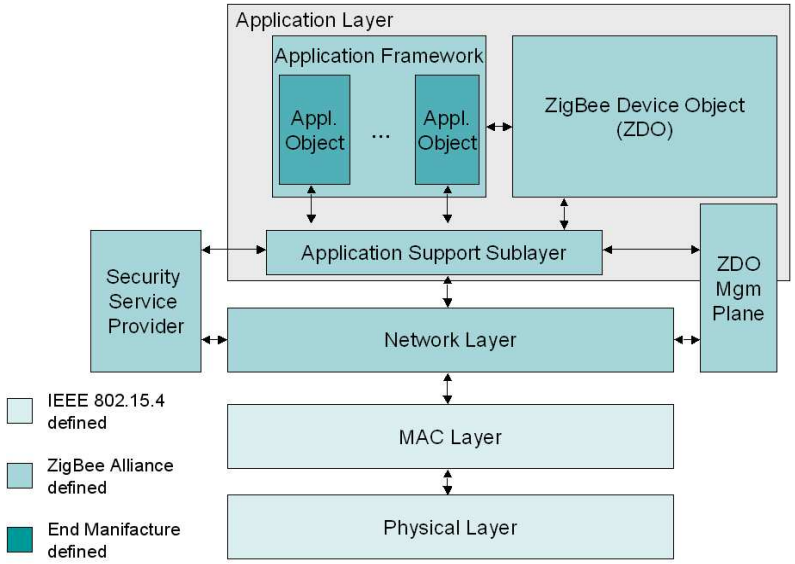

Figure 1.21: A detailed overview of ZigBee stack architecture.

and/or responding to binding requests, establishing secure relationships between network devices, discovering devices in the network, and determining which application services they provide.

1.5 Other Technologies

1.5.1 Ultrawide Bandwidth Technology

Ultrawide bandwidth radio is a fast emerging technology with uniquely attractive features that has attracted a great deal of interest from academia, industry, and global standardization bodies. The ultrawide bandwidth (UWB) technology has

been around since 1960, when it was mainly used for radar and military applications, whereas nowadays it is a very promising technology for advances in wireless communications, networking, radar, imaging, positioning systems and, in particular, WSNs.

The most widely accepted definition of a UWB signal is a signal with instantaneous spectral occupancy in excess of 500 MHz or a fractional bandwidth of more than 20%.

One of the most promising UWB technique, especially for WSN applications, is named impulse radio UWB (IR-UWB) [53]. The IR-UWB technique relies on ultra-short (nanosecond scale) waveforms that can be free of sine-wave carriers and do not require intermediated frequency (IF) processing because they can operate at baseband. The IR-UWB technique has been selected as the PHY layer of the IEEE 802.15.4a Task Group for WPAN Low Rate Alternative PHY layer [54]. The baseline of 802.15.4a is based on two optional PHYs consisting of a UWB impulse radio (operating in unlicensed UWB spectrum) and a chirp spread spectrum (CSS) (operating in unlicensed 2.4 GHz spectrum), where the former will be able to deliver communications and high precision ranging. In particular the UWB PHY supports an over-the-air mandatory data rate of 851 [Kbit/s], with optional data rates of 110 [Kbit/s], 6.81 [Mbit/s], and 27.24 [Mbit/s]. The choice of the PHY depends on the local regulations, application and user preferences. Table 1.1 reports the frequency bands foreseen by the standard (some of them are optional). The modulation used combines both BPSK and pulse position modulation (PPM) signaling so that both coherent and low complexity noncoherent receivers can be used to demodulate the signal.

PHY mode	Frequency band [MHz]
UWB Sub-GHz	250-750
2450 CSS	2400-2483.5
UWB low-band	3244-4742
UWB high-band	5944-10234

Table 1.1: IEEE 802.15.4a PHY layer frequency bands

1.5.2 Bluetooth Technology

Bluetooth wireless technology is a short-range communication system intended to replace the cables in WPANs.[3] The key features of Bluetooth wireless technology are robustness, low power, and low cost and many features of the core specification are optional, allowing product differentiation.

The IEEE Project 802.15.1 [55] has derived a WPAN standard based on the Bluetooth v1.1 Foundation Specifications.[4]

The Bluetooth RF (physical layer) operates in the unlicensed ISM band, for the majority of countries around 2.4 [GHz] in $(2400, 2483.5)$ [MHz]. The system employs a frequency hop transceiver (the nominal hop rate is 1600 [hops/s]) to combat interference and fading, and provides many FHSS carriers. RF operation uses a Gaussian shaped, binary frequency shift keying (GFSK) modulation to minimize transceiver complexity, and a forward error correction (FEC) coding technique. The bit rate is of 1 [Mbps] or, with Enhanced Data Rate, a gross air bit rate of 2 or 3 [Mbps]. These modes are known as Basic Rate and Enhanced Data Rate, respectively.

The equipment is classified into three power classes (given as power levels at the antenna connector of the equipment, if the equipment does not have a connector, a reference antenna with 0 [dBm] gain is assumed): (class 1) with maximum output

[3]Several information on Bluetooth can be found on the web site: `http://www.bluetooth.com`
[4]See also IEEE 802.15.1 web site: `http://www.ieee802.org/15/pub/TG1.html`

power of 20 [dBm], (class 2) with maximum output power of 4 [dBm], and (class 3) with maximum output power of 0 [dBm].

During typical operation, a physical radio channel is shared by a group of devices that are synchronized to a common clock and frequency hopping pattern. One device provides the synchronization reference and is known as the master. All other devices are known as slaves. A group of devices synchronized in this fashion form a piconet. This is the fundamental form of communication for Bluetooth wireless technology.

Devices in a piconet use a specific frequency hopping pattern which is algorithmically determined by certain fields in the Bluetooth specification address and clock of the master. The basic hopping pattern is a pseudo-random ordering of the 79 frequencies[5] with channel spacing of 1 [MHz] in the ISM band (e.g., $f = 2402 + k$ [MHz], with $k = 0, \ldots, 78$). To comply with out-of-band regulations in each country, a guard band is used at the lower and upper band edge, respectively of 2 [MHz] and 3.5 [MHz]. The hopping pattern may be adapted to exclude a portion of the frequencies that are used by interfering devices. The adaptive hopping technique improves Bluetooth technology co-existence with static (non-hopping) ISM systems when these are co-located.

The physical channel is sub-divided into time units known as slots with duration 625 [μs]. Data is transmitted between Bluetooth enabled devices in packets that are positioned in these slots. When circumstances permit, a number of consecutive slots may be allocated to a single packet. Frequency hopping takes place between the transmission or reception of packets. Bluetooth technology provides the effect of full duplex transmission through the use of a time-division duplex (TDD) scheme.

[5] In some countries, like France the number of frequencies is 23.

1.6 Channel and Link Models

In this section we introduce the channel and link models used hereafter.

Many works in the WSNs scientific literature assume deterministic distance- dependent and threshold-based packet capture models. In other words, all nodes within a circle centered at the transmitter, with given radius, can receive a packet sent by the transmitting one; if a receiver is outside the circle, reception is impossible [56–58]. While the threshold-based capture model, which assumes that a packet is captured if the signal-to-noise ratio (in the absence of interference) is above a given threshold, is a good approximation of real capture effects, the deterministic channel model does not represent realistic situations in most cases. The use of realistic channel models is therefore of paramount importance in wireless systems. In this thesis, a narrow-band channel, accounting for the power loss due to propagation effects including a distance-dependent path loss, the slow and the fast channel fluctuations, is considered.

In [35] results of experiments made with nodes using the IEEE 802.15.4 standard devices at 2.4 [GHz] ISM band, deployed in different environments (grass, asphalt, indoor, etc), are reported. The measurements provide inputs for understanding the basic aspects of narrow-band propagation in typical WSNs scenarios at 2.4 [GHz]. In particular, suitable comparison between the measurements performed and some simple analytical expressions has been conducted for different environments [35]. It was found for the received power in logarithmic scale that in general a Gaussian model can approximate the measurements fairly well, with different values of the standard deviation. Also some papers in the literature report results achieved in similar environments, and the Gaussian model seem to be accredited. Note that, since the scenario is stationary, the assumption of a (slow-varying) shadowing environment is

acceptable, as the log-normal distributed variable models the randomness of the geometry (presence of obstacles, etc). This is also done in other papers in the literature on WSNs (see, e.g., [59]). Channel reciprocity is also assumed.

It is assumed that the ratio between the transmit power, P_{T} and the received power, P_{R}, is given by $k \cdot d^{\beta} \cdot S$, where k is the propagation coefficient, d is the distance from the transmitter and the receiver, β is the attenuation coefficient which commonly ranges from 2 to 5, finally, S is the long-term (shadowing) fading component. We define $L = k \cdot d^{\beta} \cdot S$ as the averaged (with respect to fast fading) loss (in linear scale). By introducing the logarithmic scale, we obtain

$$L[dB] = k_0 + k_1 \ln d + s[dB], \tag{1.6.1}$$

where $k_0 = 10 \log_{10} k$, $k_1 = \beta \frac{10}{\ln 10}$, and s [dB] is a Gaussian random variable, with zero mean and variance σ_s^2. Note that in (1.6.1) the dependence on distance is through a natural logarithmic function, instead of a more typical base 10 log function; however, the transformation is quite simple, and this notation is the same used in works taken from the literature whose results are used as starting point in this section [60]. This channel model was also adopted by Orriss and Barton [61] and other Authors [62,63]. By suitably setting k_1, it is possible to accommodate an inverse square law relationship between power and distance ($k_1 = 8.69$), or an inverse fourth-power law ($k_1 = 17.37$), as examples.

For what concerns the link model, a radio link between two nodes is said to exist, which means that the two nodes are *connected* or *audible* one each other [6], if $L < L_{\mathrm{th}}$, where L_{th} represents the maximum loss tolerable by the communication system. The

[6] links reciprocity is assumed.

threshold L_{th} depends on the transmit power and the receiver sensitivity. By solving (1.6.1) for the distance d with $L = L_{\text{th}}$, we can define the transmission range

$$TR = e^{\frac{L_{\text{th}} - k_0 - s}{k_1}}, \tag{1.6.2}$$

as the maximum distance between two nodes at which communication can still take place. Such range defines the connectivity region of the sensor. Note that by adopting independent random variable (r.v.)'s, s, for separate links, we have different values of TR for every nodes pair. This means that any sensor observes a different realization of the r.v. TR depending on the direction of the potential interlocutor, thus acquiring a jaggy wireless footprint. In other words, circles to predict sensor connectivity, are not used here. However, by setting $\sigma_s = 0$, we neglect the channel fluctuations and may still define an ideal transmission range, as a reference, as

$$TR_{\text{i}} = e^{\frac{L_{\text{th}} - k_0}{k_1}}, \tag{1.6.3}$$

which is the radius of the circular deterministic footprint.

According to this channel model, we can also define the probability that two nodes are audible, $C(d)$, as the probability that $L < L_{\text{th}}$, given by

$$C(d) = \mathbb{P}\{L < L_{\text{th}}\} = 1 - 0.5\, erfc\left(\frac{L_{\text{th}} - k_0 - k_1 ln(d)}{\sqrt{2}\sigma_s}\right) \tag{1.6.4}$$

where $\mathbb{P}\{\mathcal{E}\}$ denotes the probability of the event $\mathcal{E}$ and $erfc()$ is the complementary error function. The disk model is obtained by considering $\sigma_s \to 0$, that is, $s = 0$, thus leading

$$C(d) = \begin{cases} 1 & \text{for } d \leq TR \\ 0 & \text{for } d > TR\,. \end{cases} \tag{1.6.5}$$

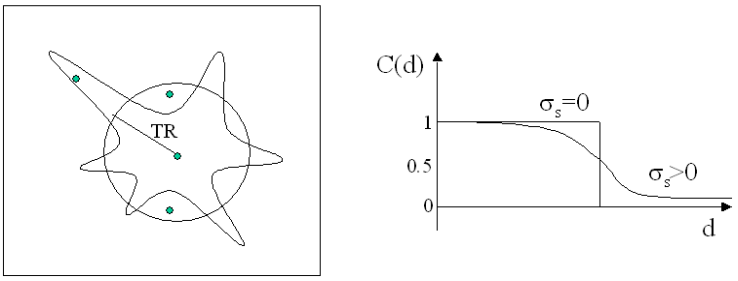

Figure 1.22: Link connectivity with and without shadowing effects.

As we can see in Fig. 1.22, taking into account a specific transmitting node, the effect of the shadowing is to make audible some nodes that are not reachable when adopting the disk model ($\sigma_s = 0$) because outside the circumference having radius TR; but, on the other side, also making non audible some nodes which are inside the circumference.

1.6.1 Connectivity Theory

The *connectivity theory* studies networks formed by large numbers of nodes distributed according to some statistics over a limited or unlimited region of $\mathbb{R}^d$, with d=1,2,3, and aims at describing the potential set of links that can connect nodes to

each other, subject to some constraints from the physical viewpoint (power budget, or radio resource limitations).

Connectivity depends on the number of nodes for unit area (nodes' density), and on the transmission power. The choice of an appropriate transmit power level is an important aspect of network design as it affects network connectivity. In fact, with a high transmit power a large number of nodes are expected to be reached via a direct link. On the contrary, a low transmit power would increase the possibility that a given node cannot reach any other node, that is, it is isolated.

In ad-hoc networks the best performance is achieved when data generated by a node can flow along the network and reach any possible endpoint. Thus the goal of connectivity is to make it possible for any node to reach any different node, perhaps in a multi-hop fashion. Although WSN are sometimes thought of as a special case of ad-hoc networks, they present a substantial difference, that is, nodes are at least of two different types: sensor and sink nodes. The purpose of this kind of networks is to process data originated by sensors, and sinks are in charge of collecting such data. Thus, the goal of connectivity is somewhat different here because it is sufficient for any sensor node to be able to reach at least one sink node, either directly or through other sensor nodes. That provided, the network is said to be *fully-connected*.

This topic is largely studied in Chapter 3.

Connectivity properties in PPP fields

Let us consider a number of nodes randomly distributed over a field. It is worth noting that, due to the random position of nodes and channel fluctuation effects, the number

of nodes which are connected [7] to whatever a node in the field, is not deterministic. This is true regardless the connectivity model we are considering. Therefore, the number of nodes connected to a give node, n, is a r.v. whose statistical properties depend on the connectivity models we are using and on the spatial distribution of nodes. In particular, when the position of nodes is distributed according to a PPP, we can apply the following theorem

Theorem 1.6.1. *Assume a Poisson distribution of nodes in a $m-$dimensional space and consider a reference node, denoted by R_N, located somewhere in the scenario. Let d, $C(d)$ and n be the euclidean distance between a generic node and R_N, the probability that a generic node is connected with R_N and the number of nodes which are connected with R_N, respectively. Then, n is a Poisson r.v..*

Proof. The proof is a consequence of the *Marking Theorem* for Poisson processes [35]. □

As a result of the previous property, the probability distribution of n is

$$\mathbb{P}\{n = n_1\} \triangleq P(n, \mu) = \frac{\mu^{n_1}}{n_1!} e^{-\mu}, \tag{1.6.6}$$

where $\mu = \mathbb{E}\{n\}$, being $\mathbb{E}\{\cdot\}$ the expectation. μ depends on the connectivity model chosen, and on the area in which nodes are distributed.

In particular, when the channel model of eq. (1.6.1) is used, the mean number of nodes audible within a range of distances r_1 and r, to a generic node ($r \geq r_1$), is denoted as $\mu_{r_1,r}$ and can be written as [60, 61]

$$\mu_{r_1,r} = \pi\rho[\Psi(a_1, b_1; r) - \Psi(a_1, b_1; r_1)], \tag{1.6.7}$$

[7] Meaning that the two nodes can reliably communicates one each other.

where ρ is the initial nodes' density and

$$\begin{aligned} \Psi(a_1, b_1; r) &= r^2 \Phi(a_1 - b_1 \ln r) \\ &- e^{\frac{2a_1}{b_1} + \frac{2}{b_1^2}} \Phi(a_1 - b_1 \ln r + 2/b_1), \end{aligned} \tag{1.6.8}$$

and $a_1 = (L_{\text{th}} - k_0)/\sigma_s$, $b_1 = k_1/\sigma_s$ and $\Phi(x) = \int_{-\infty}^{x} (1/\sqrt{2\pi}) e^{-u^2/2} du$.

By letting $r_1 = 0$ and $r \to \infty$ (which mean infinite area where nodes are distributed), $\Psi(a_1, b_1; r)$ vanishes and we can write

$$\begin{aligned} \mu_{0,\infty} &= -\pi\rho\Psi(a_1, b_1; r_1) \\ &= \pi\rho \exp[(2a_1/b_1) + (2/b_1^2)] \\ &= \pi\rho \exp[(2(L_{\text{th}} - k_0)/k_1) + (2\sigma_s^2/k_1^2)]. \end{aligned} \tag{1.6.9}$$

Note that the mean value of n, $\mathbb{E}\{n\}$, is equal to $\mu_{0,\infty}$ also in case nodes are distributed over a finite plane, but border effects are negligible (see Chapter 3), which means that the exponential $\Psi(a_1, b_1; r)$ is close to zero.

Chapter 2

Environmental Monitoring Estimation Error Through Energy-Efficient WSN

In this Chapter a self-organising single-sink WSN, aiming at estimating a scalar field over a bi-dimensional scenario (e.g., the atmospheric pressure in a wide area), is investigated. We assume that sensor devices (denoted as *nodes*, in the following) are randomly distributed, according to a PPP over the area, are organised in a *clustered* topology and access the channel through a contention-based MAC protocol. The channel and link models are those described in Chapter 1.

This Chapter provides a mathematical framework to analyse the interdependent aspects of WSN communication protocol and signal processing design. In particular, connectivity and MAC issues, randomness of the channel and the role of DDSP techniques, are accounted for. The possibility that nodes perform DDSP is studied through a distributed compression technique based on signal re-sampling. The DDSP impact on network energy efficiency is compared through a novel mathematical approach to the case where the processing is performed entirely by the sink.

The network is analysed from two different viewpoints: the estimation of the

process and the energy consumption. The trade-off between energy conservation and estimation error is discussed and a design criterion proposed. Comparison to simulation outcomes validates the model.

As an example result, the required node density is found as a trade-off between estimation quality and network lifetime for different system parameters and scalar field characteristics. It is shown that both the DDSP technique and the MAC protocol choice has a relevant impact on the performance of a WSN.

The Chapter is organized as follows: the following section deals with the aim of the model and related works, section 2.2 provides the sensing and estimation process formalization; the novel model proposed to evaluate the estimation error, is described in section 2.3 which also considers the DDSP option. Section 2.4 describes the self-organizing distributed routing and MAC algorithm used as a reference in the numerical evaluations. In section 2.5 the formulation of the energy budget is given. Finally, section 2.6 reports numerical results achieved through the mathematical framework, and compare them to simulation outcomes to validate the former.

2.1 Aims of the Framework and Related Works

The goal of the single-sink WSN considered here, is to sense a scalar field, such as, the atmospheric pressure in a wide area. To this aim nodes deployed over the area sense the physical world and transmit the measurement results to a sink, collecting data and forwarding them toward the final user. Since node battery is normally not replaced during network lifetime, the communication protocols energy efficiency is a key aspect.

The scalar field is modeled as a realization of a bi-dimensional spatial random

process. The measurements will then be subject to proper processing which might be performed either in a distributed manner by the nodes, or centrally at the sink. The specific case of random WSNs, where nodes are deployed randomly and uniformly with given density, is addressed here. In the recent literature, different works addressed the estimation of a scalar field using random WSNs. As an example, [49] presents a distributed algorithm able to estimate the gradient of a generic smooth physical process (energy constraints and nodes failure are not considered there); in [50] the relationship between the random topology of a sensor network and the quality of the reconstructed field is investigated and some guidelines on how nodes should be deployed over a spatial area for efficient data acquisition and reconstruction are derived.

Owing to the requirement for low device complexity together with low energy consumption (i.e., long network lifetime), a proper balance between communication and signal processing capabilities must be found. The adoption of DDSP techniques aims at reducing the amount of transmitted data over the wireless medium; on the other hand, the complexity of the signal processing performed at a single node has to be kept under control [64–66]. As an example, in [65] the DDSP approach has been applied to the Fast Fourier Transform algorithm showing the tradeoff between energy consumption, data latency and the number of nodes employed.

In the literature, many papers have been devoted to the subject of WSNs, with reference to DDSP, energy-efficient information routing, MAC strategies or self-organizing algorithms (see e.g., [27, 28, 32, 33]). Although these works provide insightful interesting results, the different aspects mentioned are usually accounted

separately, and in most cases performance is evaluated through simulation. Unfortunately, these aspects often drive the design of a WSN in opposite directions. In fact, as will be clear in the following, scalar field estimation errors can be reduced by increasing the connectivity between nodes at the expense of an increased energy consumption. Furthermore, the use of self-organizing communication protocols is needed, but their distributed nature determines measurement losses affecting the scalar field estimation process. Therefore, the design of an energy-efficient WSN for environmental monitoring requires a general framework able to characterize the performance jointly considering the above mentioned aspects; a mathematical approach is needed to formalize the interdependent aspects, though the random and time-varying losses in the wireless channel make connectivity between nodes complex to investigate (see e.g., [60,61,67]).

The main goal of this Chapter is neither to design specific communication protocols, nor DDSP techniques; rather, the joint consideration of all aspects mentioned, under realistic but simple working conditions, aims at stressing their interdependencies in a formalized framework. On the other hand, a novel analytical approach to assess the scalar field estimation error, evaluated as a function of the bandwidth of the target process, B, the nodes density, and the sample loss probability (caused by multiple access and routing), by means of the theory of random sampling [68,69], is also provided. In the literature, random sampling has been mainly addressed to find alias-free sampling schemes and for spectral analysis of randomly sampled stationary random processes in the mono-dimensional case [69–71]. Here this theory is revised and applied to WSN scenarios considering non stationary processes and the more general l-dimensional spatial case. In addition, a DDSP technique to increase the

network energy efficiency based on re-sampling is investigated and its performance compared with the case where all samples are processed by the sink.

2.2 Distributed Scalar Field Estimation

2.2.1 Sampling the Target Process

A scenario where nodes are randomly and uniformly placed with spatial density ρ, is considered. As will be clear later, only a subset of nodes, with density ρ_s, participate to the sampling process with known positions.[1] To save energy, nodes are normally in sleeping mode and periodically commute in receiving mode.

The sink wakes up a certain number of nodes by transmitting a sequence of packets (triggering packets, that are queries) long enough to cover the activity period of each node. Only woken nodes will participate to successive communication phases. We assume energy efficiency is not an issue for the sink, which is equipped with more complex capabilities both in terms of signal processing and transmission power, with respect to nodes.

The interval of time needed for the entire sequence of operations that start with the sink-generated triggering event and brings to the determination of the estimate at the sink, is denote as *round*. Typical environmental phenomena (e.g., temperature or pressure measurements) are slow time-varying if compared with the packet delivery time in WSNs. For this reason, we consider a quasi-static scenario, which means that the round is considered to be much smaller than the change rate of the observed field. In this scenario no stringent time synchronization constraints among nodes are

[1] Discussion on localization techniques is beyond the scope of this thesis.

present. The signal to be sampled is described here through the (target) l-dimensional spatial random process $Z(\mathbf{s})$ ($\mathbf{s}$ being the spatial variable) with realizations $z(\mathbf{s})$. The sample space is a finite region A where the process is observed, centered in the sink. Without loss of generality, we consider A a circular area with radius R. Hence, the actual (truncated) signal of interest is $x(\mathbf{s}) = z(\mathbf{s}) \cdot r_A(\mathbf{s})$, where

$$r_A(\mathbf{s}) = \begin{cases} 1 & \mathbf{s} \in A \\ 0 & \text{otherwise}\,. \end{cases} \tag{2.2.1}$$

The signal $x(\mathbf{s})$ has finite energy E_0 and belongs to the random process $X(\mathbf{s})$. The goal is to create an estimate of $x(\mathbf{s})$, denoted as $\hat{X}(\mathbf{s})$, that will be built in the following section. In Figure 2.1 a scheme of the whole estimation process is shown.

The Fourier transform, $S_X(\nu)$, the autocorrelation function, $R_X(\tau)$, and the energy spectral density, $E_X(\nu)$, of $x(\mathbf{s})$, are defined as follows

$$S_X(\nu) = \Im^{(l)}[x(\mathbf{s})] \tag{2.2.2}$$

$$R_X(\tau) = \int_{\mathbb{R}^l} x(\mathbf{s})x(\mathbf{s}-\tau)d\mathbf{s} \tag{2.2.3}$$

$$E_X(\nu) = \Im^{(l)}[R_X(\tau)]\,, \tag{2.2.4}$$

where $\tau = (\tau_1, \tau_2, ...\tau_l)$ and $\nu = (\nu_1, \nu_2, ...\nu_l)$ is a spatial frequency. The operator $\Im^{(l)}[.]$ represents the l-dimensional Fourier transform. In the following we will indicate the statistical expectation with $\mathbb{E}\{.\}$.

By assuming that $z(\mathbf{s})$ is bandlimited, $S_Z(\nu) = \Im^{(l)}[z(\mathbf{s})]$ does not contain significant spectral components outside $\mathcal{S}_0$, where $\mathcal{S}_0 = \{\nu \text{ s.t. } (-B_0 < \nu_1 < B_0, -B_0 < \nu_2 < B_0, ..., -B_0 < \nu_l < B_0)\}$ and B_0 represents the bandwidth per dimension of $z(\mathbf{s})$. The Fourier transform of $x(\mathbf{s})$ is then

$$S_X(\nu) = S_Z(\nu) \otimes R_A(\nu)\,, \tag{2.2.5}$$

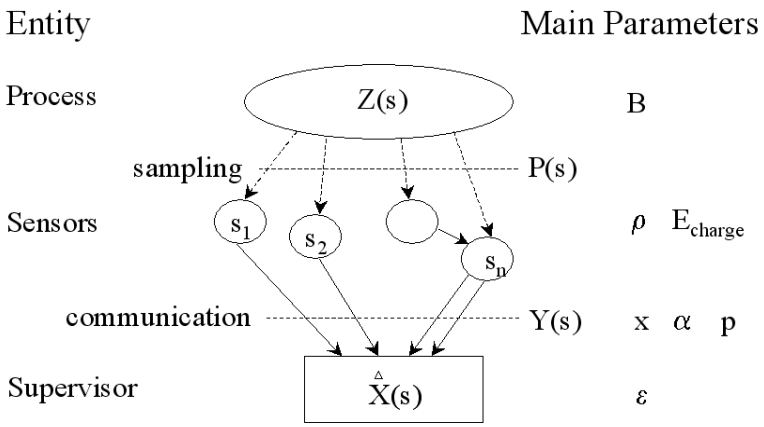

Figure 2.1: Scenario considered and main quantities involved in the process estimation.

where $R_A(\nu) = \Im^{(l)}[r_A(\mathbf{s})]$ and $\otimes$ is the convolution operator. In the practical bi-dimensional case, it is $l = 2$ and

$$R_A(\nu) = \frac{R}{\|\nu\|} J_1\left(2\pi\, R\, \|\nu\|\right), \tag{2.2.6}$$

where $J_1(.)$ is the Bessel Function of the first kind of order one and $\|.\|$ is the norm operator. Note that, due to the spatial truncation of the original signal, $x(\mathbf{s})$ is not bandlimited. However, it can be easily verified that $R_A(\nu) \approx 0$ when $\|\nu\| > \frac{1}{\pi R}$. In general, $S_X(\nu)$ and, therefore, $E_X(\nu) \approx 0$ outside $\mathcal{S}$, where $\mathcal{S} = \{\nu \text{ s.t. } (-B < \nu_1 < B, -B < \nu_2 < B, ..., -B < \nu_l < B)\}$ and, in the two-dimensional case, $B = \frac{1}{\pi R} + B_0$. The dimension of $\mathcal{S}$ is $dim(\mathcal{S}) = \beta$, where $\beta = (2B)^l$ represents the minimum Nyquist

sampling rate in the case of uniform sampling [68, 69]. In practical applications we have $\frac{1}{\pi R} \leq B_0$, that is the area of observation is chosen larger than the typical process correlation distance which is proportional to $1/B_0$: the worst case corresponding to the largest bandwidth expansion is obtained when $\frac{1}{\pi R} = B_0$.

The n-th node is located in the spatial point $\mathbf{s}_n$ and takes the sample $x(\mathbf{s}_n)$.[2] Considering the nodes randomly placed with a spatial density ρ_s in the monitored environment, we can statistically describe the sequence $\{\mathbf{s}_n\}$ of spatial samples as a homogeneous PPP [68]. The derivative of the corresponding counting process is the stationary random process $H(\mathbf{s}) = \sum_n \delta(\mathbf{s} - \mathbf{s}_n)$, having mean $\mu_H = \mathbb{E}\{H(\mathbf{s})\} = \rho_s$, and whose statistical autocorrelation function and power spectral density are given by [68, 71]

$$R_H(\tau) = \rho_s \cdot \delta(\tau) + \rho_s^2 \,, \tag{2.2.7}$$

$$S_H(\nu) = \rho_s + \rho_s^2 \cdot \delta(\nu) \,, \tag{2.2.8}$$

respectively, where $\delta(.)$ is the Dirac pseudo function, $H(\mathbf{s})$ represents the sampling process.

2.2.2 Building the Estimate

Starting from the collected samples, an estimate of the target signal can be determined through either a centralized or a distributed procedure: in the former case, nodes, via a self-organizing communication protocol, transmit their samples to the sink, which is in charge of the signal processing and the estimation (no DDSP option); in the latter, they send the samples to some elected nodes (cluster heads, CH) in a clustered architecture, that perform suitable distributed signal processing and transmit the

[2] We neglect quantization errors.

estimate to the sink which, by collecting different estimates, provides the final result as explained in the following (DDSP option).

In both cases, owing to communication failure, there exists a probability p that a node is unable to send its information to the entity performing signal processing. In this case, the corresponding sample does not contribute to the signal estimation (sample loss). The probability of correct sample reception is denoted as $h = 1 - p$.

The set of samples received by the entity performing signal processing forms a new stationary sampling process, $P(\mathbf{s})$. Using the result derived in the Appendix of this Chapter (with $P_1(\mathbf{s}) = H(\mathbf{s})$), and expressions (2.2.7), (2.2.8), the statistical autocorrelation function and mean of $P(\mathbf{s})$ are $R_P(\tau) = \delta(\tau)\ \rho_s\ h + h^2\rho_s^2$ and $\mu_P = \mathbb{E}\{P(\mathbf{s})\} = h \cdot \rho_s$, respectively. As expected the new process has the same characteristics of the original one with density $h \cdot \rho_s$ and power spectral density

$$S_P(\nu) = h\rho_s + h^2\rho_s^2 \cdot \delta(\nu). \tag{2.2.9}$$

The sampled version, $Y(\mathbf{s})$, of the target signal conditioned to the realization $x(\mathbf{s})$, can be expressed as $Y(\mathbf{s}) = x(\mathbf{s}) \cdot P(\mathbf{s})$, representing a finite energy non stationary random process. The autocorrelation function of the process realization $y(\mathbf{s})$ is

$$R_y(\tau) = \int_{\mathbb{R}^l} x(\mathbf{s})x(\mathbf{s}-\tau)p(\mathbf{s})p(\mathbf{s}-\tau)\, d\mathbf{s}\,, \tag{2.2.10}$$

where signal $p(\mathbf{s})$ is a realization of the random process $P(\mathbf{s})$.

The average statistical autocorrelation function of $Y(\mathbf{s})$, is defined as

$$\begin{aligned}\overline{R}_Y(\tau) &= \mathbb{E}\left\{\int_{\mathbb{R}^l} x(\mathbf{s})x(\mathbf{s}-\tau)P(\mathbf{s})P(\mathbf{s}-\tau)\, d\mathbf{s}\right\} = \int_{\mathbb{R}^l} x(\mathbf{s})x(\mathbf{s}-\tau)R_P(\tau)\, d\mathbf{s} \\ &= R_P(\tau) \cdot R_X(\tau)\,,\end{aligned} \tag{2.2.11}$$

and the average energy spectral density

$$\overline{E}_Y(\nu) = \Im^{(l)}[\overline{R}_Y(\tau)] = E_X(\nu) \otimes S_P(\nu)\,. \tag{2.2.12}$$

From (2.2.9), (2.2.11) and (2.2.12) it follows

$$\overline{E}_Y(\nu) = h^2 \rho_s^2 E_X(\nu) + E_0 \cdot \rho_s \cdot h\,. \tag{2.2.13}$$

We consider that the estimated signal is obtained through linear interpolation of the received set of samples $Y(\mathbf{s})$. The estimate $\hat{X}(\mathbf{s})$ can then be expressed as

$$\hat{X}(\mathbf{s}) = \phi(\mathbf{s}) \otimes Y(\mathbf{s})\,, \tag{2.2.14}$$

where $\phi(s)$ is the impulse response of the linear interpolator, whose transfer function is $\Phi(\nu) = \Im^{(l)}[\phi(\mathbf{s})]$.

In the following, let us consider the case of an ideal low-pass interpolator with transfer function

$$\Phi(\nu) = \begin{cases} 1/\mu_\phi & \nu \in \mathcal{S}^* \\ 0 & \text{otherwise}\,. \end{cases} \tag{2.2.15}$$

with μ_ϕ and $\mathcal{S} \subseteq \mathcal{S}^*$ described later.

2.3 Mathematical Derivation of the Estimation Error

A good indicator of the estimate quality is the average normalized estimation error defined as the normalized mean square error (MSE)

$$\varepsilon = \frac{1}{E_0} \mathbb{E}\left\{ \int_{\mathbb{R}^l} \left(\hat{X}(\mathbf{s}) - x(\mathbf{s}) \right)^2 d\mathbf{s} \right\}\,. \tag{2.3.1}$$

In the Appendix of this Chapter the expression for (2.3.1) is derived as a function of the spectral densities $\overline{E}_Y(\nu)$ and $E_X(\nu)$. When the ideal low-pass interpolator (2.2.15) is adopted, the expression (2.7.9) in the Appendix can be further simplified to

$$\varepsilon = 1 - 2\frac{\mu_P}{\mu_\phi} + \frac{1}{E_0\mu_\phi^2}\int_{\mathcal{S}^*} \overline{E}_Y(\nu)d\nu\,. \tag{2.3.2}$$

By substituting (2.2.13) in (2.3.2) and considering that $\int_{\mathcal{S}^*} E_X(\nu)d\nu = E_0$, we can write

$$\varepsilon = 1 - 2\frac{h\rho_s}{\mu_\phi} + \frac{h\rho_s}{\mu_\phi^2}\Big[h\rho_s + dim(\mathcal{S}^*)\Big]. \tag{2.3.3}$$

It is worthwhile noting that, due to the characteristics of Poisson sampling, no aliasing effects arise whatever reconstruction bandwidth $\mathcal{S}^*$ is chosen, unlike in the classical uniform sampling case. The only effect is an increase of the MSE. Hence, $\mathcal{S}^*$ can be different from $\mathcal{S}$ depending on the application (see later when DDSP is adopted).
Now the optimum value of μ_ϕ, minimising the estimation error ε, could be found, by constraining to zero the derivative in (2.3.3), thus[3]

$$\frac{\mathrm{d}\varepsilon}{\mathrm{d}\mu_\phi} = 0 \Longleftrightarrow \mu_\phi = h\rho_s + dim(\mathcal{S}^*)\,. \tag{2.3.4}$$

Now the value of the MSE is given by

$$\varepsilon = 1 - \frac{h\rho_s}{h\rho_s + dim(\mathcal{S}^*)} = \frac{dim(\mathcal{S}^*)}{h\rho_s + dim(\mathcal{S}^*)} = \frac{\beta\zeta}{h\rho_s + \beta\zeta}\,, \tag{2.3.5}$$

where $\zeta = dim(\mathcal{S}^*)/dim(\mathcal{S})$.

Hence, proper discussion about the meaning of this solution must be given:

- when nodes are deployed, ρ_s is known; however, during network life ρ_s decreases owing to the fact that some nodes expire, then an estimation of ρ_s is needed;

[3] With the second derivative it is possible to check that this value for μ_ϕ represents a minimum.

- knowledge of h requires knowledge of the sample loss probability, which changes during network life, and has to be estimated;
- knowledge of $dim(\mathcal{S}^*)$ requires knowledge of the dimension of the sampling space and this requires information about the process to be estimated.

For the sake of comparison, two other sub-optimal cases, which are less complex, in terms of a priori knowledge about h and $dim(\mathcal{S})$ required, are considered:

$$\mu_\phi = h\rho_s \quad \Longrightarrow \quad \varepsilon = \frac{\beta\zeta}{h\rho_s} \tag{2.3.6}$$

$$\mu_\phi = \rho_s \quad \Longrightarrow \quad \varepsilon = (1-h)^2 + \frac{h\beta\zeta}{\rho_s} \tag{2.3.7}$$

It can be easily proven that results obtained through (2.3.6) are better than (2.3.7). But even if solution given by (2.3.5) and (2.3.6) are better than (2.3.7), in some cases they could not be conveniently realized, due to the need for an estimation of h and $dim(\mathcal{S}^*)$.

2.3.1 Absence of DDSP

When DDSP is not adopted, all samples successfully received are processed by the sink, in order to determine the estimate $\hat{X}(\mathbf{s})$. Each sample has a probability equal to p to be missing because of an unconnected node, or owing to MAC failures.

It can be shown that without DDSP the best performance is obtained by fixing $\mathcal{S}^* = \mathcal{S}$, hence $\zeta = 1$.

The ratio $\eta \triangleq \rho_s/\beta$ represents the over-sampling factor with respect to the minimum Nyquist uniform sampling rate β. In general, we have $\eta \geq 1$. Expressions

(2.3.5)-(2.3.7) give the estimation error as a function of the sample loss probability and η. As can be noted, the impact of node communication failure, through the probability p, becomes more relevant as η increases, the latter being strictly related to node density. Apart from the value of $dim(\mathcal{S})$, this result does not depend on the particular realization $z(\mathbf{s})$ of the random process $Z(\mathbf{s})$. Hence, it can be extended to the whole random process. Expressions (2.3.5)-(2.3.7) can be used to measure the quality of the estimation of the random process, under observation performed at the sink, when no DDSP is implemented.

2.3.2 Presence of DDSP

In order to reduce the overall energy consumption due to the transmission of samples, it would be useful to partially decentralize the signal processing task necessary to have an estimate of the target process. In particular, considering a clustered network architecture, samples coming from nodes are not directly collected by the sink but they reach the final destination through intermediate nodes (the CHs), which perform partial signal processing. At each CH, loss-less data compression techniques can be adopted thus reducing the amount of data transmitted. Typical compression techniques take advantage of the correlation among adjacent samples. In general, the compression rate depends on the process statistics, spatial correlation and the number of samples processed. A general characterization is prohibitive and out of the scope of this thesis. An interesting survey about distributed compression in sensor networks is presented in [72].

Here the attention is focused, instead, on the possibility to compress data considering the fact that samples come from a random sampling process and making use of

a uniform re-sampling processing at the Nyquist frequency.

Let us assume that a cluster of area $A_{\rm ch}$ containing $n_{\rm p}$ nodes ($n_{\rm p}$ has mean $N_{\rm p}$) is managed by a CH which is responsible to collect samples and to re-transmit them to the sink. It is assumed that CHs can estimate a portion $x_{\rm ch}(\mathbf{s}) = z(\mathbf{s}) \cdot r_{A_{\rm ch}}(\mathbf{s})$ of the target signal in the area $A_{\rm ch}$ based on the $n_{\rm p}$ samples received. The function $r_{A_{\rm ch}}(\mathbf{s})$ is defined similarly to (2.2.1) considering the area $A_{\rm ch}$, with radius $R_{\rm ch}$, instead of A. The truncated signal $x_{\rm ch}(\mathbf{s})$, managed by the CH, is characterized by an increased bandwidth with respect to the original signal $x(\mathbf{s})$. According to (2.2.5) and (2.2.6), having substituted R with $R_{\rm ch}$, the bandwidth per dimension of $x_{\rm ch}(\mathbf{s})$ is now $B_{\rm ddsp} = B_0 + \frac{1}{\pi R_{\rm ch}}$. Indeed, to keep negligible the aliasing error due to truncation, the reconstruction filter bandwidth and the re-sampling frequency must be suitably increased, i.e., $dim(\mathcal{S}^*) = (2\,B_{\rm ddsp})^l$. Considering that $A/A_{\rm ch} \approx N_{\rm ch}$, $l = 2$ and $R_{\rm ch} \approx \sqrt{N_{\rm ch}} R$, we have

$$\zeta = \frac{dim(\mathcal{S}^*)}{dim(\mathcal{S})} = \left(1 + \sqrt{N_{\rm ch}}\right)^2 \approx N_{\rm ch}\,, \tag{2.3.8}$$

where $N_{\rm ch}$ is the average number of CHs in the sampling area A and is considered to be much larger than one. In deriving (2.3.8) the worst case where $\frac{1}{\pi R} = B_0$, is considered. The CH then makes a re-sampling of the estimated signal at the Nyquist frequency, now $\beta \cdot \zeta$, and transmits the new set of Nyquist samples to the sink which collects all the estimated portions of the original signal. Considering that the original set of samples comes from a node density ρ_s, the average number M of samples composing the new set to be transmitted is

$$M = \frac{[N_{\rm p} \cdot P_{\rm MAC} + 1]\beta\,\zeta}{\rho_s} = [N_{\rm p} \cdot P_{\rm MAC} + 1]/\delta\,, \tag{2.3.9}$$

where $[N_{\rm p} \cdot P_{\rm MAC} + 1]$ is the average number of samples received by the CH plus

the one generated by itself, taking the possibility that a packet is lost owing to the MAC protocol into consideration, through the success probability P_{MAC} (derived in section 2.4), that is the probability that a node succeeds in accessing the channel and in transmitting its packet (i.e., without collisions). The ratio $\delta = \eta/\zeta$ represents the signal compression factor due to re-sampling of the estimated signal at the Nyquist frequency. When $\delta \gg 1$ then $M \ll N_{\mathrm{p}}$ thus a drastic reduction of the transmission throughput (and energy cost) is expected. The augmented energy consumption due to signal processing at the CH in DDSP mode will be also taken into account.

No transmission errors between the CHs and the sink are assumed, because, as stated in the following section, it is assumed that during a single round the wireless channel is time-invariant and thus all CHs self-elected in a specific round can hear the sink, otherwise they would not have been triggered. Moreover, it is assumed that collisions between CHs packets are negligible (see section 2.4.2); hence, the total estimation error at the sink can be still evaluated through (2.3.5)-(2.3.7) by putting $\zeta = N_{ch}$ according to (2.3.8). As a consequence, with respect to the no DDSP case, larger values of estimation error are expected, but, as will be shown in the numerical results, a longer network lifetime, due to reduced amount of transmitted data.

2.4 The self-organizing distributed WSN

In the previous section, it has been shown that the evaluation of the MSE requires the knowledge of some network parameters such as p, and N_{ch}, that are strictly related to the way the information is delivered. In this section a typical WSN clustered architecture is analytically investigated to derive these parameters, without any aim at considering complex protocol strategies. Notre that those parameters also depend on

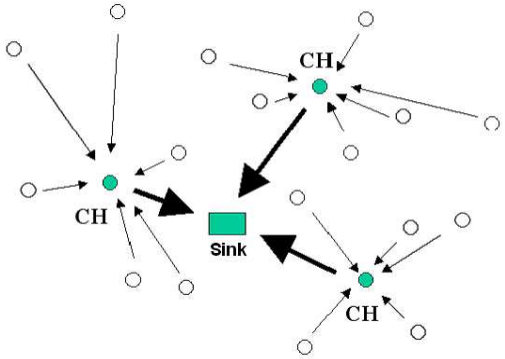

Figure 2.2: Transmission flow in the clustered topology. Rectangle: sink; filled circle: CHs; circle: non CH nodes.

the propagation characteristics of the environment, modelled as described in Chapter 1, through eq. (1.6.1).

2.4.1 Information Routing Through a Clustered Architecture

A clustered architecture seems particulary suitable for DDSP [66]. Typically, most of cluster based algorithms consider a distributed cluster head (CH) self election algorithm, such as LEACH-based algorithms investigated in [73, 74]. Also note that this architecture corresponds to a three-level tree-based topology, having the sink at

the lowest level, CHs at level 1 and non CH nodes at level 2 (see Figure 1.11).

In a clustered architecture, the nodes triggered by the sink organise themselves into clusters, with one node per cluster acting as CH. Non CH nodes transmit packets to their CHs and then CH nodes transmit the packets received plus the one generated by themselves to the sink via a direct link (see Fig. 2.2). Therefore, being a CH is much more energy intensive than being a non CH node. If the CHs were chosen a priori and fixed throughout the network lifetime, these nodes would quickly use up their limited energy: once the CH runs out of energy, it is no longer operational. Thus, it is assumed that the algorithm incorporates a randomized rotation of the CH role among the nodes in the network: at each round a node autonomously decides to elect itself CH with probability x. Decisions taken in different rounds are uncorrelated. In this way, the energy load of being a CH is evenly distributed among nodes during network lifetime.

2.4.2 Communication Protocol

The simple communication protocol considered is based on the following steps, performed at each round. As far as MAC is concerned (described in section 2.4.3), since it is assumed that the shadowing sample varies in different rounds, the natural choice brings to a contention-based protocol which minimizes control overhead with respect to a centralized algorithm [5].

The communication protocol steps are:

- *Trigger and Wake up*

The sink transmits the triggering sequence with power $P_{\mathrm{T}} = P_{\mathrm{su}}$; a random number, n_{t}, of nodes is triggered: those for which $L_{\mathrm{th}} \leq L_{\mathrm{su}}$, with L_{su} depending on P_{su}

and the receiver sensitivity. Being nodes Poisson distributed, from Theorem 1.6.1 we derive that n_t is a Poisson r.v., with a mean value, N_t, which depends on the channel model. By using the channel model of eq. (1.6.1) we can write

$$N_{\mathrm{t}} = \mathbb{E}\{n_{\mathrm{t}}\} = \rho\pi \left[e^{2(\sigma_s^2/k_1^2 - k_0/k_1 + L_{\mathrm{su}}/k_1)} + \Psi\left(\frac{L_{\mathrm{su}} - k_0}{\sigma_s}, \frac{k_1}{\sigma_s}, R \right) \right], \tag{2.4.1}$$

where $\Psi(a_1, b_1, r)$ is given by eq. (1.6.8). The second exponential takes border effects due to area limitation into account. When these border effects are negligible (the exponential is close to one), the following simplified expression, related to an infinite area, holds

$$N_{\mathrm{t}} = \mathbb{E}\{n_{\mathrm{t}}\} = \pi\ \rho\ e^{2(\sigma_s^2/k_1^2 - k_0/k_1 + L_{\mathrm{su}}/k_1)}. \tag{2.4.2}$$

It must be noted that the probability that a node situated at distance d from the sink is triggered, equals the probability $C(d)$ given by eq. (1.6.4), with $L_{\mathrm{th}} = L_{\mathrm{su}}$. This probability is a decreasing function of distance; that produces two side effects. First, the woken node density, $\rho_w(d) = \rho\, C(d)$, is distance-dependent, so the process is not uniformly sampled. Second, nodes closer to the sink participate more frequently to the transmission than far nodes and they tend to discharge their batteries prematurely.

To overcome this situation, the protocol requires that woken nodes randomly decide whether to participate to the following phases: we assume they will, with probability $w(d) = w_0/C(d)$, otherwise they switch to sleeping mode. The constant w_0 defines the sampling space A that will provide contributions to the target process estimation, as the maximum distance R will be obtained by resolving $w_0/C(R) = 1$. Moreover, it is assumed that all nodes are aware of their own position and that the sink, when triggers nodes, informs them about its position and the propagation

parameters characterizing the environment, that could be estimated, for example, from the Received Signal Strength Indication (RSSI) measurements, so that each node can compute $C(d)$.

The density of participating nodes results in

$$\rho(d) = \rho_w(d)\, w(d) = \rho\, w_0 = \rho_s \tag{2.4.3}$$

which is constant for $d < R$, as desired.

- *Self-Election*

The participating nodes initiate the self-election phase: each of them elects itself CH with probability equal to x, where x is a system parameter to be optimized. The number of CHs is n_{ch}, with mean $N_{\text{ch}} = x \cdot N_{\text{t}} \cdot w_0$. The correspondent CH and non CH densities are given by $\rho_{\text{ch}} = \rho_s \cdot x$, and $\rho_{\text{nch}} = \rho_s \cdot (1 - x)$, respectively. To notify its election both to sink and surrounding nodes, each CH transmits a broadcast packet with power $P_{\text{T}} = P_{\text{su}}$. CHs will access the channel through a contention-based mechanism, but the number of CHs is in general not very large (x is usually much less than one) and collisions can be easily avoided through standard techniques. It is also assumed that the sink sends acknowledgments to the CHs, indicating the radio channel to be used in the following phases. We will consider negligible the packet loss in this phase.

- *Cluster Selection*

Each node receiving the packet(s) sent by the CHs decides which CH to refer to (i.e., which cluster to subscribe to), based on the packet received with largest power. We assume that non CH nodes transmit with power $P_{\text{T}} = P_{\text{su}} \cdot \alpha$; where $\alpha \leq 1$ is a system parameter to be optimized. In this case the maximum tolerable path-loss

becomes $L_{\rm p} = L_{\rm su} + 10\log_{10}\alpha$. Hence, the number of CHs reachable by a generic node and the number of nodes forming a given cluster are random variables denoted as $n_{\rm rch}$ and $n_{\rm p}$, respectively; their means are $N_{\rm rch}$ and $N_{\rm p}$.

From [60, 61] and by assuming that the CHs are uniformly and randomly distributed over the infinite plane, with density $\rho_{\rm ch}$, the number $n_{\rm rch}$ of CHs reachable by a generic node is also Poisson distributed, with mean

$$N_{\rm rch} = \mathbb{E}\{n_{\rm ach}\} = \pi\ \rho_{\rm ch}\ e^{2(\sigma_s^2/k_1^2 - k_0/k_1 + L_{\rm p}/k_1)}\,. \tag{2.4.4}$$

Though the CHs can be assumed to be uniformly located owing to the distributed self-election strategy, they are not distributed over the infinite plane, as they belong to the finite set of nodes that have been triggered by the sink. Therefore, the above expression represents an approximation whose validity decreases for nodes farther from the sink. However, the approximation seems reasonable as it will be shown by simulation in the numerical results.

The number n_p of nodes that subscribe to a specific CH (i.e., the number of nodes composing a cluster), can be considered as Poisson distributed with mean [75, 76]

$$N_{\rm p} = \mathbb{E}\{n_{\rm p}\} = \pi\ \rho_{\rm nch}\ e^{2(\sigma_s^2/k_1^2 - k_0/k_1 + L_{\rm p}/k_1)}\cdot\frac{1 - e^{-N_{\rm rch}}}{N_{\rm rch}}\,, \tag{2.4.5}$$

where $N_{\rm rch}$ is given by (2.4.4).

- *Sample Transmission*

Nodes generate the packet containing the samples and transmit it; having assumed that all nodes (both CHs and non CHs) have the same receiver sensitivity, and that power loss is constant during one round, this packet will be correctly received by the relevant CH due to channel reciprocity, unless interference between packets takes place. The contention between nodes must be managed by the MAC protocol (see

below). Inter-cluster collisions are avoided as the CHs use separate radio channels assigned by the sink during the self-election notify phase.

- *Transmission to the sink without DDSP*

If DDSP is not implemented, then the CHs transmit the sequence of n_{p} samples received plus the one generated by itself; under the assumptions of this thesis, this packet will be correctly received by the sink, which will receive on average $N_{\mathrm{s}} = (N_{\mathrm{p}} + 1) \cdot N_{\mathrm{ch}}$ samples, if no packet collisions occur; they can be avoided if the sink requires packets transmission through a polling scheme. In fact, the sink knows the identity of the participating CHs from the previous self-election notify phase.

- *Transmission to the sink with DDSP*

If DDSP is implemented, then the CHs perform suitable signal processing and transmit the new m samples (with mean M) of an estimated version of the target process; under the same assumptions as for no DDSP (see subsection above), this packet will be correctly received by the sink.

The probability that a node, triggered by the sink, is able to connect to at least one CH, is denoted as P_{CON}, that is the probability that a non CH node is not isolated. If a node is isolated it will not belong to any cluster, and will never send its sample. The probability of non isolated node can be evaluated recalling the Poisson nature of n_{ach} and (2.4.4):

$$P_{CON} = 1 - \mathbb{P}\{n_{\mathrm{rch}} = 0\} = 1 - e^{-N_{\mathrm{rch}}}\,, \tag{2.4.6}$$

where $\mathbb{P}\{\mathcal{E}\}$ denotes the probability of the event $\mathcal{E}$. We will consider the network to be dense if P_{CON} assumes large values, that is, the network is essentially connected, which corresponds to high values of ρ.

2.4.3 Medium Access Control

In general, having fixed a certain MAC protocol, the information needed to evaluate the impact of such protocol on system performance, in terms of energy efficiency and sample loss probability, is the probability P_{MAC} that a packet is not lost due to interference problems, or more generally MAC failures; it is a function of the average number of transmissions per packet, $R(N)$, which depends on the specific MAC protocol adopted, of protocol parameters/contraints and of the average number of nodes N competing for transmission. An evaluation of this function for different protocols is out of the scope of this thesis: in the following an example will be given for a simple case.

Once P_{MAC} is known, it is possible to derive the probability p, that a sample in the sample space is lost due to communication. In fact, the latter event occurs if the non CH node is isolated or the packet is lost due to MAC; the probability of sample loss is thus

$$p = (1 - x)\left[(1 - P_{CON}) + P_{CON} \cdot (1 - P_{\mathrm{MAC}}(N_{\mathrm{p}})\right] , \tag{2.4.7}$$

where the second factor accounts for MAC losses during sample transmission (recall that N_{p} is the average number of nodes aggregated to each CH).

An example of the evaluation of $P_{\mathrm{MAC}}(N)$ for a simple slotted random channel access protocol without retransmissions, i.e., with $R(N) = 1$, is provided here.
The time is divided in frames and each frame is further subdivided in Z slots. We have n nodes, where n is Poisson distributed with mean $N = \mathbb{E}\{n\}$. Each node transmits a packet randomly choosing one of the Z available slots in the frame. To

reduce collisions, we choose a value for Z high enough with respect to N; moreover, since N is not constant, but depends on ρ, x and α, it could be reasonable to set Z to be dependent on ρ. In fact, if Z is constant it might occur that for high values of ρ, Z is too low with respect to N and so there are too many collisions. To avoid this problem, we fix $Z = c \cdot N$ where c is a parameter that must be suitably set.

The probability of packet loss is the probability that two or more nodes select the same slot and collide. This probability, recalling that the number of nodes, n, is Poisson distributed with mean N, is given by

$$\begin{aligned} 1 - P_{\mathrm{MAC}}(N) &= \sum_{n=2}^{\infty} \left[1 - \left(1 - \frac{1}{Z} \right)^{n-1} \right] \mathbb{P}\{n\} \\ &= 1 + \frac{e^{-N} - Ze^{-N/Z}}{Z-1} \leq 1 - e^{-N/Z} = 1 - e^{-\frac{1}{c}}. \end{aligned} \tag{2.4.8}$$

The upper-bound reported in the right hand in (2.4.8) is tight for $N > 10$ and shows that $(1 - P_{\mathrm{MAC}}(N))$ mainly depends on the ratio $c = Z/N$. For example, collision probabilities below 10% require $c = 10$, which is a reasonable value adopted in section 2.6.

Other MAC protocols used in WSNs [31, 77–79] can be considered by properly modifying (2.4.8) and $R(N)$. In particular, in Chapter 4 the probability P_{MAC} for the IEEE 802.15.4 MAC protocols, is derived. The application of the 802.15.4 to this framework is straightforward.

2.5 Energy Budget

Now, let us derive the mean energy consumption of each node during one round. This is a focal point in the WSN design because directly connected to node lifetime. By

means of the previously defined probability of CH election x, we obtain the mean energy consumption per round with and without DDSP. In particular, we have

$$E_{\text{round}} = w_0 \cdot [E_{\text{non CH}}\ (1-x)P_{CON} + x\ E_{\text{CH}}]\ , \tag{2.5.1}$$

where the first term represents the consumption if the node is non CH(multiplied by the correspondent probability) and the second term the consumption for a CH. The factor w_0 accounts for the nodes that do not participate. By considering that each non CH consumes energy when transmitting the data packet to its CH once or more times depending on the collisions, we have

$$E_{nonCH} = E_L\, R(N_{\text{p}})\, \theta_{\text{d}}\ . \tag{2.5.2}$$

where

- $E_L = E_H \cdot \alpha$ and E_H is the energy spent to transmit a bit at power P_{su};
- θ_{d} is the size (in bits) of the data packet.

The total average energy spent per round by a CH is given by

$$E_{\text{CH}} = E_{\text{H}} \cdot \theta_{\text{c}} + (N_{\text{p}}\, P_{\text{MAC}}(N_{\text{p}}) + 1)\, E_{\text{H}} \cdot \theta_{\text{d}} + f(R(N_{\text{p}}))\,, \tag{2.5.3}$$

for the no DDSP case and

$$E_{\text{CH}}^{(ddsp)} = E_{\text{H}} \cdot \theta_{\text{c}} + M\, E_{\text{H}}\, \theta_{\text{d}} + E_{\text{ddsp}} + f(R(N_{\text{p}})), \tag{2.5.4}$$

when DDSP is adopted.

The first term of (2.5.3) and (2.5.4) refers to the energy spent by a CH to transmit the broadcast packet to inform all other nodes and the sink of its role; θ_{c} is the size (in

bits) of the broadcast packet. The second term is related to the energy consumed for the data transmission to the sink: in the no DDSP case the average number of packets sent by a CH is the average number of packets correctly received by its non CHs, that is $N_{\mathrm{p}}\, P_{\mathrm{MAC}}(N_{\mathrm{p}})$, plus the one generated by the CH itself; whereas in DDSP case each CH has to transmit M data packets on average (see section 2.3.2). The generic function $f(r)$ represents the energy spent by CHs to transmit r average retransmission requests. Finally E_{ddsp} quantifies the energy spent by the CH to reconstruct and re-sample the portion of process sensed by nodes within the cluster if DDSP is adopted. We assume this portion of energy is proportional to the number of samples processed and is given by

$$E_{\mathrm{ddsp}} = E_{\mathrm{H}} \cdot \theta_{\mathrm{d}}\, \gamma\, \left(N_{\mathrm{p}} \cdot P_{\mathrm{MAC}}(N_{\mathrm{p}}) + 1\right), \tag{2.5.5}$$

where γ is a parameter to be defined according to the circuital characteristics of the node; it represents the ratio between the average energy needed to process one sample and the energy required for the sample transmission. The smaller γ, the more advantageous the DDSP strategy. According to the literature (see, e.g., [64]), the ratio of energy consumption for processing and communication of one bit is in the range of 0.001-0.0001. In the case of adoption of other compression techniques, eq. (2.5.5) has to be modified.

Now, for a given initial battery charge, E_{charge}, the mean number of rounds achievable during the life of each node is given by

$$N_{\mathrm{round}} = \frac{E_{\mathrm{charge}}}{E_{\mathrm{round}}}\,. \tag{2.5.6}$$

Note that the energy spent to receive packets is not taken into consideration, assuming that it is negligible with respect to the one used for the packet transmission; this condition occurs in some cases [64].

Table 2.1: Values adopted for propagation, process, system and project parameters if not otherwise specified.

k_0 [dB]	25.1
k_1	13.03
σ_s [dB]	4
β [m^{-2}]	4 10^{-6}
L_{su} [dB]	120
E_{charge} [J]	1
E_H [μJ]	$3,9$
θ_c [bit]	48
θ_d [bit]	1024
γ	0.001
w_0	0.462
R [m]	1500
c	10

2.6 Numerical Results

In this section, numerical results related to the mathematical framework, proposed here, will be provided to highlight the interdependency of several network design issues when the performance is investigated, both in terms of process estimation quality and network life-time. In particular, the performance is affected by a large set of parameters related to different aspects such as

- propagation (k_0 and k_1 for the path-loss model, σ_s for shadowing);
- the spatial characteristics of the target process (β);
- system choices (the density of nodes ρ, the maximum loss L_{su} for high power transmitting nodes, the initial battery energy E_{charge} for each node, the energy E_H consumed to transmit a bit in high power transmission mode, the ratio γ describing energy consumption for single sample elaboration in DDSP mode,

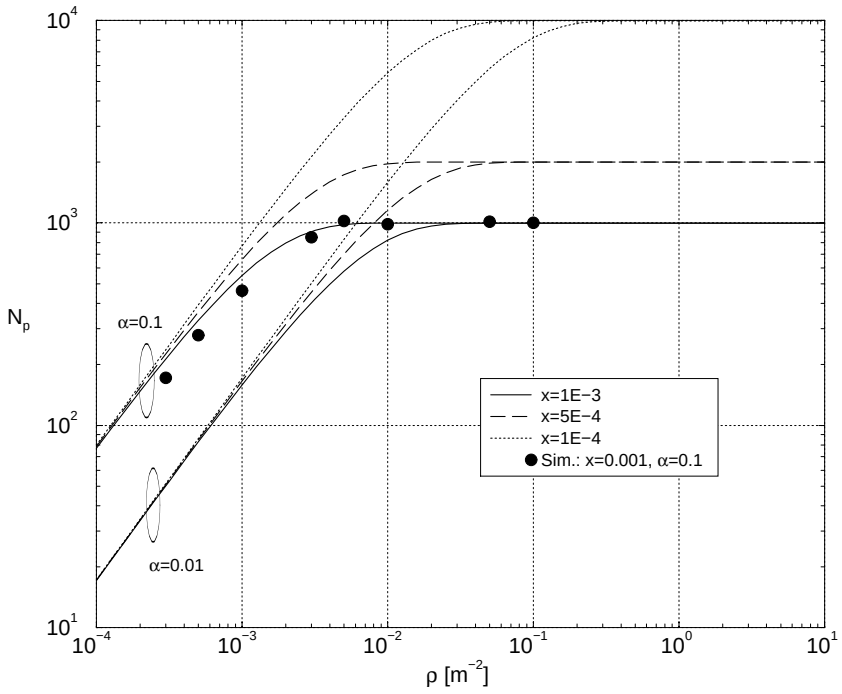

Figure 2.3: Mean cluster size as a function of density for different values of parameters x and α.

the parameter α characterizing energy consumption in low power transmission mode);

- the transmission protocol (the probability x to become a CH).

In the following, results are given as a function of ρ, x and α; the other parameter settings, if not otherwise specified, are reported in Table 2.1.

In particular, the constant $w_0 = \Phi(R)$ is chosen to be ≈ 0.5 which corresponds to a radius $R = 1500$ [m]. Within this circular area, nodes participating to the following phases result to be uniformly distributed.

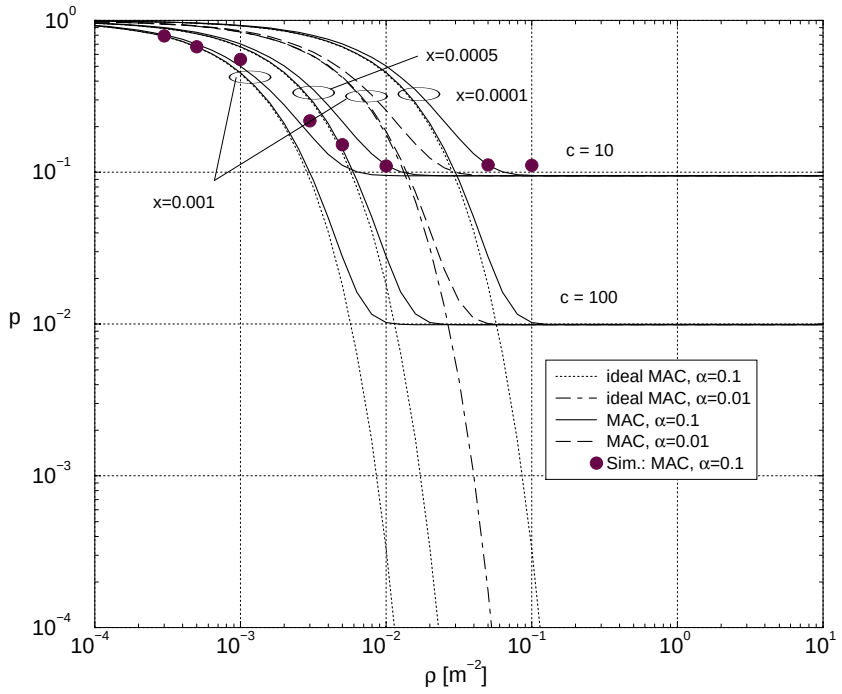

Figure 2.4: Probability of sample loss as a function of density for different values of parameters x, α and c.

Mathematical results on N_p, p, N_{round}, and ε, which are based on some approximations neglecting border effects, have also been validated through Monte Carlo simulations. The difference between simulations and the mathematical model is that in the first case the reference scenario is constituted by a circular area, having ray $R = 1500$ [m], whereas the second refers to an infinite plane; in both cases nodes are uniformly distributed over the area. However in the latter case the real scenario considered is limited by the transmission range of the sink; therefore, simulations are used to validate such approximate approach.

Due to the clustered architecture of the WSN, the mean cluster size, N_{p}, and the sample loss probability, p, play an important role on the overall network performance.

For this reason, both N_{p} and p, evaluated through eqs. (2.4.5)-(2.4.8), are reported as a function of node density ρ for different values of x and α in Figs. 2.3 and 2.4, respectively. It is interesting to observe that, as the node density increases, the cluster size tends to saturate to an asymptotic value which is a function of parameters x and α.

In Fig. 2.4, it is also possible to analyze the MAC impact on the probability of sample loss p for different values of the MAC parameter c, when $c = 10$ and $c = 100$. According to (2.4.7), for low values of ρ the sample loss probability is dominated by the probability $(1 - P_{CON})$ that a node is isolated (connectivity), whereas, for large values of ρ, it is lower bounded by the packet loss probability $(1 - P_{\mathrm{MAC}})$ (MAC effect).

For ρ approaching to infinite, we can obtain the floor value, p_{floor}, that is given by:

$$p_{\mathrm{floor}} = (1 - x) \cdot \left(1 + \frac{e^{-\frac{1-x}{x}} - c \cdot \frac{1-x}{x} e^{-\frac{1}{c}}}{c \cdot \frac{1-x}{x} - 1} \right). \tag{2.6.1}$$

This bound is absent if the effect of MAC is neglected (ideal MAC, $P_{\mathrm{MAC}} = 1$, that is $c \to \infty$, thus $p_{\mathrm{floor}} = 0$) and the performance depends only on the network connectivity which always increases with ρ. Note that for both the mean cluster size and the probability of samples loss, a very good agreement with simulations is verified.

In Fig. 2.5, the MSE as a function of ρ, for $\alpha = 0.1$ and $x = 0.001$, is reported in the absence and in the presence of DDSP, for different choices of μ_ϕ. In particular, case 1 corresponds to (2.3.7), case 2 refers to (2.3.6) and case 3 is the optimum one given by (2.3.5). Note that the floor on the MSE is due to the floor on p (see Fig. 2.4). Hence, we obtain the floors on the MSE, called $\varepsilon_{\mathrm{floor}}$. In particular, in the absence of

DDSP only in case 1 exists a floor, given by:

$$\varepsilon_{\text{floor}} = p_{\text{floor}}^2, \tag{2.6.2}$$

where p_{floor}, is given by (2.6.1).

When DDSP is adopted, all three cases provide floors, given by:

- case 1:

$$\varepsilon_{\text{floor}} = p_{\text{floor}}^2 + (1 - p_{\text{floor}}) \cdot \beta x \tilde{K} \tag{2.6.3}$$

  where $\tilde{K} = \pi e^{2(\sigma_s^2/k_1^2 - k_0/k_1 + L_{\text{su}}/k_1)}$

- case 2:

$$\varepsilon_{\text{floor}} = \frac{\beta x \tilde{K}}{1 - p_{\text{floor}}} \tag{2.6.4}$$

- case 3:

$$\varepsilon_{\text{floor}} = \frac{\beta x \tilde{K}}{\beta x \tilde{K} + 1 - p_{\text{floor}}} \tag{2.6.5}$$

With the parameters in Table 2.1, the floors values obtained through (2.6.2), (2.6.3), (2.6.4) and (2.6.5) are, respectively, 0.009, 0.038, 0.036 and 0.034, which are perfectly verified by Figure 2.5. Again, simulation results show very good agreement with mathematical models.

In all cases the introduction of DDSP leads to a significant degradation on the MSE. However, as will be clear in the following, there are relevant benefits of DDSP on WSN lifetime, and the trade-off between performance and lifetime will be discussed.

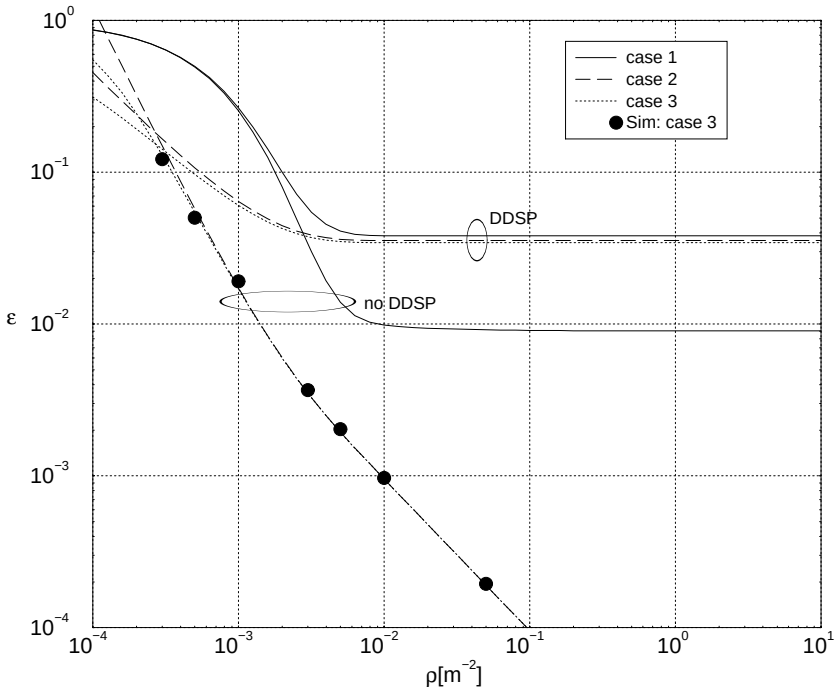

Figure 2.5: MSE with and without DDSP as a function of nodes density for different values of μ for $\alpha = 0.1$ and $x = 0.001$ in the three different cases for linear interpolator.

The effect of parameters x and α is shown in Fig. 2.6 where the MSE is plotted with and without DDSP and in the presence or not of the described MAC protocol (concerning μ_ϕ, the case 2 is considered). Analytical and simulative results are in agreement also in this case. Note that, when ideal MAC and no DDSP are considered, the MSE, according to (2.3.7), can be made arbitrary small by increasing the density ρ. However, this situation (ideal MAC) should be regarded as a performance bound since constraints due to MAC are normally present. In the following Figures, the MAC protocol described is considered.

As already mentioned, the quality of process estimation is not the only focal point that drives the choice of the node density. In fact, the mean nodes lifetime,

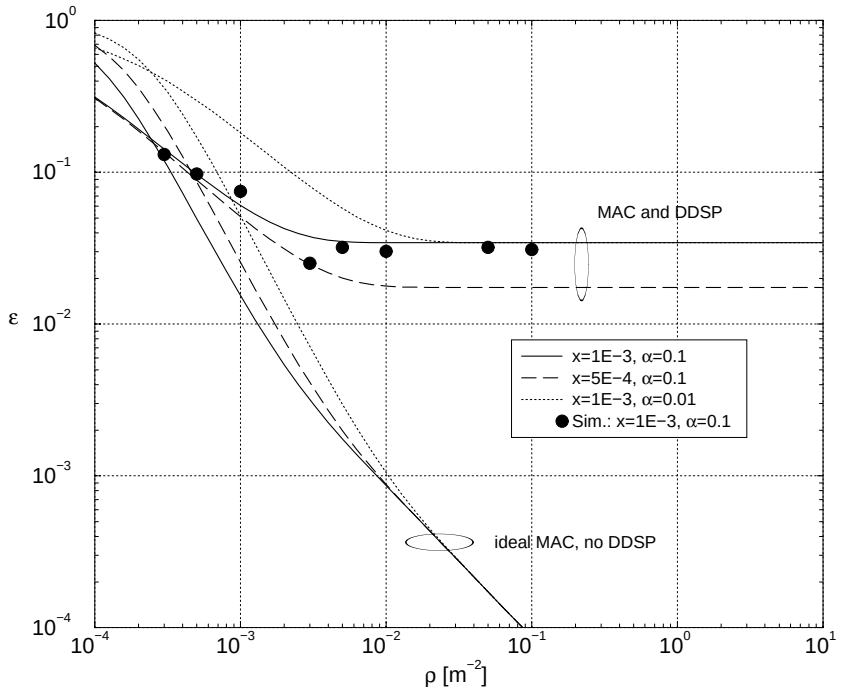

Figure 2.6: MSE with and without DDSP, as a function of density for different values of α and x.

measured in terms of the mean number of rounds achieved before they expire, is also important. It depends on a large set of parameters, such as node density and the cluster size, the energy consumed for transmitting a packet in high power mode (when the node is CH) with respect to that consumed in low power mode, the parameter α, and the operational processing mode (DDSP or not). With DDSP it also depends on the processing consumption through the parameter γ and the spatial correlation properties of the process under analysis, that is β. The mean nodes lifetime is defined in terms of the achievable average number of rounds, N_{round} through (2.5.6).

In Figs. 2.7 and 2.8, the mean number of rounds N_{round} (referred to a battery charge of $E_{\text{charge}} = 1$ Joule) is reported as a function of node density for different

values of x and α in the absence (Fig. 2.7) and in the presence (Fig. 2.8) of DDSP. By fixing a minimum number of rounds that has to be guaranteed it is possible to obtain a constraint on the maximum tolerable node density ρ. Note that for dense WSNs (high values of ρ), the life-time tends to an asymptotical value as a consequence of the asymptotical behavior of p. It is also possible to note that DDSP strongly increases the mean lifetime of nodes.

Also for the network lifetime we evaluate the floor, $N_{\text{round}_{floor}}$, for ρ approaching to infinite. The asymptotic values for N_{round} in the no DDSP and in the DDSP cases follow:

- case no DDSP:

$$N_{\text{round}_{floor}} = \frac{E_{\text{charge}}}{w_0 \left\{(1-x)E_L\theta_d + x\left[E_H\theta_c + E_H\theta_d(\frac{1-p_{\text{floor}}}{x})\right]\right\}} \tag{2.6.6}$$

- case DDSP:

$$N_{\text{round}_{floor}} = \frac{E_{\text{charge}}}{w_0 \left\{(1-x)E_L\theta_d + xE_H\theta_c + xE_H\theta_d \cdot (\beta x\tilde{K} + \gamma) \cdot (\frac{1-p_{\text{floor}}}{x})\right\}}. \tag{2.6.7}$$

For example, in the no DDSP case with $\alpha = 0.1$, we obtain a floor $N_{\text{round}_{floor}}$ equal to 539, whereas in the DDSP case, for $x = 10^{-4}$ and $\alpha = 0.01$, we obtain $N_{\text{round}_{floor}} = 38224$ which are the same values shown in Figures 2.7 and 2.8.

The three key parameters on which the trade-off design of WSN is played are ρ, x and α, and the two performance metrics considered are ε and N_{round}. A possible design criterion is the following: given a certain requirement, ε_{req}, on the MSE, find the values of ρ, x and α such that the network lifetime, N_{round}, is maximized.

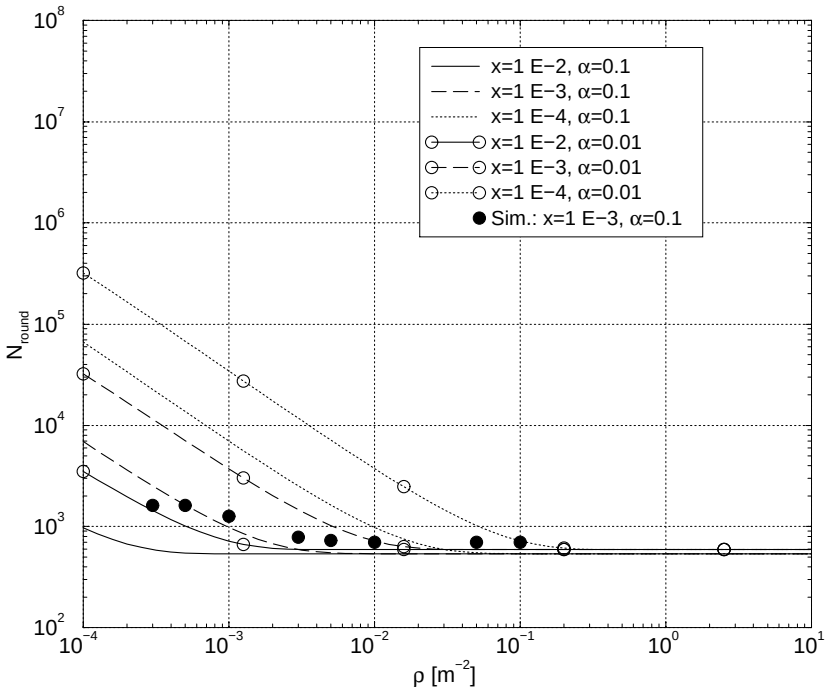

Figure 2.7: Mean node life duration (in terms of number of rounds as a function of density for different values of parameters x and α without DDSP.

According to this criterion, the algorithm which allows the evaluation of the three parameters can take advantage of floor expressions we derived, as in the following:

With requirement $\varepsilon = \varepsilon_{\mathtt{req}}$ and given $c, \sigma_s, k_0, k_1, L_{\mathtt{su}}, \beta, w_0, \gamma, \theta_d, \theta_c$

find $x_{\mathtt{req}}$ s.t. $\varepsilon_{\mathtt{floor}}(x_{\mathtt{req}}) \cdot (1 + y\%) = \varepsilon_{\mathtt{req}}$; (e.g., y=10)

find $\tilde{\alpha}(\rho)$ s.t. $\varepsilon(\rho, x_{\mathtt{req}}, \tilde{\alpha}) = \varepsilon_{\mathtt{req}}$

find $\rho_{\mathtt{req}} = \arg\max_{\rho} N_{\mathtt{round}}(\rho, x_{\mathtt{req}}, \tilde{\alpha}(\rho))$

$\alpha_{\mathtt{req}} = \tilde{\alpha}(\rho_{\mathtt{req}})$

giving $N_{\mathtt{round}}(\rho_{\mathtt{req}}, x_{\mathtt{req}}, \tilde{\alpha}_{\mathtt{req}})$

As an example design we consider the reconstruction case 1 with DDSP: by fixing $\varepsilon_{\mathrm{req}} = 4 \cdot 10^{-2}$, from the above described project criterion, we obtain $x_{\mathrm{req}} = 10^{-3}$,

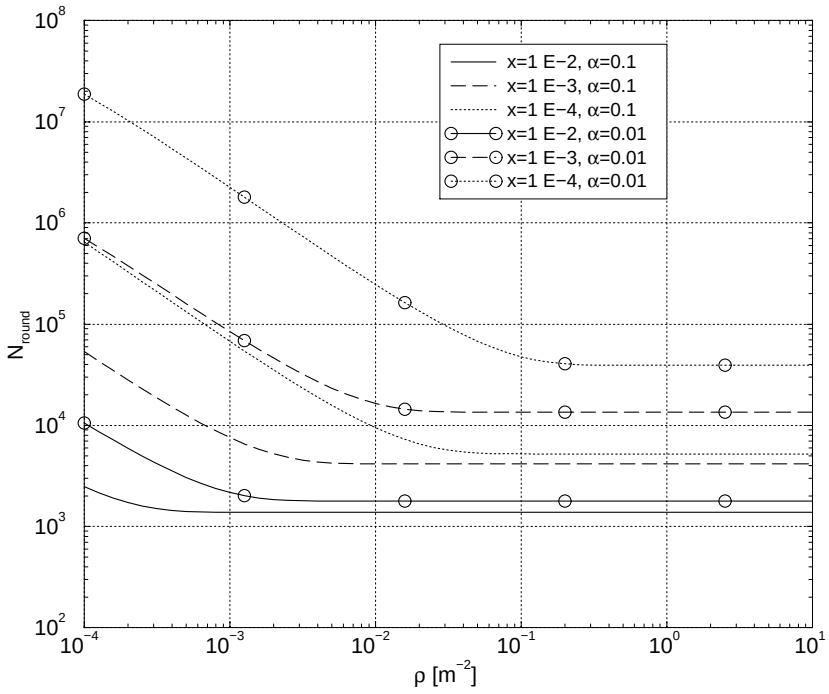

Figure 2.8: Mean node life duration (in terms of number of rounds as a function of density for different values of parameters x and α with DDSP.

$\alpha_{\text{req}} = 2.5 \cdot 10^{-3}$ and $\rho_{\text{req}} = 3.5 \cdot 10^{-2}$ $[m^{-2}]$. These parameters' values bring to a mean number of round N_{round} per Joule of charge of about 18000.

2.7 Conclusions

In conclusion, results show that:

- the DDSP technique proposed provides relevant advantages in terms of energy efficiency (see Figs. 2.7 and 2.8) at the expense of an increased estimation error;
- the role of MAC protocol can be very significant and its choice affects overall performance (see Fig. 2.4);

- a saturation effect on the performance when node density is increased is present due to the clustering architecture and MAC (see Figs. 2.5- 2.8).

The main advantage of this mathematical framework is to rapidly investigate the sensitivity, of both process estimation and WSN lifetime, to different parameter settings. An accurate evaluation through mathematical handling of all issues accounted for in this Chapter. However, the framework developed here has the limits explained in the Introduction of this thesis: (i) a single-sink scenario and not the more general multi-sink scenario, is accounted for; (ii) border effects are not taken into consideration; (iii) the model is valid only for cluster-based topology, therefore node have to reach the sink through a two-hop communication and the more general case of multiple hops is not treated; (iv) the MAC protocol is very simple, and we do not refer to any specific standard air interface; (v) the model assumes no interference between CHs in the transmissions toward the sink. In the rest of the thesis other mathematical models aiming at overcoming these limits, are proposed. In particular, Chapter 3 deals with connectivity models for multi-sink scenarios, whereas Chapter 4 introduces a model for the 802-15.4 MAC protocol. These two models are, then, integrated in Chapter 5 for the realisation of a mathematical framework for studying 805.15.4 multi-sink WSNs under connectivity, MAC and energy consumption viewpoints. However, the model described in Chapter 5, does not consider signal processing issues. The application of the signal processing issues introduced in this Chapter, to the model developed in Chapter 5, could be applied for future works.

Appendix

Point Process with losses

If the stationary random process $P_1(\mathbf{s}) = \sum_n \delta(\mathbf{s} - \mathbf{s}_n)$, with mean μ_{P_1}, is related to the point process $\{\mathbf{s}_n\}$ and p is the probability to lose a sample, the resulting thinned random process can be described as follows

$$P_2(\mathbf{s}) = \sum_n a_n \delta(\mathbf{s} - \mathbf{s}_n)\,, \tag{2.7.1}$$

where $\{a_n\}$ is an independent and identical distributed random sequence with $a_n \in \{0, 1\}$ and p is the probability to have $a_n = 0$ (sample loss) and $h = 1 - p$ the probability to have $a_n = 1$. The corresponding statistical autocorrelation function $R_{P_2}(\tau)$ can be expressed as a function of the original autocorrelation $R_{P_1}(\tau)$ as follows

$$R_{P_2}(\tau) = h^2 R_{P_1}(\tau) + \mu_{P_1}\, p\, h\, \delta(\tau)\,. \tag{2.7.2}$$

Proof.

Recalling the definition of the statistical autocorrelation function of a stationary random process we can write

$$\begin{aligned} R_{P_2}(\tau) &= \mathbb{E}\left\{P_2(\mathbf{s})P_2(\mathbf{s}-\tau)\right\} = \\ &= \mathbb{E}\left\{\sum_n \sum_i a_n a_i \delta(\mathbf{s} - \mathbf{s}_n)\delta(\mathbf{s} - \tau - \mathbf{s}_i)\right\} = \\ &= \sum_n \sum_k R_a(k)\mathbb{E}\left\{\delta(\mathbf{s} - \mathbf{s}_n)\cdot\delta(\mathbf{s} - \tau - \mathbf{s}_{n-k})\right\}, \end{aligned} \tag{2.7.3}$$

with

$$R_a(k) = \mathbb{E}\{a_n a_{n-k}\} = \begin{cases} h & k = 0 \\ h^2 & k \neq 0 \end{cases} . \tag{2.7.4}$$

By substituting (2.7.4) in (2.7.3) we get

$$R_{P_2}(\tau) = h^2 \cdot \mathbb{E}\left\{\sum_k \sum_n \delta(\mathbf{s} - \mathbf{s}_n)\delta(\mathbf{s} - \tau - \mathbf{s}_{n-k})\right\} +$$

$$(h - h^2)\sum_n \mathbb{E}\{\delta(\mathbf{s} - \mathbf{s}_n)\delta(\mathbf{s} - \tau - \mathbf{s}_n)\} =$$

$$= h^2 R_{P_1}(\tau) + p \cdot h \cdot \delta(\tau)\mathbb{E}\left\{\sum_n \delta(\mathbf{s} - \mathbf{s}_n)\right\} , \tag{2.7.5}$$

that leads to the result in (2.7.2).

Estimation error

By expanding the definition (2.3.1) we can write

$$\varepsilon = \frac{1}{E_0}\left[\mathbb{E}\left\{\int_{\Re^l} \hat{X}^2(\mathbf{s})\, d\mathbf{s}\right\} + \int_{\Re^l} x^2(\mathbf{s})\, d\mathbf{s} - 2\mathbb{E}\left\{\int_{\Re^l} \hat{X(\mathbf{s})} \cdot x(\mathbf{s})\, d\mathbf{s}\right\}\right] . \tag{2.7.6}$$

Using the Parseval's relationship we have

$$\varepsilon = \frac{1}{E_0}\int_{\Re^l} |\Phi(\nu)|^2 \overline{E}_Y(\nu) d\nu + 1 - \frac{2}{E_0}\int_{\Re^l} \Phi(\nu)\mathbb{E}\{S_Y(\nu)\} S_X^*(\nu)\, d\nu . \tag{2.7.7}$$

where $S_Y(\nu) = \Im^{(l)}[Y(s)]$.

Due to the stationarity of the random process $P(\mathbf{s})$ it is

$$\mathbb{E}\{S_Y(\nu)\} = \mathbb{E}\left\{\Im^{(l)}[x(\mathbf{s}) \cdot P(\mathbf{s})]\right\} = \mu_P \cdot S_X(\nu) . \tag{2.7.8}$$

By substituting (2.7.8) in (2.7.7) we obtain the final relationship

$$\varepsilon = 1 + \frac{1}{E_0}\int_{\Re^l} |\Phi(\nu)|^2 \overline{E}_Y(\nu) d\nu - \frac{2\mu_P}{E_0}\int_{\Re^l} \Phi(\nu) E_X(\nu)\, d\nu\,. \tag{2.7.9}$$

This expression gives the normalised estimation error as a function of $\overline{E}_Y(\nu)$, defined in (2.2.12), and $E_X(\nu)$.

Chapter 3

Tree-Based Topologies for Multi-Sink Networks

This Chapter deals with some statistical models to characterize network connectivity which provide useful general insights on network parameters design rules, such as node density and transmission power, in WSNs.

In particular, we consider a multi-sink WSN where sensors transmit data to one sink selected among many through multi-hop communication; nodes are organised in trees rooted at the sinks.

The optimal design of these trees, assuming that sensors and sinks are uniformly and randomly distributed over an infinite plane, is treated first. In particular, once the trees height is fixed, the optimum number of children per parent, maximising network connectivity, is derived. This analysis is performed through mathematical approaches and by means of simulations.

Then, a mathematical framework to derive some metrics providing the network connectivity level, is developed. Bounded and unbounded regions are considered in this case.

The Chapter is organised as follows. The following section introduces the aim of

the work. Section 3.2 deals with the related works in the literature. Then the design of the optimum tree-based topology, showing both mathematical and simulation results, is dealt with. Finally, the multi-sink multi-hop connectivity model for bounded and unbounded regions, is described.

3.1 Aims of the Study

A multi-sink WSN, collecting data from the environment through the sampling of some physical entities and sending them to a user, through multiple sinks, is considered. Nodes transmit samples taken from the environment to one sink, selected among many. The user, by collecting samples taken from different locations, and observing their temporal variations, can estimate the realisation of the observed process, as shown in Chapter 2. Good estimates require sufficient data taken from the environment.

The data taken from the area where sensors are distributed, are transmitted to a centralised unit by means of wireless links connecting sensors to sinks, which collect the samples and forward them to the unit through a proper network. If few sensor nodes are deployed and the target area is small, a single sink can be used. When the number of sensors or the target area is large, nodes are often organised in clusters; one sink per cluster forwards the queries to sensors, and collects the responses.

Sinks are sometimes specifically deployed in optimised and planned locations with respect to sensors. However, opportunistic exploitation of the presence of sinks, connected to the centralised unit through a mobile radio interface, is an option in some cases (see the Appendix of this thesis). Under these circumstances, many sinks can be present in the monitored space, but their positions are unknown and unplanned;

therefore, achievement of a sufficient amount of samples is not guaranteed, because sensor nodes might not reach any sink (and thus be isolated) due to the limited transmission range.

According to the type of enabling technology used (e.g., Bluetooth or IEEE 802.15.4), different network topologies might be conveniently created such as, for instance, trees, or rings, or cluster-based topologies [80, 81]. For WSNs, where the set of destination nodes, that are the sinks, is separated by those of sources, namely sensor nodes, tree-based topologies seem to be more efficient than the others: in fact, routing is much simpler, and also distributed data aggregation mechanisms are more efficient. Moreover, as stated in Chapter 1, this topology is one of the topologies defined by the Zigbee Alliance [51, 82], therefore suitable for 802.15.4 networks. As dealing with a multiple sink scenario, formally a forest of (disjoint) trees is formed.

In such scenario, being an uncoordinated environment, network connectivity is a relevant issue, and it is basically dominated by the randomness of radio channel and the density of sinks.

In this Chapter connectivity issues in tree-based multi-sink WSNs, by considering two separate studies, having different aims, are dealt with.

The first study focuses on properly designing the tree-based topology on the basis of connectivity requirements. The objective of the work is to maximise the number of samples reported to the sink(s), that is, network coverage, whereas the tree height should be set keeping energy consumption under control. The study has been carried out through simulations and mathematical analysis. In particular, we study: (i)

a multiple level tree topology using a deterministic MAC, based on Bluetooth or the CFP of the IEEE 802.15.4 superframe (allocation of GTSs to nodes) and (ii) a three-level topology using both the CAP and CFP of the 802.15.4 superframe. The latter case is studied through simulation [9], while the former can be mathematically handled through a statistical approach. The mathematical analysis to derive the statistics of the number of samples received at each sink is reported in [83, 84] and is based on the basic concepts of connectivity in PPP fields, reported in Chapter 1. The mathematical model is derived, assuming that both, sensors and sinks, are uniformly distributed over an infinite area. It is shown that in both cases (i) and (ii), once tree height is fixed, network is maximised by a proper choice of the average number of nodes at each level (and therefore of the average number of children per parent). However, the choice of the tree height has a relevant impact on such optimisation.

In the second study, instead, a bounded scenario where, once again, sinks and sensors are uniformly and randomly distributed, is accounted for. In this work, the probability that sensor nodes are connected to at least one sink, is mathematically derived. Starting from such a result, the probability that all nodes, or a subset of them, are connected, is computed. The work is based on previous papers published in the literature that provided results in the case of an infinite plane [61, 85]. This work differs from the previous ones, since it takes into consideration bounded scenarios, a situation which of course is way more realistic and requires suitable consideration of the border effects. The analysis is first performed in the case of single-hop communication (i.e., every sensor transmits the sensed data directly to a sink). Then, the multi-hop case (i.e., sensors may also act as routers) is considered.

In both the above works the link power loss introduced in Chapter 1 (see eq.

(1.6.1)), which takes dependance on distance and channel randomness into account, is used.

3.2 Related Works

Many papers in the literature based on random graph theory, continuum percolation and geometric probability [86–90] devoted their attention to connectivity issues of networks. In particular, wireless ad hoc and sensor networks have recently attracted a growing attention [56–58, 63, 91, 92]. A great insight on connectivity of ad hoc wireless networks is provided in [56–58]. Nonetheless, the authors do not account for random channel fluctuations and do not explicitly discuss the presence of one or more fusion centers (sinks) in the given region. Connectivity-related issues of WSNs are addressed in [63, 91]. In [63], while considering channel randomness, the authors restrict the analysis to a single-sink scenario. Single-sink scenarios have attracted more attention so far. Although such scenarios have been more examined, multi-sink scenarios, have been increasingly considered. Furthermore, the models based on bounded domains turn out to be of more practical use. As an example, [91] addresses the problem of deploying multiple sinks in a multi-hop limited WSN. However, the work presents a deterministic approach to distribute the sinks on a given region, rather than considering a more general uniform random deployment.

To the best of our knowledge, no one has so far introduced any connectivity model for WSNs while jointly considering the following aspects: presence of both sensors and multiple sinks, random deployment of nodes, multi-hop communication, bounded scenarios and channel fluctuations.

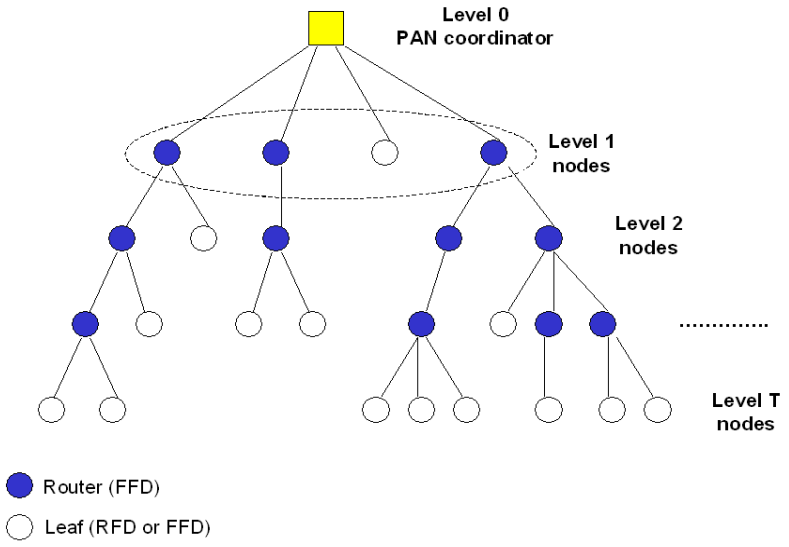

Figure 3.1: ZigBee-compliant tree network topology.

3.3 Reference Scenario

We assume that sensors and sinks are uniformly and randomly distributed over the bi-dimensional plane with densities ρ_s and ρ_0, respectively, with the latter much smaller than the former. We denote as Δ the ratio between these two densities, therefore $\Delta = \rho_s/\rho_0$.

The sensor nodes deployed in the monitored area (that could be bounded or unbounded) need to communicate the sensed data to one sink, responsible for collection of information from the area.

Communication can take place through multi-hop paths. Sensors are assumed

to be split into T groups (that we call *levels*) obtained through a random procedure which lets nodes belonging to each level be all uniformly distributed in the area (bounded or unbounded); the nodes are then connected through a hierarchical architecture, where nodes at a given level need to connect to nodes at a lower level to reach a sink (sinks belonging to the lowest level, in our formalism, see Figure 3.1). As an example, it takes 3 hops to a node belonging to level 3 to reach the sink: two nodes (one belonging to level 2 and the other belonging to level 1) will act as relays. This assumption, that we denote as *a-priori* level partitioning, accounts for networks where a node belongs to one out of T categories of devices, each one having different physical features. The expression *a-priori* stems from the fact that the partitioning procedure occurs independently from the nodes positions. Just to give a practical example, in 802.15.4 [52] networks, devices (such as the 13192 Evaluation Boards by Freescale [93]) operating on a peer-to-peer topology, can be either FFD or RFD: hence, since RFD devices may only talk to FFD ones, if the latter belongs to level i, the former will necessarily belong to level i-1. We emphasize that the nodes are then grouped with fixed densities a-priori: in fact, regardless of whether we are dealing with two diverse boards or with the same board running two different pieces of software, both the hardware (in the first case) and the software (in the second) remain the same for the entire operational time of the network (e.g., the software may not be re-compiled on-the-fly). Hence, although it is not the optimal situation from a connectivity perspective (not all possible paths to the sinks are exploitable), the a-priori partitioning assumption is noteworthy because it is widely adopted in practice. Moreover, connectivity models for two-dimensional T-hop networks under more general conditions are still being studied [94].

We denote as ρ_i nodes density at level i, with $i \in [1, .., T]$ and we assume that a node belongs to level i with a probability p_i (equal for all nodes), fixed a-priori as stated above; therefore $\rho_i = p_i \rho_s$. Whatever the strategy used, the density of nodes at all levels must satisfy the constraint

$$\sum_{i=1}^{T} \rho_i = \rho_s \, . \tag{3.3.1}$$

3.4 On the Design of Optimum Tree-Based Topologies

The aim of this part of the Chapter is to optimally design the tree topology, accounting for connectivity issues.

We assume that the air interface imposes a maximum number of nodes that can be connected to a given node. As an example, in case Bluetooth is used [55], a maximum number of seven slaves can be connected to the master of the piconet (see Chapter 1). Also, the Zigbee Alliance is providing profiles where the maximum number of children per parents is fixed a priori, to avoid the risk of many contentions during the CAP and addressing problems [82]. In particular, we will denote as c_i, the capacity of level i-1 nodes, that is the maximum number of i level nodes that can be serviced by an i-1 level node. When it does not depend on i, we denote it as c and also refer to the maximum number of children per parent in the tree.

Two different scenarios are addressed here: (i) a multiple level tree topology using a deterministic MAC, that could be based on Bluetooth or 802.15.4 in case a maximum number of seven children per parent is imposed, therefore, $c \leq 7$ (in this case, in fact, all nodes can use GTSs) and (ii) a three-level tree topology using

both CAP and CFP of 802.15.4, where the capacity constraint could be imposed or not, and the contention-based MAC protocol is accounted for. The first scenario is studied through mathematical analysis; whereas the second one is implemented through simulations.

The rest of this section is devoted to the description of these two scenarios and approaches and shows numerical results obtained.

3.4.1 The multi-level tree: mathematical analysis

Being sensors and sinks Poisson distributed over the infinite bi-dimensional plane, the number of samples reported to a generic sink through the tree is, once again, a r.v., denoted as n, having a probability distribution, denoted as $f(n)$. When a capacity constraint is imposed, n is upper-bounded by $n_{max} = \sum_{i=1}^{T} c^i$, whereas more generally it is unlimited.

The probability that the number of samples received by a given sink is above (or equal to) a fixed fraction x of the mean, Δ, is given by:

$$R = \mathbb{P}\{n \geq x\Delta\} = \sum_{x\Delta}^{\infty} f(n), \tag{3.4.1}$$

assuming $x\Delta$ is an integer. If $x\Delta$ is not an integer, extension is straightforward.

Once $f(n)$ is known (this distribution is derived in the following), the only degree of freedom, in order to properly design the trees, is the set of values ρ_i $(i = 1, \cdots, T)$, that need to be designed according to the constraint (3.3.1).

For the sake of simplicity here it is assumed that the ratio between the node density at a given level and the one at the next higher level is set to a common value

η, except for the T-th level that will include the remaining nodes. Formally,

$$\rho_i/\rho_{i-1} = \eta \quad i = 1, \cdots, T-1 \quad and \quad \rho_T/\rho_{T-1} \leq \eta. \tag{3.4.2}$$

Thus η is the mean number of children per parent, and the probability of blocking (i.e. the transmission of the samples collected to the higher level is not possible because of capacity limits, or collisions) will be the same at all levels from T-1 to 1. It is worth noting that this choice is not necessarily optimized, as the optimum choice should reflect a compromise between the cost of blocking the transmission at higher levels (where a node needs to report the many samples collected by its children) and the overall network energy efficiency. This will be matter for future work.

As a result, T and η should be fixed according to the constraint (3.3.1) and expressions given in (3.4.2).

Clearly, when η increases, the minimum value T needed to satisfy constraint (3.3.1) will decrease. In particular, using equations (3.4.2) and (3.3.1) the minimum value of T is found using the following formula:

$$\sum_{i=1}^{T-1} \eta^i + \eta^{T-1} \cdot \rho_T/\rho_{T-1} = \Delta. \tag{3.4.3}$$

On the other hand, if η significantly exceeds the air interface capacity, the probability of blocking will increase.

Thus, the objective of our analysis is to derive the value of η such that R is optimised.

According to the channel model described in Chapter 1, a node can hear a transmitting one in case $L \leq L_{\text{th}}$; thus, the number of level i sensors audible at a random point on the plane has a Poisson distribution with mean

$$\mu_i = \pi \rho_i e^{\frac{2(L_{th}-k_0)}{k_1}+\frac{2\sigma_s^2}{k_1^2}}, \tag{3.4.4}$$

which corresponds to eq. (1.6.9) by replacing ρ with ρ_i. As all sensors at all levels are randomly distributed, this applies to the number of level i sensors audible to every other sensor. This result is derived, in a different context, in [61].

Assuming that every sensor will seek service at the loudest sensor at the next level, it is shown in [83] that the number of level i sensors seeking service at a given level $i-1$ one has a Poisson distribution with a given mean. In our case, the mean number of level 1 sensors seeking service at a given sink is $[1-e^{\mu_0}]\frac{\mu_1}{\mu_0}$. The ratio $\frac{\mu_1}{\mu_0}$ is the mean number of level 1 sensors per level 0 one, and the factor $[1-e^{\mu_0}]$ eliminates those which cannot hear at least one level 0 one.

To deal with the hierarchical case we define a probability generating function $\Pi_i(s)$ for the number of level i sensors being serviced by a given level $i-1$ sensor. Then the probability generating function for the number of level $i+1$ sensors being serviced by a given level $i-1$ sensor through level i sensors (a three-level hierarchy) is

$$\Pi_i(s\Pi_{i+1}(s)). \tag{3.4.5}$$

Here, within the bracket, the term $\Pi_{i+1}(s)$ "counts" the level $i+1$ sensors reporting to a given level i one, and the additional s adds the latter before the report is sent up to the next level.

The extension to higher level hierarchies is immediate. Thus the probability generating function for the number of level $i+2$ sensors being serviced by a given level $i-1$ sensor through level i and level $i+1$ sensors (a four-level hierarchy) is

$$\Pi_i(s\Pi_{i+1}(s\Pi_{i+2}(s))), \tag{3.4.6}$$

and similarly for yet higher levels.

In these circumstances, denoting as $\mu_{(i)}$ the mean number of level i sensors being serviced by a given level $i-1$ sensor, it follows that the mean number of level $i+1$ sensors being serviced by a given level $i-1$ sensor through level i sensors is

$$\mu_{(i)}(\mu_{(i+1)}+1), \tag{3.4.7}$$

while for the four-level hierarchy this becomes $\mu_{(i)}\mu_{(i+1)}\mu_{(i+2)}+\mu_{(i)}\mu_{(i+1)}+\mu_{(i)}$.

With no capacity limitation this generating function is that of the Poisson distribution of the number of sensors seeking service described above. With capacity limitation, we start with that Poisson distribution (whose mean we take as μ), but cumulate all probabilities from the term in s^{c_i} onwards. The probability generating function therefore becomes

$$\Pi_i(s)=\sum_{u=0}^{c_i-1}\frac{\mu^u s^u}{u!}e^{-\mu}+s^{c_i}\sum_{u=c_i}^{\infty}\frac{\mu^u}{u!}e^{-\mu}. \tag{3.4.8}$$

The number of levels in the hierarchy depends on η and Δ. At one extreme, if $\eta \geq \Delta$, then all sensors are at level 1, and we have a 2-level hierarchy. If $\eta < \Delta$, then the density of level 1 sensors is $\rho_0\eta$, leaving a density of $\rho_0(\Delta-\eta)$ of sensors to allocate to lower levels: these will all remain at level 2 if $\eta^2 \geq \Delta-\eta$. Otherwise the density of level 2 sensors will be $\rho_0\eta^2$, leaving a density of $\rho_0(\Delta-\eta-\eta^2)$ for level 3 or lower. Repeating as often as necessary, we find that in general the hierarchy will be of level $T+1$ if $0 < \Delta-\eta-\eta^2-\cdots-\eta^{T-1} \leq \eta^T$.

3.4.2 Mathematical Analysis Results

The following parameters are set: $k_0 = 40$ [dB], $k_1 = 15$, $\sigma_s = 4$ [dB], $L_{\text{th}} = 110$ [dB], $\rho_0 = 10^{-4}$ $[m^{-2}]$ and $\Delta = 100$. The default requirement is to have at least 90 samples

received at each sink (therefore, $x = 0.9$). Capacity limit is $c = 7$.

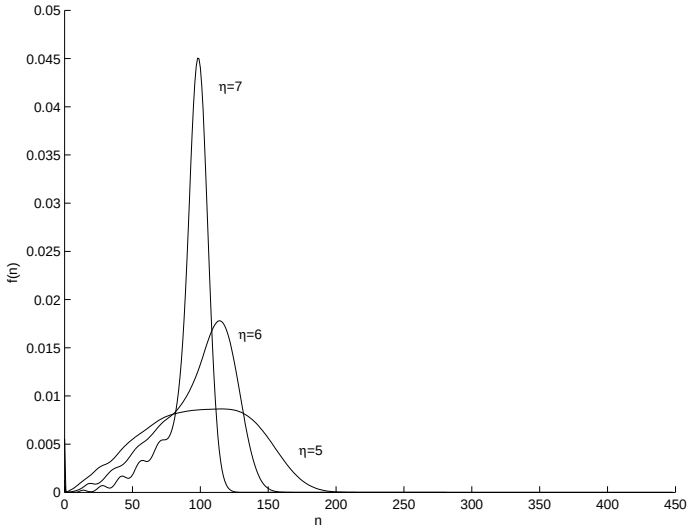

Figure 3.2: The probability distribution of number of nodes serviced, $f(n)$, for different values of η, $T = 3$.

Let us consider $T = 3$. According to the constraints (3.3.1) and (3.4.2), the values of η that should be considered approximately range from 4.3 to 9.5. Fig. 3.2 shows the probability $f(n)$ as a function of n for $\eta = 5, 6, 7$. As expected, the means tend to converge to Δ when η increases, as all trees will find a sufficient number of nodes to fill all levels. Is it worth noting that as η gets larger, the variance of these statistics decreases.

Figure 3.3 shows the effect of x on the probability R, plotted on the vertical axis as a function of η, for $T = 3$, again. According to the relevant variations on the standard deviation of $f(n)$, the curves vary significantly depending on x. In all cases, an optimum value of η can be determined by these curves, depending on the requirement set. Note that the optimum value is close to seven (i.e. the capacity limit), or a bit larger. The sudden decrease of R after the maximum is determined

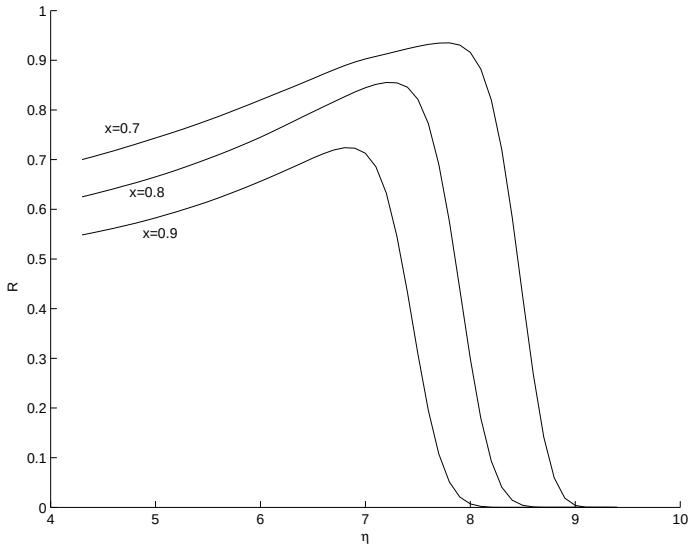

Figure 3.3: R as a function of η, by varying x, having fixed $T = 3$.

by the increase in the blocking probability. Also note that, as expected, when x is larger, the probability R gets smaller.

Figure 3.4 shows R as a function of η for $\Delta = 50$, $c = 7$, having set $k_0 = 40$ [dB], $k_1 = 13.03$, $\sigma_s = 3.5$ [dB], $L_{\text{th}} = 95$ [dB], and $\rho_0 = 4 \cdot 10^{-4}$ $[m^{-2}]$. Here we consider the options $T = 4$, 3 and 2: η can approximately range from 2.4 to 3.2, from 3.2 to 6.5 and from 6.5 to 10, respectively. Note that the cases with $T = 2$ and 3 should converge for $\eta = 6.5$, where we have a four-level tree with the lowest level empty, or a three-level tree with the lowest level having node density which is η times larger than that at the higher level; in fact, this happens. The same holds for $T = 4$ and 3 at $\eta = 3.2$. Note that the larger x (i.e. a more stringent requirement is set), the smaller the probability R, as expected. However, the most important aspect stands in the maximum value of R; depending on x, optimum performance is achieved for $T = 2$ or 3. In other words, the optimum tree height depends on the coverage requirement.

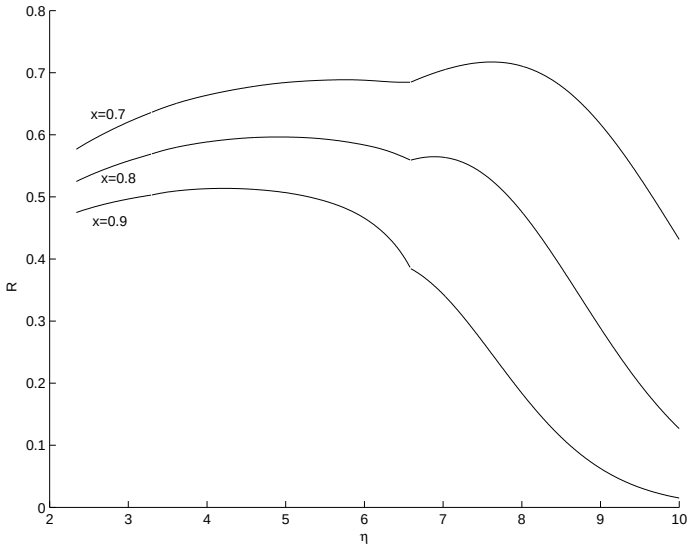

Figure 3.4: R as a function of η. $\Delta = 50$, $c = 7$.

From Fig. 3.4 it can be seen that for $x = 0.7$ the optimum topology requires $T = 2$, $\eta \approx 7.7$, while for $x = 0.9$ it is given by the pair $T = 3$, $\eta \approx 4.5$. In [9] this effect is more thoroughly discussed and it is shown that this depends on the shape of the number of nodes reporting to a given sink distribution.

In Figure 3.5, instead, we set $\Delta = 200$ and we left the other parameters at the same values used in Figure 3.4. Here the two cases $T = 4$ (η ranging in this case from 3.5 to 5.5) and 3 (from 5.5 to 9.5) are considered. Similar considerations to the case of Fig. 3.4 can be done. However, given the larger average number of nodes per tree with respect to Fig. 3.4, the optimum topology requires $T = 3$ or 4.

Finally, in Figure 3.6 we show the behavior of R, for different capacities, having fixed $\Delta = 50$, $T = 2$ and $x = 0.7$. In particular, the capacity limit for sinks is $c_1 = 13$ while c_2 ranges from 3 to 13. The graph shows that reducing c_2 affects only the left part of the curves, at least if the value is not too low. This can be motivated by

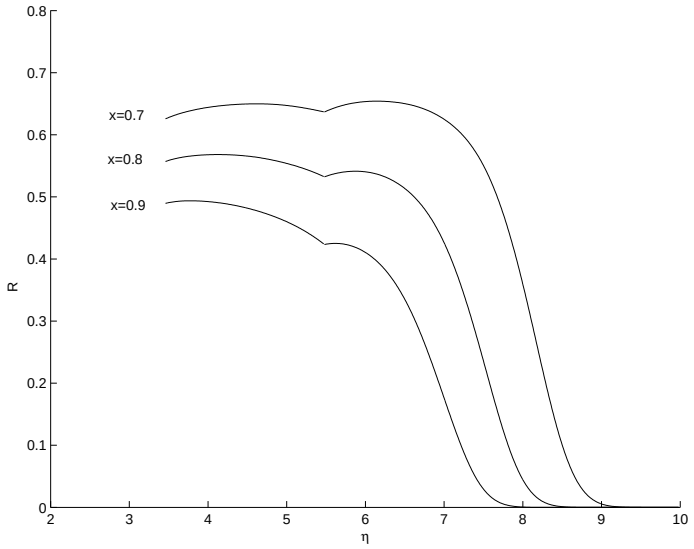

Figure 3.5: R as a function of η. $\Delta = 200$, $c = 7$.

the fact that for lower values of η, the lowest level in the tree is the one hosting the majority of nodes, and a capacity limitation at the penultimate level strongly affects the possibility to collect information from the field; on the opposite, for large values of η, the lowest level tends to become empty, and such capacity limitation does not affect significantly the probability R.

By comparing the curve for $x = 0.7$ in Fig. 3.4 to those of Fig. 3.6, it can be seen that the capacity increase from 7 to 13 clearly shows an improvement on network coverage. However, R does not reach unity. Indeed, it was found that with c tending to infinity, R monotonically increases with η, and the maximum is reached for $\eta = 50$ where R becomes approximately 0.98. The difference between this value and unity is due to the statistical behaviour of the number of nodes per tree: even if there are no capacity limitations and network connectivity is assured, the probability of any given numbers of nodes being connected to a sink does not reach unity because there

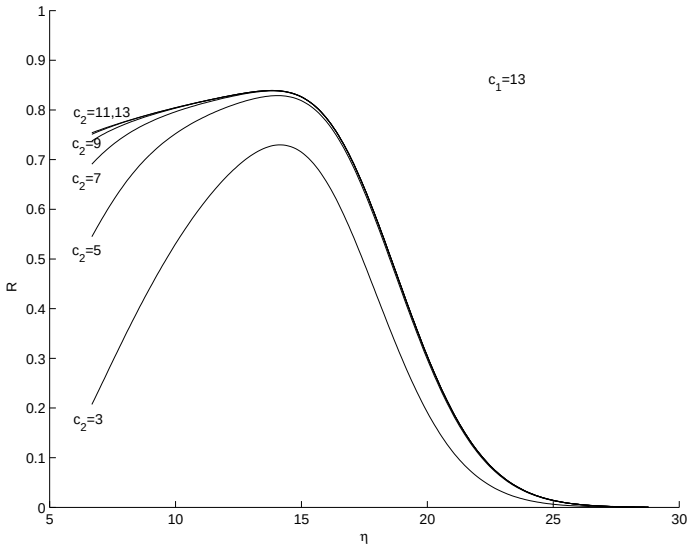

Figure 3.6: R as a function of η. $\Delta = 50$, $c_1 = 13$, $T = 2$, $x = 0.7$.

is non-zero probability of trees with very few nodes (even zero, with low probability).

Finally, results having fixed $\rho_0 = 5 \cdot 10^{-4}$ $[m^{-2}]$, $\Delta = 10$, $k_0 = 40$ [dB], $k_1 = 13.03$, $\sigma_s = 3.5$ [dB] and $L_{\text{th}} = 95.6$ [dB], are shown.

Figure 3.7 shows R as a function of η for $x = 0.7$, 0.8 and 0.9. As we can see, by increasing x, R decreases, as expected. According to the constraints (3.3.1) and (3.4.2), the values of η that should be considered depend on T. Here we consider $T = 2$, 3 and 4, which corresponds to η ranging in [2.71, 10], [1.74, 2.71] and [1.4, 1.74], respectively. Note that the cases with $T = 2$ and 3 converge for $\eta = 2.71$, because in this point we have a four-level tree with the lowest level empty, or a three-level tree with the lowest level having nodes density which is η times larger than that at the higher level. The same holds for $T = 3$ and 4, at $\eta = 1.74$. In all cases the

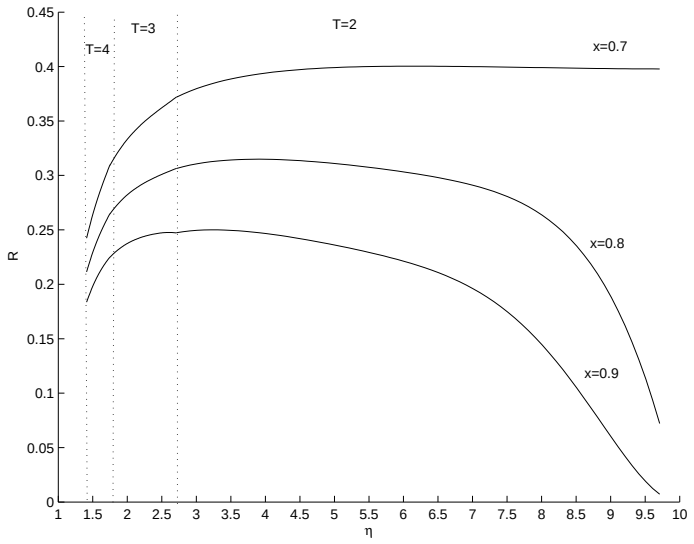

Figure 3.7: R as a function of η for $\rho_0 = 5 \cdot 10^{-5}$ $[m^{-2}]$ and $x = 0.7$, 0.8 and 0.9.

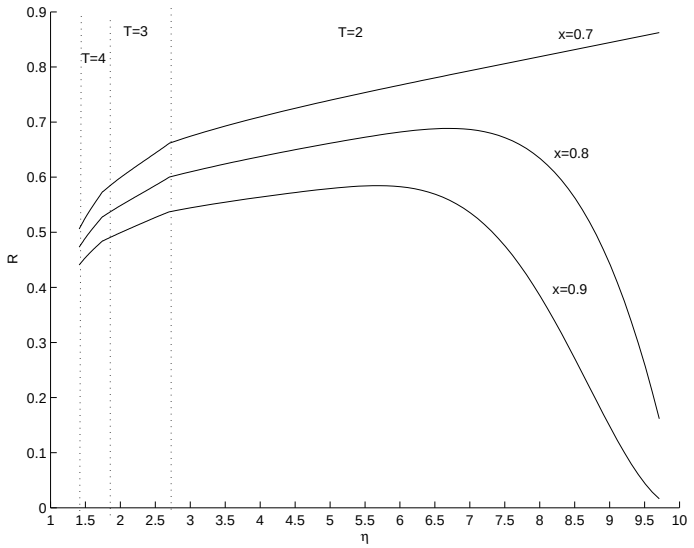

Figure 3.8: R as a function of η for $\rho_0 = 5 \cdot 10^{-4}$ $[m^{-2}]$ and $x = 0.7$, 0.8 and 0.9.

maximum value of R is reached for $T = 2$, whereas the optimum value of η decreases by increasing x. As we can see, even in the case $x = 0.7$, R assumes a maximum value of 0.4, that is quite low: the reason is that performance has been evaluated for a network with low density, which has connectivity problems. Thus, in Figure 3.8, we show R as a function of η for a network having $\rho_0 = 5 \cdot 10^{-4}$ $[m^{-2}]$ and $\Delta = 10$, for T=2, 3 and 4 and $x = 0.7$, 0.8 and 0.9. As we can see, this network is more connected than the one considered in Fig. 3.7; in fact R reaches the values of 0.85 for $x = 0.7$. The optimum value of R is reached for $T = 2$ and for $\eta = 10$, 7 and 6.3 in the three cases $x = 0.7$, 0.8 and 0.9, respectively. Moreover, we can note that for $x = 0.8$ and 0.9, when η assumes value larger than 7, R decreases; this is due to the capacity limit imposed ($c = 7$) which affects R, for large values of η.

3.4.3 The Three-Level Tree: Simulation Environment

Simulation results have been achieved through a C language simulation tool specifically developed to model the environment and protocols described in the following.

The reference scenario considered consists of a number of nodes randomly and uniformly distributed over a square area (having side L meters, so that $\rho_s = 1/L^2$), which is Poisson distributed with given mean, N_s.

Both single-sink and multi-sink scenarios are simulated. In the first case only one sink is located in a given position of the area and we fix N_s such that $\Delta = N_s$. In the multi-sink scenario, instead, a number of sinks are Poisson distributed in the square, with given mean, M.

As stated above, in the simulation environment, 802.15.4 devices are considered. Therefore, the sinks are the Personal Area Network (PAN) coordinators, managing a

PAN, composed of a given number of sensors and formed according to a procedure described in the following. Nodes work in beacon-enabled mode, therefore sinks periodically send beacon packets.

The network must be able to provide the information detected by nodes to the sinks within the superframe starting with the transmission of the beacon from sinks. We denote as *round* the period of time between two successive beacon packets sent by the sinks (i.e., the beacon interval). It is also assumed that all sinks are time synchronised, thus they transmit the beacon packets at the same time.

Note that here, we do not consider the Zigbee tree-based topology: tree formation and the access to the channel is managed through a different communication protocol, described in the following.

The channel model is the one described in Chapter 1. Finally, we impose a capacity constraints, thus we fix a maximum number of children per parent.

The tree topology

The network is organised in a three-level hierarchical topology: the sink is at level zero, level one is constituted by nodes denoted as CHs and level two is constituted by non CH nodes. Nodes elect themselves CHs with probability p_1. Therefore, we have $\rho_1 = p_1 \cdot \rho_s$ and consequently $p_1 = \eta/\Delta = \eta/M$. Recall that η is the mean number of children per parent. Having fixed M, and by varying p_1, this observation allows to draw curves of R, that can be easily derived through simulation, as a function of η.

The tree is formed according to the following steps:

1. PANs formation - each sink transmits a beacon packet and nodes select the PAN to belong to on the basis of the received power: each node selects the sink

from which it receives the largest power.

2. Clusters formation - in each PAN a certain number of nodes elect themselves CHs, with probability p_1. Each CH broadcasts a packet informing of its role and those nodes that did not elected themselves as CHs (non-CHs) select their CHs to transmit to, on the basis of the power received by each CH. In particular, once again, each node selects the loudest CH.

3. Transmissions - each non-CH node, transmits its packet to the respective CH, which, on its turn, sends all packets received, plus the one it generated, to the selected remote sink via a direct link. If a non-CH node does not receive correctly any broadcast packets coming from CHs, or there are not elected CHs in a PAN, its packet is lost (transmissions from level two to level zero are not allowed).

As will be clarified in the following, two supeframes are needed for exploiting the protocol: a superframe is used for PANs and clusters formation and another one is devoted to transmissions. In particular, a superframe for the tree formation, is followed by N_{tr} superframes where sample transmissions take place. Therefore, tree are formed every N_{tr} round (see Figure 3.9). It is reasonable, if we assume that the channel has a coherence time equal to N_{tr} round.

MAC layer protocol

The beacon-enabled mode, with acknowledge transmission, is considered.

Three kinds of packets can be transmitted in the network: the beacon, having a size of 62 bytes (i.e., it is transmitted in $124T_s$, since a bit rate of 250 [kbit/sec] is

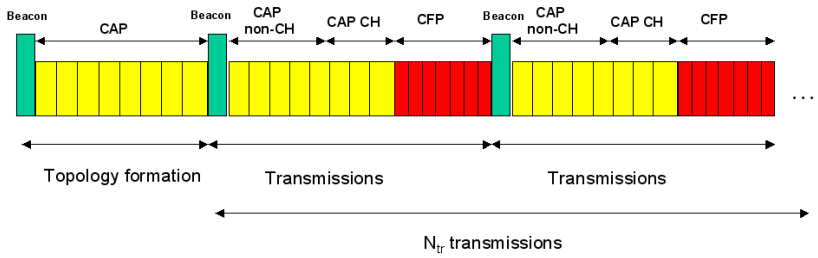

Figure 3.9: The 802.15.4 superframe used in the communication protocol.

used); the ACK packet sent to notify the correct reception of a data packet, having a size of 5 bytes, and data packets, containing the measurement result and having a size of 25 bytes (with a payload of 10 bytes).

At the end of the topology formation phase, it is assumed that the sinks are aware of the topology. This is possible because of CH broadcasts and the ACK packets sent by non CHs to notify the broadcast reception are received by the final sink too (assuming reciprocal links, if a node correctly receives the beacon, it can reach the sink). Since CHs have to transmit to the final sink all packets received inside their clusters plus the one generated by themselves, the loss of a CH packet implies the loss of a large number of samples. For this reason we decide to assign GTSs to CHs. Then, when the sink transmits the beacon which starts the sample transmission phase, it

assigns the GTSs to the CHs whose clusters are larger: in other words we introduce a priority for those CHs which have the largest cluster sizes. Moreover the sink assigns a specific channel to each cluster, that is each non CH belonging to a given cluster uses the same channel: in this way, collisions between clusters are avoided, while non CHs compete during the CAP on a given channel (in case of more than 16 clusters a spatial frequency reuse is performed). Thus, both CAP and CFP are present: the CAP duration ranges from $T_{CAP_{max}} = 960 \cdot 2^{SO} \cdot T_s - 124T_s$, when there are no CHs, and GTSs are not allocated, to $T_{CAP_{min}} = 60 \cdot 2^{SO} \cdot T_s \cdot (16 - 7) - 124T_s$, when there are seven or more than seven CHs and all GTSs are allocated (see Figure 3.9). A large value of SO is set such that the packets (and the inter-frame space) could be contained in the minimum duration of a GTS ($60 \cdot 2^{SO} T_s$) and seven GTSs could be allocated (see Chapter 1). When the number of CHs is lower than seven, all the CAP is used by non CHs that have to transmit to their CHs, through CSMA/CA: no mechanism to handle hidden terminals is performed, therefore, collisions occur and some packets are lost. When, instead, the number of CHs is larger then seven, the CFP is used and the CAP duration is $T_{CAP_{min}}$. In this case the CAP is subdivided into two parts: the first part, $T_{CAP_{nonCH}}$, set to the C % of $T_{CAP_{min}}$, is devoted to non CHs transmissions, whereas the second part, $T_{CAP_{CH}}$, set to $(100 - C)\%$ of $T_{CAP_{min}}$ is devoted to transmissions of the CHs that do not have a GTS assigned. These nodes use the default frequency to transmit to the final sink, thus they could collide. We show in the following curves for different values of C.

To realistically account for collisions, capture effect is taken into consideration: we assume a packet is captured by the receiver, even in case of packet collisions (i.e.

simultaneous transmission of packets by separate nodes), if

$$\frac{P_{R0}}{\sum_{i=1}^{N_c} P_{Ri}} > \alpha \tag{3.4.9}$$

where

- P_{R0} is the power received from the useful signal;
- P_{Ri} is the i-th interference power;
- N_c is the number of colliding packets;
- α is the capture threshold, set to 4 [dB].

When condition (3.4.9) is not fulfilled, the packet is lost and the receiving node does not transmit the acknowledge packet.

3.4.4 Simulation Results

In this section we report the numerical results obtained through simulations, in the mono- and multi-sink scenarios.

1000 rounds are simulated and then, 10 different and uncorrelated realisations of node locations are considered. At each round the packet error rate, obtained dividing the number of samples lost by the number of nodes in the network, is computed and, at the end, R is evaluated.

The packet losses are caused by the following events:

- a node is isolated: it does not receive the beacon packet or it does not receive any CH broadcast packets and it cannot reach directly the final sink; this event has very low probability with the system parameters considered in this paper;

- a node tries to access the channel for more than NB_{max} consecutive times without success (see Chapter 1);
- a node does not succeed in correctly transmitting its packet by the end of the superframe portion devoted to it;
- when a capacity constraint is imposed it may happen that some nodes (CHs or non CHs) cannot transmit their packets to their parent (the selected sink, or CH).

As in the mathematical analysis, the objective is to maximise the probability, R, that the number of samples received by the final sink is above (or equal to) a fixed fraction, x, of the mean Δ. To do this we have studied the behaviour of R by varying η (and thus p_1): results show that there exists an optimum value of η, maximising R. This optimum number can be easily motivated by the need to compromise between the load within clusters, which depends on their size and is controlled by increasing the number of CHs, and the probability of collisions among CH packets, that can be minimised by decreasing the number of CHs.

The first results are obtained in the single-sink scenario, by setting $N_s = \Delta = 100$, $L = 100$ [m] (i.e., $\rho_0 = 10^{-4}$ $[m^{-2}]$), $SO = 10$, $k_0 = 40$ [dB], $k_1 = 15$, $\sigma_s = 4$ [dB] and $L_{\text{th}} = 110$ [dB].

In Figure 3.10 R as a function of η, by varying the threshold x, is shown for the percentage C set to 70. No capacity constraints are imposed here. By increasing x, R decreases, as expected. As we can see, the curves show a maximum, that is there exists an optimum value of η, η_{opt}, for which R assumes a maximum value. In fact,

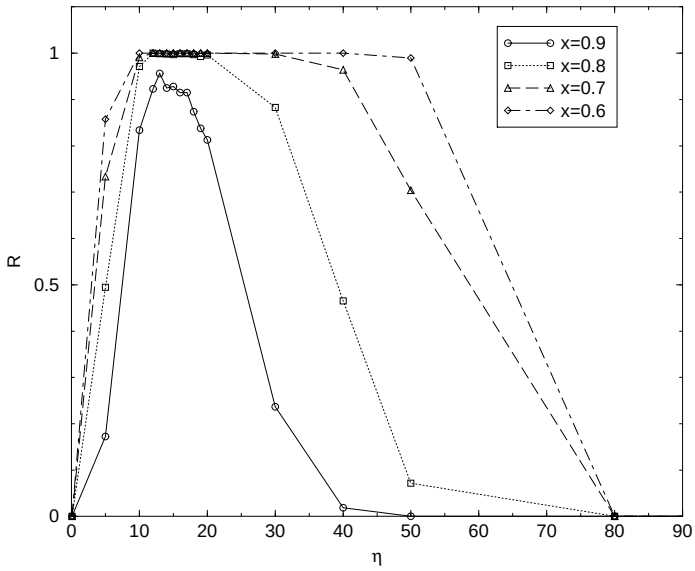

Figure 3.10: R as a function of η, in the case C=70.

when η is too low, GTSs are not exploited and the number of non CHs which compete for the channel is large and collisions inside clusters have larger probabilities. On the other hand, when η increases, the number of CHs using the CAP becomes large and the collision probability increases in the superframe portion devoted to CHs. We note that by varying x the value of η_{opt} is approximately the same.

In Figure 3.11, instead, the case $C = 100$ is shown. In this case the maximum number of CHs that can be connected to the final sink is seven; therefore, it is equivalent to impose the constraint $c_1 = 7$, whereas no constraint is imposed on c_2. In this way if the number of CHs is larger than seven the samples gathered by those having smaller clusters are lost. As we can see in the Figure, the curves present a maximum value in correspondence of an optimum value, η_{opt}; once again by increasing x, R decreases and η_{opt} is approximately the same for the different values of x.

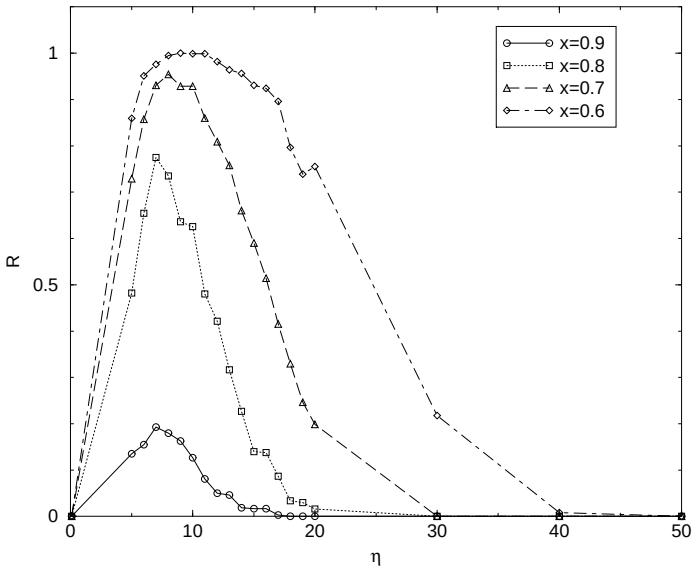

Figure 3.11: R as a function of η, in the case C=100.

If we compare Figures 3.10 and 3.11, we can observe that when $T_{CAP_{CH}}$ is set to zero, performance worsens, because when the number of CHs is larger than seven all their packets are lost; consequently the η_{opt} values in this case are lower than the one obtained with $T_{CAP_{CH}}$ set to 70% of $T_{CAP_{min}}$, because the network works better when the number of CHs is lower.

In the following Figures a comparison between the results obtained through simulations and the mathematical results for the single-sink scenario while setting $T = 2$ (three-level tree), is provided. Owing to the different strategies to access the channel, contention-based in simulations and contention-free in mathematical model, the comparison has not the aim to validate the model, but to show how the use of different MAC protocols impact performance.

The following values for the parameters are set: $N_s = \Delta = 50$, $L = 50$ [m] (i.e., $\rho_0 = 4 \cdot 10^{-4}$ $[m^{-2}]$), $SO = 10$, $k_0 = 40$ [dB], $k_1 = 13.03$, $\sigma_s = 3.5$ [dB] and $L_{\text{th}} = 92$ [dB].

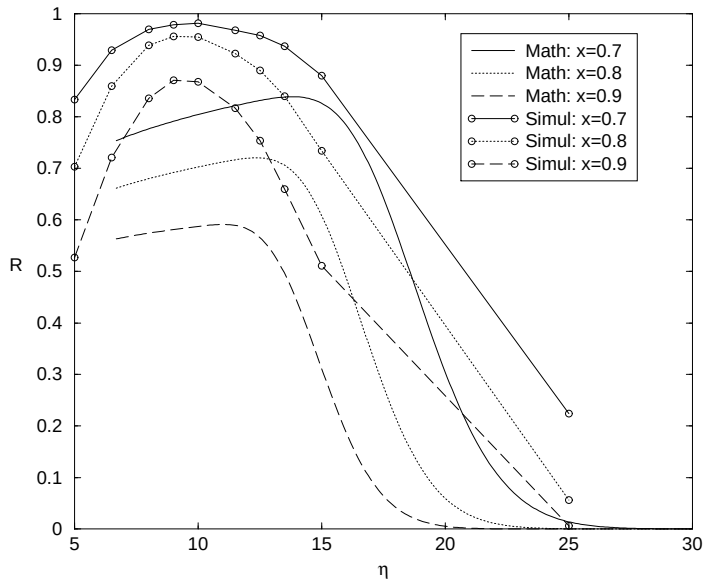

Figure 3.12: R as a function of η. $\Delta = 50$, $c = 13$. Mathematical and simulation results are reported.

Figure 3.12 shows R as a function of η for $\Delta = 50$, $c = 13$, with x taking values 0.7, 0.8, 0.9. Simulation and mathematical results are reported. With such large value of node capacity, for large η the number of collisions during the CAP can be high. In fact, this scenario is characterised by soft capacity constraints. As a result, the optimum value of η is smaller than in the case of deterministic access, accounted for by the mathematical model. Simulations report better performance for the optimum values of η, because of the border effects introduced by the limited area considered in the simulated scenario.

With smaller capacity values (see Fig. 3.13 with c set to 7), leading to situations

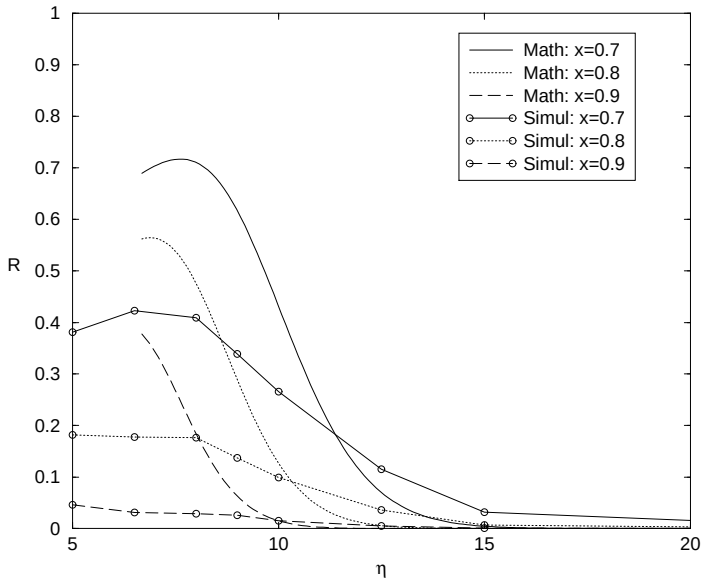

Figure 3.13: R as a function of η. $\Delta = 50$, $c = 7$. Mathematical and simulation results are reported.

where coverage is limited by hard capacity constraints, we found that simulation results give smaller values of R than the mathematical analysis; however, in this case (where collisions play a minor role) the optimum value of η found with the mathematical and simulation approaches coincide, confirming the motivation given above to the different optimum values of η.

Finally, Fig. 3.14 reports simulation outcomes achieved for the same set of parameters as in Fig. 3.12. The trends for the various values of c_2 are very similar, and the differences are motivated by the effects mentioned in the previous paragraphs.

In Figure 3.15 we compare results obtained in the single-sink and in the multi-sink scenarios. For a fair comparison, we set a common value for the sink density,

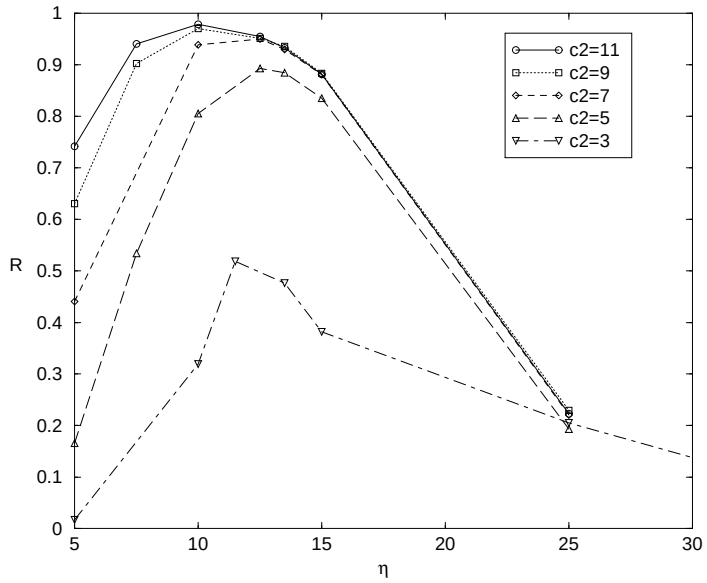

Figure 3.14: R as a function of η. $\Delta = 50$, $c_1 = 13$, $x = 0.7$. Simulation results.

$\rho_0 = 4 \cdot 10^{-4}$, $[m^{-2}]$ and $\Delta = 50$. As a consequence, the square side varies with the number of sinks: if the latter is equal to one, $L = 50$ [m], in case $M = 9$ $L = 150$ [m], and so on. The other parameters are set as follows: $SO = 10$, $k_0 = 40$ [dB], $k_1 = 13.03$, $\sigma_s = 3.5$ [dB] and $L_{\text{th}} = 92$ [dB]. The Figure reports R as a function of η (equal to $p_1 \cdot \Delta$) in three different situations: i) the single-sink deterministic scenario (with sink located in the centre of the area); (ii) the single-sink random scenario (where the sink is located in a random position); and (iii) the multi-sink case. We set $SO = 10$, $x = 0.7$ and $c_1 = c_2 = 13$. This makes R decrease rapidly when η takes values larger than 13 (many nodes belong to level 1 but they are blocked, and few level two nodes attach to the level one nodes that are accepted by the sink). In the deterministic single-sink case, according to the propagation parameters used, and the side of the area, the majority of nodes can hear the sink and there are no

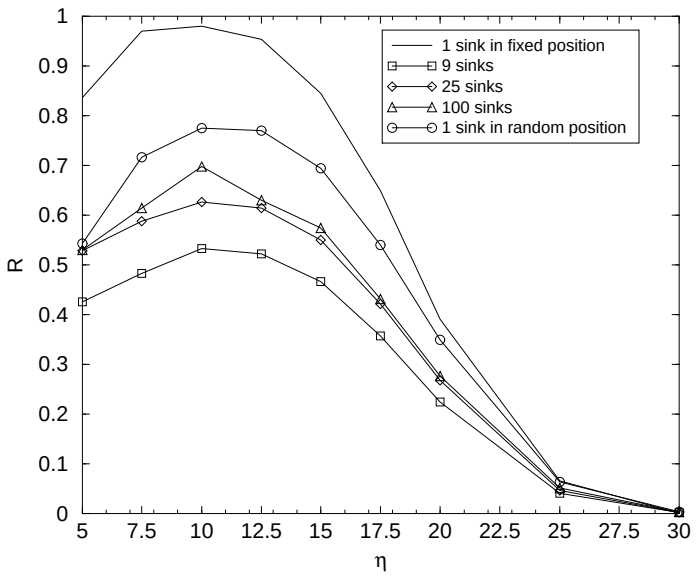

Figure 3.15: R as a function of η in the single-sink and multi-sink scenarios, with different values of M, having fixed $\Delta = 50$ and $c = 13$.

isolated nodes; thus losses are due to MAC failures and capacity constraints. In the multi-sink case, instead, R assumes smaller values, because of a larger probability to have isolated nodes that can hear no sinks. As M increases the dispersion in the number of nodes that join a sink decreases, and the distribution of the PAN sizes has smaller variance. As a result, R increases.

The distributions of the PAN sizes are reported in Fig. 3.16 for $M = 100$ and 200. They are compared to a Poisson distribution having proper mean: according to [10], in an infinite plane the PAN sizes should be Poisson distributed with mean that can be calculated starting from node and sink densities, and propagation and physical layer parameters. The Figure shows that the limited area brings to larger variances in such distributions with respect to the infinite plane case. As a result of

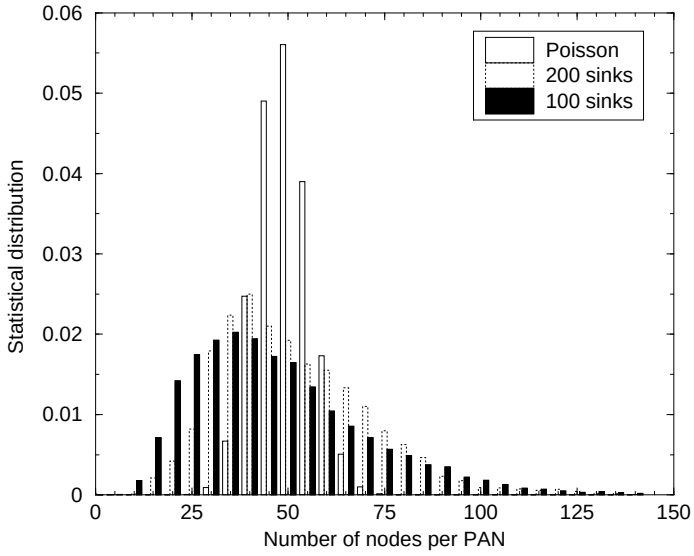

Figure 3.16: Statistical distribution of the number of nodes per PAN in the 100 sinks and 200 sinks scenarios.

such discussion, one can conclude that the multi-sink scenario gives smaller values of R when η is given, owing to the larger variances of the PAN size distributions.

In Figure 3.17 we show R as a function of η for a network having side $L = 150$ [m] (thus $M = 9$), having fixed $x = 0.7$ and $c_1 = 13$, for c_2 ranging from 3 to 13. The curves behaviour is the same observed in Figure 3.6, obtained through the mathematical model. The values of R, obtained through simulations are lower to the correspondent values obtained through the mathematical model. This is due to MAC failures and to the fact that we consider a network with $M = 9$, which is affected by border effects (here, in fact, different packets are lost for connectivity issues), whereas by increasing M (as shown in Figure 3.15), R increases (losses due to connectivity issues decrease) and for high values of M we could reach the value obtained in the mathematical model (we cannot show here results obtained for larger

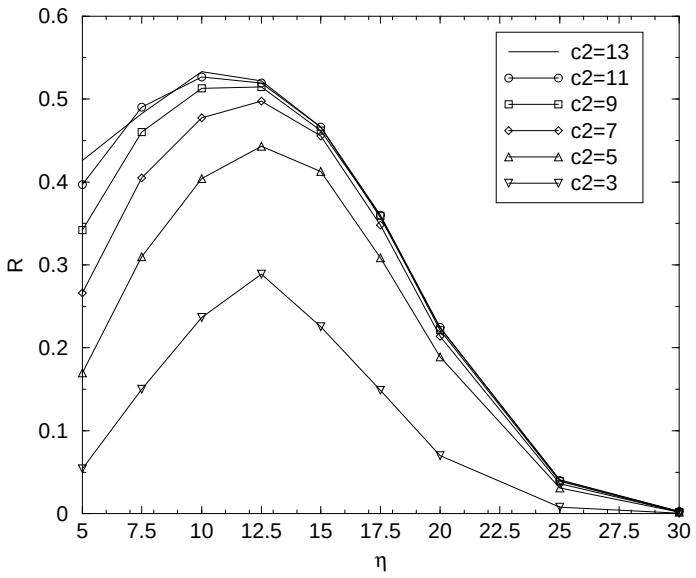

Figure 3.17: Multi-sink scenario ($M = 9$). R as a function of η for different values of c_2, having fixed $c_1 = 13$.

values of M, owing to too long simulation time needed). The other difference is that the maximum of R is obtained for different values of η; this is caused by the fact that the mathematical model requires an a priori definition of which level each node belongs to, whereas in the simulation environment a real topology formation algorithm is considered.

Finally, in Figure 3.18 two new performance metrics, W and K, are introduced. W is defined as the probability that the number of packets correctly received in the network, considering all sinks, is larger than a percentage, x, of the real number of nodes in the network. Whereas K is defined as the probability that the number of packets correctly received in the network, considering all sinks, is larger than a percentage, x, of the mean number of nodes in the network. Thus, in the Figure we

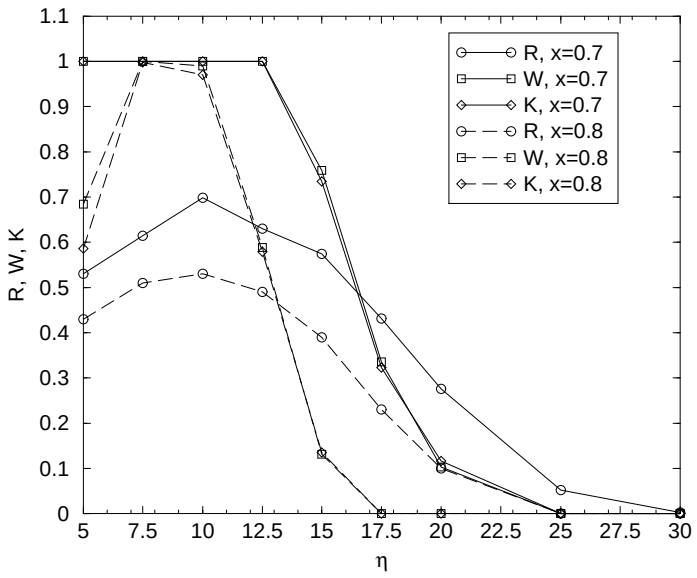

Figure 3.18: Multi-sink scenario (M=9). R, W and K as a function of η for x=0.7 and x=0.8, having fixed $c_1 = c_2 = 13$.

show R, W and K as a function of η for $x = 0.7$ and $x = 0.8$ for a network having side $L = 250$ [m] ($M = 100$), $\rho_s = 0.2$ $[m^{-2}]$, $\rho_0 = 0.002$ $[m^{-2}]$ and $c = 13$. As we can see, the W and K curves are overlapped; on the other hand, W and K show different values with respect to R. When η is smaller than the capacity limit, W and K tend to one because the distribution of the total number of nodes attached to any sink shows a smaller variance with respect to the distribution of the number n of nodes attached to a generic sink; when capacity limits become significant (for larger η), the different clusters tend to be equally limited in size and this reduces the probability of large values of the sum of all cluster sizes, thus reducing W and K.

3.5 Connectivity of Multi-Sink Multi-Hop WSNs in Bounded Regions

In this section we mathematically derive the probability that sensor nodes uniformly distributed in the monitored area are connected to at least one sink, where multiple sinks are also uniformly distributed over the same region. Starting from such a result, we also derive the probability that all nodes, or a subset of them, are connected. Such derivation is performed assuming a link power loss which takes both dependance on distance and random channel fluctuations into account (the channel model of eq. (1.6.1)) and considering border effects due to finiteness of the deployment region. The latter is assumed to be a square as it often happens (see, e.g., [95]), because of its simplicity. Nonetheless, rectangular networks exhibit very similar connectivity properties unless one side is much greater than the other [96].

The work is based on previous papers [61, 96] devoted to single hop networks. Here, bounded scenarios are accounted for, and this requires suitable consideration of the border effects. It is also shown that this model converges to the ones applied in the case of infinite plane, when the bounded region has area which is sufficiently large.

The analysis is first carried out in the case of single-hop communication (i.e., every sensor transmits the sensed data directly to a sink). Then, the multi-hop case (i.e., sensors may also act as routers) is considered assuming tree-based topologies of various heights and widths.

Finally, the mean energy consumed by the network is evaluated, and the tradeoff between connectivity and energy consumption is shown.

In the following, the connectivity model for infinite networks, which represents the starting point of the analysis, is introduced. Then, in section 3.5.2 the bounded region is introduced and the full and partial connectivity probabilities are derived for the single-hop case. In section 3.5.3 the multi-hop case is considered. In section 3.5.4 the mean energy consumption is examined and numerical results are shown in section 3.5.5.

3.5.1 Connectivity in Unbounded Single-hop Networks

The first scenario consists of an infinite bi-dimensional plane with sensors and sinks distributed according to a homogeneous PPP, with densities ρ_s and ρ_0, respectively. Since the channel model descried by eq. (1.6.1) is used, the number of audible sinks within a range of distances r_1 and r from a generic sensor node ($r \geq r_1$), $n_{r_1,r}$, is Poisson distributed with mean $\mu_{r_1,r}$, given by eq. (1.6.7) by simply substituting ρ with ρ_0. Then by letting $r_1 = 0$ and $r \to \infty$, we obtain

$$\mu_{0,\infty} = \pi\rho_0 \exp[(2(L_{\text{th}} - k_0)/k_1) + (2\sigma_s^2/k_1^2)]\,. \tag{3.5.1}$$

Equation (3.5.1) represents the mean value of the total number, $n_{0,\infty}$, of audible sinks for a generic sensor, obtained considering an infinite plane [61].

Its non-isolation probability is simply the probability that the number of audible sinks is greater than zero

$$q_\infty = 1 - e^{-\mu_{0,\infty}}\,. \tag{3.5.2}$$

3.5.2 Connectivity in Bounded Single-hop Networks

When moving to networks of nodes located in bounded domains, two important changes happen. First, even with ρ_0 unchanged, the number of sinks that are audible from a generic sensor will be lower due to geometric constraints (a finite area contains (on average) a lower number of audible sinks than an infinite plane). Second, the mean number of audible sinks will depend on the position (x, y) in which the sensor node is located in the region that we consider. The reason for this is that sensors which are at a distance d from the border, with $d \sim TR_{\rm i}$, have smaller connectivity regions and thus the average number of audible sinks is smaller. These effects, known in literature as *border effects* [57], are accounted for in our model.

The result (1.6.7) can be easily adjusted to show that the number of audible sinks within a sector of an annulus having radii r_1 and r and subtending an angle 2θ, is once again Poisson distributed with mean

$$\mu_{r_1,r;\theta} = \theta\rho_0[\Psi(a_1, b_1; r) - \Psi(a_1, b_1; r_1)], \tag{3.5.3}$$

$0 \leq \theta \leq \pi$. If the annulus extends from r to $r + \delta r$, and $\theta = \theta(r)$, this mean value becomes

$$\mu_{r,r+\delta r;\theta} = \theta(r)\rho_0 \frac{\delta\Psi(a_1, b_1; r)}{\delta r}\delta r,\ 0 \leq \theta \leq \pi. \tag{3.5.4}$$

Consider now a polar coordinate system whose origin coincides with a sensor node. As a consequence of (3.5.4), if a region is located within the two radii r_1 and r_2 and its points at a distance r from the origin are defined by a $\theta(r)$ law (see [96], Fig. 1), then the number of audible sinks in such a region is again Poisson distributed with mean $\mu_{r_1,r_2;\theta(r)} = \int_{r_1}^{r_2} \theta(r)\rho_0 \frac{d\Psi(a_1,b_1;r)}{dr} dr$, that is, from (1.6.8) and after some algebra,

$$\mu_{r_1,r_2;\theta(r)} = \int_{r_1}^{r_2} 2\theta(r)\rho_0 r\Phi(a_1 - b_1 \ln r)dr. \tag{3.5.5}$$

Now consider a square SA of side L meters and area $A = L^2$, sensors and sinks uniformly distributed on it with densities ρ_s and ρ_0, respectively. Equation (3.5.5) is suitable for expressing the mean number of audible sinks from an arbitrary point (x, y) of SA, provided that such point is considered as a new origin and that the boundary of SA is expressed with respect to the new origin as a function of r_1, r_2 and $\theta(r)$. In order to apply equation (3.5.5) to this scenario and obtain the mean number, $\mu(x, y)$, of audible sinks from the point (x, y), it is needed to set the origin of a reference system in (x, y), partition SA in eight subregions $(S_{\mathrm{r},1} \ldots S_{\mathrm{r},8})$ by means of circles whose centers lie in (x, y) (see [96], Fig. 2). Thank to the properties of Poisson r.v.'s, the contribution of each region can be summed and we obtain an exact expression for

$$\mu(x, y) = \sum_{i=1}^{8} \int_{r_{1,i}}^{r_{2,i}} 2\theta_i(r) \cdot \rho_0 \cdot r \cdot \Phi(a_1 - b_1 \ln r) dr, \tag{3.5.6}$$

which is the mean number of sinks in SA that are audible from (x, y), where $r_{1,i}$, $r_{2,i}$, $\theta_i(r)$ are reported in [96], Tables 1-2.

If we assume a single-hop network, a sensor potentially located in (x, y) is isolated (i.e., there are no audible sinks from its position) with probability $p(x, y) = e^{-\mu(x,y)}$ and it is non isolated with probability

$$q(x, y) = 1 - e^{-\mu(x,y)} \,. \tag{3.5.7}$$

Having assumed that sensor nodes are uniformly and randomly distributed in SA, if we now want to predict the probability that a randomly chosen sensor node is not isolated, we need to average $q(x, y)$ on SA. In fact, the probability that a randomly chosen sensor node is not isolated (which is an ensemble measure) and the average

non-isolation probability over a single realization coincides due to the ergodicity of stationary Poisson processes (see [97], page 104). This was also verified by simulation.

Recalling that we have considered the lower half of the first quadrant, which is one eighth of the totality, we have

$$\overline{q} = \frac{8}{A} \int_0^{L/2} \int_0^x q(x,y) dy dx. \tag{3.5.8}$$

For the sake of simplicity, we define the function $F_{\text{con}}(\cdot,\cdot)$ to be equal to the right side of (3.5.8), so that

$$\overline{q} = F_{\text{con}}(\rho_0, L). \tag{3.5.9}$$

Several results may be derived from (3.5.9). First, we compute the probability, R, that the network is fully connected (i.e. every sensor can directly reach at least one sink). Assume that we have k sensors in SA with positions $(x_1,y_1),(x_2,y_2),\ldots,(x_k,y_k)$. By indicating with F the event of full connectivity and with n_{s} the number of sensors in a scenario, we have

$$\mathbb{P}\{F|n_{\text{s}}=k;(x_1,y_1),\ldots,(x_k,y_k)\} = \prod_{i=1}^{k} q(x_i,y_i), \tag{3.5.10}$$

where we assumed that sensors connect to the sink independently from each others, which is a realistic assumption in networks that are not capacity-limited. $\mathbb{P}\{\mathcal{E}\}$ denotes the probability of the event $\mathcal{E}$.

Now, by deconditioning with respect to the nodes positions, we have

$$\begin{aligned}\mathbb{P}\{F|n_{\text{s}}=k\} = &\underbrace{\int \ldots \int}_{2k} \prod_{i=1}^{k} q(x_i,y_i) f_{X_1,Y_1}(x_1,y_1)\ldots \\ &\ldots f_{X_k,Y_k}(x_k,y_k) dx_1 dy_1 \ldots dx_k dy_k \\ = &\left[\int\int q(x_1,y_1) f_{X_1,Y_1}(x_1,y_1) dx_1 dy_1\right] \cdot \ldots \\ &\ldots \cdot \left[\int\int q(x_k,y_k) f_{X_k,Y_k}(x_k,y_k) dx_k dy_k\right],\end{aligned}$$

$$f_{X_i,Y_i}(x_i,y_i) = \begin{cases} 1/A, & (x_i,y_i) \in SA \\ 0, & \text{otherwise} \end{cases}$$

is the p.d.f. of the position of the ith node.

Note now that the same assumption (i.e., uniform distribution) holds for all nodes, thus we have

$$\mathbb{P}\{F|n_{\mathrm{s}}=k\} = \left[\int\int q(x,y) f_{X,Y}(x,y)dxdy\right]^k \tag{3.5.11}$$

$$= \left[\frac{1}{A}\int_{-L/2}^{L/2}\int_{-L/2}^{L/2} q(x,y)dxdy\right]^k \tag{3.5.12}$$

$$= \left[\frac{8}{A}\int_0^{L/2}\int_0^{x} q(x,y)dydx\right]^k = \overline{q}^k. \tag{3.5.13}$$

Since n_{s} is Poisson distributed with mean $\rho_s A$, we can decondition (3.5.13) with respect to n_{s} and obtain

$$Z = \mathbb{P}\{F\} = \sum_{k=1}^{+\infty} \mathbb{P}\{F|n_{\mathrm{s}}=k\} \cdot \mathbb{P}\{n_{\mathrm{s}}=k\}$$

$$= \sum_{k=1}^{+\infty} \bar{q}^k \cdot \frac{e^{-\rho_s A}}{k!}(\rho_s A)^k. \tag{3.5.14}$$

Equation (3.5.14) represents the probability that a sensor network performs at best (full connectivity), but the event F turns out to be a strict requirement for most of them. In other words, for many applications it is sufficient to guarantee that a certain amount of sensors can transmit their data to the sinks. For this reason, it is of interest to compute the probability of the event, C_j, of having at least a number, j, of connected sensor (partial connectivity). We first consider the event C_j^* of having exactly j connected sensors. When $n_{\mathrm{s}} = k$, the probability of having j connected sensors is

$$\mathbb{P}\{C_j^*|k\} = \binom{k}{j} \bar{q}^j (1-\bar{q})^{k-j}, \tag{3.5.15}$$

$j \leq k$, where the binomial coefficient $\binom{k}{j} = \frac{k!}{j!(k-j)!}$ accounts for all the possible ways to group j sensors out of k. Note that for the events C_j and C_j^* the following holds:

$$C_j = \{C_j^* \cup C_{j+1}^* \cup \ldots \cup C_k^*\}. \tag{3.5.16}$$

Thus, if we consider the event C_j we need to add contributions similar to (3.5.15) for all j, $j \leq k$, to obtain

$$\mathbb{P}\{C_j | n_{\mathrm{s}} = k\} = \sum_{l=j}^{k} \binom{k}{l} \bar{q}^l (1-\bar{q})^{k-l}, \tag{3.5.17}$$

$j \leq k$. Once again, by deconditioning (3.5.17) with respect to n_{s} we have

$$\begin{aligned} \mathbb{P}\{C_j\} &= \sum_{k=j}^{+\infty} \mathbb{P}\{C_j|k\} \cdot \mathbb{P}\{k\} \\ &= \sum_{k=j}^{+\infty} \sum_{l=j}^{k} \binom{k}{l} \bar{q}^l (1-\bar{q})^{k-l} \cdot \frac{e^{-\rho_s A}}{k!} (\rho_s A)^k. \end{aligned} \tag{3.5.18}$$

Note that the outer sum in (3.5.18) starts at j instead of 1, because when $k < j$ it gives no contribution (i.e., the probability of having j connected sensors in a network with less than j sensors is zero). For this reason, we want to highlight the fact that $\mathbb{P}\{C_j\}$ of (3.5.18) depends also on ρ_s: in fact, the probability of having at least j connected sensors is affected, besides $\bar{q}$, also by how many sensors we have at all in the network (i.e., either connected or not). In order to emphasize this, a new notation, $Z_{\bar{m}}(j)$, is introduced and, after some simple algebra, we have

$$\begin{aligned} Z_{\bar{m}}(j) &= \mathbb{P}\{C_j\} \\ &= e^{-\bar{m}} \cdot \sum_{k=j}^{+\infty} \sum_{l=j}^{k} \binom{k}{l} \frac{\bar{m}^k \bar{q}^l (1-\bar{q})^{k-l}}{k!}, \end{aligned} \tag{3.5.19}$$

with $\bar{m} = \rho_s A$ being the average number of sensors in SA. Thus, $Z_{\bar{m}}(j)$ of (3.5.19) has the meaning of probability of having at least j connected sensors in a network with (on average) $\bar{m}$ sensors.

3.5.3 Connectivity in Bounded Multi-hop Networks

Now we wish to extend our analysis to the case of multi-hop wireless sensor networks. Each sensor is allowed to forward its data to another sensor instead of trying to communicate directly with the sinks, with the constraint of a fixed maximum number of hops.

The *a-priori* partitioning of nodes described in section 3.3 is considered also here. Each node belongs to one out of T levels, meaning that an i-th level node can send its data only to an $(i-1)$-th level node, hence, it will take i hops to such a node to communicate with a sink (which is considered a zero level node according to this formalism). This approach is justified by the fact that in some classes of sensor networks each node has a certain probability p_i to be a level i node, with $i \in [0, T]$ (p_0 is the probability of being a sink). Thus the parental relations between nodes are in some sense pre-assigned. If ρ_{tot} is the overall nodes density (i.e., $\rho_{\text{tot}} = \rho_0 + \rho_s$) and ρ_s is the overall sensor nodes density, we have for the generic i-th level density $\rho_i = \rho_{\text{tot}} \cdot p_i,\ 0 \leq i \leq T$, with $\sum_{i=0}^{T} \rho_i = \rho_{\text{tot}}$ and $\sum_{i=1}^{T} \rho_i = \rho_s$. We also assume that nodes at each level are uniformly distributed in SA.

We now want to find the probability $\bar{q}_1$ that a randomly chosen sensor is connected and that it is one hop away from the sink. In terms of the F_{con} function introduced in (3.5.9), we can write

$$\bar{q}_1 = p_1 \cdot F_{\text{con}}(\rho_0, S), \tag{3.5.20}$$

where the two factors account for the events of belonging to the 1st level and being actually connected to a sink, respectively. Note that $\bar{q}_1$ of (3.5.20) has the same meaning of $\bar{q}$ in (3.5.8) when $T = 1$. If we consider multi-hop paths, we can define the probability $\bar{q}_i$ that a randomly chosen sensor has a connection to the sink through

a path containing at most i hops. In other words, it must be a connected 1st level sensor, or a connected 2nd level sensor, ..., or a connected i-th level sensor. As an example, the probability $\bar{q}_2$ may be written as

$$\begin{aligned}\bar{q}_2 &= p_1 \cdot F_{\text{con}}(\rho_0, L) + p_2 \cdot F_{\text{con}}(\rho_{\text{tot}} \cdot \bar{q}_1, L) \\ &= \bar{q}_1 + p_2 \cdot F_{\text{con}}(\rho_{\text{tot}} \cdot \bar{q}_1, L),\end{aligned} \tag{3.5.21}$$

where $p_2 \cdot F_{\text{con}}(\rho_{\text{tot}} \cdot \bar{q}_1, L)$ is the probability that the sensor belongs to level 2 and has a connection to any 1st level sensor which is, in turn, connected to a sink. As for $\bar{q}_3$, the chain is one hop longer, thus we need to write

$$\bar{q}_3 = \bar{q}_2 + p_3 \cdot F_{\text{con}}(\rho_{\text{tot}} \cdot p_2 \cdot F_{\text{con}}(\rho_{\text{tot}} \cdot \bar{q}_1, L), L). \tag{3.5.22}$$

In general, for an T-level network we have the recursive expression

$$\begin{aligned}\bar{q}_T = \bar{q}_{T-1} &+ p_T \cdot F_{\text{con}}(\rho_{\text{tot}} \cdot p_{T-1} \\ &\cdot F_{\text{con}}(\ldots \rho_{\text{tot}} \cdot p_2 \cdot F_{\text{con}}(\rho_{\text{tot}} \cdot \bar{q}_1, L) \ldots, L), L),\end{aligned} \tag{3.5.23}$$

with (3.5.20) providing expression for $\bar{q}_1$.

We can now introduce the probability, $Z^{(T)}$, of having all sensors connected in an T-level network by following the same reasoning as in the 1-hop case (see equations (3.5.13-3.5.14)). We recognize that, once the parameters of the network A and ρ_s are fixed, the only difference between the 1-hop and the multi-hop case resides in how the non-isolation probability is computed, i.e., we have $\bar{q}$ for the 1-hop case and $\bar{q}_T$ for the multi-hop case. In virtue of this, we can generalize (3.5.14) as

$$Z(x) = \sum_{k=1}^{+\infty} x^k \cdot \frac{e^{-\rho_s A}}{k!}(\rho_s A)^k, \tag{3.5.24}$$

where we preserved the structure and set the non-isolation probability as variable. Recalling (3.5.15-3.5.19), we find that the same holds for (3.5.19), which yields

$$Z_{\bar{m}}(j;x) = e^{-\bar{m}} \cdot \sum_{k=j}^{+\infty} \sum_{l=j}^{k} \binom{k}{l} \frac{\bar{m}^k x^l (1-x)^{k-l}}{k!}, \tag{3.5.25}$$

where we set, once again, the non-isolation probability as variable. Thus, for $Z^{(T)}$ we can simply use (3.5.24) with $x = \bar{q}_T$, getting

$$Z^{(T)} = Z(\bar{q}_T) = \sum_{k=1}^{+\infty} \bar{q}_T^k \cdot \frac{e^{-\rho_s A}}{k!} (\rho_s A)^k. \tag{3.5.26}$$

Similarly, we also compute the probability, $Z_{\bar{m}}^{(T)}(j)$, of having at least j connected sensors in an T-level network with (on average) m sensors by using (3.5.25) with $x = \bar{q}_T$ and obtain

$$\begin{aligned} Z_{\bar{m}}^{(T)}(j) &= Z_{\bar{m}}(j;\bar{q}_T) \\ &= e^{-\bar{m}} \cdot \sum_{k=j}^{+\infty} \sum_{l=j}^{k} \binom{k}{l} \frac{\bar{m}^k \bar{q}_T^l (1-\bar{q}_T)^{k-l}}{k!}. \end{aligned} \tag{3.5.27}$$

The way in which the densities ρ_i ($i \geq 1$) are defined can follow, as an example and without loss of generality, the simple partitioning criterion

$$\rho_{i+1}/\rho_i = \eta, \quad 0 \leq i < T, \tag{3.5.28}$$

where η is a constant (i.e., level densities follow an exponential growth, which is kind of a 'natural' law in hierarchical networks). Note that (3.5.28) holds only for $i < T$: in fact, if we fix ρ_0 and ρ_s, the T-th level nodes must have density $\rho_T = \rho_s - \sum_{j=1}^{T-1} \rho_j$ in order for the sensor densities to sum up to ρ_s. Moreover, by fixing ρ_0, ρ_s and η (or equivalently ρ_0, $\Delta = \rho_s/\rho_0$ and η), there are no longer degrees of freedom and the number R of levels in the network is also consequently assigned.

3.5.4 Energy Consumption

We assume that each node consumes energy when transmits and receives packets, whereas we neglect the energy spent by the node to stay in idle or sleeping states. We also assume that the sinks do not have energy consumption problems, thus we do not consider the energy spent by them. The mean energy spent in the network for each transmission towards the sink is given by

$$E = \sum_{i=1}^{T} [E_{rx} + E_{tx} \cdot i + E_{rx} \cdot (i-1)] \cdot (\overline{q}_i - \overline{q}_{i-1}), \tag{3.5.29}$$

where E_{rx} is the energy spent to receive a packet, E_{tx} is the energy spent to transmit a packet, and $\bar{q}_i$ is given by (3.5.20), (3.5.21), (3.5.22) and (3.5.23). $(\overline{q}_i - \overline{q}_{i-1})$ is the probability that a generic node belongs to level i of a connected tree. The energy spent in the network to deliver a packet from a source node to the final sink, instead, depends on the level at which the source node is located. In particular, if the source node is at level one, the packet can reach the sink through a single transmission; if, instead, the node is at level two its packet must be (i) transmitted by the source node, (ii) received by the level one node and (iii) transmitted by the latter node to the final sink, therefore two transmissions and one reception are needed. We also consider the energy spent by each node to receive the triggering packet coming from its parent in the tree (tree formation). According to the Freescale devices data sheets [93], we set the energy spent to transmit a bit equal to 0.3 $[\mu J/bit]$ and the energy spent to receive a bit equal to 0.33 $[\mu J/bit]$. Moreover, we set the packet size equal to 20 bytes, therefore $E_{tx} = 48$ $[\mu J]$ and $E_{rx} = 52.8$ $[\mu J]$.

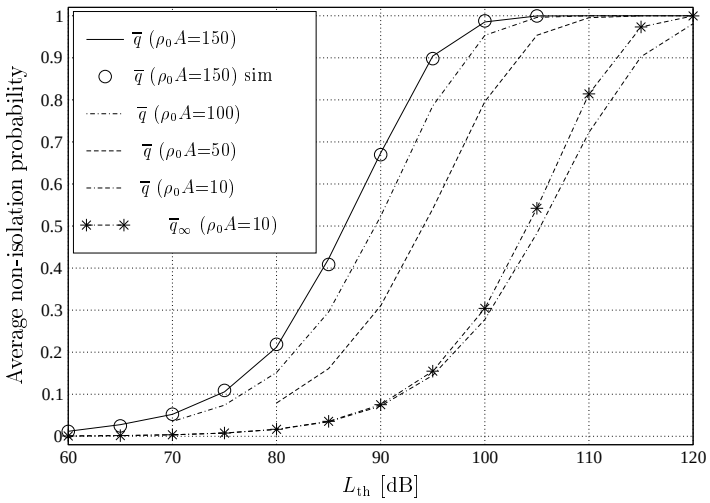

Figure 3.19: $\overline{q}$ as a function of $L_{\rm th}$ for different values of ρ_0, with $L = 1000$ [m], $k_0 = 40$ [dB], $k_1 = 13.03$, $\sigma_s = 3.5$ [dB].

3.5.5 Numerical Results

Fig. 3.19 shows $\overline{q}$ for different sink densities as a function of $L_{\rm th}$, proportional to the transmit power if the receiver sensitivity is fixed: clearly, as such density grows, for a fixed transmit power it is more likely for a sensor to reach at least a sink and thus $\overline{q}$ also grows. For example, if we want a randomly chosen sensor to be connected with 90% probability, we need $L_{\rm th} \approx 95$ [dB] when $\rho_0 A = 150$, $L_{\rm th} \approx 98$ [dB] when $\rho_0 A = 100$, $L_{\rm th} \approx 103$ [dB] when $\rho_0 A = 50$ and $L_{\rm th} \approx 115$ [dB] when $\rho_0 A = 10$. Also note the comparison to the curve for q_∞ obtained with no consideration of border effects: the error becomes non negligible for transmission ranges which are of the same size as the side L of the domain (e.g., $TR_{\rm i}(L_{\rm th} = 115[\text{dB}]) \approx 316$ [m]), a typical case for WSNs.

In Figs. 3.20 and 3.21 connectivity results related to multi-hop WSNs are reported. The criterion of a-priori partitioning is used in accordance with (3.5.28). Observe that for $T = 5\ \eta$ ranges from 1.9 to 2.3. This means that when $\eta = 2.3$ the network has 4

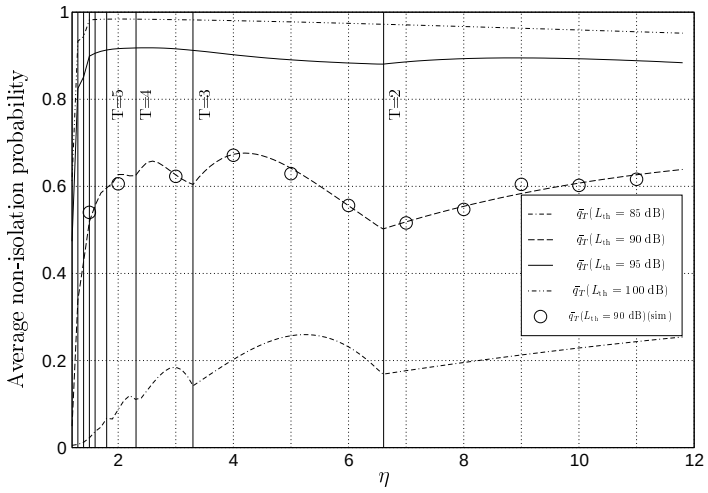

Figure 3.20: $\bar{q}_T$ as a function of η with $\rho_0 = 50/L^2$, $\rho_s = 2500/L^2$ ($\Delta = 50$), $L = 1000$ [m], $k_0 = 40$ [dB], $k_1 = 13.03$, $\sigma_s = 3.5$ [dB].

levels or, equivalently, 5 levels with the 5th being empty. $\bar{q}_R$ and $Z_{\bar{m}}^{(T)}(j)$ are plotted as functions of η, respectively. They show arches and local optima which depend on the loss threshold $L_{\rm th}$, η and T. In particular, from Fig. 3.20, we conclude that a large value of T is opportune only if $L_{\rm th}$ (and, consequently, the transmit power) is large enough: in fact, when $T = 5$ (η ranging from 1.9 to 2.3) we have global optima for $L_{\rm th} = 95$ [dB] and $L_{\rm th} = 100$ [dB] but only local optima for $L_{\rm th} = 85$ [dB] and $L_{\rm th} = 90$ [dB].

Finally, in Figure 3.22 we show the mean energy spent, E, as a function of η and T for different values of $L_{\rm th}$. As we can see E increases by increasing T, since (on average) more transmissions and receptions are needed to reach the sink. Therefore, for large values of $L_{\rm th}$ a tradeoff between connectivity and energy consumption should be found: in fact, large T improves connectivity but also increases energy consumption. Moreover, the evaluation of the energy consumption behavior is useful to select the optimum values of η and T, for a desired degree of connectivity. As an example,

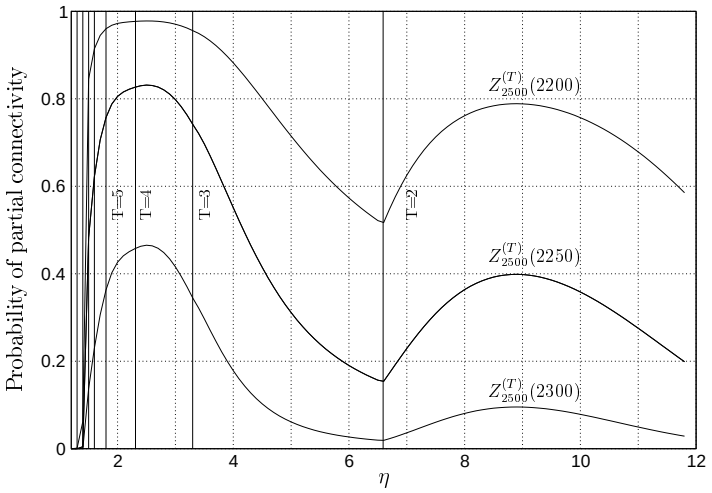

Figure 3.21: $Z^{(T)}_{2500}(2200)$, $Z^{(T)}_{2500}(2250)$ and $Z^{(T)}_{2500}(2300)$ as functions of η with $L_{\rm th} = 95$ [dB], $\rho_0 = 50/L^2$, $\rho_s = 2500/L^2$ ($\Delta = 50$), $L = 1000$ [m], $k_0 = 40$ [dB], $k_1 = 13.03$, $\sigma_s = 3.5$ [dB].

when we set $L_{\rm th} = 90$ [dB], we obtain approximatively the same maximum of $\bar{q}_T$ for $T = 4$ and $T = 3$; however, the consumed energy is notably larger for $T = 4$.

3.6 Conclusions

A novel mathematical model for studying the connectivity of multi-sink WSNs over unbounded and bounded regions, has been proposed. The practical outcome of this approach is the possibility: i) to set the proper power level of nodes and their density, given a requirement in terms of connectivity; ii) to select the optimum height and average number of children per parent in the tree; iii) to evaluate the trade-off between connectivity and energy consumption. As an example, results of Fig. 3.19 could be useful to fix the sinks density, once the transmit power (i.e., $L_{\rm th}$), is set: the application requires a minimum average non isolated probability, $\bar{q}$, that must be satisfied and, once $L_{\rm th}$ is fixed (being defined the technology used), we can obtain the

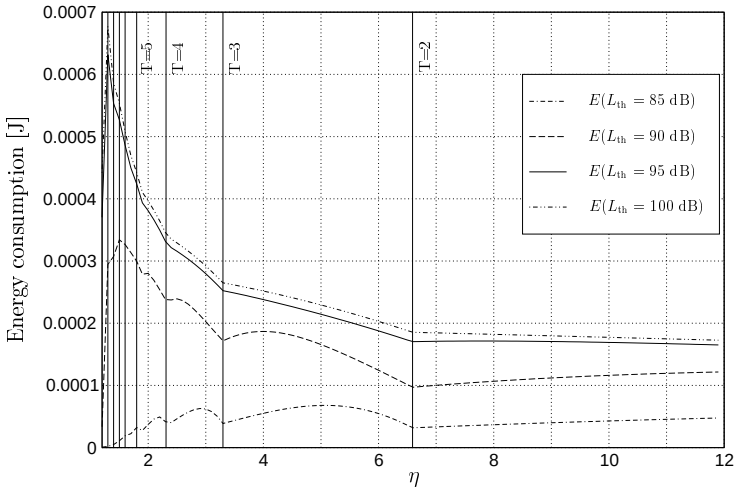

Figure 3.22: Average energy consumption E [J] as a function of η with $\rho_0 = 50/L^2$, $\rho_s = 2500/L^2$ ($\Delta = 50$), $L = 1000$ [m], $k_0 = 40$ [dB], $k_1 = 13.03$, $\sigma_s = 3.5$ [dB].

average number of sinks that must be distributed in the network. Similarly, once the sink density is fixed we can obtain the power that must be used for transmissions. Similarly, from Fig. 3.20, as an example, if the application requires $\bar{q}_T \geq 0.6$ and $L_{\text{th}}$is set to 90 [dB], $T = 4$ or 3 and $\eta \simeq 4$ should be set. But being the case $T = 3$ less energy expensive, it will be the best choice, satisfying the requirement.

The main limit of the mathematical models developed in this Chapter is that no MAC issues are accounted for. In fact, in section 3.4 a capacity constrained air interface is assumed, so that resources can be allocated to nodes and no contentions are present. However contention-based protocols are more suitable for WSNs. In this case, an hard capacity constraint, as that introduced here, does not exist, even if a sort of soft constraint could be defined. This constraint is due to the fact that, as will be clear in the following, the increasing of the number of nodes competing for the channel significantly decreases the success probability, therefore not too many nodes should be allowed to try to access the channel simultaneously. To account for

a contention-based protocol, in the following Chapter the MAC protocol defined by the 802.15.4 is modeled and in Chapter 5 the model described in section 3.5 of this Chapter is integrated with the one presented in Chapter 4, to study WSNs under a new perspective.

Chapter 4

Performance Analysis of the IEEE 802.15.4 MAC protocol

As stated in Chapter 1, the IEEE 802.15.4 MAC protocol allows two types of channel access mechanisms: beacon- or non beacon-enabled. The latter case uses unslotted CSMA/CA channel access mechanism, whereas bacon-enabled networks use both contention-based (a slotted CSMA/CA) and contention-less mechanisms to access the channel. In this Chapter an analytical model for both the modalities, is provided.

We consider a WSN composed of a number of sensor devices (hereafter denoted as *nodes*); each node upon reception of a query from the PAN coordinator (denoted as *sink* in the following) takes one sample of a given phenomenon (e.g., atmospheric pressure or temperature) and forwards it through a direct link, or possibly through multiple hops, to the sink. The nodes compete to access the channel, to transmit the data required. Once transmission is performed, they move to an idle state, till the next query is received. The interval of time between two successive queries is denoted as *round*, and its duration is denoted as T_q. Note that in the beacon-enabled case, the query coincides with the beacon packet and the round is the beacon interval, therefore $T_q = BI$ (see eq. (1.4.1)), which means that T_q may assume only a finite

set of values. Whereas in the non beacon-enabled case, T_q may assume whatever a value.

Concerning network topology, both stars and tree-based topologies are accounted for, in this Chapter. Star topologies are preferable when the PAN area is small; the number of nodes that could be associated to the sink, in fact, should range from three to seven, as it is widely accepted that 802.15.4 does not support larger network sizes in this case [82]. Nevertheless, for the sake of completeness and validation of the model, also results for networks composed of a number of nodes larger than seven, are shown. Trees, instead, are used in case of large networks. Since trees can be formed only when nodes operate in the beacon-enabled mode [51], this topology is implemented only in this modality.

Given this scenario, the aim of the model is to provide an analytical description of the transitions between node states (backoff, sensing, transmit, idle) of the CSMA/CA algorithm.

The mathematical model developed, allows the evaluation of the statistical distribution of the traffic generated by the nodes. In particular, the statistics of the delays with which the nodes access to the channel, and with which their packets are received by the sink, are provided. The knowledge of the statistics of the traffic generated by the PAN, is useful, for example in those applications in which the sink acts as gateway toward an infrastructure-based wireless network (e.g., UMTS). Such knowledge is, in fact, useful to schedule radio resources for the gateway (see the Appendix).

The model is then finalized to derive the probability that a node succeeds when accessing the channel, and in transmitting its packet, the overall throughput generated by the network and the energy consumption.

To validate the mathematical model, comparison to simulations is performed.

The model differs from those previously published by other authors in the literature as it precisely follows the MAC procedure defined by the standard, in the context of the WSN scenario described.

In the Chapter, after an overview of the literature, the two models related to the two modalities with the results are given. Finally, a comparison between the two modalities is provided.

4.1 Related Works

In the literature, performance evaluation of the 802.15.4 MAC protocol has been carried out by means of simulation for small and low-load networks in [98] and for dense networks in [99]. In [100] the performance of the beacon-enabled slotted CSMA/CA is evaluated through ns-2 simulator for different network settings to understand the impact of the protocol attributes (superframe order, beacon order and backoff exponent) on network performance. Also, some studies have tried to describe analytically the behavior of the 802.15.4 MAC protocol. Few works devoted their attention to non beacon-enabled mode [101]; most of the analytical models are related to beacon-enabled networks [102–106].

In [101], the authors try to model the unslotted CSMA/CA protocol for non beacon-enabled networks, but they do not capture correctly the protocol, because they include in the Markov chain two subsequent sensing phases, and not one, as fixed in the standard (see section 4.2).

The analytical models for the slotted CSMA/CA 802.15.4 protocol developed in [102], [103], [104] fail to match simulation results (see [105]), as the authors use the

same Markov formulation and assumptions made by Bianchi in [107], where the 802.11 MAC protocol is considered. This protocol, in fact, is significantly different from the one defined by the 802.15.4 standard (see section 4.2). A better, even if similar, model is proposed in [106] and [108], where, however, the sensing states are not correctly captured by the Markov chain. In [105] the main gaps of the previous models are overcome. However, in all the previous works, [101], [105], and [106], the probability to find the channel busy is evaluated regardless of the backoff stage in which the node is. This model, instead, captures the different probabilities (i.e., the probability of being in sensing, of finding the channel busy, etc.) at the different backoff stages.

In contrast with these works, this thesis provides a new analytical model, which predicts the statistical distribution of the traffic generated by an 802.15.4 WSN, by using a two-dimensional chain analysis. The form of the analysis is similar in some aspects to the one used by Bianchi [107], but, owing to the differences between the two CSMA/CA algorithms defined in the standards, Bianchi's model cannot be applied to the 802.15.4 MAC protocol, and a new model is needed.

Furthermore, all the works cited here studied the asymptotic behavior of the network, i.e., the behavior of the system at the equilibrium conditions, evaluating the stationary probabilities, obtained when time, t, tends to infinite ($t \to \infty$). This analysis, instead, evaluates the statistical distribution of some metrics (the probability that a node succeeds when accessing the channel, that a node transmits its packet correctly, and that the sink receives a packet) over time, starting from the reception of the query sent by the sink.

Another important difference between this model and the aforementioned models is that those studies assume that nodes have always [105–107], or with a certain

probability [101–104] a packet to be transmitted. In this case, when a node succeeds in transmitting its packet, it will start again the backoff algorithm, possibly with a certain probability: this assumption makes the Markov chain close and simplifies the analysis. Therefore, the number of nodes that have to compete for the channel is known (or is defined with a simple statistical distribution). In the model proposed here, instead, we assume that nodes are triggered by the sink, which then waits for the replies; each node has only one packet per round to be transmitted, as usual in WSN scenarios. Therefore, the number of nodes competing for channel access decreases with time. The probability of being in a certain state (sensing, transmission, or backoff) thus depends on time.

4.2 The Non Beacon- and Beacon-Enabled MAC protocols

The details of the non beacon- and beacon-enabled MAC protocols are reported here even if they have been introduced in Chapter 1, to facilitate the reading of this Chapter.

As stated in Chapter 1, in the non beacon-enabled mode nodes use an unslotted CSMA/CA protocol, implemented using units of time called backoff periods, having a duration denoted as d_{bo}, equal to $20T_s$, where $T_s = 16$ $[\mu sec]$ is the symbol time [52].

Each node maintains two variables for each transmission attempt: NB and BE. NB is the number of times the CSMA/CA algorithm was required to backoff while attempting the current transmission; this value will be initialized to 0 before each new transmission attempt and cannot assume values larger than NB_{max}, equal to

4. BE is the backoff exponent related to the maximum number of backoff periods a node will wait before attempting to assess the channel. BE will be initialized to the value of BE_{min}, equal to 3, and cannot assume values larger than BE_{max}, equal to 5. Figure 4.1 illustrates the steps of the CSMA/CA algorithm, starting from when the node has data to be transmitted. First, NB and BE are initialized and then the MAC layer will delay any activities for a random number of backoff periods in the range (0, 2^{BE}-1) [step (1)]. After this delay, channel sensing is performed for one unit of time [step (2)]. If the channel is assessed to be busy [step (3)], the MAC sublayer will increase both NB and BE by one, ensuring that BE is not larger than BE_{max}. If the value of NB is less than or equal to NB_{max}, the CSMA/CA algorithm will return to step (1). If the value of NB is larger than NB_{max}, the CSMA/CA algorithm will terminate with a "Failure," meaning that the node does not succeed in accessing the channel. If the channel is assessed to be idle [step (4)], the MAC layer will begin transmission of data immediately ("Success" in accessing the channel).

In the beacon-enabled mode [52], a superframe, starting with the beacon packet (corresponding to the query in the scenario considered here), transmitted by the sink, is established.

As stated above the duration of the whole superframe (including active and inactive parts) is BI, given by eq. (1.4.1), whereas the duration of the active part of the superframe, containing CAP and CFP, namely the superframe duration, is $SD = 16 \cdot 60 \cdot 2^{SO} \cdot T_s$.

In the star topology case, we set $SO = BO$, therefore $BI = SD = T_q$ (hereafter denoted as T_q for the star topology case) and no inactive part is present, whereas the

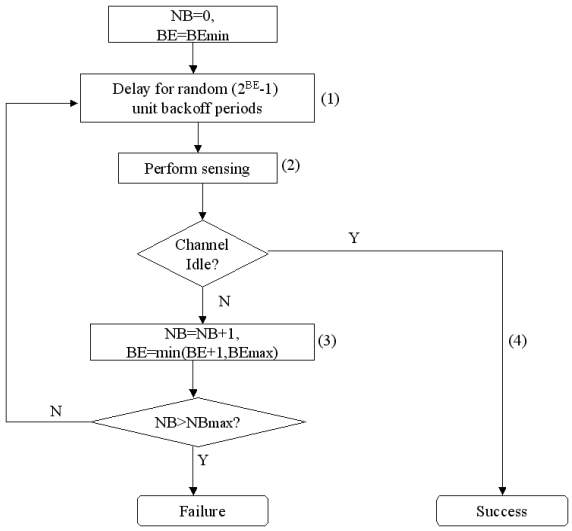

Figure 4.1: The IEEE 802.15.4 CSMA/CA algorithm in the non beacon-enabled case.

cases $SO \leq BO$ are considered in the tree topology case. According to the standard, each GTS must have a duration multiple of $60 \cdot 2^{SO} \cdot T_s$; we denote this duration as d_{GTS}, equal to $D_{GTS} \cdot 60 \cdot 2^{SO} \cdot T_s$, with D_{GTS} integer (see Figure 4.2, above part). Since an inter-frame space, equal to 40 T_s, between two successive packets received by the sink must be guaranteed [52], D_{GTS} is chosen such that the GTS may contain the packet and the inter-frame space. The sink may allocate up to seven GTSs, but a minimum CAP duration of 440 T_s, must be guaranteed.

For what concerns the CSMA/CA algorithm used in the CAP portion of the superframe the only difference with the non beacon-enabled case is that nodes have to find the channel free for two subsequent backoff periods before transmitting the packet (see Figure 1.13). To this aim, each node maintains another variable, called CW, denoting the number of backoff periods that need to be clear of channel activity

before the transmission can start. First, CW is initialized to 2. When channel sensing is performed for one backoff period [step (2)], if the channel is assessed to be busy, CW is set to 2 and if $NB < NB_{max}$ the algorithm returns to step (1); otherwise the algorithm will unsuccessfully terminate, meaning that the node does not succeed in accessing the channel. If the channel is assessed to be idle, instead, CW is decremented by 1 and compared with 0. If $CW > 0$, the algorithm returns to step (2); otherwise a transmission may start.

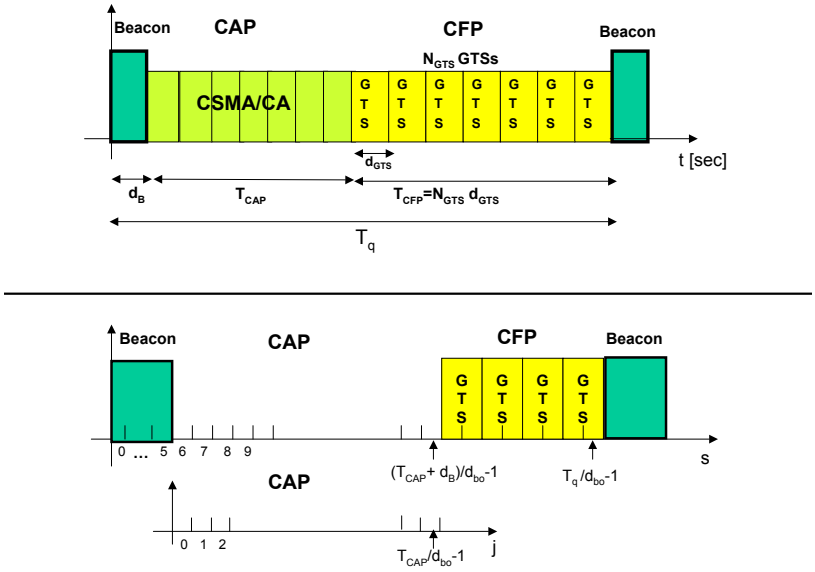

Figure 4.2: The IEEE 802.15.4 superframe, considering the time axis, t, (above part), and the number of slots, s, (below part).

4.3 Reference Scenario and Model Assumptions

We consider N nodes in the network. We assume that each node transmits a packet, having size, z, equal to $D \cdot 10$ bytes, being D an integer. The time needed to transmit a packet will be equal to $D \cdot d_{bo}$, as a bit rate of 250 [kbit/sec] is used; therefore, each packet occupies D backoff periods. We also set the query (i.e., the beacon in the beacon-enabled case) size equal to 60 bytes, and denoting the time needed to transmit this packet as d_B, we have $d_B = 120\ T_s$.

Finally, in the beacon-enabled case, we set the GTSs duration equal to the minimum possible duration which allows to contain the packet and the inter-frame space, occupying 2 backoff periods. Therefore, $D_{GTS} = \lceil (D+2)/(3 \cdot 2^{SO}) \rceil$, and the number of backoff periods occupied by each GTS is equal to $D_{GTS} \cdot 3 \cdot 2^{SO}$.

Ideal channel conditions are assumed: all nodes can "hear" each other, and, therefore, no hidden terminal problem is accounted for. Similar scenarios and assumptions are considered in many studies in the literature [98–107]. Collisions between nodes may occur in case two or more nodes perform channel sensing at the same time, find the channel free and transmit simultaneously their packets. For the sake of energy efficiency, no acknowledge and retransmission mechanism is implemented; therefore, when a packet collides it is definitely lost in that round.

In the model, the resolution time (hereafter denoted as slot) is set equal to the backoff period, d_{bo}, which corresponds also to the duration of the single sensing phase and to the packet transmission time when $D = 1$.

In the non beacon-enabled mode, it is assumed that all nodes start the backoff algorithm at the same time, when the query transmitted by the sink is received (no propagation delay is present due to short distances), and we fix the origin of the time

axis ($t = 0$) at the instant in which all nodes receive the query. Then, the behavior of the network from $t = 0$ to the instant in which all possible transmissions have taken place (as will be clarified in the following, in fact, there exists a maximum delay affecting packets transmissions), is modeled.

In the beacon-enabled case, instead, the origin of time axis is fixed at the beginning of the superframe ($t = 0$), therefore nodes will receive the beacon and they will start the CSMA/CA algorithm at $t = d_B$ (see Figure 4.2 above part). Therefore, the alignment between the first backoff period of each node and the beginning of the beacon transmission, is ensured. In case a node does not succeed in accessing the channel or in transmitting the packet correctly (i.e., without collisions), by the end of the superframe, the packet will be lost. Since one of the aims of the model is to derive the statistic of the traffic generated by nodes in the whole superframe, the behavior of the network in each slot, will be studied. In the following we denote as s, the s-th slot in the supeframe, being $s \in [0, T_q/d_{bo} - 1]$ (see Figure 4.2, below part).

4.4 The Non Beacon-Enabled Model

In this part of the Chapter the non beacon-enabled model is presented, starting from the modelling of node states, passing through the description of the finite-state transition diagram developed to model all the possible states in which a node could be and the transitions between the states, ending with the derivation of performance metrics. Finally, numerical results are shown. Have in mind that in this modality only the star topology case is accounted for, since according to Zigbee specifications trees could be formed only when nodes work in the beacon-enabled mode.

4.4.1 Node States

Generally speaking, a node accessing the channel during a round can be in one of four states: backoff, sensing, transmission, or idle. However, if after sensing the channel is free, transmission immediately occurs, followed by a sequence of idle states till the end of the round. Thus, given the objectives of this work, only the backoff and sensing states, must be modeled.

The node state is modelled as a bidimensional process $Q(\hat{t}) = \{BO_c(\hat{t}), BO_s(\hat{t})\}$, where $\hat{t}$ is an integer, representing the time slot and, more precisely, the j-th slot (from $j \cdot d_{bo}$ to $(j+1) \cdot d_{bo}$) is denoted by $\hat{t} = j$. $BO_c(\hat{t})$ and $BO_s(\hat{t})$ represent the backoff time counter and the backoff stage at time $\hat{t}$, respectively. Both are time-discrete stochastic processes assuming discrete values. Therefore, the process is a chain; however, it is not a Markovian chain [109] because $BO_c(\hat{t})$ is not a memoryless process as its value depends on its history (i.e., its value depends on how many times the node has tried to access the channel without success).

The initial value of backoff time counter, $BO_c(0)$, is uniformly distributed in the range $[0, W_{NB}-1]$, where $W_{NB} = 2^{BE}$ is the dimension of the contention window and $NB \in [0, NB_{max}]$. The value of BE depends on the second process characterizing the state: $BO_s(\hat{t})$. We can identify $NB_{max}+1$ different backoff stages obtained by considering the different possible combinations of the pair (NB, BE). In Table 4.1, the different backoff stages with the correspondent W_{NB} values (denoted as W_0 ,.., $W_{NB_{max}}$) are shown.

The 802.15.4 MAC protocol states that at the beginning of the backoff algorithm, each node sets $NB = 0$ and $BE = 3$ (corresponding to $W_0 = 8$). Then, each time the channel is sensed busy, NB and BE are increased by 1 (cases $BO_s = 1$ and 2).

When BE reaches its maximum value, there is no more increase. The case $BO_s = 4$ is the last case, because here NB reaches its maximum value, and it cannot be further increased.

Because there exists a maximum value for NB, there will be also a maximum delay affecting the transmission of a packet. This maximum is reached in case a node extracts at every backoff stage the higher backoff time counter and at the end of each backoff stage it always finds the channel busy. In this case, the node is in backoff state for $\sum_{k=0}^{NB_{max}}(W_k - 1)$ slots and in sensing for $NB_{max} + 1$ slots. Therefore, the last slot in which a transmission can start is

$$\hat{t}_{max} = \sum_{k=0}^{NB_{max}} W_k = 120\,, \tag{4.4.1}$$

and the last slot in which a transmission can finish is $(\hat{t}_{max} + D - 1)$. Sensing, instead, is possible only for $\hat{t} \in [0, \hat{t}_{max} - 1]$.

In the following, the generic state will be denoted as $Q(\hat{t}) = \{BO_c, BO_s, \hat{t}\}$ and the probability of being in a generic state will be denoted as $P\{BO_c = c, BO_s = i, \hat{t} = j\} = P\{c, i, j\}$.

Table 4.1: The backoff stages.

BO_s	NB	BE	$W_{NB} = 2^{BE}$
0	0	3	$W_0 = 8$
1	1	4	$W_1 = 16$
2	2	5	$W_2 = 32$
3	3	5	$W_3 = W_2 = 32$
4	4	5	$W_4 = W_2 = 32$

4.4.2 Formulation of the Mathematical Model

Steps Followed by the Model

Let us denote as b^j the probability that in the j-th slot the channel is found to be busy after sensing. This probability will be initially left as parameter, and its computation will be provided at the end of section 4.4.3.

The model provides the following metrics:

1. the probability that a node ends the transmission of its packet in a given slot, j, denoted as $P\{T^j\}$, with $j \in [0, \hat{t}_{max} + D - 1]$;

2. the probability that the sink receives the end of a packet, coming whatever a node, in a given slot j, denoted as $P\{R^j\}$, with $j \in [0, \hat{t}_{max} + D - 1]$;

3. the success probability for a transmission, i.e., the probability that a node succeeds in transmitting its packet in a round whatever the slot, denoted as p_s.

The probability $P\{T^j\}$ depends on the probability of being in sensing state in the slot $j - D$. Because a packet occupies D slots, a node sensing the channel in slot $j - D$ and finding it free, will end its transmission in slot j. To determine the sensing probabilities, we model the behavior of a single node, using a state-transition diagram [109], describing the relation between all possible states in which a node can be (Figures 4.3, 4.4, 4.5, 4.6 and 4.7). From this diagram, we obtain the probability of being in sensing state at the j-th slot and at the i-th backoff stage ($BO_s = i$), denoted as $P\{S_i^j\} = P\{0, i, j\}$, whatever j and i. This is made in the remainder of this section. From these probabilities, we can derive the probability of being in sensing state at the j-th slot, denoted as $P\{C^j\}$ with $j \in [0, \hat{t}_{max} - 1]$, and therefore

$P\{T^j\}$. $P\{T^j\}$, $P\{R^j\}$, p_s, E_{mean} and b^j are derived in section 4.4.3. In this section is also provided the algorithm used to compute all the target performance metrics.

Sensing Probabilities

The state-transition diagram of the bidimensional process $Q(\hat{t})$ is presented through five different Figures (4.3, 4.4, 4.5, 4.6 and 4.7), each one related to a specific backoff stage. In particular, Figure 4.3 addresses the case $BO_s = 0$, Figure 4.4 $BO_s = 1$, Figure 4.5 $BO_s = 2$, Figure 4.6 $BO_s = 3$, and Figure 4.7 $BO_s = 4$. As will be clarified in the following, they are linked together through transitions that originate from some states of a Figure and terminate in the states of the subsequent Figure. Because each Figure is related to a specific value of BO_s, for the sake of simplicity in the drawings, the generic backoff state (ovals in the Figures) is simply denoted as $\{c, j\}$, omitting the value of BO_s; the sensing states (squares) are denoted as S^j with no pedex i.

In the following the different parts of the state-transition diagram will be described. For each case, the probabilities of being in the different states of the chain and the transition probabilities between the states will be provided.

First Backoff Stage ($BO_s = 0$)

At the beginning of the backoff algorithm, each node extracts an integer, uniformly distributed between 0 and $W_0 - 1 = 7$. At $t = 0$ a node enters, with probability $1/W_0$, one of the states $\{c, 0, 0\}$ with $c \in [0, 7]$. If the extracted value is 0, the node in slot 0 will sense the channel and in slot 1 it will transmit its packet, because no transmission may occur in the first slot ($P\{T^0 = 0\}$) and, therefore, the channel will be certainly

found free ($b^0 = 0$). In case a value larger than 0 is extracted, the node will decrease its backoff counter at each slot until the counter will reach the zero value, when the node will sense the channel. After the sensing phase the node will transmit the packet, in case the channel is found free; otherwise it will pass to the following backoff stage and another value, uniformly distributed between 0 and $W_1 - 1 = 15$, will be extracted. In Figure 4.3, the transitions that originated from the sensing states enter in the states of Figure 4.4. For example, if a node is in the state S_0^1 and it finds the channel busy, it will enter the state S_1^2, or one of the states $\{c, 1, 2\}$, with $c \in [0, 15]$, with the same probability b^1/W_1. The state of arrival depends on the new backoff counter value extracted.

Denoting as $P\{BO_c = c_1, BO_s = i_1, t = j_1 | BO_c = c_0, BO_s = i_0, \hat{t} = j_0\} =$ $P\{c_1, i_1, j_1 | c_0, i_0, j_0\}$, the transition probability from the state $\{c_0, i_0, j_0\}$ to the state $\{c_1, i_1, j_1\}$, the transition probabilities between the backoff states are given by:

$$P\{c, 0, j + 1 | c + 1, 0, j\} = 1 \ , \tag{4.4.2}$$

for $c \in [0, W_0 - 2]$ and $j \in [0, W_0 - 2]$.

This equation accounts for the fact that, at the beginning of each time slot, the backoff time counter is decreased by 1 until it reaches the zero value, with probability 1.

The probabilities of being in a sensing state are given by:

$$P\{S_0^j\} = \begin{cases} \frac{1}{W_0} & \text{for } j \in [0, W_0 - 1] \\ 0 & \text{for } j > W_0 - 1 \ . \end{cases} \tag{4.4.3}$$

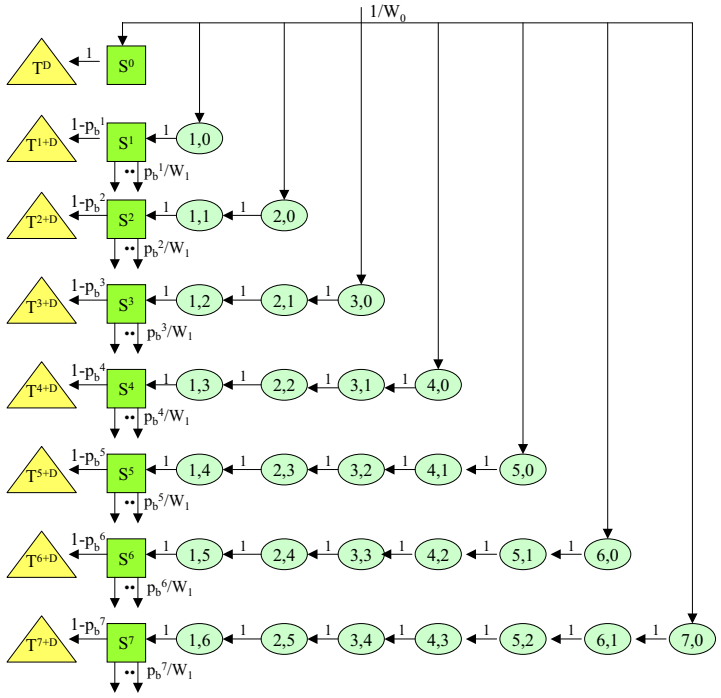

Figure 4.3: The state-transition diagram related to the first backoff stage.

Second Backoff Stage ($BO_s = 1$)

As a node can arrive in this backoff stage only after it has finished the first backoff stage, it cannot reach this stage before $j = 2$; therefore, S_1^0 and S_1^1 (and so T_1^1 and T_1^2) do not appear in the diagram.

As in the previous case, the transition probabilities between backoff states are given by:

$$P\{c, 1, j+1 | c+1, 1, j\} = 1 \ , \tag{4.4.4}$$

for $c \in [0, W_1 - 2]$ and $j \in [2, W_{0,1} - 2]$, where $W_{0,1} = W_0 + W_1$. In the following, we will denote as $W_{x,y,z}$, the sum $W_x + W_y + W_z$.

The transition probabilities between the states of the first backoff stage ($BO_s = 0$) and the ones of the second backoff stage ($BO_s = 1$) are given by:

$$P\{c, 1, j+1 | 0, 0, j\} = \frac{b^j}{W_1} \ , \tag{4.4.5}$$

for $c \in [0, W_1 - 1]$ and $j \in [1, W_0 - 1]$. This equation accounts for the fact that in case the channel at the j-th slot is found busy, the node will go to one of the states $\{c, 1, j+1\}$, with $c \in [0, W_1 - 1]$, with the same probability $1/W_1$.

The probabilities of being in sensing are given by:

$$P\{{S_1}^j\} = \begin{cases} 0 & \text{for } j < 2 \\ \sum_{v=1}^{j-1} P\{{S_0}^v\} \cdot \frac{b^v}{W_1} & \text{for } j \in [2, W_0] \\ P\{S_1^{W_0}\} & \text{for } j \in [W_0 + 1, W_1 + 1] \\ P\{S_1^{W_0}\} - \sum_{v=1}^{j-W_1-1} P\{S_0^v\} \cdot \frac{b^v}{W_1} & \text{for } j \in [W_1 + 2, W_{0,1} - 1] \\ 0 & \text{for } j > W_{0,1} - 1 \ . \end{cases} \tag{4.4.6}$$

The second equation derives from the fact that until $j \leq W_0$, the probability of being in sensing in the second backoff stage depends on the probabilities of being in sensing in the first backoff stage and to find the channel busy. As an example, a node can arrive in S_1^3 if it is in S_0^1, finds the channel busy, and extracts the value 1 for the second backoff stage; or it is in S_0^2, finds the channel busy, and extracts the value 0 for the second backoff stage (see Figures 4.3 and 4.4).

The third equation accounts for the fact that for $j > W_0$, there are no more transitions between the states of $BO_s = 0$ and the ones of $BO_s = 1$, because the last slot in which a node can sense the channel in the first backoff stage is $j = W_0 - 1 = 7$.

Finally, when j reaches $W_1 + 2 = 18$, $P\{{S_1}^{18}\}$ is obtained by subtracting the probability $P\{S_0^1\}\frac{b^1}{W_1}$ from $P\{S_1^{W_0}\}$. Therefore, $P\{{S_1}^{18}\} = \sum_{v=2}^{W_0-1} P\{{S_0}^v\} \cdot \frac{b^v}{W_1}$. In

fact, if a node is in S_0^1 it moves (in case of channel busy) to states $\{c, 1, 2\}$ with $c \in [0, 15]$; therefore the state $\{16, 1, 2\}$ does not exist (see the Figure).

The last sensing state we can have in this part of the chain is S_1^{23}, which means that the second backoff stage will be completed by a node at maximum in the 24-th slot.

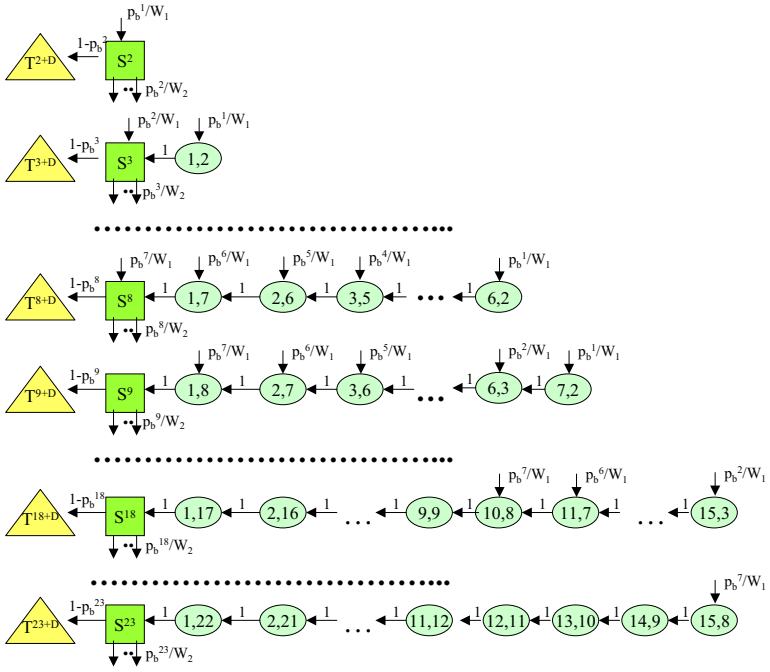

Figure 4.4: The state-transition diagram related to the second backoff stage.

Third Backoff Stage ($BO_s = 2$)

Following similar considerations made, and observing the part of the state-transition diagram depicted in Figure 4.5, we can derive the following probabilities.

The transition probabilities between the backoff states are given by:

$$P\{c, 2, j+1 | c+1, 2, j\} = 1 \ , \tag{4.4.7}$$

for $c \in [0, W_2 - 2]$ and $j \in [3, W_{0,1,2} - 2]$.

The transition probabilities between the states of the second backoff stage ($BO_s = 1$) and the ones of the third backoff stage ($BO_s = 2$) are given by:

$$P\{c, 2, j+1 | 0, 1, j\} = \frac{b^j}{W_2} \ , \tag{4.4.8}$$

for $c \in [0, W_2 - 1]$ and $j \in [2, W_{0,1} - 1]$.

The probabilities of being in sensing state are given by:

$$P\{{S_2}^j\} = \begin{cases} 0 & \text{for } j < 3 \\ \sum_{v=2}^{j-1} P\{{S_1}^v\} \cdot \frac{b^v}{W_2} & \text{for } j \in [3, W_{0,1}] \\ P\{S_2^{W_{0,1}}\} & \text{for } j \in [W_{0,1}+1, W_2+2] \\ P\{S_2^{W_{0,1}}\} - \sum_{v=2}^{j-W_2-1} P\{S_1^v\} \cdot \frac{b^v}{W_2} & \text{for } j \in [W_2+3, W_{0,1,2}-1] \\ 0 & \text{for } j > W_{0,1,2} - 1 \ . \end{cases} \tag{4.4.9}$$

Fourth Backoff Stage ($BO_s = 3$)

Similarly, and observing the part of the state-transition diagram depicted in Figure 4.6, we can derive the following probabilities.

The transition probabilities between the backoff states are given by:

$$P\{c, 3, j+1 | c+1, 3, j\} = 1 \ , \tag{4.4.10}$$

for $c \in [0, W_2 - 2]$ and $j \in [4, W_{0,1,2,3} - 2]$.

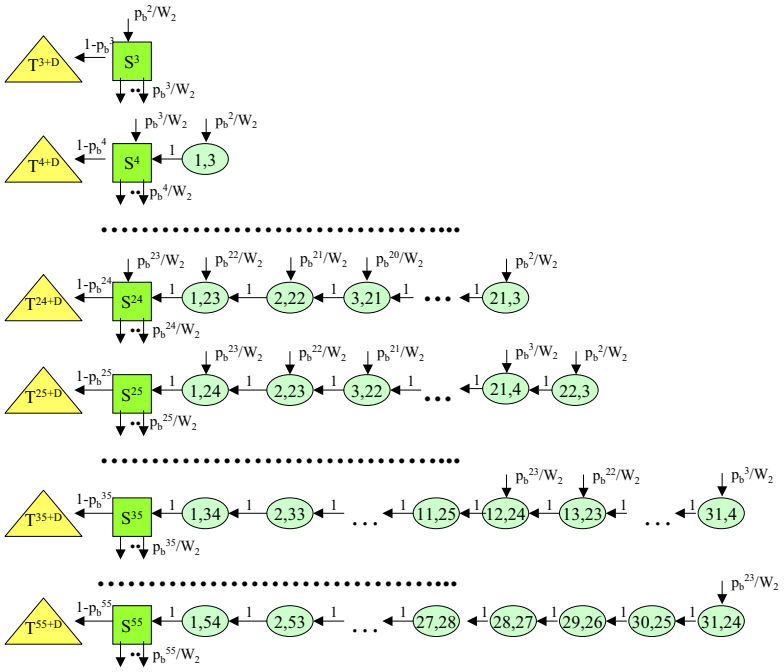

Figure 4.5: The state-transition diagram related to the third backoff stage.

Moreover, we have to evaluate the transition probabilities between the states of the third backoff stage ($BO_s = 2$) and the ones of the fourth backoff stage ($BO_s = 3$); these probabilities are given by:

$$P\{c, 3, j+1 | 0, 2, j\} = \frac{b^j}{W_2} \,, \tag{4.4.11}$$

for $c \in [0, W_2 - 1]$ and $j \in [3, W_{0,1,2} - 1]$.

The probabilities of being in sensing state are given by:

$$P\{S_3{}^j\} = \begin{cases} 0 & \text{for } j < 4 \\ \sum_{v=3}^{j-1} P\{S_2{}^v\} \cdot \frac{b^v}{W_2} & \text{for } j \in [4, W_2+3] \\ \sum_{v=3}^{j-1} P\{S_2{}^v\} \cdot \frac{b^v}{W_2} - \sum_{v=3}^{j-W_2-1} P\{S_2{}^v\} \cdot \frac{b^v}{W_2} & \text{for } j \in [W_2+4, W_{0,1,2}] \\ P\{S_3{}^{W_{0,1,2}}\} - \sum_{v=W_{0,1}}^{j-W_2-1} P\{S_2{}^v\} \cdot \frac{b^v}{W_2} & \text{for } j \in [W_{0,1,2}+1, W_{0,1,2,3}-1] \\ 0 & \text{for } j > W_{0,1,2,3}-1 \ . \end{cases} \tag{4.4.12}$$

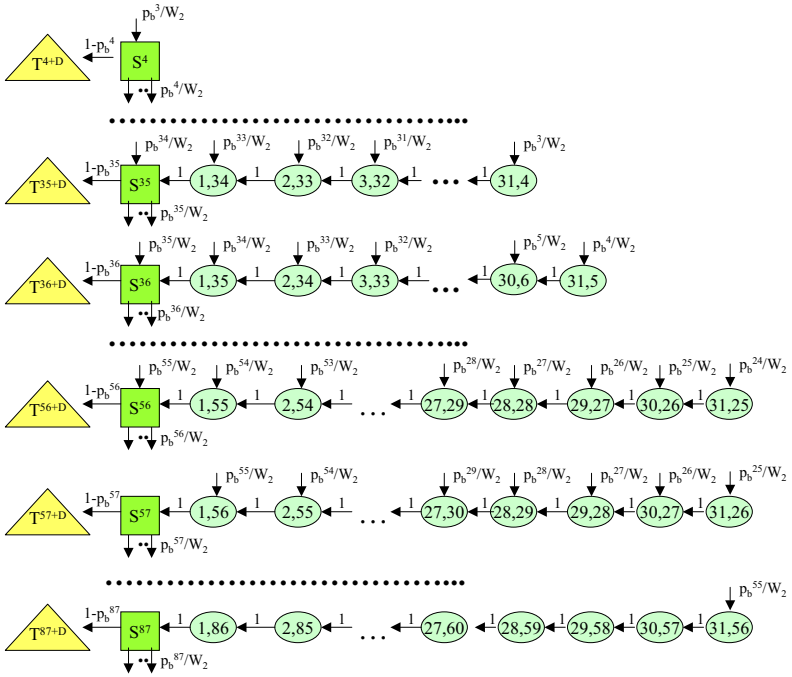

Figure 4.6: The state-transition diagram related to the fourth backoff stage.

Fifth Backoff Stage ($BO_s = 4$)

Similarly, and observing the part of the state-transition diagram depicted in Figure

4.7, we can derive the following probabilities.

The transition probabilities between the backoff states are given by:

$$P\{c, 4, j+1 | c+1, 4, j\} = 1 \ , \tag{4.4.13}$$

for $c \in [0, W_2 - 2]$ and $j \in [5, W_{0,1,2,3,4} - 2]$.

Moreover, we have to evaluate the transition probabilities between the states of the fourth backoff stage ($BO_s = 3$) and the ones of the fifth backoff stage ($BO_s = 4$); these probabilities are given by:

$$P\{c, 4, j+1 | 0, 3, j\} = \frac{b^j}{W_2} \ , \tag{4.4.14}$$

for $c \in [0, W_2 - 1]$ and $j \in [4, W_{0,1,2,3} - 1]$.

The probabilities of being in sensing state are given by:

$$P\{{S_4}^j\} = \begin{cases} 0 & \text{for } j < 5 \\ \sum_{v=4}^{j-1} P\{{S_3}^v\} \cdot \frac{b^v}{W_2} & \text{for } j \in [5, W_2 + 4] \\ \sum_{v=4}^{j-1} P\{{S_3}^v\} \cdot \frac{b^v}{W_2} - \sum_{v=4}^{j-W_2-1} P\{{S_3}^v\} \cdot \frac{b^v}{W_2} & \text{for } j \in [W_2 + 5, W_{0,1,2,3}] \\ P\{{S_4}^{W_{0,1,2,3}}\} - \sum_{v=W_{0,1,2}}^{j-W_2-1} P\{{S_3}^v\} \cdot \frac{b^v}{W_2} & \text{for } j \in [W_{0,1,2,3} + 1, W_{0,1,2,3,4} - 1] \\ 0 & \text{for } j > W_{0,1,2,3,4} - 1 \ . \end{cases} \tag{4.4.15}$$

4.4.3 Performance Metrics Derived from the Model

Transmission Probabilities

As stated, the aim of the model is to evaluate the probability that a generic node ends its packet transmission in slot j, $P\{T^j\}$, with $j \in [0, \hat{t}_{max} + D - 1]$.

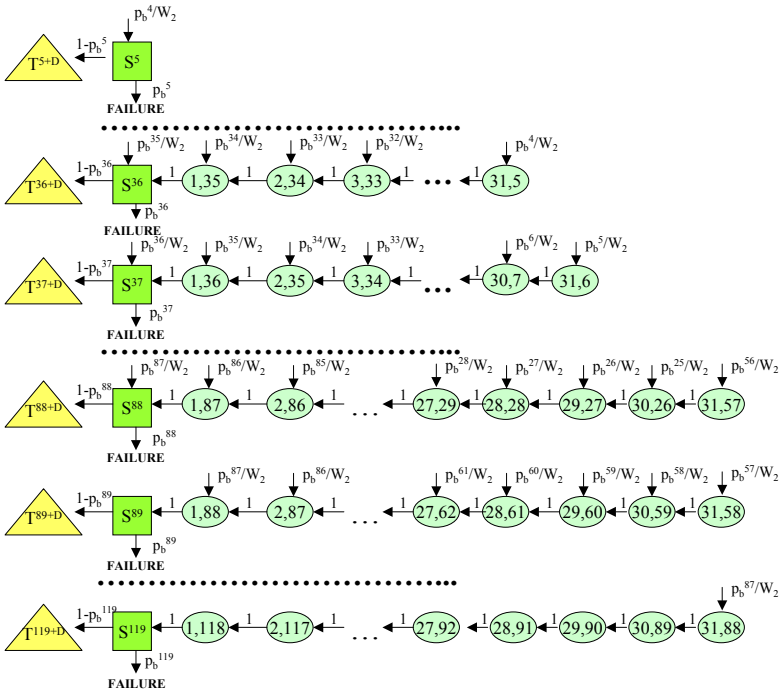

Figure 4.7: The state-transition diagram related to the fifth backoff stage.

A node finishes its transmission in slot j, if in slot $j - D$, it senses the channel finding it free; therefore, this probability is given by:

$$P\{T^j\} = P\{C^{j-D}\} \cdot (1 - b^{j-D}) \ . \tag{4.4.16}$$

Because a node transmits a packet occupying D slots, we associate $P\{T^j\}$ to the slot in which the transmission terminates; therefore, for $j < D$, $P\{T^j\} = 0$.

The cumulative function, $F_T(j)$, defined as the probability that a packet coming from whatever a node, is transmitted in the channel within slot j, is given by:

$$F_T(j) = \sum_{v=0}^{j} P\{T^v\} \ . \tag{4.4.17}$$

The probability of being in sensing state at the different instants j is given by:

$$P\{C^j\} = \sum_{i=0}^{NB_{max}} P\{S_i^j\}\,. \tag{4.4.18}$$

Reception and Success Probability

To evaluate the other target probabilities, we have to model how the number of nodes that compete for accessing to the channel varies with time. We denote as N_c^j the number of nodes which have not transmitted yet at the end of slot (j-1) and that will compete for slot j. In particular, in slot 0, the number of nodes which compete for the channel is equal to N and as none can transmit in slot 0 ($P\{T^0\} = 0$) N_c^1 is equal to N too (see Figure 4.8). Whereas if we set $D = 1$, in slot 1 some nodes may terminate the transmission, each with probability $P\{T^1\}$, and at the end of this slot the number of nodes that still have to transmit their packets, N_c^2, will depend on $P\{T^1\}$ and could be lower than N. In Figure 4.8 is shown an example (considering the case $D = 1$), in which one of the five competing nodes transmits in slot 1, and therefore in the second slot we have four nodes competing for the channel ($N_c^2 = 4$). Therefore, N_c^j is a random variable, binomially distributed. In the case $D = 1$, the probability that k over $\hat{N}$ nodes at slot j have not transmitted yet the packet, conditioned on the fact that at slot $j-1$ $\hat{N}$ nodes are competing for the channel ($N_c^{j-1} = \hat{N}$), is given by:

$$\begin{aligned} P\{N_c^j = k | N_c^{j-1} = \hat{N}\} &= B^j(k, \hat{N}) = \\ &= \binom{\hat{N}}{k} \left(1 - b^{j-2}\right) \left(P\{C^{j-2}\}\right)^{\hat{N}-k} \cdot \prod_{i=0}^{NB_{max}} \left(1 - P\{S_i^{j-2}\}\right)^k, \end{aligned} \tag{4.4.19}$$

where $(1-b^{j-2})(P\{C^{j-2}\})^{\hat{N}-k}$ is the probability that $\hat{N}-k$ nodes transmit in j and $\prod_{i=0}^{NB_{max}}(1-P\{S_i^{j-2}\})^k$ is the probability that the remaining k nodes do not transmit, as they do not sense the channel in slot $j-2$.

In eq. (4.4.19), N_c^{j-1} is, in its turn, a random variable, binomially distributed, having a probability distribution that depends on the probabilities $P\{T^l\}$ with $l \in (1,..,j-2)$. Therefore, to find the statistics of N_c^j, eq. (4.4.19) should be averaged over the statistics of N_c^{j-1}, whose determination would depend on the statistics of N_c^{j-2} and so on. By increasing the initial number of nodes in the network, N_c^0, and the time slot considered (i.e., the value of j), the complexity of the evaluation of the statistics of N_c^{j-1} increases exponentially, because of the need to follow all possible combinations of values of N_c^2, N_c^3, etc. To reduce such complexity we have introduced an approximation: we do not model N_c^{j-1} as a random variable, but we set its value at the value of k that corresponds to a maximum value of the probability $B^{j-1}(k,\hat{N})$. Therefore N_c^{j-1} is given by:

$$N_c^{j-1} = \arg\max_k B^{j-1}(k,\hat{N}). \tag{4.4.20}$$

Moreover, we have also evaluated performance by simply setting $N_c^j = N$, whatever be j. In section 4.4.4, simulation results are compared with the mathematical analysis results considering both the models of N_c^j. Results show that the two models bring approximatively to the same results and that a good agreement with simulations is obtained in both cases. Therefore, the approximation introduced does not affect performance too much.

The modelling of N_c^j in the case $D > 1$ is even more complex than the case $D = 1$, because N_c^j will depend on the number of nodes starting their transmission in the last

D slots. But as by increasing D each node occupies the channel for a longer time, N_c^j will decrease more slowly with time; therefore it is reasonable to set $N_c^j = N$ whatever be j. If, in fact, this approximation is good for $D = 1$, it will be fine for $D > 1$ all the more. Therefore, only the case $N_c^j = N$ whatever be j has been considered in section 4.4.4 for $D > 1$.

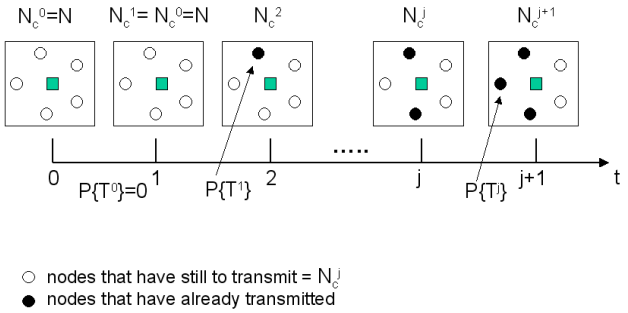

Figure 4.8: The behavior of the number of nodes that have still to access the channel in the different time slots (example).

Now, we can evaluate the probability, p_s, that a generic packet is transmitted successfully on the channel given by:

$$p_s = \sum_{j=0}^{\hat{t}_{max}+D-1} P\{Z^j\} \ , \tag{4.4.21}$$

where $P\{Z^j\}$ is the probability that a successful transmission ends in slot j, which means that one and only one transmission starts in $j-D+1$. Because we assume that all nodes can hear each other, if in slot $j-D+1$ only one node starts its transmission,

the sink will receive correctly (i.e., without collisions) the end of the packet in j. From the law of total probability we obtain:

$$P\{Z^j\} = P\{1\ tx\ in\ (j-D+1) | channel\ free\ in\ (j-D)\} \cdot P\{channel\ free\ in\ (j-D)\} + \\ + P\{1\ tx\ in\ (j-D+1) | channel\ busy\ in\ (j-D)\} \cdot P\{channel\ busy\ in\ (j-D)\}, \tag{4.4.22}$$

where $P\{1\ tx\ in\ (j-D+1) | channel\ free\ in\ (j-D)\}$ and $P\{1\ tx\ in\ (j-D+1) | channel\ busy\ in\ (j-D)\}$, are the probabilities that one and only one transmission starts in slot $j-D+1$ conditioned to the fact that the channel in $j-D$ is free or busy, respectively. As only one transmission starts in slot $j-D+1$ if only one node, over N_c^{j-D}, senses the channel in slot $j-D$ and as no transmissions may start in $j-D+1$ if the channel in $j-D$ is busy, $P\{Z^j\}$ is given by:

$$P\{Z^j\} = (1-b^{j-D}) P\{C^{j-D}\} \cdot \prod_{i=0}^{NB_{max}} \left(1 - P\{S_i^{j-D}\}\right)^{N_c^{j-D}-1}, \tag{4.4.23}$$

where $P\{C^{j-D}\}$ is the probability that one node senses the channel in $j-D$ and $\prod_{i=0}^{NB_{max}} (1 - P\{S_i^{j-D}\})^{N_c^{j-D}-1}$ is the probability that the remaining $N_c^{j-D}-1$ nodes do not sense the channel in slot $j-D$.

Finally, the probability $P\{R^j\}$ that in slot j the sink receives the end of a packet, coming from whatever a node, is given by:

$$P\{R^j\} = N_c^j \cdot P\{Z^j\}\ . \tag{4.4.24}$$

The Energy Consumption

Here, the mean energy consumed by a node during a round, is derived. A node spends energy when it receives or transmits a packet and also when it is in backoff state. After the transmission of the packet, the node switches off and does not consume energy. The node will stay in the off state till the reception of the following query.

We let $P_{\rm s} = 82.5$ [mW] be the power spent in receiving and sensing states; $P_{\rm bo} = 50$ [mW] the power spent in backoff state and $P_{\rm t} = 75.8$ [mW] the power spent during transmission (see Freescale IEEE 802.15.4 devices [93]).

The mean energy spent by a node in a round, is given by:

$$E_{mean} = \sum_{j=0}^{\hat{t}_{max}+D-1} E_{\rm t}^{j} + E_{\rm s}^{j} + E_{\rm bo}^{j}, \tag{4.4.25}$$

where E_t^j, E_s^j, and E_{bo}^j are the different energy contributions spent in transmission, sensing and backoff, respectively, for a node ending its transmission in slot j.

Since no retransmission is performed, each node will transmit only one packet per round. Therefore,

$$E_{\rm t}^{j} = P_{\rm t} \cdot \frac{D \cdot N_{\rm bit}}{R_{\rm b}} \cdot P\{T^j\}, \tag{4.4.26}$$

where $N_{\rm bit} = 10$ bytes is the number of bits transmitted in one slot (having duration d_{bo}). The energy spent in the sensing state depends on how many slots are used by the node for sensing the channel. A node transmitting in slot j could have sensed the channel for one slot, in case it has found the channel free at the end of the first backoff stage, for two slots in case it has found the channel free at the end of the second backoff stage, etc. This energy is given by

$$E_s^j = P_s \cdot \frac{N_{bit}}{R_b} \cdot (1 - b^{j-D}) \sum_{k=0}^{NB_{max}} (k+1) \cdot P\{S_k^{j-D}\}, \tag{4.4.27}$$

where b^j is the probability to find the channel busy in slot j, and $(1-b^{j-D})\cdot P\{S_k^{j-D}\}$ is the probability that a node at the end of the k-th backoff stage, finds the channel free and ends transmitting in slot j. Finally, the energy spent in the backoff state depends on how many slots are occupied by the node for the backoff procedure. This number depends, in turn, on the number of backoff stages performed. Therefore, we have

$$E_{bo}^j = P_{bo}\cdot\frac{N_{bit}}{R_b}\cdot(1-b^{j-D})\sum_{k=0}^{NB_{max}}(j-k-D)\cdot P\{S_k^{j-D}\}, \tag{4.4.28}$$

where $j-k-D$ is the number of slots during which a node that has finished the k-th backoff stage, has performed backoff. This value is the same no matter what values of backoff counter are extracted at each backoff stage.

Derivation of the probability that the channel is found busy

By denoting as f^j the probability that the channel in j is free, the probability to find the channel busy in j is given by:

$$b^j = 1 - f^j\ . \tag{4.4.29}$$

From the law of total probability we can express p_f^j as:

$$\begin{aligned} f^j = {} & P\{no\ tx\ in\ j | channel\ free\ in\ (j-1)\}\cdot P\{channel\ free\ in\ (j-1)\}+ \\ & + P\{no\ tx\ in\ j | channel\ busy\ in\ (j-1)\}\cdot P\{channel\ busy\ in\ (j-1)\}. \end{aligned} \tag{4.4.30}$$

where $P\{no\ tx\ in\ j|channel\ free\ in\ (j-1)\}$ and $P\{no\ tx\ in\ j|channel\ busy\ in\ (j-1)\}$, are the probabilities that no transmissions occur in slot j conditioned to the fact that the channel in $j-1$ is free or busy, respectively.

When $D = 1$, $P\{no\ tx\ in\ j | channel\ free\ in\ (j-1)\} = \prod_{k=0}^{NB_{max}} (1 - S_k^{j-1})^{N_c^{j-1}-1}$, as if the channel in $j-1$ is free, no transmissions occur in j if no nodes sense the channel in $j-1$. When, instead, the channel in $j-1$ is busy, no transmissions may certainly occur in j. Therefore, in this case, p_f^j is given by:

$$f^j = \left(1 - b^{j-1}\right) \prod_{i=0}^{NB_{max}} \left(1 - P\{S_i^{j-1}\}\right)^{N_c^{j-1}-1} + b^{j-1} \ . \tag{4.4.31}$$

When, instead, $D > 1$ the second term of eq. (4.4.30) coincides with the probability that in slot $j-1$ a transmission ends, i.e., the probability that at least one transmission starts in slot $j-D$, given by: $(1-b^{j-D-1}) \cdot [1 - \prod_{k=0}^{NB_{max}} (1 - S_k^{j-D-1})^{N_c^{j-D-1}-1}]$.

Therefore, in this case, f^j is given by:

$$\begin{aligned} f^j = & \left(1 - b^{j-1}\right) \prod_{i=0}^{NB_{max}} \left(1 - P\{S_i^{j-1}\}\right)^{N_c^{j-1}-1} \\ & + \left(1 - b^{j-D-1}\right) \cdot \left[1 - \prod_{k=0}^{NB_{max}} \left(1 - S_k^{j-D-1}\right)^{N_c^{j-D-1}-1}\right] . \end{aligned} \tag{4.4.32}$$

Obviously, when $j \leq D$ the second term of eq. (4.4.32) becomes null.

The Algorithm

The algorithm that allows the evaluation of all the aformentioned performance metric follows. The simplest case of $N_c^j = N$ whatever be j is considered, but the algorithm can be used for any modelling of how N_c^j evolves with time (i.e., with j), by simply substituting the formula to derive N_c^j in the sequence of steps below (see first instruction of For cycle).

`Initialisation of the parameters for` j`=0:`

- `set` $N_c^0 = N$`;`

- set $b^0 = 0$;
- set $P\{S_0^0\} = 1/W_0$, $P\{S_k^0\} = 0$ for $k \in [1, NB_{max}]$;
- set $P\{C^0\} = P\{S_0^0\}$;
- set $P\{T^0\} = 0$;
- set $P\{Z^0\} = 0$;
- set $P\{R^0\} = 0$.

For $(j = 1; j <= \hat{t}_{max} + D - 1; j++)$

{

- set $N_c^j = N$;
- compute b^j according to eq. (4.4.29), by using eq. (4.4.31) in the case $D = 1$ and eq. (4.4.32) in the case $D > 1$;
- compute $P\{S_0^j\}$ according to eq. (4.4.3)
- compute $P\{S_1^j\}$ according to eq. (4.4.6)
- compute $P\{S_2^j\}$ according to eq. (4.4.9)
- compute $P\{S_3^j\}$ according to eq. (4.4.12)
- compute $P\{S_4^j\}$ according to eq. (4.4.15)
- compute $P\{C^j\}$ according to eq. (4.4.18)
- compute $P\{T^j\}$ according to eq. (4.4.16)
- compute $P\{Z^j\}$ according to eq. (4.4.23)
- compute $P\{R^j\}$ according to eq. (4.4.24)

}

compute p_s through eq. (4.4.21) and E_{mean} through eq. (4.4.25).

4.4.4 Numerical Results

For the purpose of numerical comparison, a dedicated simulation tool has been developed. We consider N nodes and a sink, sending queries and waiting for the data from nodes. In each round, nodes receive the query and transmit directly to the sink the data, by using the 802.15.4 CSMA/CA protocol described in section 4.2. Ideal channel conditions are assumed; therefore, all nodes can "hear" each other and can receive correctly the query at each round. No capture effect is considered: in case two or more packets collide, they are all lost. Finally, no acknowledge and retransmission mechanisms are performed. 10^4 rounds are simulated.

Figures 4.9, 4.10 and 4.11 show the probability $P\{T^j\}$ as a function of time $\hat{t} = j$, representing the time slot, for $N = 3$, 5 and 7, respectively, having fixed $D = 1$. Even if these probabilities could be larger than zero for $j \in [0, \hat{t}_{max} + D - 1]$, as, in all the three case, for $j > 26$ $P\{T^j\}$ tend to zero, the curves are shown for $j \leq 26$.

Both mathematical analysis and simulation results are reported, considering the two models: N_c^j variable according to eq. (4.4.20), and $N_c^j = N$. As we can see, the two mathematical models bring approximatively the same results, and both do not present relevant differences with respect to simulations; therefore, the model is validated. Owing to its simplicity, all the other results shown here have been obtained by considering $N_c^j = N$, whatever be j.

It can be seen in the Figures that, in all cases, no traffic is present in the first slot, because no transmissions may occur: a node that extracts the 0 value at the

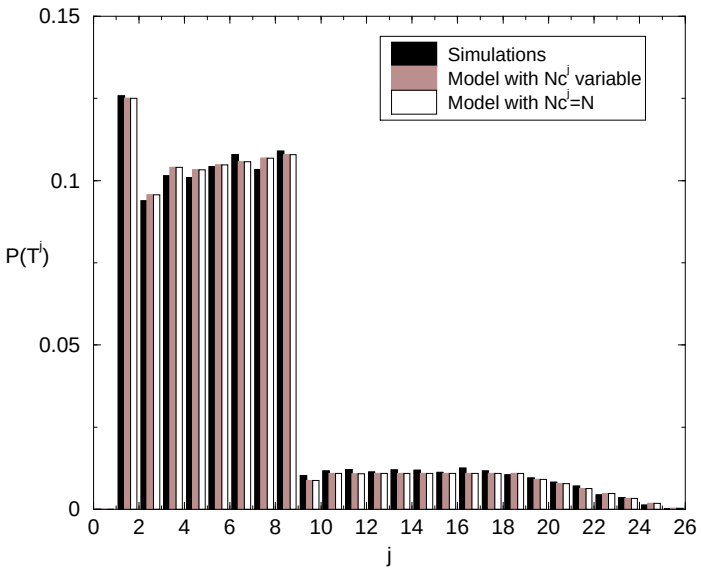

Figure 4.9: The probabilities $P\{T^j\}$ obtained through simulation and through the mathematical model considering $N_c^j = N_c^0$ for every j and N_c^j variable, in the case N=3 and $D = 1$.

first backoff stage will sense the channel in slot 0 and will transmit in slot 1. This happens with probability $1/W_0 = 1/8$, whatever be N, and this is also the maximum value that $P\{T^j\}$ can assume. If a node extracts the value 0 at the first backoff stage, in fact, it will certainly transmit in slot 1, whereas if a larger value is extracted there is a certain probability that the channel is found busy. Therefore, $P\{T^j\}$ assumes lower values for $j > 1$. When a node tries to access the channel for the first time, it will delay the transmission for a random number of slots in the range $[0, 7]$. As the network is composed of few nodes, the probability to find the channel busy is low; therefore, $P\{T^j\}$ for $j \in [1, 8]$, which correspond to the cases in which the node extracts the value 0, or 1, .. , or 7 respectively, are the largest. Lower probabilities are associated to the slots from 9 to 23, in which only nodes that have found the

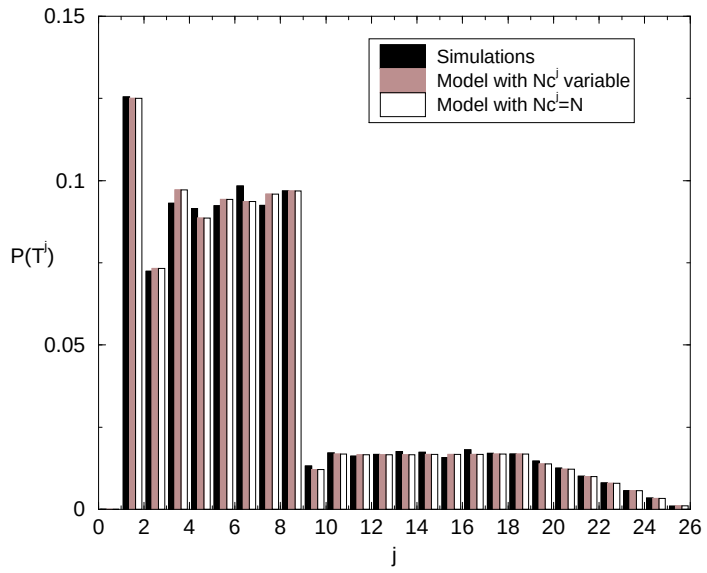

Figure 4.10: The probabilities $P\{T^j\}$ obtained through simulation and through the mathematical model considering $N_c^j = N_c^0$ for every j and N_c^j variable, in the case N=5 and $D = 1$.

channel busy and are performing the second backoff stage (plus some nodes already performing the third of fourth of fifth backoff stage, which are a minority) transmit. From slot 24, the probabilities show a further decrease, because in these slots there are only transmissions of nodes that have ended the second backoff too (as can be seen in Figure 4.4 the last slot in which there could be transmissions of the second backoff stage is 23) and are running the third or fourth or fifth backoff stage; once again the probability that the channel is found busy for two or three times is very low, and few nodes will transmit after slot 24. If we compare Figures 4.9, 4.10 and 4.11 we can note that by increasing N the probabilities to have transmissions in slots from 2 to 8 decrease and, consequently, the probabilities to have transmissions in slots from 9 to 23 increase. The reason is that by increasing the number of nodes, the probability

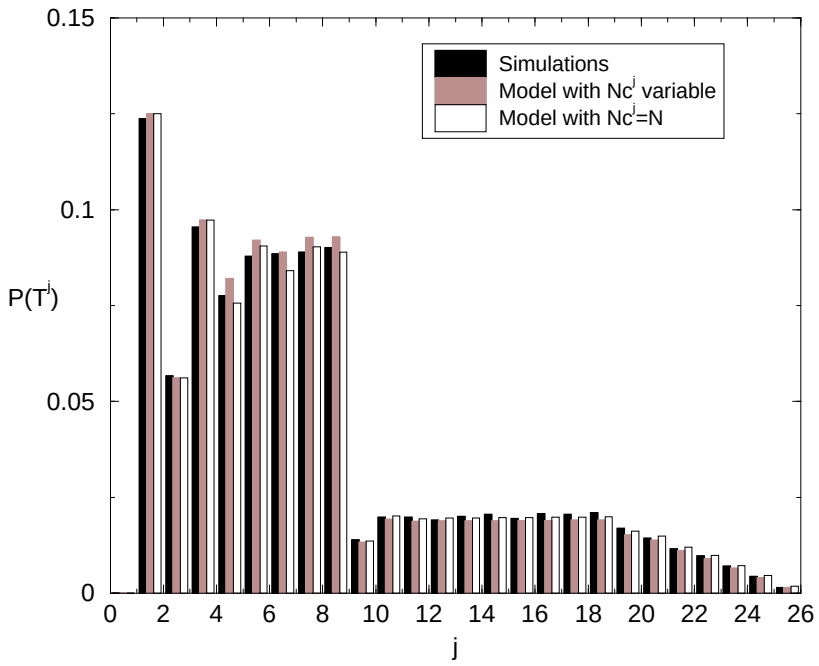

Figure 4.11: The probabilities $P\{T^j\}$ obtained through simulation and through the mathematical model considering $N_c^j = N_c^0$ for every j and N_c^j variable, in the case N=7 and $D = 1$.

to find the channel busy at the end of the first backoff increases. Finally, it can be noted that in all cases we have two relative minima in slot 2: as the probability to transmit a packet in slot 1 is large, the probability to find the channel busy in this slot is also large; therefore, the probability to transmit in the following slot is quite small (see eq. (4.4.16)).

In Figures 4.12 and 4.13, the probabilities $P\{Z^j\}$ and $P\{R^j\}$ as a function of j, representing the time slot, are shown for $N = 3$, 5, and 7. Once again, the model is validated by simulations: the values obtained through the analysis and simulations are very similar. The differences are due to the approximation we have made in modeling

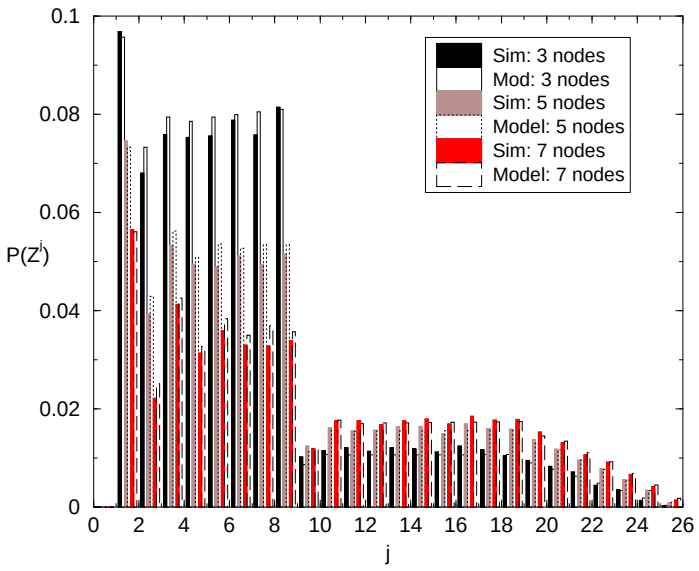

Figure 4.12: The probabilities $P\{Z^j\}$ obtained through simulation and through the mathematical model for $N = 3$, 5 and 7, having fixed $D = 1$.

N_c^j (set equal to N, whatever be j). The trends are very similar to those obtained for $P\{T^j\}$: the largest values of probabilities are for slots 1 to 8; lower probabilities are present for slots from 9 to 23 and then the probabilities tend to zero. Moreover, we have a maximum in slot 1 and a relative minimum in slot 2.

To validate the model for the cases $D > 1$, in Figure 4.14, $F_T(j)$ as a function of j, for different values of N and D, is shown. Both mathematical analysis (lines) and simulation results (symbols) are reported to validate the model: a good agreement between the two results can be found in all cases. The non linear behavior of the curves for small values of the ordinate are due to the sudden changes in values of $P\{T^j\}$ already commented before. As we can see, in all cases no traffic is present for $j < D$, and when $j = D$ $P\{T^j\}$ assumes its maximum value, equal to 1/8, whatever be N (as in the case $D = 1$). Moreover, by increasing N and D, the delay with which

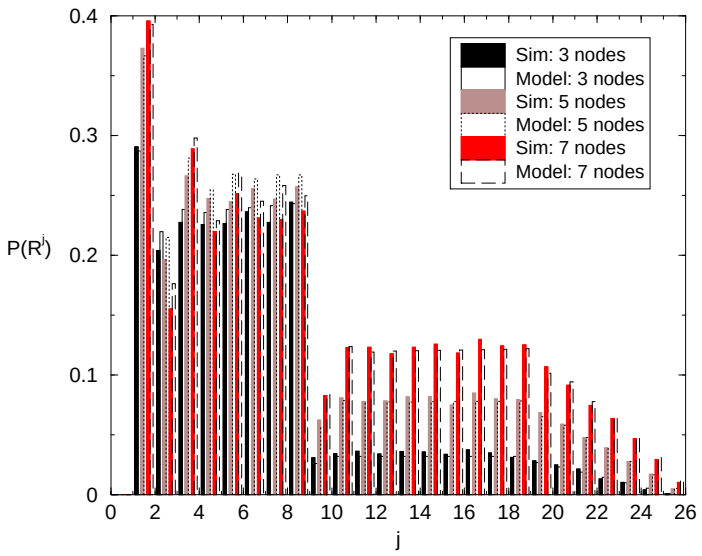

Figure 4.13: The probabilities $P\{R^j\}$ obtained through simulation and through the mathematical model, for $N = 3$, 5 and 7, having fixed $D = 1$.

a node accesses the channel increases. Moreover, in the case $N = 10$ and $D = 10$, we can note that $F_T(j)$ does not reach the value 1, as there is a certain probability that a node cannot succeed in accessing the channel.

In Figure 4.15, p_s as function of N for different values of D is shown. Results obtained through simulation (symbols) and through the mathematical model (lines) are reported. Once again, simulations validate the model. As we can see, p_s decreases monotonically by increasing N, because the number of nodes competing for the channel increases. Moreover, we can note that there exists an optimum value of D, D_{opt}, maximizing p_s, and this value depends on N. For the sake of legibility of drawings, here only the curves obtained for $D = 1$, 3 and 5, are shown. However, the model has been validated for $1 \leq D \leq 10$ and $1 \leq N \leq 50$. From these results, we have found also that for $1 < N < 12$, $D_{opt} = 7$; for $12 < N < 18$, $D_{opt} = 5$; for $N > 68$, $D_{opt} = 2$.

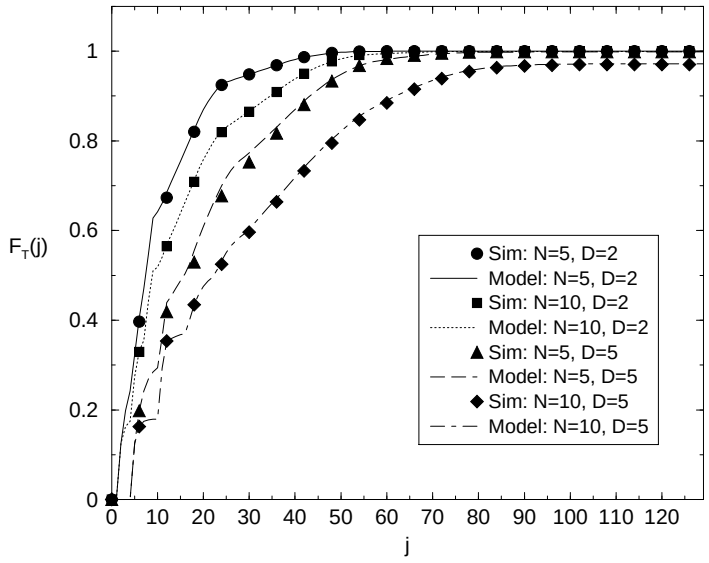

Figure 4.14: The cumulative function $F_T(j)$ as a function of j, obtained through simulations (symbols) and through the mathematical model (lines), for different values of N and D.

Therefore, it clearly appears that D_{opt} decreases when increasing N.

To better understand how the distribution of the traffic varies when low, medium, and high offered load are present, in Figure 4.16 the cumulative function of $P\{Z^j\}$, $F_Z(j)$, as a function of j, for different values of N and D, is shown ($F_Z(j)$ is obtained by substituting $P\{T^v\}$ with $P\{Z^v\}$ in eq. (4.4.17)). Both mathematical analysis (lines) and simulation results (symbols) are reported to validate the model: a good agreement between the two results can be found in almost all cases. As expected, once we fix D, by decreasing N (therefore the offered load), $F_Z(j)$ decreases. Once we fix N, instead, the value of D maximizing $F_Z(j)$ depends on N as stated earlier. As an example, for $N = 10$, to obtain the largest value of $F_Z(j)$ we have to fix $D = 10$, whereas for $N = 40$, the largest value is reached for $D = 1$. However, if we set

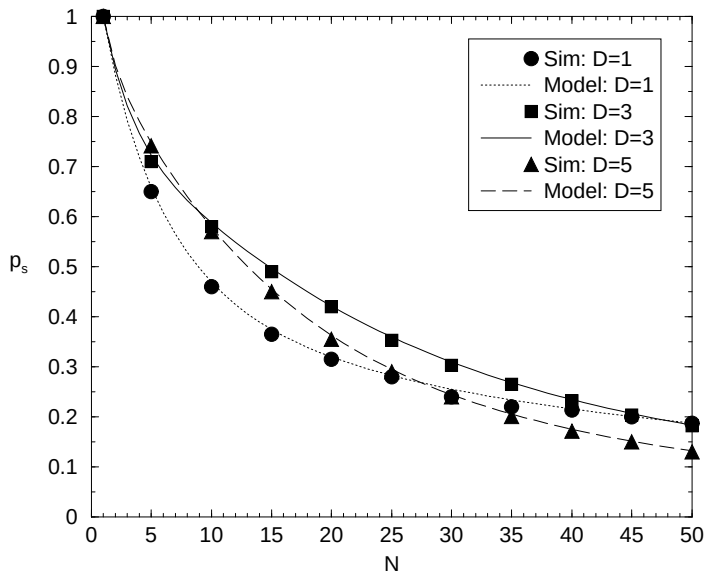

Figure 4.15: The success probability, p_s obtained through simulations (symbols) and through the mathematical model (lines), as a function of N, for different values of D.

$D = 10$, the maximum value of $F_Z(j)$ is reached with a higher delay. As it can be seen, in fact, the curves with $D = 1$ have a larger slope and reach the maximum value with lower delays.

Now, the behavior of p_s and E_{mean}, by varying the interval of time between two successive queries, T_q, having fixed $D = 5$ and 10, is studied.

Figure 4.17 reports p_s as a function of N. As expected by increasing T_q, p_s gets larger, because nodes have more time to access the channel. However note that the increase of p_s is obtained at the cost of larger delays, resulting also in an increasing of E_{mean}. In Figure 4.18, E_{mean} as a function of N is shown, for the same set of parameters D and T_q considered in Figure 4.17. As it can be noted, here the increasing

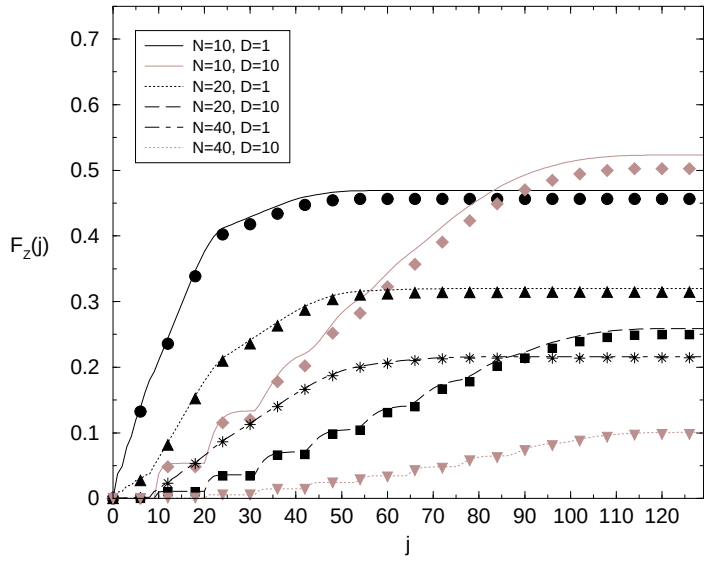

Figure 4.16: The cumulative function, $F_Z(j)$, as a function of j, obtained through simulations (symbols) and through the mathematical model (lines), for different values of N and D.

of T_q results in an increasing of E_{mean}, since nodes will stay on for more time, and also have larger probability to transmit their packets. For low N, by increasing D, E_{mean} gets larger, because of the greater amount of energy spent for transmitting larger packets. Conversely, for high N, the larger D, the lower will be the probability that a node succeeds in accessing the channel, decreasing the energy spent by the node.

By comparing Figures 4.17 and 4.18 we can deduce that a tradeoff between energy consumption and success probability should be found.

Finally, performance, in terms of p_s and E_{mean}, for different values of parameters characterising the backoff algorithm is evaluated, to compare possible variations of

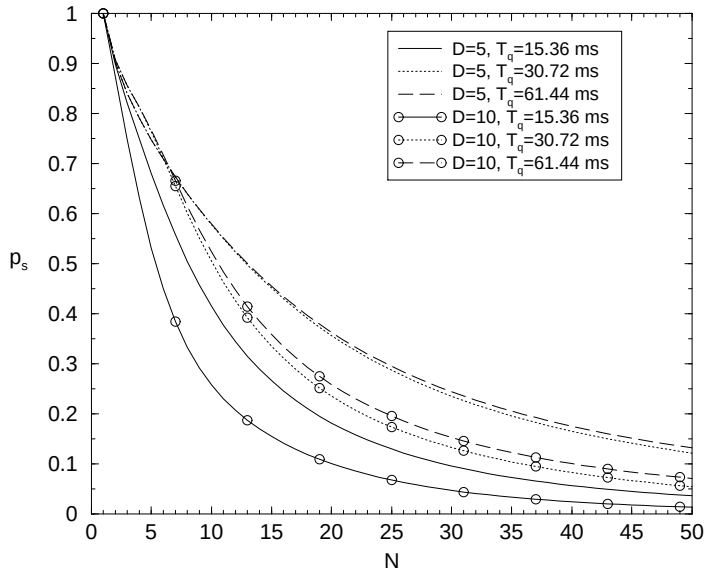

Figure 4.17: The success probability, p_s as a function of N, for different values of D and T_q.

the algorithm with respect to the one defined by the 802.15.4 standard. All results are obtained, by setting $D = 1$. The symbols in the Figures (e.g., circles, squares, stars, etc..) represent simulations, whereas the curves are obtained through the mathematical model. Once again a good agreement between results has been found.

In Figures 4.19 and 4.20 p_s and E_{mean} as a function of N for different values of W_k, with $k \in [0, NB_{max}]$, having fixed $NB_{max} = 4$, are reported, respectively. In particular, we consider the cases of absence of exponential backoff, that is $BE_{min} = BE_{max}$ =2, 3, 4 and 5 (corresponding to W_k =4, 8, 16 and 32), and the cases in which the exponential backoff is implemented, for which we set $BE_{max} = 5$ and BE_{min} =2, 3 (the standard case) and 4 (corresponding to W_k =4, 8 and 16).

In Figure 4.19 by increasing W_0, p_s increases, as the probability that two or more

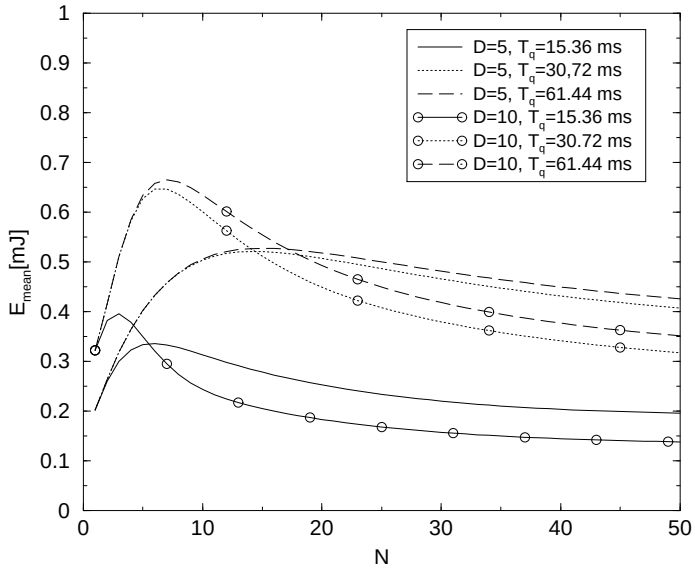

Figure 4.18: The mean energy consumed per round, E_{mean}, as a function of N, for different values of D and T_q.

nodes extract the same counter decreases. Having fixed W_0, the use of the exponential backoff improves performance. This improvement is more significant the larger is N and the smaller W_0.

By observing Figure 4.20, it can be seen that the backoff algorithms leading to better performance in terms of reliability are less energy efficient. Therefore, for example, the case $W_k = 4$ is the best from the energy consumption viewpoint and the worst from the reliability viewpoint.

For low values of N if we pass from the standard values of W_k to the case $W_k = 32$, a 10% improvement for p_s is obtained, but also a large worsening in the energy consumption (the energy consumed is three times larger). For large values of N, instead, if we pass from the standard case to $W_k = 32$, we obtain an improvement of

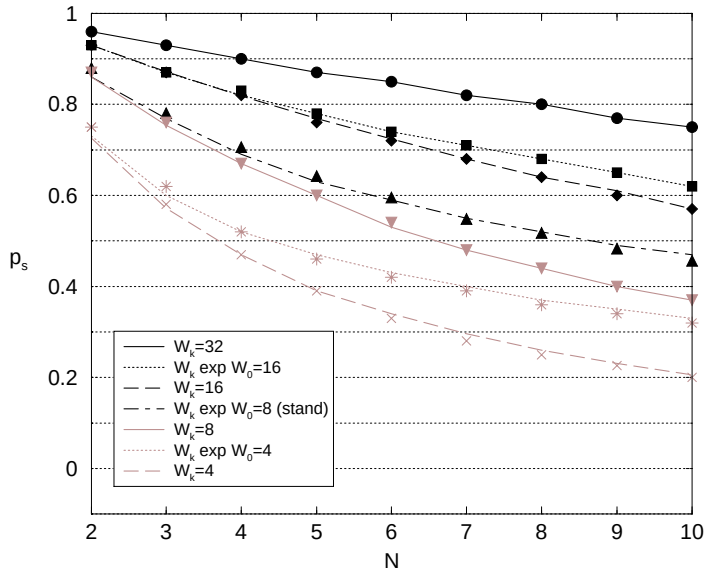

Figure 4.19: The probability p_s obtained through simulation and through the mathematical model for different value of N, by varying the values of W_k, having fixed $NB_{max} = 4$.

almost 30% for p_s while the energy is less than doubled; therefore, in some cases it could be a convenient option.

However, the choice of the backoff algorithm to be implemented depends on the application: in case energy efficiency is a more stringent requirement with respect to reliability, low values of W_0 must be considered; on the opposite, larger values of W_0 should be used in case reliability is the main requirement of the application. As we can see form the Figures, the protocol defined by 802.15.4 realizes a good trade-off between all requirements.

Finally, in Figures 4.21 and 4.22 p_s and E_{mean} as a function of N, by varying NB_{max} are reported, respectively. Here W_k are set to the values defined by the standard and $W_k = 4$ for every k. As we can see, no differences are present in all

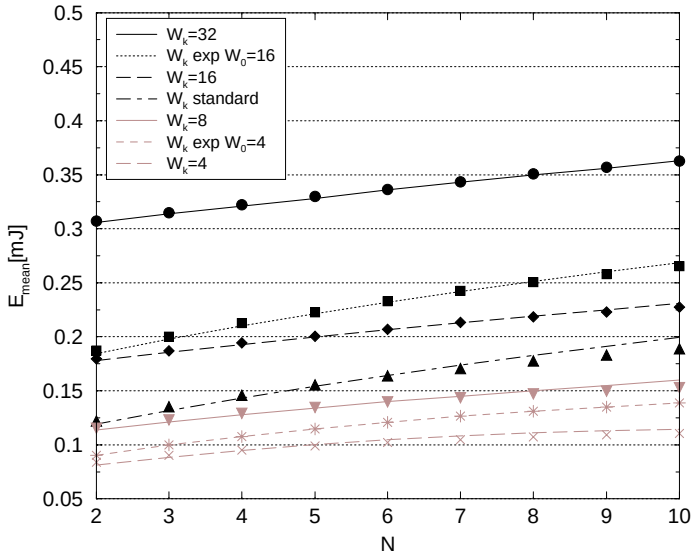

Figure 4.20: The mean energy spent, E_{mean} [mJ] obtained through simulation and through the mathematical model for different values of N, by varying the values of W_k, having fixed $NB_{max} = 4$.

performance metrics when the standard values of W_k are fixed. In the case $W_k = 4$, instead, there is a small difference for large values of N. Therefore, we can deduce that for the number of nodes considered here, increasing NB_{max} does not affect performance since in most cases all nodes succeed in accessing the channel before $\hat{t}_{max}$.

4.5 The Beacon-Enabled Model

In this section the beacon-enabled model, considering both star and tree-based topologies, is derived. The section is outlined as follows: section 4.5.1 introduces the metrics derived from the model, whereas in the sections 4.5.2 and 4.5.3 the mathematical

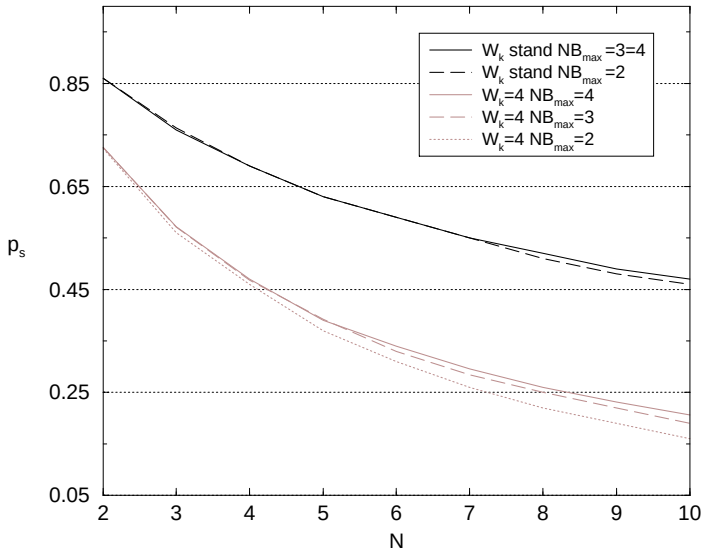

Figure 4.21: The probability p_s obtained through the mathematical model for different values of N, by varying NB_{max}, having fixed the W_k standard values and W_k=4 for $k \in (0, NB_{max})$.

model of the CSMA/CA algorithm and the performance metrics related to the CAP portion of the superframe, are derived. All the previous sections are related to star topologies, and the related results are discussed in section 4.5.4. In section 4.5.5, finally, the tree-based topology is dealt with.

4.5.1 Performance Metrics Derived from the Model

Have in mind that in case of star topologies, we set $BI = SD = T_q$ and also that we denote as s, the s-th slot (i.e., backoff period) in the superframe. Note that here we introduce a new variable for denoting the generic slot, s, which is different from j, previously defined; the relationship between s and j will be explained in the following.

The model provides the following metrics:

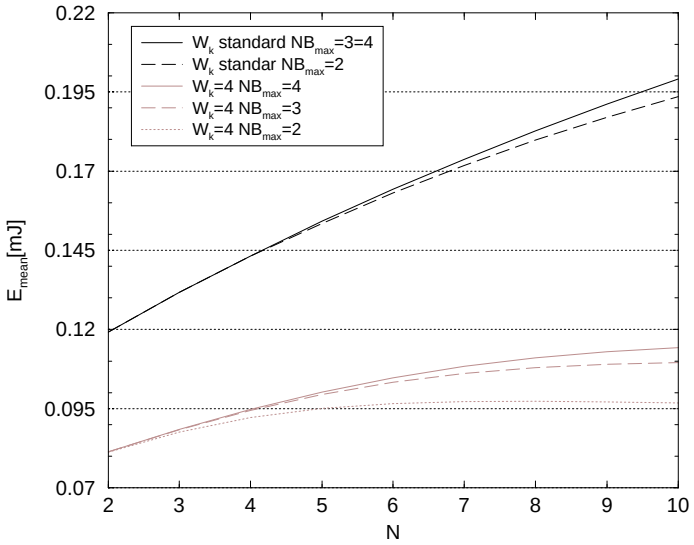

Figure 4.22: The mean energy spent, E_{mean} [mJ], obtained through the mathematical model for different values of N, by varying NB_{max}, having fixed the W_k standard values and W_k=4 for $k \in (0, NB_{max})$.

- the probability that a node ends the transmission of its packet in a given slot s, denoted as $P\{T^s\}$, with $s \in [0, T_q/d_{bo} - 1]$;

- the probability that the sink receives the packet tail, coming from a node, in a given slot s, denoted as $P\{Z^s\}$, with $s \in [0, T_q/d_{bo} - 1]$;

- the success probability for a transmission, that is the probability that a node succeeds in transmitting its packet in the superframe whatever the slot, denoted as p_s.

We assume that when N_{GTS} GTSs are used, the sink will assign these slots to N_{GTS} different nodes randomly selected among the N nodes of the network. Therefore, no resource allocation strategies are accounted for, in the model. For the scenario

considered, this assumption is reasonable, since we assume that all nodes transmit packets of the same size and no priority policy between nodes is needed.

In these conditions, the probability that a node may use the CPF to access the channel is equal to N_{GTS}/N; whereas the probability that a node has to use the CAP is equal to $(N - N_{GTS})/N$.

To simplify formulas in the following, we will denote as j the slots in the CAP portion, and as $P\{T^j\}_{CAP}$ and $P\{Z^j\}_{CAP}$, the probabilities that a node succeeds in accessing the channel and in transmitting its packet in slot j of the CAP portion, being $j \in [0, T_{CAP}/d_{bo} - 1]$. Therefore, we simply set $j = s - 6$ (see Figure 4.2, below part).

The probabilities $P\{T^s\}$ and $P\{Z^s\}$ in the CAP portion are given by:

$$P\{T^s\} = \begin{cases} 0 & \text{for } s \in [0, 5] \\ P\{T^j\}_{CAP} \cdot \frac{N - N_{GTS}}{N} & \text{for } s \in [6, (T_{CAP} + d_B)/d_{bo} - 1] \\ & \text{and } j \in [0, T_{CAP}/d_{bo} - 1] \,, \end{cases} \tag{4.5.1}$$

and

$$P\{Z^s\} = \begin{cases} 0 & \text{for } s \in [0, 5] \\ P\{Z^j\}_{CAP} \cdot \frac{N - N_{GTS}}{N} & \text{for } s \in [6, (T_{CAP} + d_B)/d_{bo} - 1] \\ & \text{and } j \in [0, T_{CAP}/d_{bo} - 1] \,. \end{cases} \tag{4.5.2}$$

Whereas, in the CFP, we have:

$$P\{T^s\} = P\{Z^s\} = \begin{cases} \frac{1}{N} & \text{for } s = (T_{CAP} + d_B)/d_{bo} + k \cdot D_{GTS} \cdot 3 \cdot 2^{SO} + D - 1 \\ & \text{and } k \in [0, N_{GTS} - 1] \\ 0 & \text{otherwise} \,. \end{cases} \tag{4.5.3}$$

Have in mind that transmissions are referred to the slot in which the transmission ends.

The cumulative functions, $F_T(s)$ and $F_Z(s)$, defined as the probability that a node transmits its packet within slot s, and that a node transmits correctly its packet within s, respectively, are given by: $F_T(s) = \sum_{v=0}^{s} P\{T^v\}$, and $F_Z(s) = \sum_{v=0}^{s} P\{Z^v\}$.

Finally, the success probability, p_s, for a packet transmitted by a node in a network composed by N nodes organised in a star topology, $p_s(N)$, is:

$$p_s(N) = p_{s_{CAP}}(N - N_{GTS}) \cdot \frac{N - N_{GTS}}{N} + \frac{N_{GTS}}{N}, \tag{4.5.4}$$

where $p_{s_{CAP}}(N - N_{GTS})$ is the success probability for a packet transmitted in the CAP portion, through the CSMA/CA algorithm, when $N - N_{GTS}$ nodes are competing for the channel. The success probability for a packet transmitted in the CFP, instead, is equal to one.

The probabilities $P\{T^j\}_{CAP}$, $P\{Z^j\}_{CAP}$ and $p_{s_{CAP}}$, related to the CAP portion, are derived in the following sections where the mathematical model of the CSMA/CA algorithm is introduced.

4.5.2 Formulation of the Mathematical Model of the CSMA/CA Algorithm

Node States

As in the non beacon-enabled case, a node accessing the channel during the CAP portion of the superframe can be in one of four states: backoff, sensing, transmission, or idle, and given the objectives of this work, we need to model only the backoff and

sensing states.

The node state is modeled as a three-dimensional process $Q(\hat{t})$= $\{BO_c(\hat{t})$,$BO_s(\hat{t})$, $CW(\hat{t})\}$, where $\hat{t}$ is an integer, representing the time, expressed in number of slots, having set the origin of this time axis ($\hat{t} = 0$) at the instant when nodes receive the beacon. Therefore, $\hat{t} = j$ denotes the j-th slot (from $j \cdot d_{bo}$ to $(j + 1) \cdot d_{bo}$), after the reception of the beacon, that is the interval of time between $120T_s + j \cdot d_{bo}$ and $120T_s + (j + 1) \cdot d_{bo}$.

$BO_c(\hat{t})$ and $BO_s(\hat{t})$ represent, once again, the backoff time counter and the backoff stage at time $\hat{t}$, respectively, and $CW(\hat{t})$ is the value of CW at time $\hat{t}$.

As in the non beacon-enabled case, we can identify $NB_{max} + 1$ different backoff stages obtained by considering the different possible combinations of the pair (NB, BE), shown in Table 4.1.

Since there exists a maximum value for NB, there will be also a maximum delay affecting the transmission of a packet. This maximum is reached in case a node extracts at every backoff stage the higher backoff time counter and at the end of each backoff stage it always finds the channel busy. Therefore, the last slot in which a transmission can start is $\hat{t}_{max} = \sum_{k=0}^{NB_{max}} W_k + 5 = 125$, and the last slot in which a transmission can finish is $(\hat{t}_{max} + D - 1)$.

In the following, the generic state will be denoted as $Q(\hat{t})$=$\{BO_c, BO_s, CW, \hat{t}\}$ and the probability of being in a generic state will be denoted as $P\{BO_c$=c, BO_s=i, CW=$w, \hat{t}$=$j\}$=$P\{c, i, w, j\}$. In particular, the probability of being in a backoff state, will be denoted as $P\{c, i, 2, j\}$, since in these states CW is equal to 2. Whereas the probability of being in the first sensing phase (i.e., when CW=2) and in the second sensing phase (i.e., when CW=1) at the j-th slot and in the i-th backoff stage, will

be denoted as $P\{S2_i^j\}$=$P\{0, i, 2, j\}$ and $P\{S1_i^j\}$=$P\{0, i, 1, j\}$, respectively. Note that when a node is in sensing state, BO_c, is equal to zero.

Steps Followed by the Model

Let us denote as b_w^j the probability that in the j-th slot when $CW = w$ the channel is found to be busy after sensing. Since CW is equal to 2 when a node performs the first sensing phase and to 1 when it performs the second sensing phase, we will denote as b_2^j the probability to find the channel busy in the first phase and as b_1^j the probability to find the channel busy in the second phase. Finally, we will denote as f^j, the joint probability to find the channel free in slot j and in slot $j-1$ (i.e., the probability that a node starting sensing in slot $j-1$ finds the channel free for two subsequent slots). These probabilities will be initially left as parameters, and their computation will be performed in section 4.5.3. The model provides $P\{T^j\}_{CAP}$ and $P\{Z^j\}_{CAP}$, with $j \in [0, T_{CAP}/d_{bo} - 1]$, and $p_{s_{CAP}}$.

The probability $P\{T^j\}_{CAP}$ depends on the probability of being in sensing state in the slot $j - D - 1$ (since a packet occupies D slots) and to find the channel free for two subsequent slots. To determine the sensing probabilities, the behavior of a single node is modeled, using a state-transition diagram [109], describing the relation between all possible states in which a node can be (see the following section). From this diagram, we obtain the probabilities $P\{S1_i^j\}$ and $P\{S2_i^j\}$, whatever be j and i. This is made in the remainder of this section. From these probabilities, we can derive the probabilities $P\{T^j\}_{CAP}$, $P\{Z^j\}_{CAP}$, $p_{s_{CAP}}$ are derived in section 4.5.3. At the end of this section are also given b_1^j, b_2^j and f^j. The algorithm used to compute all the target performance metrics is not reported owing to its similarity with the one

illustrated in section 4.4.3.

Sensing Probabilities

The state-transition diagram of the bidimensional process $Q(\hat{t})$ is presented through five different Figures (4.23, 4.24, 4.25, 4.26 and 4.27), related to the backoff stages $BO_s = 0$, 1, 2, 3 and 4, respectively. Because each Figure is related to a specific value of BO_s, for the sake of simplicity in the drawings, the generic backoff state (ovals in the Figures) is simply denoted as $\{c, j\}$, omitting the value of BO_s, and also the value of CW, equal to 2 for all backoff states. The sensing states (squares) are denoted as $S1^j$ and $S2^j$ with no pedex i.

In the following the probabilities of being in the different states of the chain and the transition probabilities between the states will be provided, for the different backoff stages. The description of the different finite state transition diagrams are omitted owing to their similarity with the diagrams of the non beacon-enabled mode. Therefore, we refer to section 4.4.2 for these descriptions.

First Backoff Stage ($BO_s = 0$)

Denoting as $P\{BO_c = c_1, BO_s = i_1, CW = w_1, \hat{t} = j_1 | BO_c = c_0, BO_s = i_0, CW = w_0, \hat{t} = j_0\}$=$P\{c_1, i_1, w_1, j_1 | c_0, i_0, w_0, j_0\}$, the transition probability from the state $\{c_0, i_0, w_0, j_0\}$ to the state $\{c_1, i_1, w_1, j_1\}$, the transition probabilities between the backoff states are given by:

$$P\{c, 0, 2, j+1 | c+1, 0, 2, j\} = 1 \,, \tag{4.5.5}$$

for $c \in [0, W_0 - 2]$ and $j \in [0, W_0 - 2]$. This equation accounts for the fact that, at

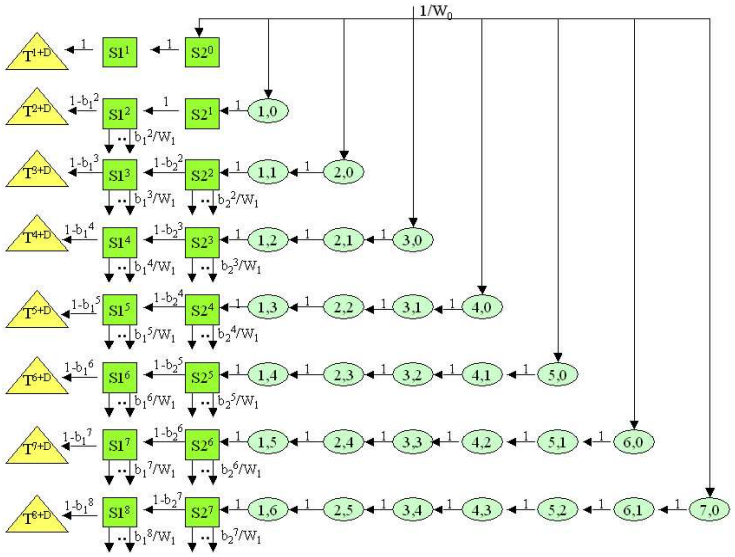

Figure 4.23: The state-transition diagram of the first backoff stage ($BO_s = 0$).

the beginning of each time slot, the backoff time counter is decreased by 1 until it reaches the zero value, with probability 1.

The probabilities of being in a sensing state when $CW = 2$ are given by:

$$P\{S2_0^j\} = \begin{cases} \frac{1}{W_0} & \text{for } j \in [0, W_0 - 1] \\ 0 & \text{otherwise .} \end{cases} \tag{4.5.6}$$

The probabilities of being in a sensing state when $CW = 1$ are given by:

$$P\{S1_0^j\} = \begin{cases} P\{S2_0^{j-1}\} \cdot (1 - b_2^{j-1}) & \text{for } j \in [1, W_0] \\ 0 & \text{otherwise .} \end{cases} \tag{4.5.7}$$

A node, in fact, will sense the channel for the second time if and only if it finds the channel free during the first sensing phase.

Second Backoff Stage ($BO_s = 1$)

As a node can arrive in this backoff stage only after it has finished the first one, it cannot reach this stage before $\hat{t} = 3$.

As in the previous case, the transition probabilities between backoff states are given by:

$$P\{c, 1, 2, j+1 | c+1, 1, 2, j\} = 1 \ , \tag{4.5.8}$$

for $c \in [0, W_1 - 2]$ and $j \in [3, W_{0,1} - 1]$, where $W_{0,1} = W_0 + W_1$.

The transition probabilities between the sensing states at $CW = 2$ of the first backoff stage ($BO_s = 0$) and the states of the second backoff stage ($BO_s = 1$) are given by:

$$P\{c, 1, 2, j+1 | 0, 0, 2, j\} = \frac{b_2^j}{W_1} \ , \tag{4.5.9}$$

for $c \in [0, W_1 - 1]$ and $j \in [2, W_0 - 1]$. This equation accounts for the fact that in case the channel at the j-th slot is found busy, the node will go to one of the states $\{c, 1, 2, j+1\}$, with $c \in [0, W_1 - 1]$, with the same probability $1/W_1$.

The transition probabilities between the sensing states at $CW = 1$ of the first backoff stage ($BO_s = 0$) and the states of the second backoff stage ($BO_s = 1$) are given by:

$$P\{c, 1, 2, j+1 | 0, 0, 1, j\} = \frac{b_1^j}{W_1} \ , \tag{4.5.10}$$

for $c \in [0, W_1 - 1]$ and $j \in [2, W_0]$.

The probabilities of being in sensing when $CW = 2$ are given by:

$$P\{S2_1^j\} = \begin{cases} \sum_{v=2}^{j-1}(P\{S1_0^v\} \cdot \frac{b_1^v}{W_1} + P\{S2_0^v\} \cdot \frac{b_2^v}{W_1}) & \text{for } j \in [3, W_0 + 1] \\ P\{S2_1^{W_0+1}\} & \text{for } j \in [W_0 + 2, W_1 + 2] \\ \sum_{v=j-W_1}^{W_0}(P\{S1_0^v\} \cdot \frac{b_1^v}{W_1} + P\{S2_0^v\} \cdot \frac{b_2^v}{W_1}) & \text{for } j \in [W_1 + 3, W_{0,1}] \\ 0 & \text{otherwise.} \end{cases} \tag{4.5.11}$$

The first equation derives from the fact that until $j \leq W_0$, the probability of being in sensing at the second backoff stage depends on the probabilities of being in sensing at the first backoff stage and of finding the channel busy the first or the second time. As an example, a node can arrive in $S2_1^3$ if it is in $S1_0^2$ or in $S2_0^2$, finds the channel busy, and extracts the value 0 for the second backoff stage (see Figs. 4.23 and 4.24). The second equation accounts for the fact that for $j > W_0 + 1$, there are no more transitions between the states of $BO_s = 0$ and the ones of $BO_s = 1$, because the last slot in which a node can sense the channel in the first backoff stage is $j = W_0 = 8$. Finally, when j reaches $W_1 + 3 = 19$, the sum starts with $v = 3$ and not 2, since if a node is in $S1_0^2$ (or in $S2_0^2$) it moves (in case of channel busy) to states $\{c, 1, 2, 3\}$ with $c \in [0, 15]$; therefore the state $\{16, 1, 2, 3\}$ does not exist (see the Figure).

Finally, the probabilities of being in a sensing state when $CW = 1$ are given by:

$$P\{S1_1^j\} = \begin{cases} P\{S2_1^{j-1}\} \cdot (1 - b_2^{j-1}) & \text{for } j \in [4, W_{0,1}] \\ 0 & \text{otherwise .} \end{cases} \tag{4.5.12}$$

Third Backoff Stage ($BO_s = 2$)

Following similar considerations as above, and observing the part of the state-transition diagram depicted in Figure 4.25, we can derive the following probabilities.

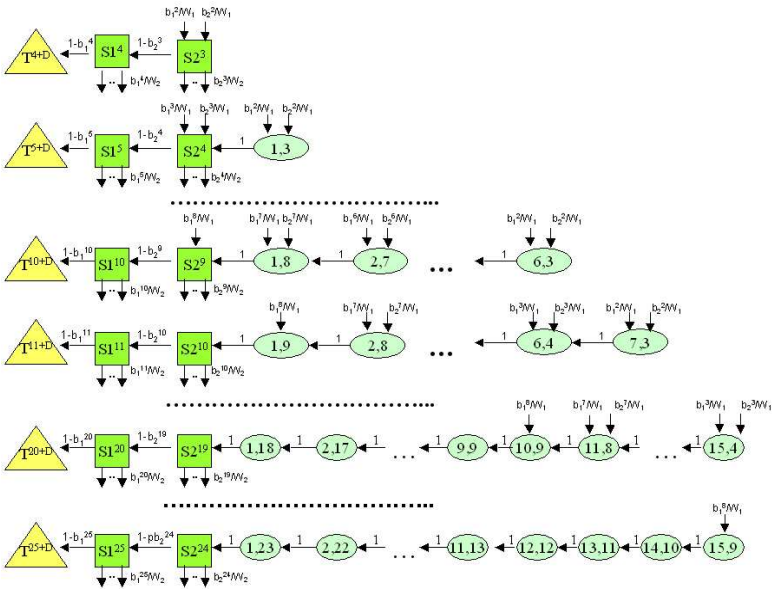

Figure 4.24: The state-transition diagram of the second backoff stage ($BO_s = 1$).

The transition probabilities between the backoff states are given by:

$$P\{c, 2, 2, j+1 | c+1, 2, 2, j\} = 1 \ , \tag{4.5.13}$$

for $c \in [0, W_2 - 2]$ and $j \in [4, W_{0,1,2}]$.

The transition probabilities between the sensing states at $CW = 2$ of the second backoff stage ($BO_s = 1$) and the states of the third backoff stage ($BO_s = 2$) are given by:

$$P\{c, 2, 2, j+1 | 0, 1, 2, j\} = \frac{b_2^j}{W_2} \ , \tag{4.5.14}$$

for $c \in [0, W_2 - 1]$ and $j \in [3, W_{0,1}]$.

The transition probabilities between the sensing states at $CW = 1$ of the second backoff stage ($BO_s = 1$) and the states of the third backoff stage ($BO_s = 2$) are given

by:

$$P\{c,2,2,j+1|0,1,1,j\} = \frac{b_1^j}{W_2} \ , \tag{4.5.15}$$

for $c \in [0, W_2 - 1]$ and $j \in [4, W_{0,1} + 1]$.

The probabilities of being in sensing state when $CW = 1$ are given by:

$$P\{S2_2^j\} = \begin{cases} \sum_{v=3}^{j-1}(P\{S1_1^v\} \cdot \frac{b_1^v}{W_2} + P\{S2_1^v\} \cdot \frac{b_2^v}{W_2}) & \text{for } j \in [4, W_{0,1} + 2] \\ P\{S2_2^{W_{0,1}+2}\} & \text{for } j \in [W_{0,1} + 3, W_2 + 3] \\ \sum_{v=j-W_2}^{W_{0,1}+1}(P\{S1_1^v\}\frac{b_1^v}{W_2} + P\{S2_1^v\}\frac{b_2^v}{W_2}) & \text{for } j \in [W_2 + 4, W_{0,1,2} + 1] \\ 0 & \text{otherwise.} \end{cases} \tag{4.5.16}$$

Finally, the probabilities of being in a sensing state when $CW = 1$ are given by:

$$P\{S1_2^j\} = \begin{cases} P\{S2_2^{j-1}\} \cdot (1 - b_2^{j-1}) & \text{for } j \in [5, W_{0,1,2} + 2] \\ 0 & \text{otherwise .} \end{cases} \tag{4.5.17}$$

Fourth Backoff Stage ($BO_s = 3$)

Similarly, and observing the part of the state-transition diagram depicted in Figure 4.26, we can derive the following probabilities.

The transition probabilities between the backoff states are given by:

$$P\{c,3,2,j+1|c+1,3,2,j\} = 1 \ , \tag{4.5.18}$$

for $c \in [0, W_2 - 2]$ and $j \in [5, W_{0,1,2,3} + 1]$.

The transition probabilities between the sensing states at $CW = 2$ of the third backoff stage ($BO_s = 2$) and the states of the fourth backoff stage ($BO_s = 3$) are given by:

$$P\{c,3,2,j+1|0,2,2,j\} = \frac{b_2^j}{W_2} \ , \tag{4.5.19}$$

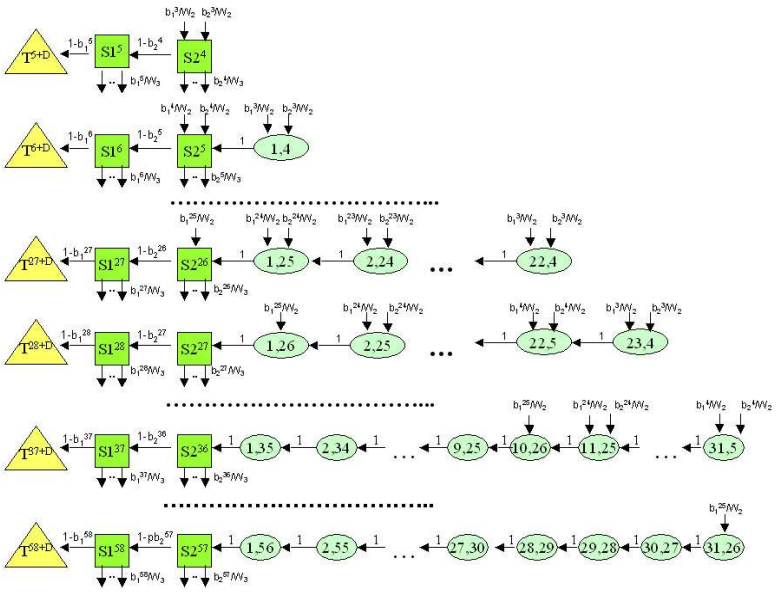

Figure 4.25: The state-transition diagram of the third backoff stage ($BO_s = 2$).

for $c \in [0, W_2 - 1]$ and $j \in [4, W_{0,1,2} + 1]$.

The transition probabilities between the sensing states at $CW = 1$ of the third backoff stage ($BO_s = 2$) and the states of the fourth backoff stage ($BO_s = 3$) are given by:

$$P\{c, 3, 2, j+1 | 0, 2, 1, j\} = \frac{b_1^j}{W_2} , \tag{4.5.20}$$

for $c \in [0, W_2 - 1]$ and $j \in [5, W_{0,1,2} + 2]$.

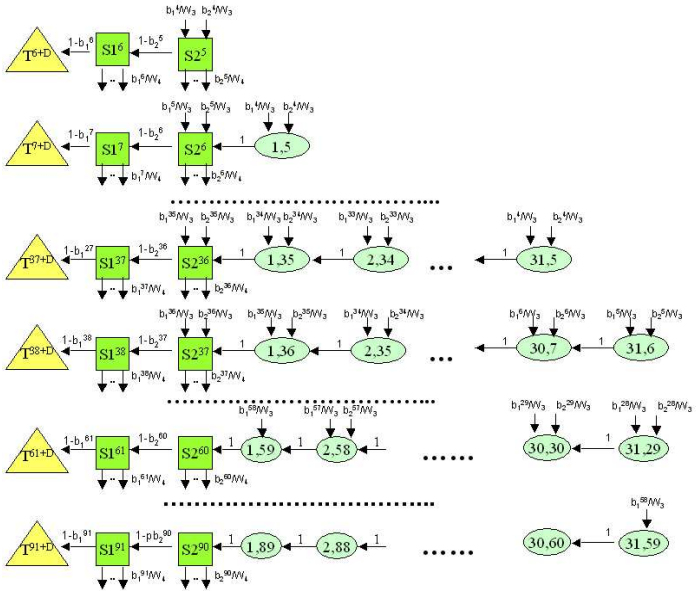

Figure 4.26: The state-transition diagram of the fourth backoff stage ($BO_s = 3$).

The probabilities of being in sensing state when $CW = 2$ are given by:

$$P\{S2_3^j\} = \begin{cases} \sum_{v=4}^{j-1}(P\{S1_2^v\} \cdot \frac{b_1^v}{W_2} + P\{S2_2^v\} \cdot \frac{b_2^v}{W_2}) & \text{for } j \in [5, W_2 + 4] \\ \sum_{v=j-W_2}^{j-1}(P\{S1_2^v\}\frac{b_1^v}{W_2} + P\{S2_2^v\}\frac{b_2^v}{W_2}) & \text{for } j \in [W_2 + 5, W_{0,1,2} + 3] \\ \sum_{v=j-W_2}^{W_{0,1,2}+2}(P\{S1_2^v\}\frac{b_1^v}{W_2} + P\{S2_2^v\}\frac{b_2^v}{W_2}) & \text{for } j \in [W_{0,1,2} + 4, W_{0,1,2,3} + 2] \\ 0 & \text{otherwise.} \end{cases} \tag{4.5.21}$$

Finally, the probabilities of being in a sensing state when $CW = 1$ are given by:

$$P\{S1_3^j\} = \begin{cases} P\{S2_3^{j-1}\} \cdot (1 - b_2^{j-1}) & \text{for } j \in [6, W_{0,1,2,3} + 3] \\ 0 & \text{otherwise .} \end{cases} \tag{4.5.22}$$

Fifth Backoff Stage ($BO_s = 4$)

Similarly, and observing the part of the state-transition diagram depicted in Figure 4.27, we can derive the following probabilities.

The transition probabilities between the backoff states are given by:

$$P\{c, 4, 2, j+1 | c+1, 4, 2, j\} = 1 \ , \tag{4.5.23}$$

for $c \in [0, W_2 - 2]$ and $j \in [6, W_{0,1,2,3,4} + 2]$.

The transition probabilities between the sensing states at $CW = 2$ of the fourth backoff stage ($BO_s = 3$) and the states of the fifth backoff stage ($BO_s = 4$) are given by:

$$P\{c, 4, 2, j+1 | 0, 3, 2, j\} = \frac{b_2^j}{W_2} \ , \tag{4.5.24}$$

for $c \in [0, W_2 - 1]$ and $j \in [5, W_{0,1,2,3} + 2]$.

The transition probabilities between the sensing states at $CW = 1$ of the fourth backoff stage ($BO_s = 3$) and the states of the fifth backoff stage ($BO_s = 4$) are given by:

$$P\{c, 4, 2, j+1 | 0, 3, 1, j\} = \frac{b_1^j}{W_2} \ , \tag{4.5.25}$$

for $c \in [0, W_2 - 1]$ and $j \in [6, W_{0,1,2,3} + 3]$.

The probabilities of being in sensing state when $CW = 2$ are given by:

$$P\{S2_4^j\} = \begin{cases} \sum_{v=5}^{j-1} (P\{S1_3^v\} \cdot \frac{b_1^v}{W_2} + P\{S2_3^v\} \cdot \frac{b_2^v}{W_2}) & \text{for } j \in [6, W_2 + 5] \\ \sum_{v=j-W_2}^{j-1} (P\{S1_3^v\} \frac{b_1^v}{W_2} + P\{S2_3^v\} \frac{b_2^v}{W_2}) & \text{for } j \in [W_2 + 6, W_{0,1,2,3} + 4] \\ \sum_{v=j-W_2}^{W_{0,1,2,3}+3} (P\{S1_3^v\} \frac{b_1^v}{W_2} + P\{S2_3^v\} \frac{b_2^v}{W_2}) & \text{for } j \in [W_{0,1,2,3} + 5, W_{0,1,2,3,4} + 3] \\ 0 & \text{otherwise.} \end{cases} \tag{4.5.26}$$

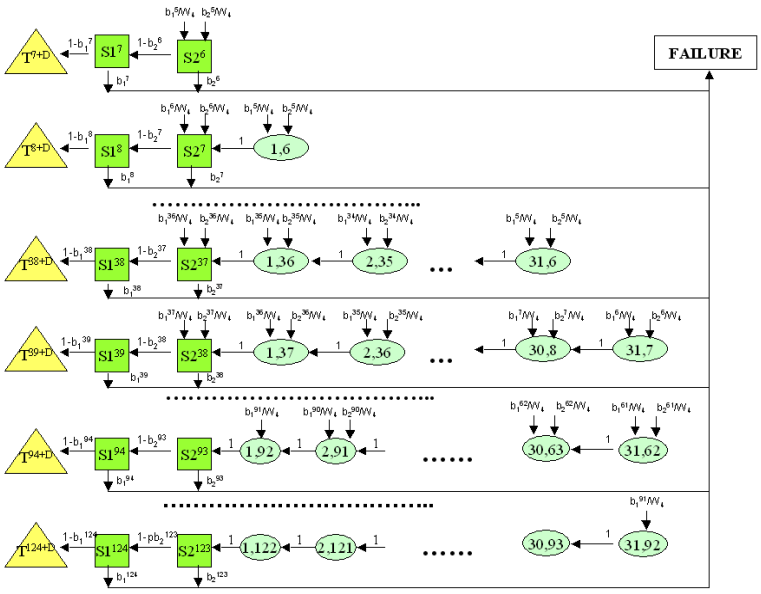

Figure 4.27: The state-transition diagram of the fifth backoff stage ($BO_s = 4$).

Finally, the probabilities of being in a sensing state when $CW = 1$ are given by:

$$P\{S1_4^j\} = \begin{cases} P\{S2_4^{j-1}\} \cdot (1 - b_2^{j-1}) & \text{for } j \in [7, W_{0,1,2,3,4} + 4] \\ 0 & \text{otherwise .} \end{cases} \tag{4.5.27}$$

4.5.3 Performance Metrics related to the CAP portion

Transmission Probabilities

As stated before, the aim of our model is to evaluate the probability that a generic node ends its packet transmission in slot j, $P\{T^j\}_{CAP}$, with $j \in [0, T_{CAP}/d_{bo} - 1]$.

A node finishes its transmission in slot j, if in slot $j - D - 1$, it starts sensing the channel finding it free for two subsequent slots. The probability that a node starts sensing in slot j, is the sum of the probabilities of starting sensing in the j-th slot

and at the i-th backoff stage, considering all possible backoff stages. Therefore, we obtain:

$$P\{T^j\}_{CAP} = \begin{cases} f^{j-D} \cdot \sum_{k=0}^{NB_{max}} P\{S2_k^{j-D-1}\} & \text{for } j \in [D+1, \hat{t}_{max}+D-1] \\ 0 & \text{otherwise} \end{cases} \tag{4.5.28}$$

Because a node transmits a packet occupying D slots, we associate $P\{T^j\}_{CAP}$ to the slot in which the transmission terminates.

The probabilities $P\{T^j\}_{CAP}$ obtained from eq. (4.5.28) are used in eq. (4.5.1) to derive the statistics in the whole superframe.

Reception and Success Probability

To evaluate the other target probabilities, we have to model how the number of nodes that compete for the access to the channel varies with time. The number of nodes which have not transmitted yet at the end of slot $j-1$ and that will compete for slot j, is denoted as N_c^j. N_c^j is a random variable, binomially distributed; however since a precise modelling of this variable, is very complex [16], an approximation in the model, by simply setting $N_c^j = N_c = N$, whatever be j, has been introduced. In section 4.5.4, simulations are compared with the mathematical approach. Results show that a very good agreement with simulations is obtained through the model, despite the approximation introduced.

The probability, p_s, that a generic packet is transmitted successfully on the channel

given by:

$$p_{s_{CAP}} = \begin{cases} \sum_{j=0}^{\hat{t}_{max}+D-1} P\{Z^j\}_{CAP} & \text{if} \quad \hat{t}_{max} + D - 1 \leq T_{CAP}/d_{bo} - 1 \\ \sum_{j=0}^{T_{CAP}/d_{bo}-1} P\{Z^j\}_{CAP} & \text{otherwise} \end{cases} \tag{4.5.29}$$

where $P\{Z^j\}_{CAP}$ is the probability that a successful transmission ends in slot j, which means that one and only one transmission starts in $j - D + 1$.

As only one transmission starts in slot $j - D + 1$ if only one node, over N_c, senses the channel in slot $j - D$ and if the channel is free in $j - D$ and $j - D - 1$, $P\{Z^j\}$ is given by:

$$P\{Z^j\}_{CAP} = f^{j-D} \sum_{k=0}^{NB_{max}} P\{S2_k^{j-D}\} \cdot \prod_{k=0}^{NB_{max}} (1 - P\{S2_k^{j-D}\})^{N_c-1}\,, \tag{4.5.30}$$

where the second factor gives the probability that one node senses the channel in $j - D$, whatever the backoff stage, and the third factor gives the probability that the remaining $N_c - 1$ nodes do not sense the channel in slot $j - D$.

Probability to find the channel busy

The channel will be found busy in slot j in case a transmission starts in slot j, or in slot $j - 1$, up to slot $j - D + 1$, since each node transmits a packet occupying D slots. Therefore, by denoting as $P\{T_1^j\}$ the probability that at least one transmission starts in slot j, the probability to find the channel busy during the first sensing phase ($CW = 2$) is given by:

$$b_2^j = \sum_{v=j-D+1}^{j} P\{T_1^v\}\,. \tag{4.5.31}$$

Whereas, b_1^j is the probability to find the channel busy conditioned to the fact that the channel in $j-1$ was free, since a node performs the second sensing phase only if it has found the channel free in the first slot. Therefore, it is the probability that slot $j-2$ is free and that there is at least one node starting sensing in this slot:

$$b_1^j = (1 - b_2^{j-2}) \cdot \left[1 - \prod_{k=0}^{NB_{max}} (1 - S2_k^{j-2})^{N_c - 1} \right], \tag{4.5.32}$$

where the second factor (between the brackets), is the probability that at least one node starts sensing in slot $j-2$.

The channel will be jointly free in slots j and $j-1$ if no transmissions start in slot j, $j-1$, up to $j-D$, therefore, the probability f^j is given by:

$$f^j = 1 - \sum_{v=j-D}^{j} P\{T_1^v\}. \tag{4.5.33}$$

Finally, the probability that at least one transmission starts in slot j is given by:

$$P\{T_1^j\} = f^{j-1} \cdot \left[1 - \prod_{k=0}^{NB_{max}} (1 - S2_k^{j-2})^{N_c - 1} \right]. \tag{4.5.34}$$

4.5.4 Numerical Results for the Star Topology

For the purpose of numerical comparison, the same simulation tool, written in C language, used for validating the non beacon-enabled mode, has been used. Obviously, in this case the slotted CSMA/CA protocol has been implemented and also the CFP of the superframe has been simulated. Once again, ideal channel conditions are assumed, no capture effect is considered, and no acknowledge and retransmission mechanisms are performed. Once again 10^4 superframes are simulated.

In Figures 4.28 and 4.29, the cumulative function $F_T(s)$, as a function of time, s, for different values of N, having set $D = 2$ when no GTSs and seven GTSs are

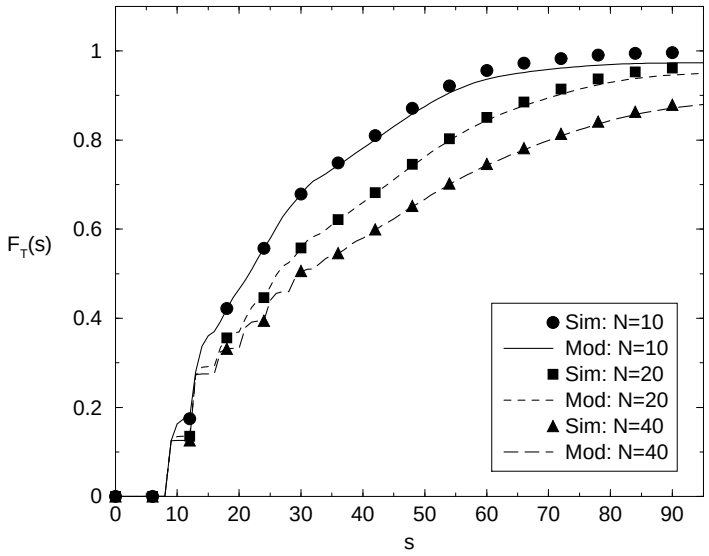

Figure 4.28: The cumulative function, $F_T(s)$, when no GTSs are allocated, having fixed $D = 2$.

allocated, are shown. Both mathematical analysis (lines) and simulation results (symbols) are reported to validate the model: an excellent agreement between results can be found in all cases. Results are obtained by setting $SO = 1$, therefore $T_q = 1920\ T_s = 30.72$ [ms]. No traffic toward the sink is present for $s < 6+(D+1) = 9$, owing to the transmission of the beacon and to the sensing phases. As expected, by increasing N, the delay with which a node accesses the channel increases. The curves do not reach the value 1, since some nodes do not succeed in accessing the channel by the end of the superframe. The step-wise behavior of curves is motivated by the move from one backoff stage to the following. $P\{T^j\}_{CAP}$, in fact, present relative maxima at the beginning of each backoff window (i.e., the interval of time in which occur transmissions of nodes performing the first, the second, etc.. backoff stage), whereas the probability to access the channel is approximately the same inside each

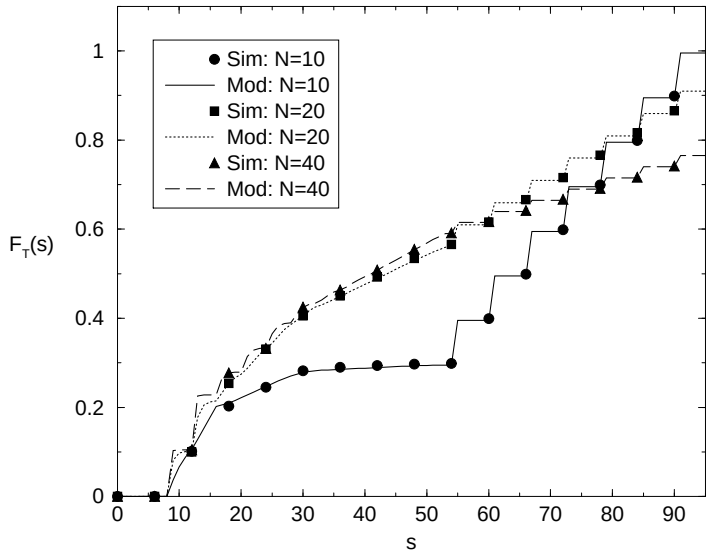

Figure 4.29: The cumulative function, $F_T(s)$, when seven GTSs are allocated, having fixed $D = 2$.

backoff window [15, 16].

In Figure 4.29 we can observe the statistic of the traffic in the CFP, characterised by steps in each GTS.

Figure 4.30 reports the cumulative function $F_Z(s)$, as a function of s, for different values of N, having set $D = 2$. The behavior of the curves is similar to that of Figure 4.28 and 4.29, the only difference is that, owing to collisions, some transmitted packets are not correctly received by the sink, therefore the curves are down translated. As we can see, a good agreement between simulation and analytical results is obtained also for this metric. A good agreement between simulation results (points) and model results (lines) has been found. The case $N = 20$ is not shown for the sake of legibility of the Figure, since curves are partially overlapped.

In Figures 4.31 and 4.32 p_s as functions of N, for different values of SO, having

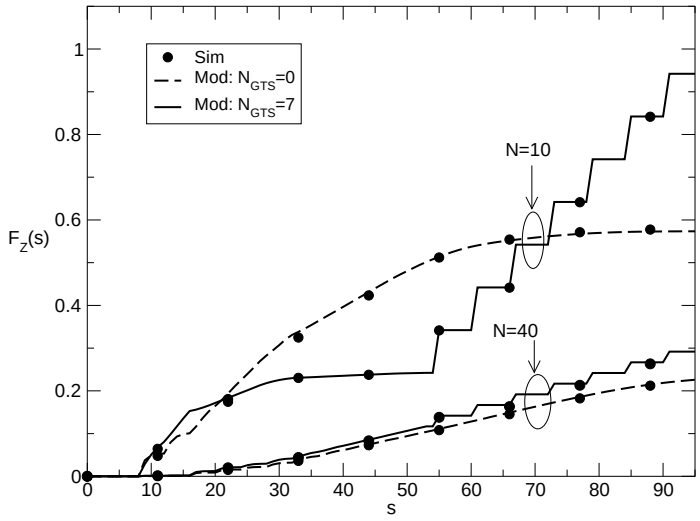

Figure 4.30: The cumulative function, $F_Z(s)$, when GTSs are allocated and not.

fixed $D = 5$ and $D = 10$ are shown, respectively. The cases of no GTSs and N_{GTS} equal to the maximum number of GTSs allocable, are considered. As explained above, this maximum number depends on the values of D and SO. As we can see, p_s decreases monotonically (for $N > 1$ when $N_{GTS} = 0$ and for $N > N_{GTS}$ when $N_{GTS} > 0$), by increasing N, since the number of nodes competing for the channel increases. As expected the use of GTSs improves performance, since less nodes compete for the channel. By increasing SO, p_s gets larger, since increases the CAP duration and nodes have more time to try to access the channel. Results for $SO > 2$ are the same obtained in the case $SO = 2$, this means that when $SO = 2$ the largest values of p_s are reached.

Now the concepts of *throughput*, denoted as S, and *offered load*, denoted as G, are introduced. We define the throughput as the number of bytes per unit of time successfully transmitted to the sink, and the offered load as the maximum number

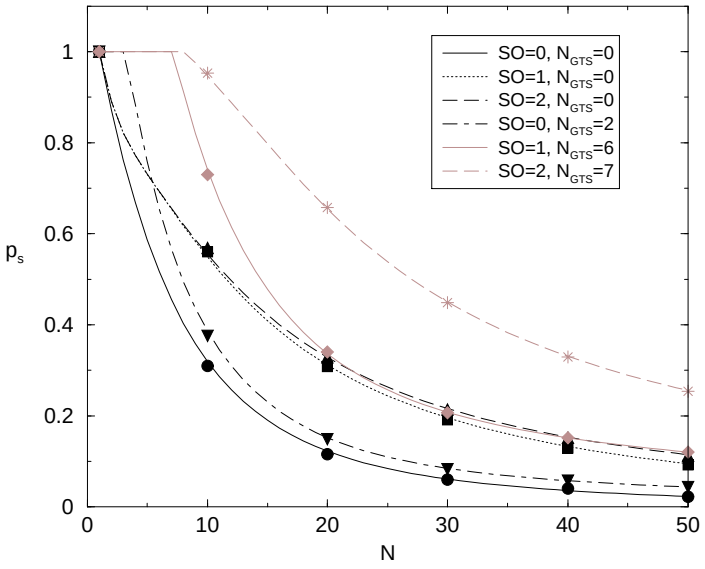

Figure 4.31: The success probability, p_s as a function of N, having fixed $D = 5$.

of bytes the network was deployed to deliver per unit of time, that is, the amount of traffic that nodes are able to offer to the sink. G is given by:

$$G = \frac{N \cdot z}{T_q} \, [bytes/sec] \, . \tag{4.5.35}$$

S is given by:

$$\begin{aligned} S = p_s \cdot G = \frac{z \cdot N}{T_q} \left(p_{s_{CAP}} \cdot \frac{N - N_{GTS}}{N} + \frac{N_{GTS}}{N} \right) = \\ = \frac{z}{T_q} \left[p_{s_{CAP}} \cdot (N - N_{GTS}) + N_{GTS} \right] \ \ [bytes/sec] \, . \end{aligned} \tag{4.5.36}$$

Have in mind that $z = D \cdot 10$ bytes and $T_q = BI = SD$, in this case.

In Figures 4.33 and 4.34, S as a function of G, when varying SO (i.e., T_q) and D, when no GTSs and when the maximum number of GTSs is allocated, respectively, are shown. When few nodes are distributed in the network, by increasing G, S gets larger. When, instead, many nodes are distributed, an increasing of G results in a

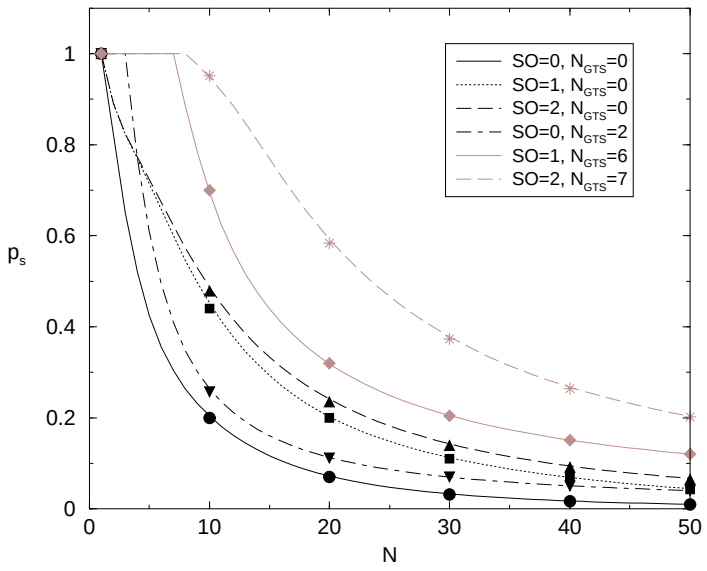

Figure 4.32: The success probability, p_s as a function of N, having fixed $D = 10$.

decrease of S, since many nodes are competing for the channel. This means that in star topologies it is not convenient to increase too much N (i.e., the cost of the network), since many packets will be lost. Moreover this results confirm that star topology is not suitable for large N. Moreover, we can note that there exists a value of SO maximising S, which depends on G and D. As an example, for $D = 5$ when G is low, an increase of SO (i.e., T_q), even though increases p_s, results in a decrement of S, since S depends also on $1/T_q$. When, instead, the offered load gets larger, collisions increase and larger values of SO are required. On the other hand, when $D = 10$, the optimum value of SO is 1, for low G. This is due to the fact that, having large packets, when $SO = 0$ too many packets are lost, owing to the short duration of the superframe.

When no GTSs are allocated (Figure 4.33) S decreases monotonically since

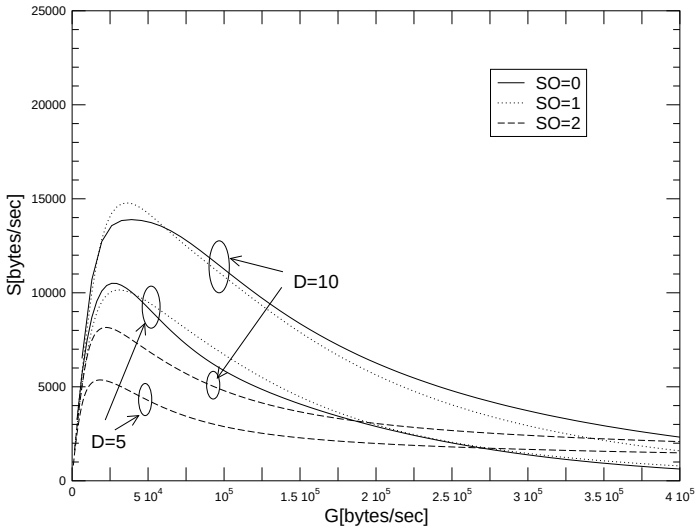

Figure 4.33: The throughput S as a function of G, when no GTSs are allocated.

$\lim_{G\to\infty} p_{s_{CAP}} = 0$. When, instead, GTSs are allocated (Figure 4.34), there exists an horizontal asymptote, derived as follows.

$$\lim_{G\to\infty} S = \lim_{G\to\infty} \left(\frac{z}{T_q} \cdot p_{s_{CAP}} \cdot (N - N_{GTS}) + \frac{z \cdot N_{GTS}}{T_q} \right) = \frac{z \cdot N_{GTS}}{T_q} \,. \qquad (4.5.37)$$

As an example, when $SO = 1$ and $D = 10$, the maximum number of GTSs allocable is $N_{GTS} = 6$ and the horizontal asymptote is $S = 19531.25$ $[bytes/sec]$.

4.5.5 The Tree-Based Topology

As stated above when the number of nodes in the PAN increases, star topologies are not suitable, and peer-to-peer or tree-based topologies should be used [51]. The tree-based topology defined by the Zigbee Alliance [51] for 802.15.4 networks, is considered here.

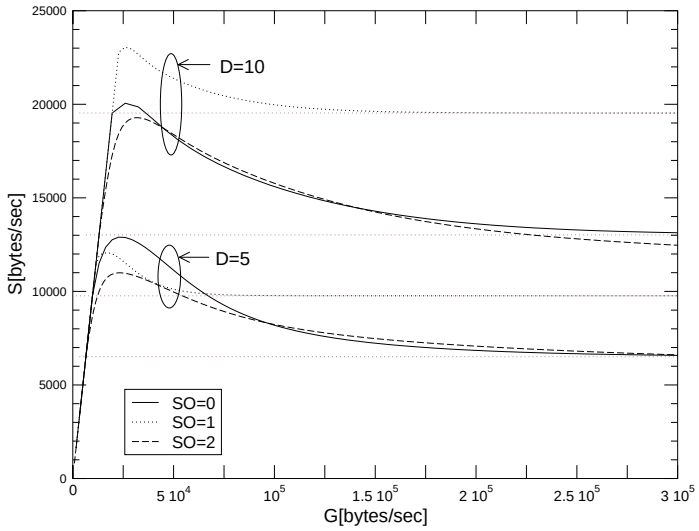

Figure 4.34: The throughput S as a function of G, when the maximum number of GTSs is allocated.

We consider a $(T+1)$-level tree-based topology, where the tree is rooted at the sink (namely, at level zero), and level i nodes receive data from level $i+1$ nodes and forward them to level $i-1$ nodes, toward the sink (see Figure 1.11).

As stated in Chapter 1, the tree formation procedure is started by the sink, which broadcasts beacons to nodes. A candidate node receiving the beacon may request to join the network at the sink. If the sink allows the node to join, it will begin transmitting periodic beacons so that other candidate nodes may join the network. In particular, each router in the tree, after the reception of the beacon coming from the parent, will select the instant when transmitting its beacon. Each child node tracks the beacon of its parent and transmits its own beacon at a predefined offset with respect to the beginning of its parent beacon. Obviously the beacon packets are sent only by the routers in the tree.

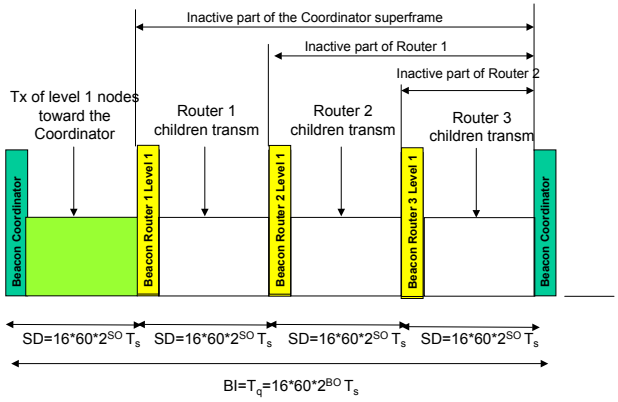

Figure 4.35: The superframe structure used in the tree-based topology.

It is assumed that all the active parts of the superframes generated by the routers and by the sink have the same duration, SD; therefore, we fix a unique value of SO. In this conditions, once we set the value of BO, the number of routers (including the sink) that will have a portion of superframe allocated for the reception of data coming from their children, will be equal to 2^{BO-SO} (see Figure 4.35).

We denote as p_i the probability that a node is at level i of the hierarchy and with $p_s(n_i)$, the success probability for a level i node competing for the channel with the other $n_i - 1$ nodes, connected to the same parent at level $i-1$. The success probability for a node accessing the channel in the tree is:

$$p_{s_{tree}} = \sum_{i=1}^{T} p_i \cdot \prod_{k=1}^{i} \overline{p_{s_k}}\,, \tag{4.5.38}$$

where $\overline{p_{s_k}} = \sum_{j=1}^{N_k} p_s(n_k) \cdot \mathbb{P}\{n_k\}$, is the average success probability for a node being at level k, and $\mathbb{P}\{n_k\}$ is the probability that n_k nodes at level k are attached to the

same parent at level $k-1$. A packet coming from a level i node will be correctly received by the sink, in case it is successfully transmitted by the level i node from which it is generated, and by all the routers from level $i-1$ till level 1, forwarding it toward the sink. According to the channel access strategy defined above, only the children of a given parent compete for the channel, therefore the tree could be seen as a set of stars, each formed by a parent and its children, operating independently (i.e., without collisions). Therefore, $p_s(n_k)$ is given by eq. (4.5.4), by simply setting $N = n_k$.

Note that equation (4.5.38) could be used to evaluate the success probability for a node accessing the channel when a $T+1$-level tree-based topology is established, whatever be the strategy used to realise the tree.

Now the success probability $p_{s_{tree}}$ is evaluated in the particular case of a three-level tree. We denote as $N_i = p_i \cdot N$, the number of level i nodes, with $i = 1, 2$. We assume that level 2 nodes select randomly the level 1 node parent, and that the active part of the superframe defined by the sink is used by level 1 nodes, whereas the remaining $2^{BO-SO} - 1$ superframe portions are randomly allocated to level 1 routers for the reception of packets coming from their children. Under these assumptions, there exists a certain probability that a level 1 router has not a portion of the superframe allocated, therefore the packets coming from its children will be lost. We denote as p_{frame} the probability that a level 2 node may try to access the channel, since its parent has a portion of the superframe allocated. This probability is given by:

$$p_{frame} = \frac{2^{BO-SO} - 1}{N_R}\,, \tag{4.5.39}$$

where N_R is the mean number of level 1 routers, that is the number of level 1 nodes that have at least one child, given by:

$$N_R = \sum_{i=0}^{N_1} \binom{N_1}{i} (p_{child})^i \cdot (1 - p_{child})^{N_1 - 1} \ , \tag{4.5.40}$$

where $p_{child} = 1 - (1 - \frac{1}{N_1})^{N_2}$ is the probability that a level 1 node has at least a child, and $1/N_1$ is the probability that a level 2 node is connected to a given level 1 node.

Being the number of level 2 nodes connected to the same level 1 node binomially distributed, we can evaluate the average success probability for a node being at level 2:

$$\overline{p_{s_2}} = \sum_{i=0}^{N_2} p_s(i) \cdot \binom{N_2}{i} \left(\frac{1}{N_1}\right)^i \cdot \left(1 - \frac{1}{N_1}\right)^{N_2 - 1} \ , \tag{4.5.41}$$

where $p_s(i)$ is the success probability given by eq. (4.5.4) when i nodes at level 2 are competing for transmitting to the same level 1 node. Finally,

$$p_{s_{tree}} = p_1 \cdot \overline{p_{s_1}} + p_2 \cdot p_{frame} \cdot \overline{p_{s_1}} \cdot \overline{p_{s_2}} \, , \tag{4.5.42}$$

where p_{frame} is given by eq. (4.5.39), and $\overline{p_{s_1}} = p_s(N_1)$.

Numerical Results for the Tree-Based Topology

Numerical results obtained in the three-level tree are discussed here, and compared with results obtained in the star topology case. Since the success probability $p_{s_{tree}}$ depends on p_s obtained in the star topology case, that has been validated in section 4.5.4, simulation results are not reported here.

In Figure 4.36 $p_{s_{tree}}$ as a function of N_1, for different values of N, D and SO, having set $BO = 5$, is shown. There exists an optimum value of N_1 maximising $p_{s_{tree}}$, and this value, obviously increases by increasing N and is approximatively the same

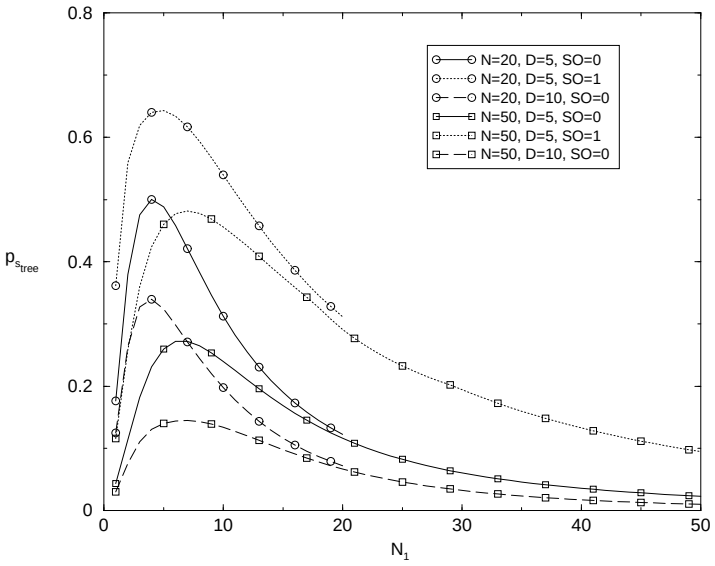

Figure 4.36: The success probability, $p_{s_{tree}}$ as a function of N_1 for a tree-based topology.

when varying D and SO. This means that, once we fix N there exists an optimum split between level 1 and level 2 nodes, maximising the success probability.

In Figure 4.37 results related to the two topologies, showing the success probability as a function of N, for different values of SO and BO, are compared. For a fair comparison, the success probability is computed by fixing the same value of $T_q = BI$, therefore giving to nodes the same time to try to access the channel. To this aim, we set $SO = BO$ for the star topology, and we compare the case "star" with $SO = BO = 1$ with the case "tree" with $BO = 1$ and $SO = 0$. Whereas the case "star" with $SO = BO > 1$ (note that the cases $SO = BO$ =2,3, etc.. bring to the same p_s) are compared with the cases "tree" with $BO > 1$, whatever be SO. In the tree case N_1 is set to the optimum value maximising $p_{s_{tree}}$ obtained from curves in the Figure 4.36. As we can see, when $BO = 1$, the star is preferable, since in the tree

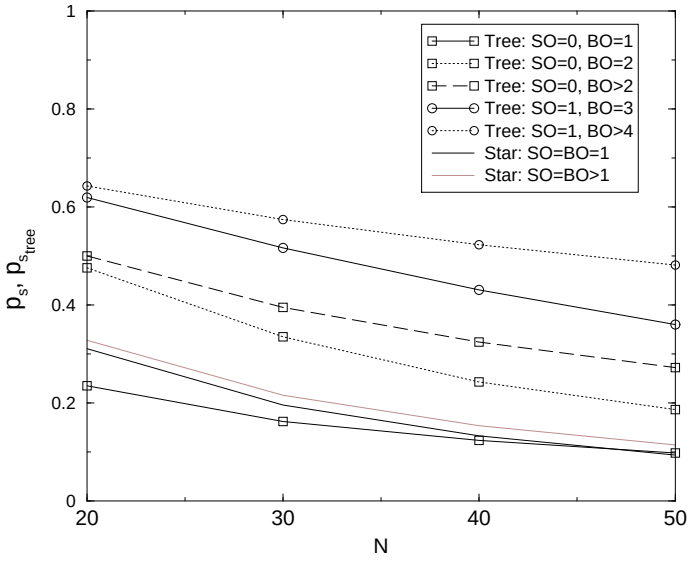

Figure 4.37: The success probability as a function of N when a star and tree topologies are used.

only one router has a part of the superframe allocated, therefore, many packets of level 2 nodes will be lost. For $BO > 1$, instead, the tree outperforms the star. The difference between the star and the tree, obviously, increases by increasing BO and SO, resulting in an increase of p_{frame} and p_s, respectively.

4.6 Comparison between the two Beacon- and Non Beacon-Enabled Modes

The comparison is performed in terms of success probability, p_s and throughput S (defined in section 4.5.4), considering the star topology (since trees may not be formed in the non beacon-enabled case [51]). Have ion mind that T_q is given by eq. (1.4.2) for

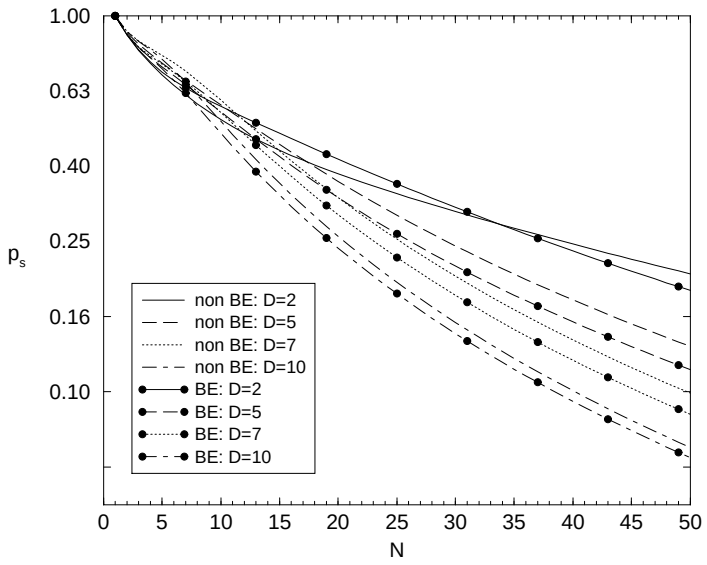

Figure 4.38: The success probability, p_s for the beacon- and non beacon-enabled modes, as a function of N.

the beacon one, and can be set whatever a value in the non beacon-enabled case [16].

Figure 4.38 compares the values of p_s obtained in the two modes, when no GTSs are allocated. Results are obtained through the mathematical models. Here $T_q = 61.44$ [ms], which corresponds to $SO = 2$ in the beacon-enabled case and is larger than the maximum possible delay in the non beacon-enabled mode. This means that the largest values of p_s that could be obtained in both the modalities, are considered. A logarithmic scale is used to better visualise the differences between the curves. It can be seen that there are no relevant differences between the two modalities, when no GTSs are allocated. When instead GTSs are used, relevant differences are present.

If we compare Figures 4.31 and 4.32, related to the beacon-enabled mode (with $D = 5$ and 10, respectively) with results of the non beacon-enabled mode shown in Figure 4.17, we can note that in both cases, $D = 5$ and 10, once we fix the round or

superframe duration, results are approximatively the same if no GTSs are allocated, whereas, there is a notable increasing of p_s in the beacon-enabled case when GTSs are allocated. Note that the cases $T_q = 15.36$ [ms], $T_q = 30.72$ [ms] and $T_q = 61.44$ [ms] correspond to $SO = 0$, 1 and 2, respectively.

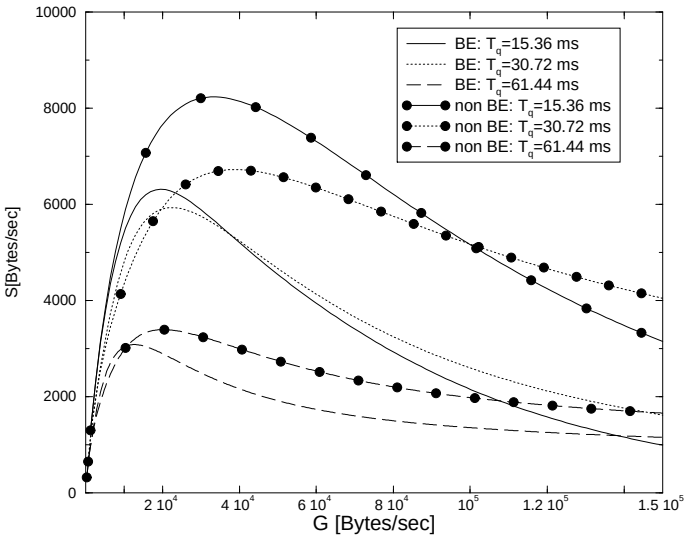

Figure 4.39: The throughput, S, as a function of G for $D = 2$, for the beacon- and non beacon-enabled modes.

In Figures 4.39 and 4.40, S as a function of G, when varying T_q, for $D = 2$ and $D = 10$, respectively, are shown. Both beacon- and non beacon-enabled modes are considered. In both Figures, once G is fixed there exists a value of SO (i.e., T_q) maximising S. For $D = 2$ (Figure 4.39) when G is low, an increase of T_q results in a decrement of S since, even though p_s gets greater (since nodes have more time to transmit their packets), the query interval is longer and, therefore, the number of bytes per second received by the sink decreases. When, instead, the offered traffic gets larger, collisions increase and larger values of T_q are required, to increase S. On

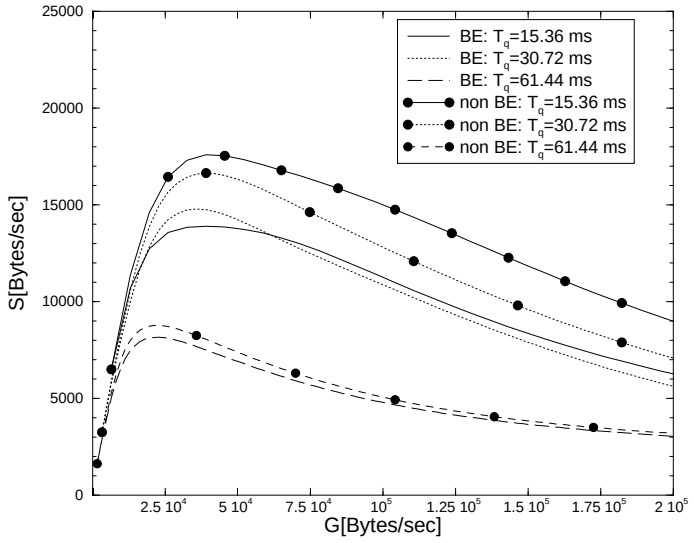

Figure 4.40: The throughput, S, as a function of G, for $D = 10$, for the beacon- and non beacon-enabled modes.

the other hand, when $D = 10$ in the beacon-enabled case, the optimum value of SO is 1, for low G. This is due to the fact that, having large packets, when $T_q = 15.36$ [ms] too many packets are lost, owing to the short duration of the superframe. If the curves obtained in the two modalities are compared, we see that (especially in the case $D = 2$) the non beacon-enabled mode outperforms the beacon-enabled mode. The differences in terms of p_s, in fact, are few when $T_q = 61.44$ [ms], but increase when T_q gets lower, since, on average, the delays in the beacon-enabled case are larger [16]. This results in notably larger values of S in the non beacon-enabled case, for low T_q.

Finally, for comparison of Figures 4.39 and 4.40, we note that, once G is fixed, S gets notably larger when D increases, since more bytes/sec are correctly transmitted toward the sink.

In Figures 4.39 and 4.40 simulation results are not reported, since S depends on

p_s, validated in many Figures of this Chapter.

4.7 Conclusions

A novel analytical model for the IEEE 802.15.4 MAC protocol, considering both non beacon- and beacon-enabled PANs, where nodes are organised in a star topology (or possibly, a tree, in the beacon-enabled case), is provided. The model does not suffer from the limitations shown by related works in the literature; however, more importantly, it also introduces a very new challenge in the modelling of CSMA-based MAC protocols for WSNs. This challenge regards the application scenario considered here: the sink periodically triggers nodes and waits for replies. This implies that each node has one and only one packet to be transmitted at each query received, and also that the number of nodes competing for the channel decreases by passing time. Therefore, this scenario imposes the use of a new approach in modeling the MAC protocol, different from that developed by Bianchi [107] and followed by almost all the successive literature from 2000 till now. As stated above, in fact, in [107] the network is studied in saturated conditions, or, anyway, in conditions in which the statistics of the traffic generated by node is defined a priori. The other relevant issue of this model is that it allows the evaluation of the statistical distribution of the traffic generated by nodes toward the sink, never investigated before analytically, and significantly useful when WHNs are considered.

Chapter 5

Area Throughput for Multi-Sink Wireless Sensor Networks

In this Chapter the models for the evaluation of connectivity properties in multi-sink WSNs and of the 802.15.4 MAC protocols, described in Chapters 3 and 4 respectively, have been integrated in a unique framework. In particular, here the concept of *area throughput*, that is the amount of data per second successfully transmitted to the sinks from a given area, is introduced. This performance metric is strictly related to both connectivity and MAC issues: it depends, in fact, on the probability that a given sensor node is not isolated and that it succeeds in transmitting its packet (i.e., the packet does not collide).

Two different scenarios, characterised by two different sensors and sinks distributions are accounted for: PPP distribution for both sensors and sinks, and Thomas Point Process (TPP) distribution (described in the following). In both cases, either bounded or unbounded regions, are considered. Note that even if the model is thought for CSMA-based MAC protocols, with particular attention toward the 802.15.4 protocol, it could be easily applied to any MAC protocol. The link model considered is the one described in Chapter 1, taking into consideration random channel fluctuations

(see eq. (1.6.1)).

After an introduction of the reference scenario, motivations and aims of the work, the PPP scenario is dealt with leaving the TPP distributed scenario for the second part of the Chapter.

5.1 Reference Scenario and Aims of the Model

A multi-sink WSN, collecting data from the environment through the sampling of some physical entities and sending them to some external user, through multiple sinks, is considered. The reference application is spatial/temporal process estimation [35] and the environment is observed through queries/respond mechanisms: queries are periodically generated by the sinks, and sensor nodes respond by sampling and sending data. Through a simple polling model, sinks periodically issue queries, causing all sensors perform sensing and communicating their measurement results back to the sinks they are associated with. The user, by collecting samples taken from different locations, and observing their temporal variations, can estimate the realisation of the observed process, as shown in Chapter 2. Good estimates require sufficient data taken from the environment.

Often, the data must be sampled from a specific portion of space, even if the sensor nodes are distributed over a larger area. Therefore, only a location-driven subset of sensor nodes must respond to queries. The aim of the query/response mechanism is then to acquire the largest possible number of samples from the area.

As stated in Chapter 1, when the number of sensors or the target area is large, nodes are often organised in clusters; one sink per cluster forwards the queries to sensors, and collects the responses.

Being the acquisition of samples from the target area the main issue for the application scenario considered, a new metric for studying the behavior of the WSN, namely the *area throughput*, denoting the amount of data per unit of time successfully transmitted to the centralised unit originating from the target area, is defined.

As expected, the area throughput is larger if the density of sensor nodes is larger, but, on the other hand, if a contention-based MAC protocol is used, the density of nodes significantly affects the ability of the protocol to avoid packet collisions (i.e., simultaneous transmissions from separate sensors toward the same sink). If, in fact, the number of sensor nodes per cluster is very large, collisions and backoff procedures can make data transmission impossible under time-constrained conditions, and the samples taken from sensors do not reach the sinks and, consequently, the centralised unit. Therefore, the optimisation of the area throughput requires proper dimensioning of the density of sensors, in a framework model where both MAC and connectivity issues are considered.

Even if the model described above, could be applied to any MAC protocol, we particularly refer to CSMA-based protocols, and in particular to the IEEE 802.15.4 air interface, being the reference interface of this thesis. In this case, sinks will act as PAN coordinators, periodically transmitting queries to sensors and waiting for replies. According to the standard, the different PAN coordinators, and therefore the PANs, use different frequency channels (see the scan functionality performed by the PAN coordinator for establishing a PAN, described in Chapter 1). Therefore no collisions may occur between nodes belonging to different PANs; however, nodes belonging to the same cluster, will compete to try to transmit their packets to the sink.

An infinite area where sensors and sinks are uniformly distributed at random, is

considered. Then, a specific portion of space, of finite size and given shape (without loss of generality, we consider a square), is considered as target area (see Figure 5.2), where sensors and sinks are distributed according to the two distributions accounted for.

The frequency of the queries transmitted by the sinks is denoted as $f_q = 1/T_q$. Each sensor takes, upon reception of a query, one sample of a given phenomenon and forwards it through a direct link to the sink. Once transmission is performed, it switches to an idle state until the next query is received. We denote the interval between two successive queries as *round*.

The amount of data available from the sensors deployed in the area, per unit of time, is denoted as *offered load*. The basic objective of this Chapter is thus to determine how the area throughput depends on the offered load for different scenarios and system parameters.

In general terms, it might be said that the aim is to define a picture showing how throughput varies with load, as done for many years in the literature for different types of MAC protocols. However, here connectivity and the plurality of sinks are accounted for.

In the PPP scenario case, a comparison of performance obtained with the beacon- and non beacon-enabled modes, is also provided. Whereas in the TPP case we also address energy consumption issues, by showing the trade-off between energy consumption and area throughput.

5.1.1 Related Works

Many works in the literature devoted their attention to connectivity in WSNs and to the analytical study of CSMA-based MAC protocols. Therefore, many works have dealt with these two issues separately; very few papers jointly consider the two issues under a mathematical approach. Some analysis of the two issues are performed through simulations: as examples, [110] related to ad hoc networks, and [11], to WSNs.

An overview of the literature related to connectivity issues in WSNs is provided in Chapter 3.

Concerning the analytical study of CSMA-based MAC protocols, in [111] the throughput for a finite population when a persistent CSMA protocol is used, is evaluated. An analytical model of the IEEE 802.11 CSMA based MAC protocol, is presented by Bianchi in [107]. In these works no physical layer or channel model characteristics are accounted for. Capture effects with CSMA in Rayleigh channels, are considered in [112], whereas [113] addresses CSMA/CA protocols. However, no connectivity issues are considered in these papers: the transmitting terminals are assumed to be connected to the destination node. In [114] the per-node saturated throughput of an IEEE802.11b multi-hop ad hoc network with a uniform transmission range, is evaluated under simplified conditions from the viewpoint of channel fluctuations and number of nodes. The works related to the analytical modeling of the IEEE 802.15.4, instead, have been introduced in Chapter 4.

For what concerns nodes spatial distribution, the very typical models in static wireless networks (i.e., not considering distributions originated from a particular mobility pattern of nodes) are the PPP and Binomial Point Process (BPP) with very few

exceptions ([80] is one of them). In [115] and [116] the authors use (among others) a modified Thomas model [117] for describing real-world nodes deployments with a good accuracy. All the previously cited works do not account for MAC issues, with the one exception known to us in a slightly different context, namely the work by Hoydis et al. [118].

5.2 Area Throughput for a Poisson Point Process Field

As stated above, the increasing of sensors density in the area, aiming at increasing the quantity of samples taken from the area (i.e., improving the estimation of the process), also causes many data losses, due to MAC failures. One solution can be found in the decimation of the sensor nodes to respond. Other improvements might be introduced by letting the sensor nodes apply a form of aggregation procedure, responding only sporadically to queries, with a single data packet composed of all samples taken since the previous transmission: fewer access attempts are performed, but with longer packets. Such decimation process, or the aggregation strategy, must be driven by an optimisation procedure that, by taking into account the density of sensor nodes and sinks, the frequency of queries, and the randomness of node locations, the radio channel behaviour, and CSMA mechanisms, determines the optimum number of nodes that should respond to any query, and whether aggregating samples provides advantages.

This section first addresses such optimisation problem, by showing the behaviour of the area throughput for different aggregation strategies and considering the 802.15.4

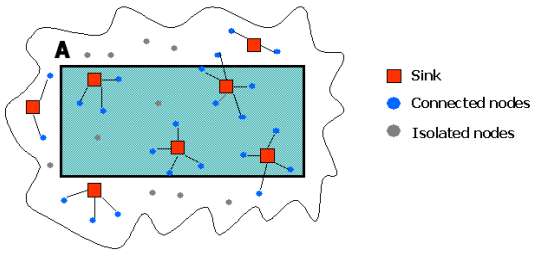

Figure 5.1: The reference scenario considered.

MAC protocol in the non beacon-enabled mode. For the sake of completeness, also an example of results obtained by applying to the framework a very simple CSMA-based MAC protocol is shown.

Finally, performance obtained with the beacon-enabled and the non beacon-enabled modes of 802.15.4, are compared.

5.2.1 Assumptions and Reference Scenario

The reference scenario considered consists of an area of finite size and given shape, where sensors and sinks are both distributed according to an homogeneous PPP. The sensors and sinks densities, are denotes as ρ_s and ρ_0, respectively, whereas A is the area of the target domain. Denoting by k the number of sensor nodes in A, k is

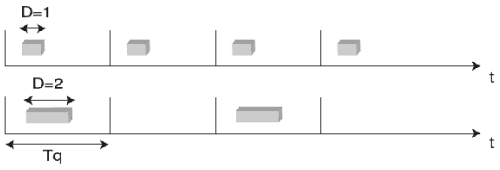

Figure 5.2: The aggregation strategy.

Poisson distributed with mean $\bar{k} = \rho_s \cdot A$ and p.d.f.

$$g_k = \frac{\bar{k}^k e^{-\bar{k}}}{k!}. \tag{5.2.1}$$

The average number of sinks in A is denoted as $I = \rho_0 \cdot A$.

The Aggregation Strategy

Sinks periodically send queries to sensors and wait for replies. In case a sensor node receives a query from more than one sink, it selects the one providing the largest received power and responds to it. It is assumed that sensors may perform some data aggregation before transmitting their packets. For instance, they perform sampling from the environment upon each query, but transmit data only when a given number

of samples have been collected. By doing so, transmissions do not occur at each query.

The time needed to transmit a unit of data, that is one sample, is denoted as T, whereas T_D is the time needed to transmit a packet. The frequency of the queries transmitted by the sinks is denoted as $f_q = 1/T_q$. T_q is the time interval between two consecutive queries. It is assumed that sensors transmit packets composed of D samples every D queries. At each query sensors take one sample and when D samples are taken, data is aggregated and transmitted. We assume that the aggregation process generates a packet whose transmission requires a time $T_D = D \cdot T$, when D units of data are aggregated. In Figure 5.2, the aggregation strategies in the cases $D = 1, 2$ are shown as examples.

5.2.2 Evaluation of The Area Throughput

The area throughput is mathematically derived through an intermediate step: first the probability of successful data transmission by an arbitrary sensor node, when k nodes are present in the monitored area, is considered. Then, the overall area throughput is evaluated based on this result.

Joint MAC/Connectivity Probability of Success

Let us consider an arbitrary sensor node that is located in the observed area A at a certain time instant. The aim is computing the probability that it can connect to one of the sinks deployed in A and successfully transmit its data sample to the infrastructure. Such an event is clearly related to connectivity issues (i.e., the sensor must employ an adequate transmitting power in order to reach the sink and not be isolated)

and to MAC problems (i.e., the number of sensors which attempt at connecting to the same sink strongly affects the probability of successful transmission). For this reason, we define $P_{s|k}(x,y)$ as the probability of successful transmission conditioned on the overall number, k, of sensors present in the monitored area, which also depends on the position (x,y) of the sensor relative to a reference system with origin centered in A. This dependence is due to the well-known border effects in connectivity [58].

In particular,

$$\begin{aligned} P_{s|k}(x,y) &= E_n[P_{MAC}(n) \cdot P_{CON}(x,y)] \\ &= E_n[P_{MAC}(n)] \cdot P_{CON}(x,y) \end{aligned} \tag{5.2.2}$$

where the impact of connectivity and MAC on the transmission of samples are separated. A packet will be successfully received by a sink if the sensor node is connected to at least one sink and if no MAC failures occur. The two terms that appear in (5.2.2) are now analysed.

$P_{CON}(x,y)$ represents the probability that the sensor is not isolated (i.e., it receives a sufficiently strong signal from at least one sink). This probability decreases as the sensor approaches the borders (border effects). P_{CON} for multi-sink single-hop WSNs, in bounded and unbounded regions, has been computed in Chapter 3. In particular, for bounded regions, $P_{CON}(x,y) \simeq P_{CON}$, that is equal to q_∞, given by eq. (3.5.2) in Chapter 3. Whereas, when unbounded regions are considered, $P_{CON}(x,y)$ is equal to $q(x,y)$ given by eq. (3.5.7) of Chapter 3.

Specifically, since the position of the sensor is in general unknown, $P_{s|k}(x,y)$ of

(5.2.2) can be deconditioned as follows:

$$\begin{aligned} P_{s|k} &= E_{x,y}[P_{s|k}(x,y)] \\ &= E_{x,y}[P_{CON}(x,y)] \cdot E_n[P_{MAC}(n)]\,. \end{aligned} \tag{5.2.3}$$

$E_{x,y}[P_{CON}(x,y)]$ is equal to $\overline{q}$ given by eq. (3.5.8) in Chapter 3, when bounded regions are accounted for. When, instead border effects are negligible, $E_{x,y}[P_{CON}(x,y)] = E_{x,y}[P_{CON}] = P_{CON}$, given by eq. (3.5.2).

Given the channel model described in Chapter 1 (see eq. (1.6.1)), the average connectivity area of the sensor, that is the average area in which the sinks audible to the given sensor are contained, can be defined as

$$A_{\sigma_s} = \pi e^{\frac{2(L_{\text{th}}-k_0)}{k1}} e^{\frac{2\sigma_s^2}{k_1^2}}\,. \tag{5.2.4}$$

In [96] it is also shown that border effects are negligible when $A_{\sigma_s} < 0.1A$. In the following only this case will be accounted for. In this case:

$$P_{CON}(x,y) \simeq P_{CON} = 1 - e^{-\mu_0}, \tag{5.2.5}$$

where $\mu_0 = \rho_0 A_{\sigma_s} = IA_{\sigma_s}/A$ is the mean number of audible sinks on an infinite plane from any position [61].

$P_{MAC}(n)$, $n \geq 1$, is the probability of successful transmission when $n-1$ interfering sensors are present. It accounts for MAC issues. When the 802.15.4 MAC protocols are considered, the models to derive $P_{MAC}(n)$ are given in Chapter 4. In particular, $P_{MAC}(n)$ is the success probability, p_s, derived in Chapter 4, when n nodes are competing for the channel. In particular, p_s is given by eq. (4.4.21), for the non beacon-enabled case and by eq. (4.5.4), for the beacon-enabled case.

In general, when CSMA-based MAC protocols are considered, $P_{MAC}(n)$ is a monotonic decreasing function of the number, n, of sensors which attempt to connect to

the same serving sink. This number is in general a random variable in the range $[0, k]$. In fact, note that in (5.2.2) there is no explicit dependence on k, except for the fact that $n \leq k$ must hold. Moreover in our case we assume $1 \leq n \leq k$, as there is at least one sensor competing for access with probability P_{CON} (5.2.5).

In [75], Orriss *et al.* showed that the number of sensors uniformly distributed on an infinite plane that hear one particular sink as the one with the strongest signal power (i.e., the number of sensors competing for access to such sink), is Poisson distributed with mean

$$\bar{n} = \mu_s \frac{1 - e^{-\mu_0}}{\mu_0}, \tag{5.2.6}$$

with $\mu_s = \rho_s A_{\sigma_s}$ being the mean number of sensors that are audible by a given sink. Such a result is relevant toward our goal even though it was derived on the infinite plane. In fact, when border effects are negligible (i.e., $A_{\sigma_s} < 0.1A$) and k is large, n can still be considered Poisson distributed. The only two things that change are:

- n is upper bounded by k (i.e., the pdf is truncated)
- the density ρ_s is to be computed as the ratio k/A $[m^{-2}]$, thus yielding $\mu_s = k\frac{A_{\sigma_s}}{A}$.

Therefore, we assume $n \sim \text{Poisson}(\bar{n})$, with

$$\bar{n} = \bar{n}(k) = k\frac{A_{\sigma_s}}{A}\frac{1 - e^{-\mu_{sink}}}{\mu_{sink}} = k\frac{1 - e^{-IA_{\sigma_s}/A}}{I}. \tag{5.2.7}$$

Finally, by making the average in (5.2.3) explicit and neglecting border effects (see (5.2.5)), we get

$$P_{s|k} = (1 - e^{-IA_{\sigma_s}/A}) \cdot \frac{1}{M} \sum_{n=1}^{k} P_{MAC}(n) \frac{\bar{n}^n e^{-\bar{n}}}{n!}, \tag{5.2.8}$$

where

$$M = \sum_{n=1}^{k} \frac{\bar{n}^n e^{-\bar{n}}}{n!} \tag{5.2.9}$$

is a normalizing factor.

Area Throughput

The area throughput has been defined as the amount of data, successfully transmitted toward the sinks, per unit of time. The data here is identify with the sample, being a sample the unit of data transmitted (packet when $D = 1$); therefore, the metric will be expressed in [samples/sec].

According to the aggregation strategy described in the previous section, the amount of samples generated by the network as response to a given query is equal to the number of sensors, k, that are present and active when the query is received. As a consequence, the average number of data samples-per-query generated by the network is the mean number of sensors, $\bar{k}$, in the observed area.

Now denote by G the average number of data samples generated per unit of time, given by

$$G = \bar{k} \cdot f_q = \rho_s \cdot A \cdot \frac{1}{T_q} \text{[samples/sec]}. \tag{5.2.10}$$

From (5.2.10) we have $\bar{k} = GT_q$.

The average amount of data received by the infrastructure per unit of time (area throughput), S, is given by:

$$S = \sum_{k=0}^{+\infty} S(k) \cdot g_k \ \text{[samples/sec]}, \tag{5.2.11}$$

where

$$S(k) = \frac{k}{T_q} P_{s|k}, \tag{5.2.12}$$

g_k as in (5.2.1) and $P_{s|k}$ as in (5.2.8).

Finally, by means of (5.2.8), (5.2.9) and (5.2.10), equation (5.2.11) may be rewritten as

$$S = \frac{1 - e^{-IA_{\sigma_s}/A}}{T_q} \cdot \sum_{k=1}^{+\infty} \frac{\sum_{n=1}^{k} P_{MAC}(n) \frac{\bar{n}^n e^{-\bar{n}}}{n!}}{\sum_{n=1}^{k} \frac{\bar{n}^n e^{-\bar{n}}}{n!}} \cdot \frac{(GT_q)^k e^{-GT_q}}{(k-1)!}. \quad (5.2.13)$$

5.2.3 Numerical Results

A square area, having area $A = 10^6$ $[m^2]$, where an average number of 10 sinks are distributed according to a PPP ($I = 10$), is considered. We also set $k_0 = 40$ [dB], $k_1 = 13.03$, $\sigma_s = 4$ [dB] (the values are taken from experimental measurements made on the field with Freescale devices [93]) and $L_{th} = 107$ [dB].

In this section the behavior of the area throughput, S, as a function of the offered load, G, is shown.

First, the optimal aggregation strategy is investigated, showing results for a single-sink scenario with no connectivity problems, with the purpose of motivating the use of the aggregation strategy, then the multi-sink scenario is considered. Then, a comparison of the area throughput obtained with the two modalities, beacon- and non beacon-enabled, is provided.

Note that the results shown in the following, obtained by applying the aggregation strategy described above, are also valid for a more general scenario, where nodes transmit packets of duration T_D every query, and no aggregation strategy is performed. In this case S, expressed in [samples/sec] is still given by eq. (5.2.13), but now a sample coincides with a packet (i.e., it has duration $D \cdot T$ and not T). If, instead, we are interested in S in [bytes/sec], to take into account the quantity

of information contained in each packet, we have simply to multiply S given by eq. (5.2.13) by $D \cdot 10$.

The optimum aggregation strategy

The single-sink scenario, without connectivity problems.

Here results obtained through the non beacon-enabled mode of the 802.15.4, related to a single-sink scenario with n sensors and no connectivity problems, are shown. These results are interesting because they motivate the choice of the above described aggregation strategy. It is shown indeed, that given n, there exists an optimum value of D, D_{opt}, maximising the throughput, S. Therefore, if sensors are aware of the size n of the cluster they belong to, they could select $D = D_{opt}$, obtained through our results, and transmit the aggregated packet every D_{opt} queries.

The interval of time T needed to transmit a unit of data will be equal to the backoff period, $d_{bo} = 320$ $[\mu sec]$, defined in Chapter 4. It is assumed that the sinks allow sensors to try to access the channel for all the time they need. Therefore, by setting the query size equal to 10 bytes (i.e., the query is transmitted in T), we fix $T_q = (\hat{t}_{max} + D + 1)\,T = (121 + D)\,T$, being $(\hat{t}_{max} + D)\,T$ the maximum delay with which a node can transmit a packet having size $D \cdot 10$ [bytes] (see eq. (4.4.1)).

Since here we have ensured connectivity, a single sink and a deterministically fixed number, $k = n$, of sensors competing for access, we have $P_{CON} = 1$ and $P_{s|k} = P_{MAC}$. Hence, the area throughput is simply:

$$S = \frac{n}{(121 + D)T} \cdot P_{MAC}(n)\,. \tag{5.2.14}$$

In Figure 5.3 S as a function of n, for different values of D, is shown. As we can

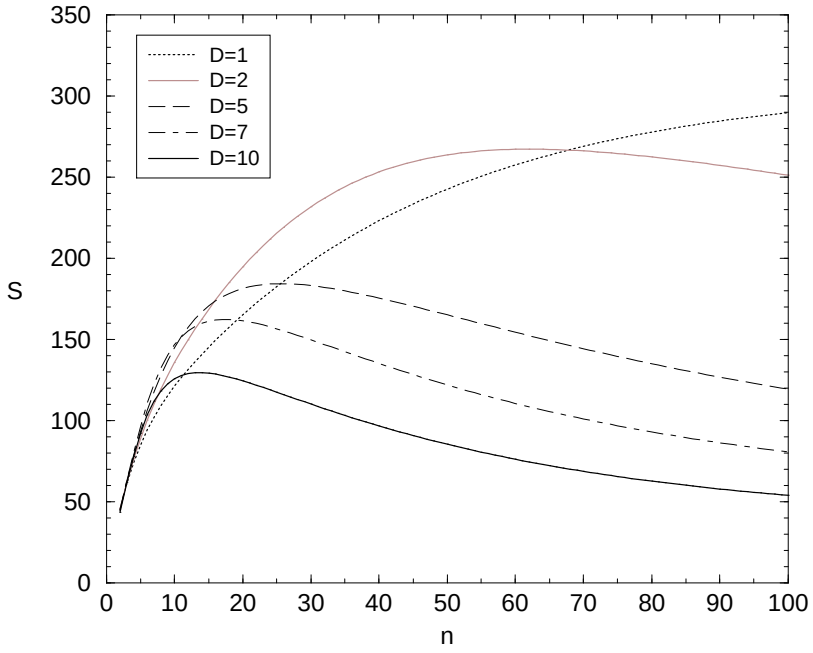

Figure 5.3: S (802.15.4 protocol) as a function of n, for different values of D, in a single sink connected case.

see, S presents a maximum. In fact, for small n, P_{MAC} approaches zero slower then $1/n$ and thus by increasing n, S also increases. On the contrary, for large n, P_{MAC} approaches zero faster then $1/n$ and thus by increasing n, the product $n \cdot P_{MAC}(n)$ decreases, and so does S. The physical interpretation is that too many packet losses occur when traffic is too heavy. The maximum values of S depend on D and are obtained for different values of n. As we can see, for $1 < n < 12$, $D_{opt} = 7$; for $12 < n < 18$, $D_{opt} = 5$; for $18 < n < 68$, $D_{opt} = 2$ and for $n > 68$ $D_{opt} = 1$. Therefore, it clearly appears that D_{opt} decreases when increasing n.

The aggregation strategy proposed here, is achievable only in case sensors know n. This parameter could be estimated by sensors, for example, by computing the number

of times the channel is found busy in a given interval of time. The probability to find the channel busy, in fact, is strictly related to n.

The multi-sink scenario

Once again the 802.15.4 in non beacon-enabled mode, is considered; therefore, $T = 320$ $[\mu sec]$ and $T_q = (121 + D)\,T$. Since a typical 802.15.4 air interface is considered, a limit on the number of sensors that could be connected to a given sink should be imposed [51, 82]. To this end, we denote as n_{max} the maximum number of sensors that could be served by a sink and define a new probability (to replace $P_{MAC}(n)$ in (5.2.13)) $P'_{MAC}(n)$ given by:

$$P'_{MAC}(n) = \begin{cases} P_{MAC}(n), & n \leq n_{max} \\ P_{MAC}(n_{max}) \cdot n_{max}/n, & n > n_{max} \end{cases} \tag{5.2.15}$$

where $P_{MAC}(n)$ is obtained through the model described in Chapter 4, and $1 - n_{max}/n$ is the probability that a sensor is not served by the sink it is connected to, owing to the capacity constraint. Performance curves are obtained by setting $n_{max} = 20$. Moreover, the case of negligible border effects is considered.

In Figures 5.4 and 5.5, S as a function of G for different values of D when $P_{CON} = 1$ and 0.67 respectively, is shown. In both Figures there exists a value D_{opt} which decreases by increasing G. Moreover, from Figure 5.4 we can see that for $0 < G <$ 3000 samples/s (when $I = 10$, $G = 3000$ corresponds to $n = 12$) $D_{opt} = 7$; for $3000 < G < 4500$ samples/s ($G = 4500$ corresponds to $n = 18$) $D_{opt} = 5$; and for $G > 4500$ samples/s $D_{opt} = 2$. Therefore, the behavior of D_{opt} as a function of G is exactly the same shown in Figure 5.3.

By comparing Figures 5.4 and 5.5, we can observe the effects of connectivity on

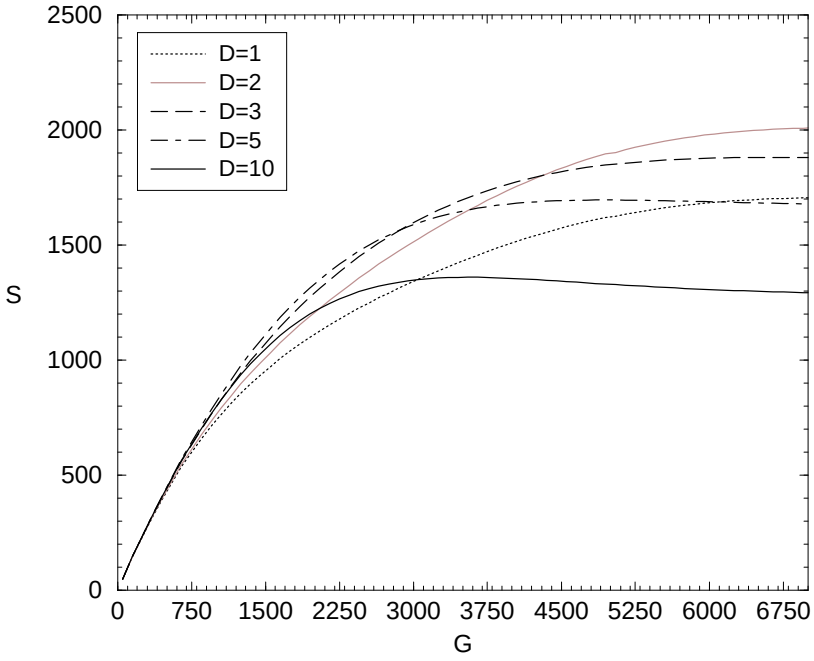

Figure 5.4: S as a function of G, for different values of D, having fixed $P_{CON}(x, y) = 1$.

S. Once D is fixed, the values of S reached for large offered load are approximatively the same reached when $P_{CON} = 1$. The decrease of P_{CON}, in fact, results in a lower mean number of sensors per sink, therefore the decreasing of P_{CON} is compensated by an increasing of $P_{MAC}(n)$. However, the behavior of the curves for low values of G is different (the curves have different slopes). If we fix $D = 5$ and we want to obtain $S = 1500$, when $P_{CON} = 0.67$, we need to deploy on average 158 sensors, whereas, when $P_{CON} = 1$, 106 sensors on average are sufficient. Therefore, the loss of connectivity brings to a larger cost in terms of number of sensors that must be deployed to obtain the desired S.

To increase the values of S, instead, we need to increase I. In fact, given a value of G, by increasing I the connectivity improves and also the losses due to MAC decrease,

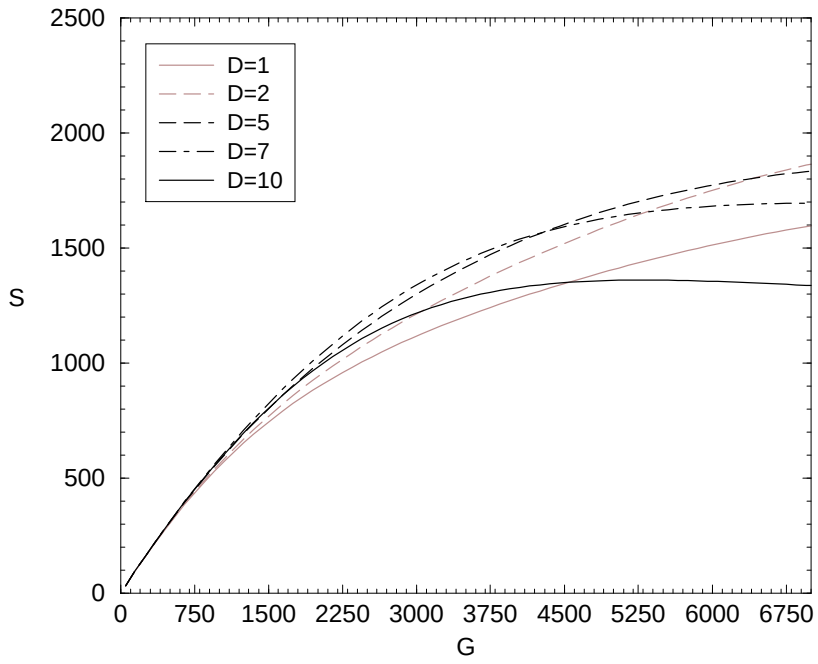

Figure 5.5: S as a function of G, for different values of D, having fixed $P_{CON}(x, y) = 0.67$.

since n decreases.

Finally, an example of results obtained by considering a simpler MAC protocol model where the probability of success, $P''_{MAC}(n)$ (to be included in (5.2.13)), is a linear function of n, is shown. In [119] it is show, in fact, that in some cases the success probability for a non-persistent CSMA protocol, decreases linearly with the number of nodes. Therefore, we model $P''_{MAC}(n)$ as:

$$P''_{MAC}(n) = m \cdot n + 1, \tag{5.2.16}$$

and we denote by n^* the value such that $P''_{MAC}(n^*) = 0$.

In Figure 5.6 three cases are accounted for: $m = -0.01$, corresponding to $n^* = 100$; $m = -0.02$, corresponding to $n^* = 50$; and $m = -0.04$, corresponding to $n^* = 25$.

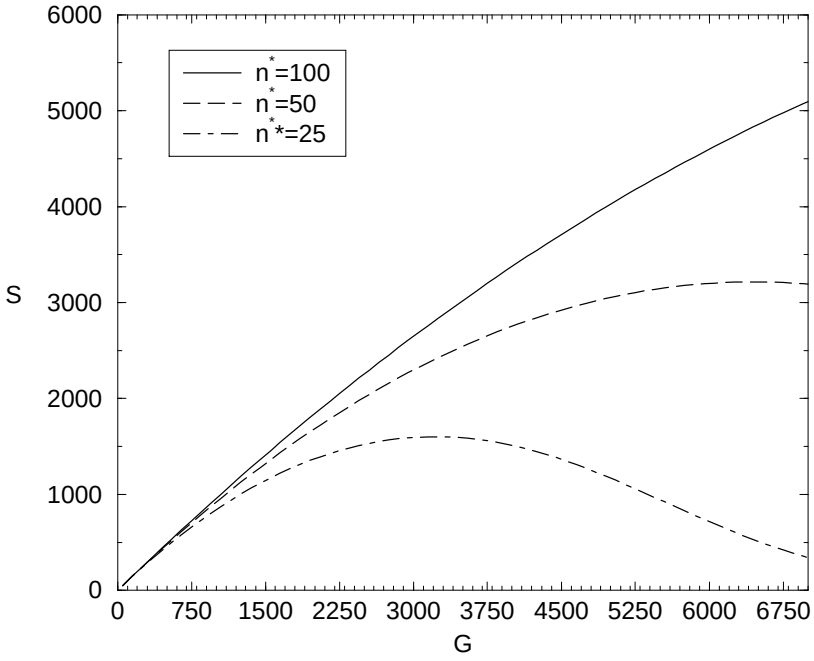

Figure 5.6: S as a function of G in the case of a CSMA based protocol, having a $P_{MAC}(n)$ decreasing linearly with n, for different values of n^*.

By decreasing n^*, the maximum of S is reached for lower values of G. Therefore, for a given value of G, by increasing the slope of $P''_{MAC}(n)$, S increases. The maximum value of S obtained with $n^* = 50$ is approximately twice as large as the one obtained with $n^* = 25$, but it is reached for an offered load that is twice over. Therefore, this increase in the maximum value is reached at the cost of deploying more sensors.

Comparing beacon- and non beacon-enabled

In this section the area throughput obtained with the two modalities beacon- and non beacon-enabled, considering different values of D, SO, N_{GTS}, T_q and different connectivity levels, is shown.

The query packet size is set equal to 60 bytes, therefore, it is transmitted in $6 \cdot T$ seconds, and $T_q = (126 + D)\,T$ for the non beacon-enabled mode, once again to allow sensors to access the channel for all the time needed.

Here a limit on the number of sensors that could be connected to the same sink is not imposed, therefore, eq. (5.2.15) is not used.

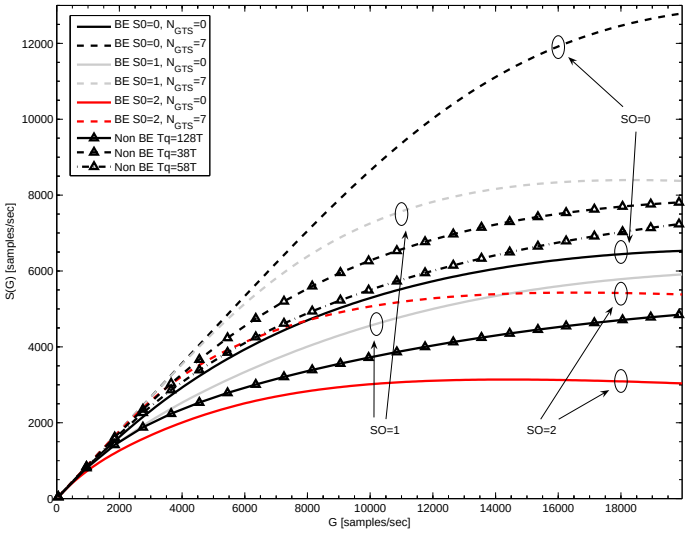

Figure 5.7: S as a function of G, for the beacon- and non beacon-enabled cases, by varying SO, N_{GTS} and T_q, having fixed $D = 2$.

In Figures 5.7 and 5.8, S as a function of G, when varying SO, N_{GTS} and T_q, for $D = 2$ and $D = 10$, is shown, respectively. The input parameters that we entered give a connection probability $P_{CON} = 0.89$. Both beacon- and non beacon-enabled modes are considered. In both Figures it can be noted that, once SO is fixed (beacon-enabled case), an increase of N_{GTS} results in an increment of S, since P_{MAC} increases. Moreover, once N_{GTS} is fixed, there exists a value of SO maximising S. When $D = 2$,

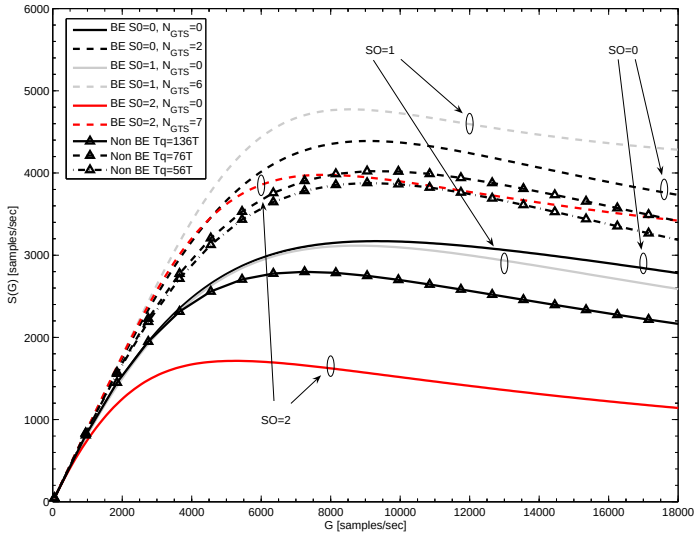

Figure 5.8: S as a function of G, for the beacon- and non beacon-enabled cases, by varying SO, N_{GTS} and T_q, having fixed $D = 10$.

an increase of SO results in a decrement of S since, even though P_{MAC} gets greater, the query interval is longer and, therefore, the number of samples per second received by the sink decreases. On the other hand, when $D = 10$ and all possible GTSs are allocated, the optimum value of SO is 1. This is due to the fact that, having large packets, when $SO = 0$ too many packets are lost, owing to the short duration of the superframe. However, when $N_{GTS} = 0$ the best case is, once again, $SO = 0$, since in this case MAC losses are approximately the same obtained in the case $SO = 1$ (see Figure 4.32), which, however, brings to a higher query interval. In conclusion, we can deduce that the use of GTSs is always advantageous, and that there exists an optimum value of SO maximising S, which depends on D and N_{GTS}.

Concerning the non beacon-enabled case, in both Figures it can be noted that,

by decreasing T_q, S gets larger even though P_{MAC} decreases, since, once again, the MAC losses are balanced by larger values of f_q.

By comparison of Figures 5.7 and 5.8, we note that, once the offered load, G, is fixed, S gets notably smaller when D increases. S, in fact, is expressed in terms of samples/sec received by the sink, and not in bytes/sec. Therefore, once T_q is fixed, by increasing D, P_{MAC} gets smaller. On the other hand, by increasing D, the maximum value of S is reached for lower values of G. This means that, when D is small, the maximum value of S is reached at the cost of deploying more sensors.

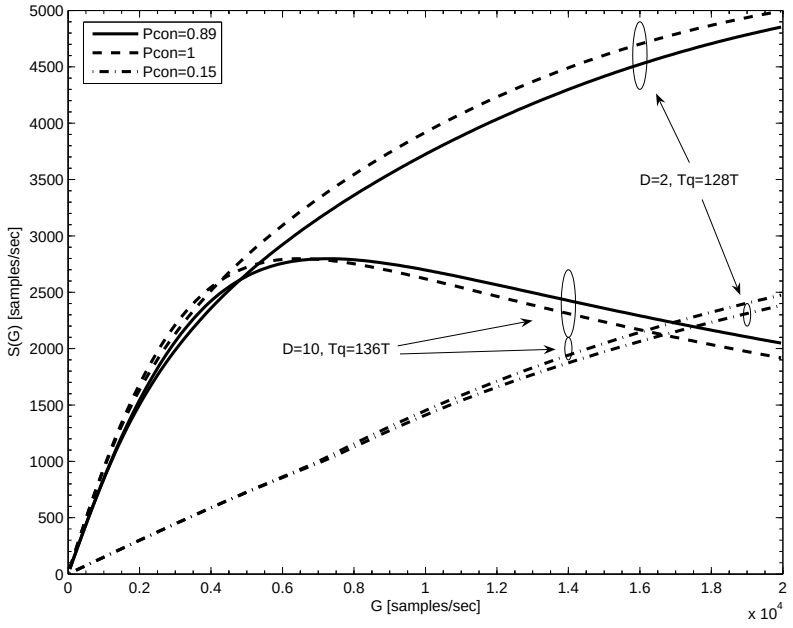

Figure 5.9: S as a function of G, in the non beacon-enabled case, for different values of D and P_{CON}, having fixed T_q to the maximum delay.

Finally, we show the effects of connectivity on the area throughput. When P_{CON} is less than 1, only a fraction of the deployed nodes has a sink in its vicinity. In

particular, an average number, $\bar{k} = P_{CON}GT_q/I$, of sensors compete for access at each sink. In Figure 5.9 we consider the non beacon-enabled case with $D = 2$, $T_q = 128T$ and $D = 10$, $T_q = 136T$. When $D = 10$, $T_q = 136T$, for high offered loads the area throughput tends to decay, since packet collisions dominate. Hence, by moving from $P_{CON} = 1$ to $P_{CON} = 0.89$, we observe a slight improvement due to the fact that a smaller average number of sensors tries to connect to the same sink. Conversely, when $D = 2$, $T_q = 128T$, S is still increasing with G, then by moving from $P_{CON} = 1$ to $P_{CON} = 0.89$, we just reduce the useful traffic. Furthermore, when $P_{CON} = 0.15$, the offered load is very light, so that we are working in the region where $P_{MAC}(D = 2, T_q = 128T) < P_{MAC}(D = 10, T_q = 136T)$ (see Fig. 4.17), resulting in a slightly better performance of the case with $D = 2$. Thus we conclude that the effect of lowering P_{CON} results in a stretch of the curves reported in the previous plots.

5.3 The Thomas Point Process Scenario

In this part of the Chapter a non uniform scenario, where sensors and sinks are distributed, over bounded or unbounded regions, according to a TPP, is considered. While uniform distribution of sensors after deployment is often a useful approximation, it is not always achievable or not even desirable in practice. For many deployment techniques, sensors tend to become placed in clusters of different sizes. The clustering of short range radios has been shown to occur also in other natural contexts, see, for example, [120]. We employ a parameterised model for describing these clusters, called the TPP. The use of TPP allows to characterise in detail the impact of the inhomogeneity and node densities on the metrics of interest.

It is assumed that sensors are deployed in clusters each containing one sink and a

number of cluster members. Sinks are deployed uniformly on finite (square having side L), or infinite plane, with overall density ρ_0 and each cluster associated to a given sink has a Poisson distributed number (with mean μ) of cluster members. The locations of these cluster members are taken to follow normal distribution with mean at the location of the sink, and with covariance matrix $\mathrm{diag}(\sigma_x^2, \sigma_y^2)$. This is a small variation of the TPP used as a sensor location distribution model in, for example, [116].

Since, as stated in Chapter 1, one of the main issues for WSNs is the energy consumption, here the behavior of both performance metrics, area throughput and energy consumption, by varying the offered load, is studied. Both metrics are analytically derived here.

5.3.1 Evaluating Audibility of Sensors

Network connectivity is enhanced as the number of sensors that can gain access to a sink is made as large as possible. As for the PPP scenario, communication from sensor to sink is permitted if the power received by the latter is sufficient (in which case the sensor is said to be audible to the sink), and if the number of (tentative) communication attempts taking place simultaneously is not too large (in which case we expect the transmission to be successful)[1]. The first aspect is treated in this section, considering both, unbounded and bounded regions.

The unbounded scenario

Recall that it is assumed that sinks are uniformly distributed on the infinite plane with density ρ_0 and that each sink gives rise to a cluster which hence contains one

[1]The reverse communication (sink to sensor(s)) only requires audibility, i.e., no MAC failures occur since different sinks use different frequencies.

sink and a number of cluster members, n, Poisson distributed with mean μ. The p.d.f. of the positions of a sensor in a cluster is a 2D Gaussian, i.e.

$$f_{X,Y}(x,y) = \frac{1}{2\pi\sigma_x\sigma_y} e^{-\frac{x^2}{2\sigma_x^2}} e^{-\frac{y^2}{2\sigma_y^2}}, \tag{5.3.1}$$

where we assumed that the cluster center lies at the origin.

Now suppose each sensor has to reach its sink through direct single hop communication. If we employ the random connection model described in Chapter 1 and recall that $C(d)$ (given by eq. (1.6.4)), is the probability that two sensors at distance d are audible, the probability that an arbitrary sensor in a cluster is audible to the sink is (after deconditioning with respect to the position)

$$p = \frac{1}{2\pi\sigma_x\sigma_y} \int_{-\infty}^{\infty}\int_{-\infty}^{\infty} C(\sqrt{x^2+y^2}) e^{-\frac{x^2}{2\sigma_x^2}} e^{-\frac{y^2}{2\sigma_y^2}}\, dx\, dy. \tag{5.3.2}$$

Assuming independence between two audibility events, we have for a single cluster

$$\mathbb{P}\{k \text{ audible sensors} | n \text{ sensors in all}\} = \binom{n}{k} p^k (1-p)^{n-k}, \tag{5.3.3}$$

yielding

$$\mathbb{P}\{k \text{ audible sensors}\} = \sum_{n=k}^{\infty} \binom{n}{k} p^k (1-p)^{n-k} \frac{\mu^n}{n!} e^{-\mu}, \tag{5.3.4}$$

where $\mathbb{P}\{\mathcal{E}\}$ denotes the probability of the event $\mathcal{E}$.

The expected number of sensors per cluster that are audible to the sink is now given by

$$\bar{k} = \sum_{k=0}^{\infty} k \cdot \sum_{n=k}^{\infty} \binom{n}{k} p^k (1-p)^{n-k} \frac{\mu^n}{n!} e^{-\mu}. \tag{5.3.5}$$

The bounded scenario

In this case sinks are uniformly distributed on a square of side L, that is in the region $[0, L] \times [0, L]$. The p.d.f. of the positions of a sensor in a cluster is

$$f_{X,Y}(x, y; x_0, y_0) = \frac{e^{-\left[\frac{(x-x_0)^2}{2\sigma_x^2} + \frac{(y-y_0)^2}{2\sigma_y^2}\right]}}{\int_0^L e^{-\frac{(x-x_0)^2}{2\sigma_x^2}} dx \int_0^L e^{-\frac{(y-y_0)^2}{2\sigma_y^2}} dy} \tag{5.3.6}$$

when $(x, y) \in [0, L] \times [0, L]$, and 0 otherwise, where (x_0, y_0) is the (unknown) position of the sink.

In this case the probability that an arbitrary sensor in a cluster is audible to a sink in (x_0, y_0) is (after deconditioning with respect to the position of the sensor)

$$\begin{aligned} p(x_0, y_0) = \int_{-\infty}^{\infty} \int_{-\infty}^{\infty} & C(\sqrt{(x - x_0)^2 + (y - y_0)^2}) \\ & \times f_{X,Y}(x, y; x_0, y_0)\, dx\, dy. \end{aligned} \tag{5.3.7}$$

By further deconditioning with respect to sink position, we get the average probability of audibility as

$$p = \frac{1}{L^2} \int_0^L \int_0^L p(x_0, y_0)\, dx_0\, dy_0. \tag{5.3.8}$$

Assuming independence between two audibility events, we have for a single cluster

$$\mathbb{P}\{k \text{ audible sensors} | n \text{ sensors in all}\} = \binom{n}{k} p^k (1 - p)^{n-k}, \tag{5.3.9}$$

yielding

$$\mathbb{P}\{k \text{ audible sensors}\} = \sum_{n=k}^{\infty} \binom{n}{k} p^k (1 - p)^{n-k} \frac{\mu^n}{n!} e^{-\mu}. \tag{5.3.10}$$

The expected number of sensors per cluster that are audible to the sink is now given by

$$\bar{k} = \sum_{k=0}^{\infty} k \cdot \sum_{n=k}^{\infty} \binom{n}{k} p^k (1 - p)^{n-k} \frac{\mu^n}{n!} e^{-\mu}. \tag{5.3.11}$$

5.3.2 Area Throughput

The derivation of the area throughput follows directly from the evaluation of the *cluster throughput*, S_c, defined as the number of samples per second successfully transmitted to a sink by the sensors belonging to its cluster.

By following the same rationale as in section 5.2.2, we first consider the probability of successful data transmission by an arbitrary sensor to its cluster head, when n sensors are present in the cluster and k sensors out of n are audible to the sink (channel fluctuations are accounted for). This probability, $P_{s|n,k}$, can be computed as (from (5.3.8) and (5.3.3))

$$\begin{aligned} P_{s|n,k} &= p \cdot P_{\mathrm{MAC}}(k) \cdot \mathbb{P}\{k \text{ audible sensors} | n \text{ sensors in all}\} \\ &= p \cdot P_{\mathrm{MAC}}(k) \cdot \binom{n}{k} p^k (1-p)^{n-k}, \end{aligned} \tag{5.3.12}$$

where once again the impact of audibility and MAC on the transmission of samples (the sensor must be both audible to the sink and able to get its packet through), are separated. In particular, p is the probability that a randomly selected sensor in a cluster is audible to the sink (5.3.8), while $P_{\mathrm{MAC}}(k)$ (with $k \geq 1$), is the probability of successful transmission when $k-1$ interfering sensors are present. Once again the case of 802.15.4 MAC protocol in the non beacon-enabled mode is considered here. Therefore, $P_{MAC}(k)$ coincides with the success probability p_s derived in Chapter 4, given by eq. (4.4.21).

Now for a cluster that has n sensors, and k of them are audible to the cluster

head, we have for the cluster throughput

$$S_{c|n,k} = n \cdot f_q \cdot P_{s|n,k} = n \cdot f_q \cdot p \cdot P_{\mathrm{MAC}}(k) \cdot \mathbb{P}\{k \text{ audible sensors}|n \text{ sensors in all}\}. \tag{5.3.13}$$

By first deconditioning (5.3.13) with respect to k we obtain

$$S_{c|n} = n \cdot f_q \cdot p \cdot \frac{1}{M} \sum_{k=1}^{n} P_{\mathrm{MAC}}(k) \cdot \binom{n}{k} p^k (1-p)^{n-k} \text{ [samples/sec]}, \tag{5.3.14}$$

which is the cluster throughput when n sensors are present in the cluster, with $M = \sum_{k=1}^{n} \binom{n}{k} p^k (1-p)^{n-k}$ being a normalizing factor. Recalling that $n \sim \mathrm{Poisson}(\mu)$, we finally obtain

$$S_c = f_q \cdot p \cdot \frac{1}{M} \sum_{n=1}^{+\infty} n \sum_{k=1}^{n} P_{\mathrm{MAC}}(k) \cdot \binom{n}{k} p^k (1-p)^{n-k} \frac{\mu^n}{n!} e^{-\mu} \text{ [samples/sec]}. \tag{5.3.15}$$

Now note that in any closed domain of area A there are on average $\rho_0 A$ clusters. For the sake of simplicity but without loss of generality a square of side length L, so that $A = L^2$, is considered. Thus by assuming independence from cluster to cluster and neglecting border effects, i.e.,

- σ_x,σ_y small enough such that each cluster having its cluster-head in A is entirely contained in A with high probability;

- $L \gg$ average transmission range;

the area throughput S, is simply given by

$$S = \rho_0 \cdot A \cdot S_c = \rho_0 \cdot A \cdot f_q \cdot p \cdot \frac{1}{M} \sum_{n=1}^{+\infty} n \sum_{k=1}^{n} P_{\mathrm{MAC}}(k) \cdot \binom{n}{k} p^k (1-p)^{n-k} \frac{\mu^n}{n!} e^{-\mu} \text{ [samples/sec]}. \tag{5.3.16}$$

Now, being the offered load G the average number of data samples per unit of time the network was deployed to deliver, it is given by

$$G = \bar{N} \cdot f_q \text{ [samples/sec]}, \tag{5.3.17}$$

where $\bar{N}$ is the average number of sensors in the selected area. By once again neglecting border effects (i.e. assuming that the border of the area does not cut off part of a cluster), the number of selected sensors is the product of two Poisson r.v.'s, namely the number of clusters times the number of sensors per cluster. As these numbers are uncorrelated, their expectations satisfy $\bar{N} = \rho_0 A \cdot \mu$, from which

$$\mu = \frac{G T_q}{\rho_0 A}. \tag{5.3.18}$$

Finally, by substitution of (5.3.18) into (5.3.16), we obtain

$$S(G) = \rho_0 \cdot A \cdot f_q \cdot p \cdot \frac{1}{M} \sum_{n=1}^{+\infty} n \sum_{k=1}^{n} P_{\mathrm{MAC}}(k) \cdot \binom{n}{k} p^k (1-p)^{n-k} \frac{\left(\frac{G T_q}{\rho_0 A}\right)^n}{n!} e^{-\frac{G T_q}{\rho_0 A}} \text{ [samples/sec]}. \tag{5.3.19}$$

5.3.3 Energy Consumption

Once a sensor receives the query coming from the sink, it starts the algorithm to try to access the channel and, in case of success in accessing the channel, it transmits the

packet. At the end of transmission, it switches off until the reception of the next query and in this state it does not consume energy. Therefore, a sensor consumes energy when it receives the query and when it performs the MAC protocol (including states such as backoff, sensing, transmission, etc.). The mean energy spent by a sensor for performing the MAC protocol, is denoted as $E_{\mathrm{MAC}}(k)$. This energy depends on the mean number, k, of sensors audible to a sink and hence competing for the channel. Recall that $k \leq n$ holds, where n is the number of sensors in the cluster. Obviously, in case a sensor is isolated (not audible by the sink) it will not spend energy for that round. Therefore, the mean energy spent by a sensor in the network in a round, E_{round}, is given by

$$E_{\mathrm{round}} = p \cdot (E_{\mathrm{rx}} + \overline{E_{\mathrm{MAC}}}) \text{ [J/sample]}, \tag{5.3.20}$$

where p is given by (5.3.8), E_{rx} is the energy spent to receive the query and $\overline{E_{\mathrm{MAC}}}$ is the mean energy spent for accessing the channel and transmitting the packet.

By following the same reasoning as before, for a cluster composed of n sensors we have

$$E_{\mathrm{MAC}}|_n = \frac{1}{M} \sum_{k=1}^{n} E_{\mathrm{MAC}}(k) \binom{n}{k} p^k (1-p)^{n-k}, \tag{5.3.21}$$

where we have averaged over the number of audible sensors (which are at most n) and $M = \sum_{k=1}^{n} \binom{n}{k} p^k (1-p)^{n-k}$. By further deconditioning with respect to n, we obtain

$$\overline{E_{\mathrm{MAC}}} = \frac{1}{M} \sum_{n=1}^{+\infty} \sum_{k=1}^{n} E_{\mathrm{MAC}}(k) \binom{n}{k} p^k (1-p)^{n-k} \frac{\mu^n}{n!} e^{-\mu}. \tag{5.3.22}$$

$E_{\mathrm{MAC}}(k)$ is the mean energy spent by a node accessing the channel through the IEEE 802.15.4 protocol. Therefore, its definition coincides with the mean spent buy a node in a round, E_{mean}, when k nodes are accessing the channel, given by eq. (4.4.25).

5.3.4 Numerical Results

In this section the behavior of the area throughput and of the energy consumption as functions of the offered load, G, for different packet sizes, clusters shaping factors and sink densities, are shown.

A square area, A, where sinks and sensors are distributed according to the small variation of the TPP described above, is considered as target area. Two reference scenarios are fixed: in the first one it is assumed that the deployment region is a large square field with $L = 1000$ [m]. The second scenario we consider is a deployment in a smaller square region of side length $L = 200$ [m]. While in the first case we assume border effects do not play a significant role, in the second we do account for them and show their impact. In both cases, results are obtained by setting $k_0 = 40$ [dB], $k_1 = 13.03$ and $\sigma_s = 4$ [dB]. Moreover, in the following, we will assume $\sigma_x = \sigma_y = \sigma$. In addition to illustrating results from the analytical calculations, in some cases we confirm these by showing results obtained from a simulator environment.

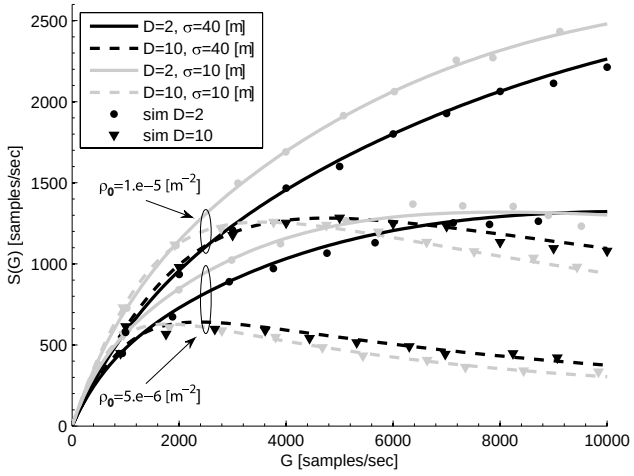

Figure 5.10: S as a function of G for different values of D, ρ_0 and σ.

In Figure 5.10, S as a function of G for different D, σ and sinks density, ρ_0, having set $L = 1000$ [m] and $L_{th} = 95$ [dB], is given. Both analytical results (lines) and simulation results (markers) are shown. In the simulator, clusters are formed in the following way: sensors choose the nearest, measured in Euclidean distance, sink to transmit to. Instead, the model forces a sensor to connect to the sink with respect to which it has been deployed according to the TPP. As we can see a good agreement between results is obtained. The differences are due to border effects and the different cluster heads selection strategies. Of course, we expect that by increasing ρ_0 and σ, results will differ owing to the overlapping of clusters. Once ρ_0 and D are fixed, for low offered load, by decreasing σ, S gets larger; conversely, for high G, larger shaping factors improve performance due to fewer packet collisions. By increasing D and ρ_0, the intersections between curves related to $\sigma = 10$ [m] and $\sigma = 40$ [m] are obtained for lower values of G. In fact, once ρ_0 is fixed, an increase of σ brings to have a larger number of isolated nodes, but also to a smaller average number of sensors trying to connect to the same sink (i.e., fewer MAC losses). Therefore, for low G, connectivity is the main cause of losses and small σ are advantageous; conversely, for high offered load, it is better to fix large σ, to decrease MAC losses. Finally, we note that S shows a maximum: S increases with G till MAC losses become significant. The maxima are reached for larger values of G, when decreasing D and ρ_0.

In Figure 5.11 the energy per second per sample consumed (on average) by a single sensor in the network, $E = E_{\text{round}}/T_q$ [mJ/sec/sample] is shown as a function of G for different values of D and σ. The Figure is obtained by setting $\rho_0 = 10^{-5}$ $[m^{-2}]$, $L = 1000$ [m] and $L_{th} = 95$ [dB]. As σ decreases, E gets larger since it is more likely that the sensor is audible to the sink and hence that it consumes energy. Moreover,

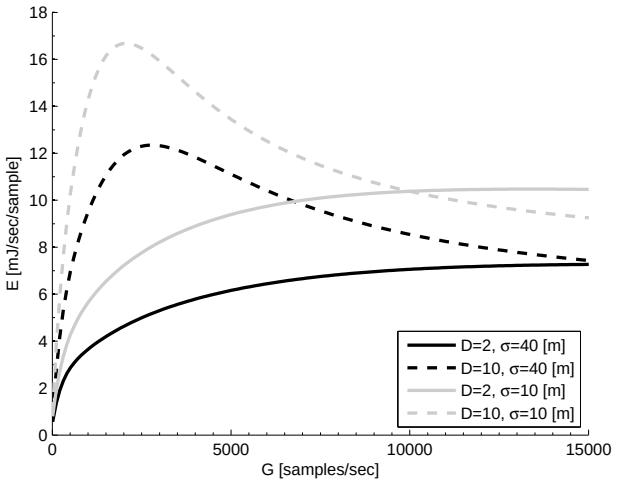

Figure 5.11: E_{round}/T_q as a function of G, by varying D and σ.

for low offered load, by increasing D, E gets larger as well, since a greater amount of energy is spent for transmitting larger packets. Conversely, for high G, the larger D is, the lower will be the probability that a node succeeds in accessing the channel, decreasing the energy spent by the node.

By comparing Figures 5.10 and 5.11 we can deduce that a trade-off between energy consumption and area throughput must be found.

In Figure 5.12 we show the behavior of $\eta = S/(T_q E_{\text{round}} G)$ [samples/sec/mJ], that is the number of samples per second received (on average) by the sinks, per mJ of energy spent. The Figure is obtained by setting $L = 1000$ [m] and $L_{th} = 95$ [dB]. As expected, η increases by increasing ρ_0, since a greater number of sinks help reducing the size of clusters (thus reducing collisions and improving efficiency), and by decreasing D, since, once again, MAC losses decrease.

The following Figures are related to the bounded region case. Therefore, are obtained by setting $L = 200$ [m] and also we set $L_{th} = 92$ [dB]. In this case we show

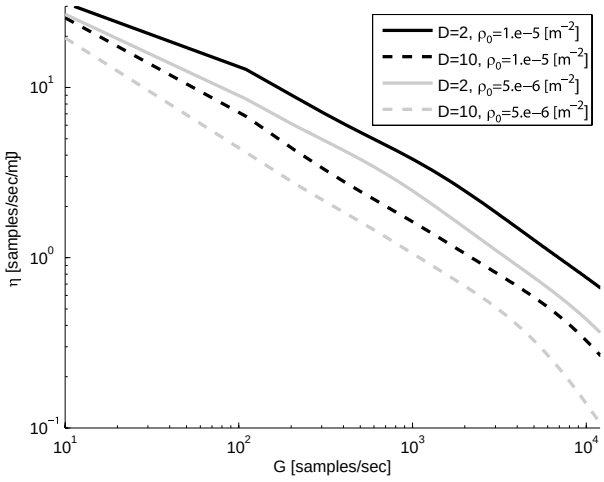

Figure 5.12: η as a function of G, by varying D an ρ_0.

the behavior of the area throughput, expressed in [bytes/sec], therefore, $S(G)$ given by eq. (5.3.19), multiplied by $10 \cdot D$, and of the energy efficiency as functions of the offered load, G, for different packet sizes, clusters shaping factors and sink densities, are shown.

In Figure 5.13 we show the impact of border effects on area throughput. Specifically, we show $S(G)$, expressed in [bytes/sec], for two different cluster size parameters, and both considering and ignoring border effects. Taking the border effects into account has a small, but noticeable effect, especially in the case the cluster size is significant compared to the size of the region under consideration. The increase in area throughput induced by the finite size of the deployment region is also quite intuitive, since the clusters near the boundaries tend to become more dense.

Finally, in Figure 5.14 the corresponding results for the energy efficiency η, is shown. Border effects are still noticeable, but smaller than contributions from changes in cluster size or the parameter D.

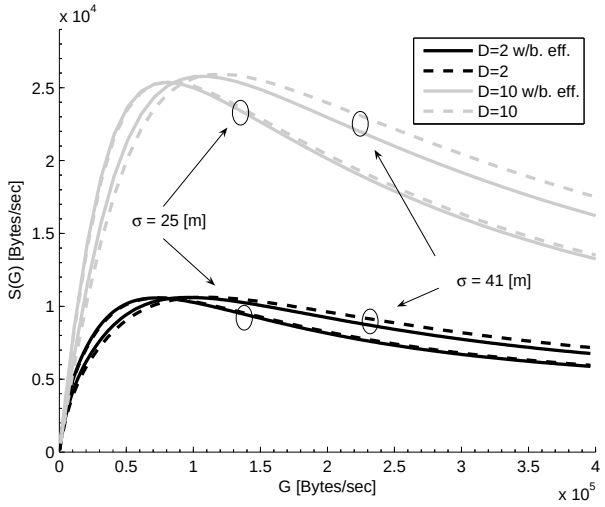

Figure 5.13: S as a function of G for different values of D, with $L = 200$ [m], $L_{\text{th}} = 92$ [dB].

Finally, in Figure 5.15 $S(G)$ for different sensors and sinks distributions is shown and demonstrate the impact of the cluster formation mechanism based on Monte Carlo simulations. An area $A = 1$ $[km^2]$ is considered here. The results clearly show the limitations on the area throughput imposed by fixed sink deployments, and the relatively good performance obtained by simple randomized cluster head selection. The feasibility of the latter approach is, however, clearly dependent on the application scenario considered.

5.4 Conclusions

A multi-sink WSN where sensor nodes transmit their packets to a sink selected among many, by using a CSMA-based MAC protocol, is studied. A new performance metric, accounting for connectivity and MAC issues jointly, namely the area throughput, has been defined. This new concept allows the study of this kind of networks under a

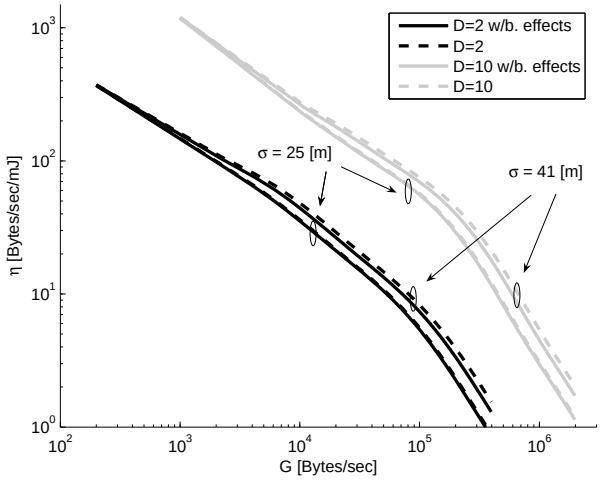

Figure 5.14: η as a function of G, with $L = 200$ [m], $L_{\text{th}} = 92$ [dB].

new perspective, even if, in general terms, the aim is to define a picture showing how throughput varies with load, as done for many years in the literature. However, here, connectivity issues and the presence of multiple sinks are accounted for. This implies, mainly, that performance depends not only on the number of nodes in the network, and on the packet size, but also on sinks density and on transmit power (i.e., L_{th}). In fact, in case the application fixes the minimum value of S, from the Figures we could obtain not only the number of nodes that must be distributed in the network (i.e., the offered load, G), but also (once G is fixed), the number of sinks that must be distributed, or the transmit power (from which depends L_{th}, and, therefore, P_{CON}). Other minor outcomes could be derived from this Chapter: i) the model developed allows the evaluation of an optimum aggregation strategy, maximising S; ii) a comparison in terms of area throughout between the beacon- and non beacon-enabled modes of the 802.15.4, is provided; iii) the energy consumption and throughput trade-off, has been evaluated. Finally, note that the model developed

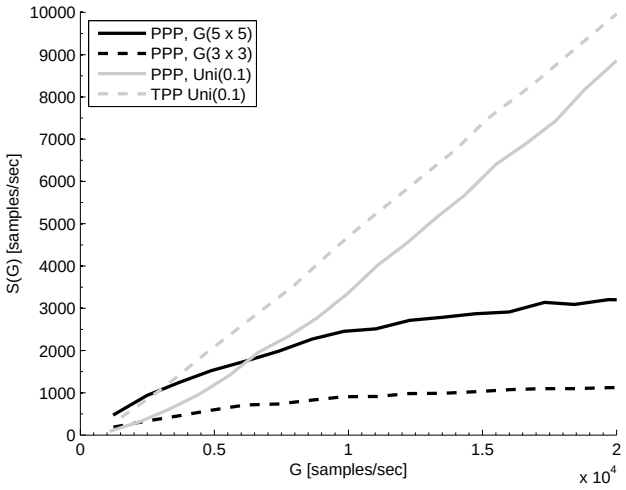

Figure 5.15: The area throughput for different node location distributions (indicated in the legend) and cluster formation techniques ($G(n \times m)$ denotes cluster heads forming an $n \times m$ grid, and Uni(p) denotes unformly random selection of cluster heads from the node population with probability p).

here has allowed to overcome most of the limits of the framework of Chapter 2, since multiple sinks, a real air interface, and border effects, have been accounted for.

Chapter 6

Capacity Analysis of Two-Hop Virtual MIMO Systems in a Poisson Field of Nodes

This Chapter is devoted to the application of MIMO systems to WSNs. Being sensor devices very tiny, they cannot be equipped with multiple antenna elements, therefore, the concept of Virtual MIMO (V-MIMO) should be used. V-MIMO systems exploit MIMO capability, by using devices having a single antenna element, thanks to cooperation between nodes. A two-hop V-MIMO system, where a source node has to transmit data to a destination node via a relay node. is considered. A number of *ancillary* nodes, distributed according to a PPP, are supposed to be distributed around the source, relay and destination, with the possibility to create clusters of cooperating nodes. It is assumed that nodes use two different air-interfaces: a short range and low rate air interface, used to exchange data for exploiting cooperation within each cluster, whereas a long range and high rate air interface can be used to transmit data from cluster to cluster.

The channel model considered is the one described in Chapter 1, therefore, once again random channel fluctuations are accounted for. Owing to the random nature of

the channel, the number of transmit and receive antennas is a random variable and a certain outage probability there exists. Performance is evaluated in terms of outage probability, defined as the probability that the achieved capacity between source and destination is smaller than a given threshold. Also energy consumption issues are taken into consideration, evaluating the total power consumed by the network for delivering the data.

6.1 Virtual Multiple-Input-Multiple-Output and Related Works

Virtual (also known as distributed) MIMO (V-MIMO) systems appear as one of the most interesting paradigms for the deployment of future wireless systems [121, 122]. The key aspect of V-MIMO communication systems is the possibility for the devices, which can be equipped with single or multiple antennas, to create clusters of cooperating nodes. The clusters of cooperating nodes are usually denoted as virtual antenna arrays (VAAs) [121]. Another interesting characteristic of V-MIMO is the possibility to use two different air interfaces for cooperation between devices and data transmission (from source to destination). For example, a short range air interface (e.g., the IEEE 802.15.4) is used for exchanging data within clusters (intra-VAA communication), whereas a high rate air interface is used for communications from cluster to cluster (inter-VAAs communication) [121, 122].

The concept of VAAs with application to cellular networks, has been introduced in 2000 [123] and the generalisation of the concept to distributed MIMO multi-stage communication networks has been introduced in [124]. In [121] and [122] the ergodic

capacity of a V-MIMO system for single and two-hop ad-hoc network scenarios, respectively, is derived. In [125] the diversity gain achieved by a V-MIMO is investigated in realistic indoor propagation environments. In more recent works the concept of V-MIMO has been applied to WSNs, where the cooperating devices are sensors, equipped with a single antenna element [126]. It is worth noting that the topology of the network considered in the previous works is assumed to be fixed and the issues related to the creation of the VAAs are not considered.

Furthermore, there exist few works related to connectivity aspects in MIMO systems in the context of ad-hoc networks (e.g., [127, 128]). In [127] the performance of some spatial diversity techniques including maximal ratio combining are investigated. In [128], a multiple access scheme with frequency hopping is considered. In [127, 128] Poisson fields of nodes are studied.

Bounds on the theoretical capacity achievable by wireless ad hoc networks with devices equipped with single antennas have been recently obtained in [129] when the node location is known, and in [130] when nodes are uniformly distributed in a d-dimensional region. Upper and lower bounds on the capacity are obtained also in [131], where the received power (averaged over fast fading fluctuations) on the terminals of a MIMO relay network is assumed to be random and i.i.d. The bounds, which become tight when the number of relaying nodes approaches infinity, do not depend on the statistical distribution of the received signal (only the hypothesis of i.i.d. is requested). The use of MIMO in ad hoc networks are also investigated in [132]; in that paper a novel connectivity metric is proposed and outage capacity is evaluated assuming different numbers of antennas. The new connectivity metric captures the

time-varying fading, transmission power, and multiple antenna characteristics of wireless nodes. However, the propagation model considered in [132] takes only Rayleigh fading into account, whereas shadowing effects are neglected.

A WSN where nodes, uniformly and randomly distributed in a given area, transmit information to a sink equipped with smart antennas, is investigated in [133]. The framework in [133], which considers a propagation environment composed by a distance-dependent loss, shadowing and Rayleigh fading, permits an analytical evaluation of the achievable rate.

By considering all the works briefly introduced above, it could be said that, no article addressing V-MIMO considering connectivity problems, which usually arise with the formation of the VAAs, can be found in the literature.

6.2 System Description and scenario

Throughout the article vectors and matrices are indicated by bold, $\mathbf{I}$ is the identity matrix and $|\mathbf{A}|$ denotes the determinant of $\mathbf{A}$. $\{a_{i,j}\}_{i,j=1,..,M}$ is an $M \times M$ matrix with elements $a_{i,j} = \{\mathbf{A}\}_{i,j}$, $\dagger$ is the operator of conjugation and transposition. Also, $\mathbb{E}\{\cdot\}$ denotes expectation, and $\mathbb{P}\{\mathcal{E}\}$ denotes the probability of the event $\mathcal{E}$.

6.2.1 Scenario

The reference scenario is illustrated in Figure 6.1. In the following, source, relay and destination nodes will be denoted as *main* nodes.

It is assumed that ancillary nodes are spatially distributed in three areas $\mathcal{A}_{\mathrm{S}}$, $\mathcal{A}_{\mathrm{R}}$ and $\mathcal{A}_{\mathrm{D}}$ according to a PPP [35]. For the sake of simplicity, the areas $\mathcal{A}_{\mathrm{S}}$, $\mathcal{A}_{\mathrm{R}}$

and $\mathcal{A}_{\mathrm{D}}$ are assumed to be circular (with centers in the main nodes) with radius r_{S}, r_{R} and r_{D}, respectively. With such model the probability of having one node in the infinitesimal area $\delta\mathcal{A}$ is $\eta\delta\mathcal{A}$, where η denotes nodes' density [35]. As a general case, nodes' density in the three areas may be different: we denote as η_{S}, η_{R} and η_{S}, the densities of the ancillary nodes distributed around the source, the relay and the destination, respectively. At the beginning of the communication, three clusters (s-VAA, r-VAA and d-VAA) are formed around source, relay and destination. The main nodes transmit a query to the ancillary nodes, by using the short-range radio interface. Owing to propagation conditions, only a subset of the ancillary nodes can really cooperate with the main nodes. The number of nodes which actually communicate with source, relay and destination is denoted by n_{S}, n_{R} and n_{D}, respectively, and are called *cooperating* nodes. We also assume that the distances source-relay and relay-destination are much larger then the distance between a main node and its cooperating nodes. So that the short-range radio interface can be used only to transmit/receive data to/from the main node and its cooperating nodes (intra-VAA communication).

It is assumed that nodes work in a half-duplex mode and that a decode and forward strategy is implemented at the relay.

The communication in the two-hop case is performed according to the following steps: (i) The source transmits data to the n_{S} cooperating nodes; (ii) the $n_{\mathrm{S}}+1$ nodes of the s-VAA transmit data toward the relay through the V-MIMO channel, using the high rate interface (inter-VAA communication); (iii) the $n_{\mathrm{R}}+1$ nodes of the r-VAA cooperate to decode the received data and forward it toward the destination; (iv) the $n_{\mathrm{D}}+1$ nodes of the d-VAA receive data from the r-VAA and cooperate to decode it. The maximum number of cooperating nodes that the main nodes can actually handle

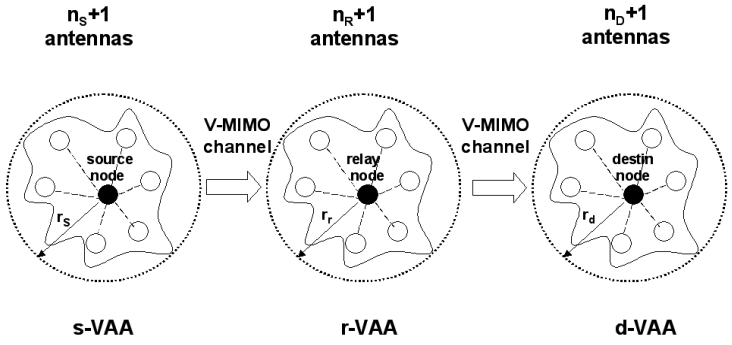

Figure 6.1: The Virtual MIMO communication system.

is obviously limited by their hardware equipment: we denote this number as M_{S}, M_{R} and M_{D} for source, relay and destination, respectively. Note that this analysis can be applied regardless the criterion for the selection of the cooperating nodes which has been chosen.

The single-hop communication protocol can be easily derived from the one described above.

6.2.2 The connectivity model

It is worth noting that, due to the random position of ancillary nodes and channel fluctuation effects, the number of cooperating nodes at the main nodes is not deterministic. This is true regardless the connectivity model we are considering. Being

ancillary nodes Poisson distributed, the number of cooperating nodes is a Poisson random variable, whose mean depends on the connectivity models selected (see Chapter 1). If the channel model described in Chapter 1 is used (see eq. (1.6.1)), the mean value of the number of nodes in $\mathcal{A}_{\rm S}$ for which $L < L_{\rm th}$, is denoted by $N_{\rm S}$, and can be written, according to eqs. (1.6.7) and (1.6.9), as

$$N_{\rm S} = \eta_{\rm S}\pi \left[e^{2L_{\rm th}/k_1 - 2k_0/k_1 + 2\sigma_s^2/k_1^2} + \Psi\left(\frac{L_{\rm th} - k_0}{\sigma_s}, \frac{k_1}{\sigma_s}, r_{\rm S} \right) \right], \tag{6.2.1}$$

where $\Psi(a_1, b_1, r)$ is given by eq. (1.6.8).

$N_{\rm R}$ and $N_{\rm D}$ (i.e., the mean number of nodes in $\mathcal{A}_{\rm R}$ and $\mathcal{A}_{\rm D}$ for which $L < L_{\rm th}$) can be easily obtained from (6.2.1) by using the couple of values ($\eta_{\rm R}$, $r_{\rm R}$) or ($\eta_{\rm D}$, $r_{\rm D}$) instead of ($\eta_{\rm S}$, $r_{\rm S}$). The parameters k_0, k_1, σ_s and $L_{\rm th}$ in (6.2.1) refer to intra-VAA transmission.

Finally, note that for each air interface (intra-VAA and inter-VAA) we could have different power transmission ($P_{\rm T}$), receiver sensitivity (which means different thresholds $L_{\rm th}$) and propagation parameters (k_0, k_1, σ_s).

6.3 Ergodic Capacity expressions for V-MIMO

In this Chapter it is assumed that the receiver has perfect knowledge of the channel state, whereas the transmitter knows only the average loss (path-loss and shadowing) [121,122]. The received signal at the $\ell^{\underline{\rm th}}$ hop can be written as

$$\mathbf{y}_\ell = \sqrt{P_\ell}\mathbf{H}_\ell \mathbf{b}_\ell + \mathbf{n}_\ell \tag{6.3.1}$$

where $\mathbf{y}_\ell$ is a $(n_{\rm R}+1)$ (for $\ell = 1$) or $(n_{\rm D}+1)$-dimensional (for ℓ=2) vector. P_ℓ, $\mathbf{H}_\ell$, $\mathbf{b}_\ell$, $\mathbf{n}_\ell$ are the averaged (over fast fading) power received by a given node of r-VAA (or

d-VAA) when transmitted by a node of s-VAA (or r-VAA), the fast fading channel matrix, the transmitted symbol vector and the thermal noise vector, respectively. It is assumed $\mathbb{E}\left\{ \mathbf{b}_\ell \mathbf{b}_\ell^\dagger \right\} = \mathbf{I}$, and $\mathbb{E}\left\{ \mathbf{n}_\ell \cdot \mathbf{n}_\ell^\dagger \right\} = \sigma_{\mathrm{N}}^2 \mathbf{I}$, where σ_{N}^2 is the thermal noise power per antenna element. We consider a flat uncorrelated Rayleigh environment so that the elements of $\mathbf{H}_\ell$, $h_{i,j}^{(\ell)}$, can be modelled by a collection of i.i.d complex-valued Gaussian r.v.'s having $\mathbb{E}\left\{ h_{i,j}^{(\ell)} \right\}$=0 and unitary mean $\mathbb{E}\left\{ |h_{i,j}^{(\ell)}|^2 \right\}$=1. Since the distances source-relay and relay-destination are much larger then the distance between a main node and its cooperating nodes, the averaged power (P_ℓ) received by a node in r-VAA ($\ell = 1$) or d-VAA ($\ell = 2$) does not depend on the specific transmit node.

The mean (with respect to fast fading fluctuations) capacity in the two-hop case, $\bar{C}^{(2)}$, is the minimum between the mean capacity of the first link (from the source to the relay) and of the second link (from the relay to the destination) [122]. Therefore, by assuming n_{S}, n_{R} and n_{D} cooperating nodes, the source-destination ergodic capacity can be written as

$$\bar{C}^{(2)}_{n_{\mathrm{S}},n_{\mathrm{R}},n_{\mathrm{D}}} = \frac{1}{2} \min \left\{ \bar{C}^{(1)}_{n_{\mathrm{S}},n_{\mathrm{R}}}(\rho_1), \bar{C}^{(1)}_{n_{\mathrm{R}},n_{\mathrm{D}}}(\rho_2) \right\}, \tag{6.3.2}$$

where the term 1/2 reflects the fact that half of the resources (in the time or frequency axes) are spent for the transmission from source to relay and half for the transmission from relay to destination. $\bar{C}^{(1)}_{n_1,n_2}(\rho_\ell)$ is the mean capacity of a MIMO channel with n_1+1 transmit (the main node plus n_1 cooperating nodes) and n_2+1 receive antennas and ρ_ℓ is the signal-to-noise ratio, defined as $\rho_\ell \triangleq P_\ell/\sigma_{\mathrm{N}}^2$. In the single-hop case, the expression for the capacity can be easily written as $\bar{C}^{(1)}_{n_{\mathrm{S}},n_{\mathrm{D}}}(\rho)$.

The mean capacity of MIMO in Rayleigh fading channels has been extensively studied in the past years, here we use a closed form expression which was derived

in [134]

$$\bar{C}^{(1)}_{n_1,n_2}(\rho) = \frac{n_{\min} K}{\ln 2} \sum_{n=1}^{n_{\min}} \sum_{m=1}^{n_{\min}} (-1)^{n+m} |\Omega| \times$$

$$\rho^{-n_{\max}+n_{\min}-n-m+1} F(n+m-1+n_{\max}-n_{\min}, 1/\rho)\,, \tag{6.3.3}$$

where $n_{\min} = 1 + \min\{n_1, n_2\}$, $n_{\max} = 1 + \max\{n_1, n_2\}$,
$K = \left[\prod_{i=1}^{n_{\min}} (n_{\max}-i)! \prod_{j=1}^{n_{\min}} (n_{\min}-i)!\right]^{-1}$, the $(i,j)^{\underline{\text{th}}}$ element of Ω is

$$\omega_{i,j} = \frac{(\alpha_{i,j}^{(n)(m)} + n_{\max} - n_{\min})!}{\sqrt[n_{\min}-1]{n_{\min}}}, \tag{6.3.4}$$

$$\alpha_{i,j}^{(n)(m)} \triangleq \begin{cases} i+j-2 & \text{if} \quad i < n \,\text{and}\, j < m \\ i+j & \text{if} \quad i \geq n \,\text{and}\, j \geq m \\ i+j-1 & \text{otherwise,} \end{cases} \tag{6.3.5}$$

and

$$F(a,d) \triangleq (a-1)! e^d \sum_{k=1}^{a} \frac{\Gamma(-a+k,d)}{d^k}, \tag{6.3.6}$$

where $\Gamma(\alpha, x)$ is the incomplete Gamma function [135].

6.4 Outage probability analysis

Since the number of cooperating nodes is a r.v., there exists a certain probability that the source-destination mean capacity, $\bar{C}^{(2)}$, is lower than a given value, C_0, which depends on the specific application considered. In such scenario, a useful performance metric is the outage probability, $P_{\text{out}} \triangleq \mathbb{P}\{\bar{C}^{(2)} < C_0\}$, which can be evaluated as

$$P_{\text{out}} = \sum_{s=0}^{M_{\text{S}}} \sum_{r=0}^{M_{\text{R}}} \sum_{d=0}^{M_{\text{D}}} \mathbb{P}\{n_{\text{S}} = s, n_{\text{R}} = r, n_{\text{D}} = d\} \times I\left(\bar{C}^{(2)}_{s,r,d}, C_0\right), \tag{6.4.1}$$

where $\mathbb{P}\{n_{\rm S}=s, n_{\rm R}=r, n_{\rm D}=d\}$ is the probability that there are s, r and d cooperating nodes at the source, relay, and destination, respectively. Finally, the indicator function, $I(x,y)$, is equal to one for $x<y$ and zero otherwise.

Owing to the presence of the limitation on the number of cooperating nodes, $n_{\rm S}$, $n_{\rm R}$ and $n_{\rm D}$ do not have Poisson distribution. However, their distribution can be easily obtained from (1.6.6) as

$$Q(s,N_{\rm S})=\begin{cases} P(s,N_{\rm S}) & \text{for } s<M_{\rm S} \\ 1-\sum_{l=0}^{M_{\rm S}-1}P(l,N_{\rm S}) & \text{for } s=M_{\rm S}\ , \end{cases} \tag{6.4.2}$$

equivalent expressions can be written for $Q(r,N_{\rm R})$ and $Q(d,N_{\rm D})$. Being $n_{\rm S}$, $n_{\rm R}$ and $n_{\rm D}$ independent r.v.s, (6.4.1) can be re-written as

$$\begin{aligned} P_{\rm out}=&\sum_{s=0}^{M_{\rm S}}\sum_{r=0}^{M_{\rm R}}\sum_{d=0}^{M_{\rm D}}Q(s,N_{\rm S})Q(r,N_{\rm R})Q(d,N_{\rm D}) \\ &\times I\left(\bar{C}^{(2)}_{s,r,d},C_0\right). \end{aligned} \tag{6.4.3}$$

Note that, with the definition of the signal-to-noise ratio given in this Chapter, $\bar{C}^{(1)}_{n_1,n_2}(\rho)=\bar{C}^{(1)}_{n_2,n_1}(\rho)$. So that, in the case of $\rho_1=\rho_2$, expression (6.3.2) can be simplified as $\bar{C}^{(2)}=\frac{1}{2}\bar{C}^{(1)}_{n_{\rm R},n_{\rm M}}(\rho)$, where $n_{\rm M}=\min\{n_{\rm S},n_{\rm D}\}$. The expression for the $P_{\rm out}$ becomes

$$\begin{aligned} P_{\rm out}=&\sum_{r=0}^{M_{\rm R}}\sum_{m=0}^{\min\{M_{\rm S},M_{\rm D}\}}Q(r,N_{\rm R})\mathbb{P}\{n_{\rm M}=m\} \\ &\times I\left(\frac{1}{2}\bar{C}^{(1)}_{r,m}(\rho),C_0\right), \end{aligned} \tag{6.4.4}$$

and the distribution of $n_{\rm M}$ can be written as

$$\begin{aligned} \mathbb{P}\{n_{\rm M}=m\}=&Q(m,N_{\rm S})Q(m,N_{\rm D})+Q(m,N_{\rm S}) \\ \times&\sum_{\nu=m+1}^{\min\{M_{\rm S},M_{\rm D}\}}Q(\nu,N_{\rm D})+Q(m,N_{\rm D})\sum_{\nu=m+1}^{\min\{M_{\rm S},M_{\rm D}\}}Q(\nu,N_{\rm S}). \end{aligned} \tag{6.4.5}$$

Starting from (6.4.3), the outage probability for the single-hop case can be easily written as

$$P_{\text{out}} = \sum_{s=0}^{M_{\text{S}}} \sum_{d=0}^{M_{\text{D}}} Q(s, N_{\text{S}}) Q(d, N_{\text{D}})\, I\left(\bar{C}_{s,d}^{(1)}(\rho), C_0\right). \tag{6.4.6}$$

6.5 Considerations on power consumption

The total power spent by the network to deliver the data from the source to the destination, depends on the power spent by each node participating in the communication. In this work, the power spent by the network for performing cooperation (i.e., we do not consider the power spent for intra-VAA transmissions) is neglected and the focus is only on inter-VAA transmissions. To have a unique performance metric, we denote as $\mathbb{E}\{P_{\text{tot}}\}$ the averaged (with respect to fast and slow fading, and to the number of cooperating nodes) power spent by all the active nodes in the network. $\mathbb{E}\{P_{\text{tot}}\}$ can be written as

$$\mathbb{E}\{P_{\text{tot}}\} = \mathbb{E}\left\{P_{\text{T}}^{(1)}\right\}(\mathbb{E}\{n_{\text{S}}\}+1) + \mathbb{E}\left\{P_{\text{T}}^{(2)}\right\}(\mathbb{E}\{n_{\text{R}}\}+1),$$

where the two terms of the sum refer to the total averaged power spent by the s-VAA and the r-VAA, respectively, being $\mathbb{E}\left\{P_{\text{T}}^{(1)}\right\}$ the averaged power used by each node of the s-VAA, and $\mathbb{E}\left\{P_{\text{T}}^{(2)}\right\}$ the averaged power used by each node of the r-VAA. $P_{\text{T}}^{(1)}$ and $P_{\text{T}}^{(2)}$ can be calculated by recalling that the power control at the transmitter exploits the knowledge of path loss and shadowing to obtain a target signal-to-noise ratio at the receiver (ρ_1 or ρ_2). For a fixed value of ρ_1 we obtain the transmit power used by each s-VAA node

$$P_{\text{T}}^{(1)} = \rho_1\, k\, d_1^{\beta}\, \sigma_{\text{N}}^2\, s, \tag{6.5.1}$$

where d_1 is the source-relay distance. $P_{\mathrm{T}}^{(2)}$, the averaged transmit power used by each node at the r-VAA, is obtained by eq. (6.5.1) by using ρ_2 instead of ρ_1 and d_2 (the relay-destination distance) instead of d_1.

Finally, we can derive the averaged transmit power used by each s-VAA node, by calculating the expectation of $P_{\mathrm{T}}^{(1)}$ with respect to shadowing

$$\begin{aligned}\mathbb{E}\left\{P_{\mathrm{T}}^{(1)}\right\} &= \rho_1 k d^{\beta} \sigma_{\mathrm{N}}^2 \int_0^{+\infty} s\, f_s(s)\, ds \\ &= \rho_1 k d^{\beta} \sigma_{\mathrm{N}}^2 e^{\frac{(\sigma_s \ln 10)^2}{200}},\end{aligned} \tag{6.5.2}$$

where $f_s(s)$ is the distribution of the shadowing in linear scale. Similarly, $\mathbb{E}\left\{P_{\mathrm{T}}^{(2)}\right\}$ can be obtained by (6.5.2) by replacing ρ_1 with ρ_2. Note that the parameters k, β, σ_s and σ_{N}^2 in (6.5.2) refer to the inter-VAA transmission.

6.6 Numerical Results

In this section the behavior of the complementary outage probability, $P_{\mathrm{in}} \triangleq 1 - P_{\mathrm{out}}$, is shown by varying different scenarios and system parameters. Results are obtained by setting, if not otherwise specified, the following parameters: $r_{\mathrm{S}} = r_{\mathrm{R}} = r_{\mathrm{D}} = 10$ [m], $\sigma_s = 4$ [dB]; $\sigma_{\mathrm{N}}^2 = 8 \cdot 10^{-15}$ [W] and $M_{\mathrm{S}} = M_{\mathrm{R}} = M_{\mathrm{D}} = 10$. We consider two different channel models for intra-VAA and inter-VAAs communication. In the first case, we set $k_0 = 41$ [dB], $k_1 = 13.03$ ($\beta = 3$), and $L_{\mathrm{th}} = 92$ [dB] (that is the IEEE 802.15.4-like air interface [35]); whereas we set $k_0 = 15$ [dB] and $k_1 = 17.37$ ($\beta = 4$) for the inter-VAAs transmissions (L_{th} is not fixed in this case, since it is assumed that the s-VAA and the r-VAA so that the r-VAA and the d-VAA are always connected). In the following, we will consider $\rho_1 = \rho_2 = \rho$ and we will fix the densities of ancillary nodes at $\eta_{\mathrm{S}} = \eta_{\mathrm{R}} = \eta_{\mathrm{D}} = \eta$. Figure 6.2 reports P_{in} as a function of C_0, for different

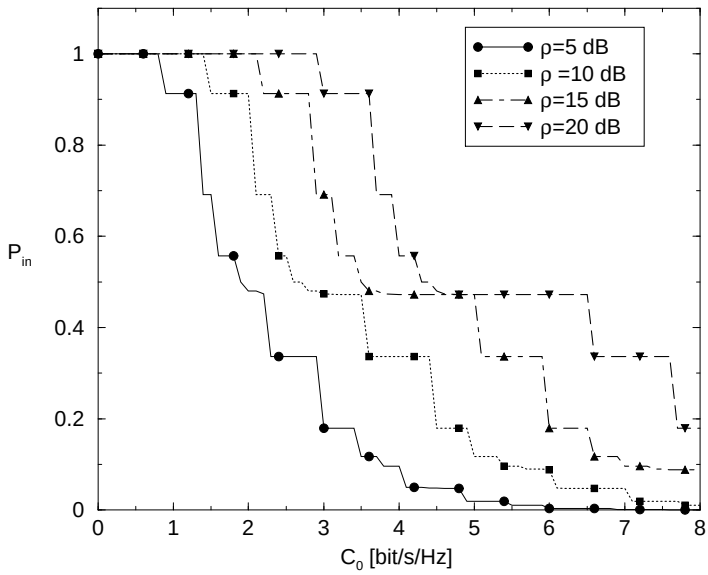

Figure 6.2: The complementary outage probability, P_{in}, as a function of C_0, for different values of ρ.

values of ρ, having set $\eta = 5\,10^{-4}$ [m^{-2}].

As expected, P_{in} decreases by increasing C_0 and the curves are translated by increasing ρ. Note that the step behavior of the curve can be explained by observing that $\bar{C}^{(2)}_{n_{\text{S}},n_{\text{R}},n_{\text{D}}}$ is a function of the three discrete r.v.s n_{S}, n_{R} and n_{D}. In Figure 6.3 P_{in} as a function of σ_s for different values of C_0 is shown, other parameters are $\rho = 10$ [dB] and $\eta = 10^{-5}$ [m^{-2}].

The Figure shows that by increasing σ_s, P_{in} increases. The beneficial (from the P_{in} point of view) effect of σ_s can be explained by observing that the presence of the shadowing leads to an increase of the number of cooperating nodes [61] and therefore, the average number of virtual antennas of V-MIMO gets larger with σ_s.

Figure 6.5 shows the impact of the distribution of the ancillary nodes. The Figure plots P_{in} as a function of $\eta_{\text{S}} = \eta_{\text{D}}$, for different values of η_{R}. The Figure has been

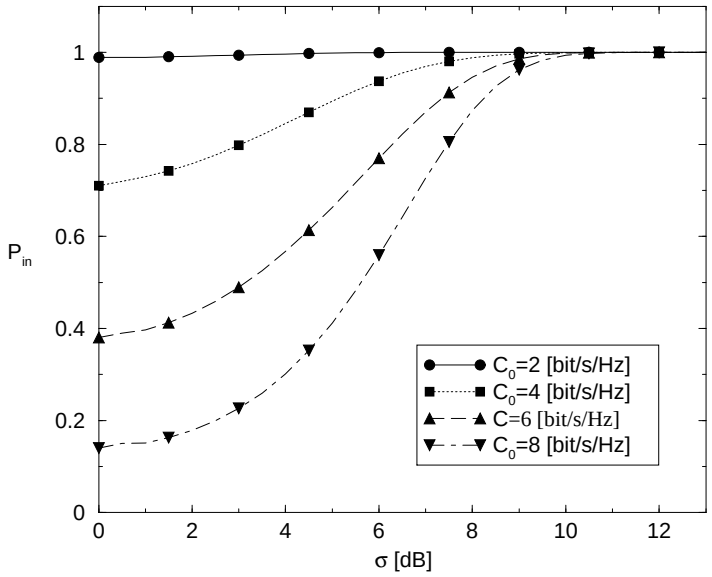

Figure 6.3: The complementary outage probability, P_{in}, as a function of σ_s, for different values of C_0.

obtained by setting $C_0 = 5$ [bit/s/Hz] and $\rho = 10$ [dB]. The curves saturate at a given value, which increases by increasing η_{R}. This behavior can be explained by recalling that when the density of the ancillary nodes at the relay is low, the number of receive antennas used in the first hop (which coincides with the number of transmit antennas used in the second hop) is small. This effect on the capacity is shown in eq. (6.4.4), where the capacity is written as a function of n_{R} and on the minimum between n_{S} and n_{D}. Since the capacity is limited by the minimum between the number of transmit and receive antennas, the value of P_{in} does not reach 1 even if η_{S} and η_{D} (but not η_{R}) become very large. This latter consideration suggests us a simple way for the dimensioning of the system: once the application fixes the minimum acceptable value of P_{in}, the minimum number of the density of ancillary nodes at the relay can be easily obtained from Figure 6.5. The previous figure can be

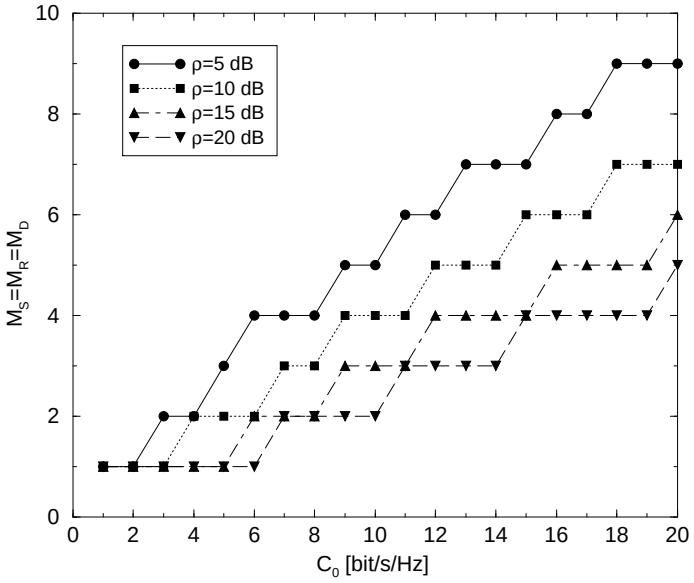

Figure 6.4: The maximum number of antennas $M_{\mathrm{S}} = M_{\mathrm{R}} = M_{\mathrm{D}}$ as a function of C_0, for different values of ρ.

also useful to evaluate the minimum value of $\eta_{\mathrm{S}} = \eta_{\mathrm{D}}$, which leads to the requested P_{in}. Since he number of cooperating nodes has an impact on the overall amount f energy consumed for inter- and intra-VAA transmissions, it is reasonable to introduce a limit on the number of cooperating nodes. In Figure 6.4 the minimum number of $M_{\mathrm{S}} = M_{\mathrm{R}} = M_{\mathrm{D}}$ which allows to obtain $P_{\mathrm{in}} \geq 0.9$ is shown as a function of C_0 for different values of ρ. Here, nodes' density is $\eta = 6.5\,10^{-3}[\mathrm{m}^{-2}]$. This Figure can be useful, for dimensioning purposes, to obtain the limit on the number of cooperating nodes which should be imposed to satisfy the application requirement and also to minimize the energy consumption.

Finally, in Figure 6.6, P_{in} as a function of $\mathbb{E}\{P_{\mathrm{tot}}\}$, for different values of η, is shown for $C_0 = 5$ [bit/s/Hz] and $d_1 = d_2 = 300$ [m]. The single and the two-hop

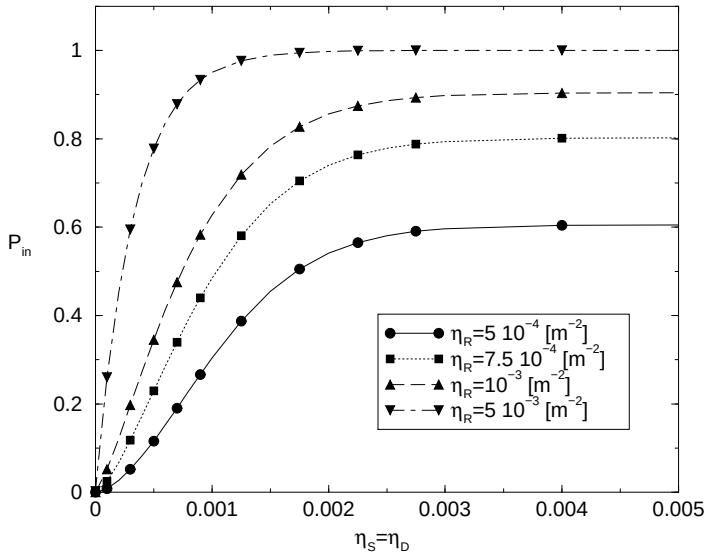

Figure 6.5: The complementary outage probability, $P_{\rm in}$, as a function of $\eta_{\rm S} = \eta_{\rm D}$, for different values of $\eta_{\rm R}$.

communication protocols are compared. As expected, the increase in the value of $P_{\rm in}$ is obtained at the cost of an increasing of the total power spent by the network. Once again the curves saturate, since, owing to the values considered for C_0 and $L_{\rm th}$, $P_{\rm in}$ cannot reach 1 even if nodes' density increases. For what concerns the comparison between two communication protocols, we can deduce that for low values of η, the single-hop protocol allows to obtain larger $P_{\rm in}$. When nodes' density increases, the two-hop protocol can exploit the additional degrees of freedom given by r-VAA and outperforms the single-hop case.

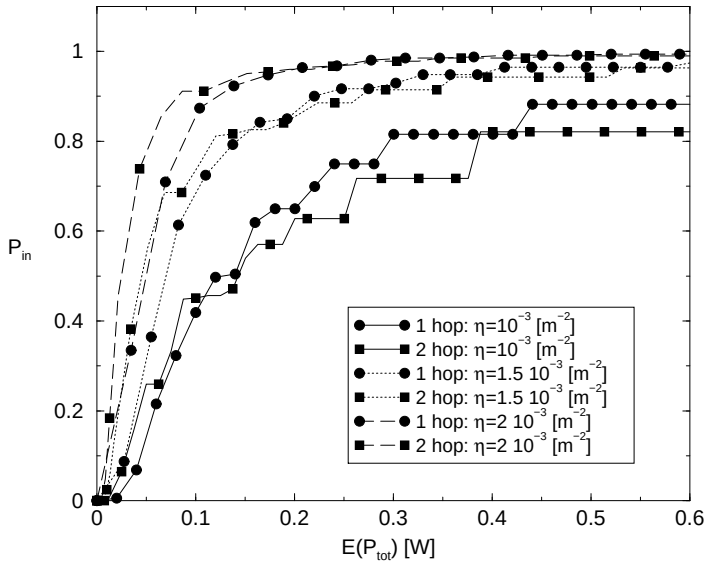

Figure 6.6: The complementary outage probability, P_{in}, as a function of $\mathbb{E}\{P_{\text{tot}}\}$ for different values of η, in the one-hop and two-hop cases.

6.7 Conclusion

In this Chapter, the performance of a two-hop V-MIMO system has been studied in the presence of randomness of nodes' location. The impact of the standard deviation of shadowing and of nodes' density has been investigated. Finally, the comparison between single and two-hop communication protocol, in terms of tradeoff between outage probability and total power consumed by the nodes, shows that the two-hop protocol outperforms the single-hop case when nodes' density increases. As already stated this represents a preliminary work on this topic.

Chapter 7

Conclusions and Open Issues

In this thesis WSNs are studied under different perspectives and some guidelines for network design are provided. Particular attention is devoted to connectivity issues, topology design and MAC protocols, and also some distributed detection techniques have been investigated. The work has been developed in three phases: i) the realisation of a mathematical framework accounting for signal processing, MAC and connectivity issues; ii) the development of connectivity models for multi-sink multi-hop networks distributed in bounded and unbounded regions and the development of an analytical model for the MAC 802.15.4; iii) the integration of the connectivity and MAC models developed at step two and, in parallel, the application of MIMO techniques to WSNs.

Even though signal processing issues are accounted for only in Chapter 2, the importance of this part must be underlined, also to justify its inclusion in the thesis. The framework described in Chapter 2, in fact, puts together many issues of WSNss: from signal processing, through connectivity and channel randomness, to MAC. Even though the model is developed under simplified assumptions and scenarios (e.g., no

border effects, single-sink scenario) and by using simple protocols, this work has the merit of defining a new approach for studying WSNss: the development of frameworks able to study these networks under different perspectives and evaluating different performance metrics jointly.

As stated in the Introduction the limits of this initial work have been overcome in the next Chapters, up to the development of the model described in Chapter 5, including, once again, different topics, but in a more complex form. However, this final model does not take into consideration distributed detection techniques. Therefore, the main and most important open issue of this thesis is the development of a mathematical framework accounting for connectivity in multi-sink multi-hop networks (with nodes distributed in bounded regions), channel randomness, MAC issues considering the 802.15.4 or other CSMA-based protocols and, finally, signal processing techniques. This could be a very interesting, new and challenging research topic, that could be investigated in the next years. By now, in fact, no works dealing with these issues together are present in the open literature (see also the Proceeding of the most important International Conference dealing with WSNs, EWSN 2009 [136]).

Regarding the 802.15.4 MAC protocols work, it is important to remark that the model developed here opens the way to a new approach to analytically study contention-based MAC protocols. This novelty derives from the application scenario considered, that is a typical application for WSNss: the sink periodically triggers nodes and waits for replies. The research devoted to random MAC modelisation started around 1980 (one of the first papers is [137], related to slotted aloha), and with the Bianchi's model has undergone a significant change, thanks to the development of a Markov Chain describing the IEEE 802.11 CSMA/CA algorithm. Many

papers followed the methodology used by Bianchi. All these papers assume that nodes work in saturated traffic conditions, or have a packet to be transmitted in the queue, with a known probability. The model developed here, instead, assume that each node has one packet to be transmitted at each query, which implies that the number of nodes competing for the channel decreases by passing time. This completely changes the form of the analysis and distinguishes this work from those already present in the literature. Obviously some open issues could be found also in this work. For example, capture effects, acknowledge transmissions and data packets retransmissions, could be introduced in the model. Also the three-level tree topology could be extended to the general case of T-level hierarchy, by considering a more realistic strategy for creating trees.

Finally, for what concerns the V-MIMO systems topic, as stated in Chapter 6, the work presented here is only preliminary and many open issues could be found. One of these, for example, could be the application of MAC issues to multi-hop V-MIMO systems.

Chapter 8

Appendix - A Hybrid Hierarchical Architecture: From a Wireless Sensor Network to the Fixed Infrastructure

8.1 Abstract

The Hybrid Hierarchical Architecture (HHA) represents a particular case of Wireless Hybrid Network, where sensor nodes transmit their samples to an infrastructure network through multiple hops. In the HHA, gateway terminals implementing both cellular and infrastructure-less air interfaces, allow integration of the two separate paradigms characterising the Wireless Sensor Network (WSN) and the cellular network. In this paper, in particular we study a hierarchical network where an IEEE

802.15.4 WSN, organised in a tree-based topology, is connected, through a mobile gateway, to an infrastructure network using a cellular air interface like UMTS.

In such scenario, the mobile gateway receives data from sensors with an inter-arrival time distribution which depends on the WSN topology, the number of sensors distributed, and the parameters which characterise the 802.15.4 Medium Access Control protocol, such as the Superframe Order, the Beacon Order, the number of Guaranteed Time Slots, etc. Such distribution is analysed in this paper through simulation. The outcome of this work provides useful hints to the characterisation of the traffic generated by the mobile gateway and provided to the infrastructure network. The design of the scheduling techniques implemented at the infrastructure side requires suitable knowledge of the characteristics of such traffic.

8.2 Reference Network Architecture

In the past few years the development of new technologies and the standardisation of new air interfaces both for infrastructure-less and infrastructure-based wireless networks (such as e.g. WiFi, WiMAX, Bluetooth, Zigbee, etc..), has increased the interest of researchers toward radio systems composed of sub-parts implementing separate technologies and network paradigms (like for instance ad hoc and cellular networks). Let us denote these systems as Wireless Hybrid Networks (WHNs) [138]. They are characterised by the coexistence of several communication technologies and the presence of devices with different functionalities and computational capabilities. This paper in particular refers to a network architecture denoted as Hybrid Hierarchical Architecture (HHA, see Figure 8.1), which in fact is a particular case of WHN. The

HHA has been selected as reference architecture in CRUISE, a Network of Excellence funded by the European Commission through the sixth Framework Program, dealing with Wireless Sensor Networks (WSNs) CRUISE IST Project [1].

The HHA is hybrid, because the mobile gateways at level 1 need to link air interfaces based on different paradigms (they should therefore be able to bridge networks implementing very different types of paradigms). At level zero, radio access ports (i.e. fixed stations covering the area through Radio Access Networks - RANs - using air interface standards like e.g. GPRS or UMTS or WiFi) provide access to mobile terminals (denoted here as Mobile Gateways, level one), carried usually by people. These mobile devices can also be connected through a different air interface (e.g. Zigbee, or Bluetooth) to a lower level of wireless nodes (level two), with limited energy and processing capabilities, which can find access to the fixed network only through the gateways. These wireless nodes, which might be sensor nodes, are distributed in the environment and provide information taken from it; moreover they interact through possibly different air interfaces with tiny devices at level three (e.g. smart tags, or very-low-cost sensors) which are part of movable objects (e.g. printers, books, tickets, etc). The hierarchy is thus composed of four levels.

As an example of application, let us consider a large office building. The area is covered by some indoor UMTS stations, and the employees working in the offices carry UMTS mobile devices also equipped with Zigbee air interfaces; these mobile terminals can interact with Zigbee-enabled small devices distributed over the corridors, and inside the offices. Such devices might provide localisation and logistic information, and are also able to detect the presence in their immediate neighbourhood of

[1] See the project website: http://www.ist-cruise.eu/

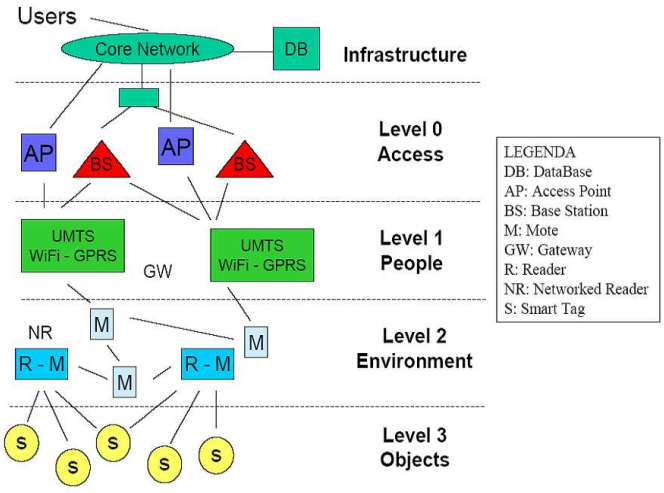

Figure 8.1: The Hybrid Hierarchical Architecture.

objects, like laptops, printers, pieces of equipment, etc, which have Zigbee-enabled, low cost devices that communicate with the nodes distributed in the environment. In this scenario, every employee can scan the environment to get the information on the localisation of movable objects. This can also be done through web services implemented in the intranet serving the building: the user sitting in his/her office will get the requested information through a sequence of links from the lower level (the objects) to the upper (the access ports, bringing the information to the infrastructure and the Internet or intranet).

In this context, this paper considers a scenario composed of three levels, namely level 0, 1 and 2: an IEEE 802.15.4 compliant WSN (level 2), which has to periodically transmit data taken from the environment to a sink, that is the mobile gateway (level 1); the latter must forward data received to a UMTS radio access port (level 0).

In this scenario a specific issue arises: the UMTS scheduler [139], [140] needs to allocate radio resources to the mobile gateway that generates data according to the

inputs received from the WSN [27], [28]. The IEEE 802.15.4 air interface is based on a random multiple access strategy (Carrier Sense Multiple Access, CSMA); as a result, the statistic of the traffic generated by the Sensor Nodes (SNs) is not known a priori, even if a periodic trigger is sent by the mobile gateway toward the environment. On the other hand, the UMTS scheduler will assign radio resources based on requests from the mobile gateway, that needs to be based on the inputs from the SNs. It is therefore very relevant to have knowledge of the statistics of the traffic received by the mobile gateway. Such traffic depends on the way the CSMA protocol is used in the WSN. The WSN, on its turn, is organised in a tree-based topology. This is the topology chosen by the Zigbee Alliance [82], [141] for the IEEE 802.15.4 networks. We denote as level $2, i$ nodes, the SNs belonging to level 2 of the HHA hierarchy and to level i of the WSN hierarchy (see Figure 8.2). In our formalism, level $2, i+1$ nodes transmit their packets to level $2, i$ nodes. Therefore, at level $2, 0$ we have the gateway, that is the root of the tree, and which belongs also to level 1 of the HHA hierarchy.

Having this scenario in mind, the goal of this paper is the description of statistics of traffic at the mobile gateway, gathering data from SNs. Results are obtained through simulations, using a simulator written in C language.

This work is an extension of a previous published paper [25], where, however, a different topology for the WSN was considered and where different metrics for the evaluation of the traffic were evaluated.

Next Section deals with the WSN, considering MAC and routing aspects and the characterisation of the traffic. Finally, simulation results and conclusions are dealt with.

8.3 The Wireless Sensor Network

The reference scenario considered consists of a number of SNs randomly and uniformly distributed over a square area (having side L) and a sink, that is the gateway, located in the centre of the area. The network must be able to provide the information detected by nodes to the gateway, hereafter denoted as Personal Area Network (PAN) coordinator [142], [52] which periodically sends a query and waits for replies from SNs.

SNs are IEEE 802.15.4 standard compliant devices. IEEE802.15.4 is an emerging standard which represents an enabling technology for WSNs. In particular, the IEEE 802.15.4 defines the physical and MAC layer aspects, while leaves the choice of routing and network formation protocols to network designers. The upper layers of the protocol stack are proposed by the ZigBee Alliance [51]: Zigbee specifications propose a tree-based topology described in the following.

The rest of the Section will introduce the IEEE 802.15.4 MAC protocol and the tree-based topology defined by the Zigbee Alliance.

8.3.1 The IEEE 802.15.4 MAC Protocol

IEEE 802.15.4 allows two types of channel access mechanisms: Beacon or non-Beacon enabled. In the first case a slotted Carrier Sensing Multiple Access protocol with Collision Avoidance (CSMA/CA) is used; whereas in non-Beacon enabled networks, an unslotted CSMA/CA is performed. We refer to the Beacon-enabled mode, since, according to Zigbee specifications, this is the modality to be used for tree-based topologies. According to the standard, time is organised in a superframe structure composed by an active and an inactive part [52]. Each superframe is started by a Beacon packet, sent by the PAN coordinator. The active part is composed of 16

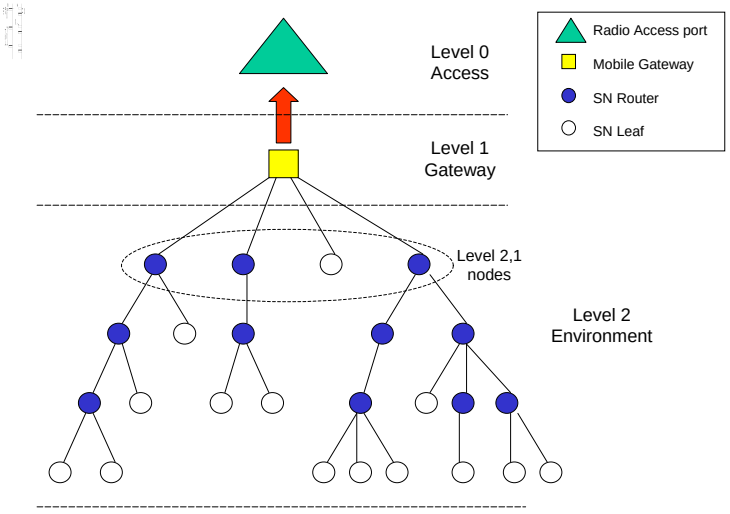

Figure 8.2: Hierarchical tree-based network topology.

equally sized slots and is divided, on its turn, into two parts: the Contention Access Period (CAP), where the access to the channel is managed by a slotted CSMA/CA protocol and the Contention Free Period (CFP), in which a maximum number of seven Guaranteed Time Slots (GTSs) can be allocated by the coordinator to specific nodes (see Figure 8.3).

The duration of the active part and of the whole superframe, depend on the value of two integer parameters ranging from 0 to 14, that are, respectively, the Superframe Order (SO) and the Beacon Order (BO). The latter, defines the interval of time between two successive Beacons, namely the Beacon Interval (BI), given by:

$$BI = 16 \cdot 60 \cdot 2^{BO} \cdot T_s \tag{8.3.1}$$

where 16 is the number of slots, T_s is the symbol time that equals 16 [μs], and $60 \cdot 2^{SO} \cdot T_s$ is the slot size.

The duration of the active part of the superframe (hereafter denoted as Superframe

Duration, SD), is given by:

$$SD = 16 \cdot 60 \cdot 2^{SO} \cdot T_s. \tag{8.3.2}$$

The replies coming from SNs, must arrive to the PAN coordinator, by the end of the active part of the superframe started with the transmission of the query, that the Beacon packet.

The CSMA/CA protocol developed in the simulator is the IEEE 802.15.4 slotted CSMA/CA protocol [52] with no battery life extension, BEmin=3, BEmax=5 and NBmax=4. The algorithm is implemented using time units called backoff periods, having duration $20T_s$. The backoff period boundaries of every SN in the PAN must be aligned with the superframe slot boundaries of the PAN coordinator. Therefore, the beginning of the first backoff period of each SN is aligned with the beginning of the Beacon transmission. All transmissions must start on the boundary of a backoff period. Each SN maintains three variables for each transmission attempt: NB, CW and BE. NB is the number of times the CSMA/CA algorithm was required to backoff while attempting the current transmission; this value is initialized to 0 before each new transmission attempt. When NB reaches its maximum value, NB_{max}, the SN cannot more try to access the channel and its packet is lost. CW is the contention window length, defining the number of backoff periods that need to be clear of channel activity before the transmission can start; this value is initialized to 2 before each transmission attempt and reset to 2 each time the channel is assessed to be busy. BE is the backoff exponent, which is related to how many backoff periods a SN has to wait before attempting to access the channel.

For the sake of conciseness we do not report the details of the algorithm, but we

refer to the standard.

An acknowledge mechanism is performed: each node, after the transmission of a packet, waits for the ACK packet for a time equals to 54 T_s, at the end of which, if it has not received the ACK, it retransmits the packet.

Three kinds of packet are thus considered:

- Beacon: the packet sent by the PAN coordinator, having size 120 T_s;
- ACK: the acknowledge sent to notify the correct reception of a data packet, having size 22 T_s;
- DATA: the data packet containing the measurement result; the size is set to 50 T_s.

The CSMA/CA algorithm must not be used for the transmission of Beacon frames and ACK.

A packet is lost in case a node tries to access the channel for more than NB_{max} consecutive times without success and in case a node does not succeed in transmitting correctly its packet by the end of active part of the superframe.

8.3.2 The Zigbee Hierarchical Tree-Based Topology

Different network topologies for WSNs might be conveniently created such as, for instance, trees, or rings, or cluster-based topologies [81], [80], but since in these networks the set of destination nodes (the sinks) are generally separated by those of sources (namely sensor nodes), tree-based topologies seem to be more efficient than the others: in fact, routing is much simpler, and also distributed data aggregation mechanisms can be used efficiently. This is, in fact, the topology chosen by the

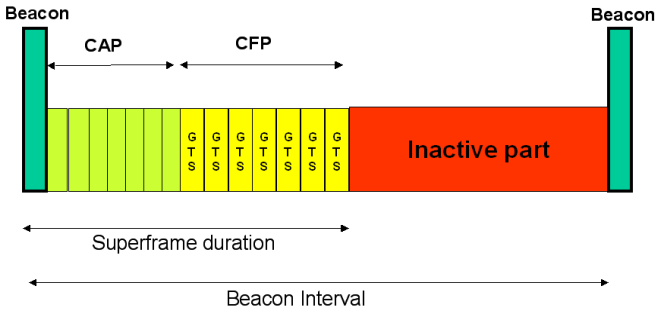

Figure 8.3: Superframe structure used in the IEEE 802.15.4 Wireless Sensor Network.

ZigBee Alliance for the IEEE 802.15.4 networks [51]. The Zigbee specifications define a Beacon-enabled tree-based topology, as a particular case of the IEEE 802.15.4 peer-to-peer networks. According to the topology formation procedure defined in the IEEE 802.15.4 standard (briefly described in the following), a tree, rooted at the PAN coordinator, is formed. As stated above, in the tree, SNs at a given level have to transmit their packets to SNs at a lower level to reach the PAN coordinator. We have two different types of nodes in the tree: the routers, which receive data from their children, aggregate them, and transmit the packet obtained to their parents; and the leafs, which have no routing functionalities and have only to transmit their packets to the parent (see Figure 8.2).

The topology formation procedure is started by the PAN coordinator, which broadcasts Beacon packets to neighbour SNs. A candidate SN receiving the Beacon may request to join the network at the PAN coordinator. If the PAN coordinator

allows the SN to join, it will begin transmitting periodic Beacons so that other candidate SNs may join the network.

As stated above, SNs must be in Beacon-enabled mode: each child node tracks the Beacon of its parent (see Figure 8.4, where the tracking period is outlined as a dashed rectangle). A core concept of this tree topology is that the child node may transmit its own Beacon at a predefined offset with respect to the beginning of its parent Beacon: the offset must always be larger than the parent SD and smaller than BI (see Figure 8.5). This implies that the Beacon and the active part of child superframe reside in the inactive period of the parent superframe; therefore, there is no overlap at all between the active portions of the superframes of child and parent. This concept can be expanded to cover more than two nodes: the selected offset must not result in Beacon collisions with neighbouring nodes. This implies that the node must record the timestamp of all neighbouring nodes and selects a free time slot for its own Beacon. Obviously a child will transmit a Beacon packet only in case it is a router in the tree; if the child is a leaf it has only to transmit the packet to its parent. Each child will transmit its packet to the parent in the active part (CAP or CFP) of the parent supeframe.

Therefore, each router in the tree, after the reception of the Beacon coming from the parent, will select the instant in which transmits its Beacon.

We assume that all the active parts of the superframes generated by the routers and by the PAN coordinator have the same duration; therefore, we fix a unique value of SO. Moreover, we fix the value of BO of the PAN coordinator superframe, so that the inactive part includes at least N_R SDs, being N_R the number of routers present in the tree (see Figure 8.5).

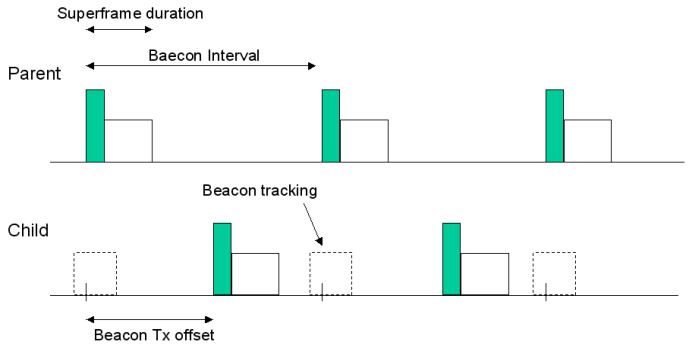

Figure 8.4: The tracking of the Beacon's parent, performed by a generic child.

Therefore, BO is chosen as the minimum integer which satisfies:

$$2^{BO} \geq (N_R + 1) \cdot 2^{SO}. \tag{8.3.3}$$

8.4 Characterisation of the traffic generated by the WSN

Since, all routers in the network aggregate the data received to create a single packet (having common size, 50 T_s) and transmit it to the parent, the statistics of the traffic generated at the PAN coordinator depends only on the instant in which packets sent by level 2,1 SNs reach the PAN coordinator.

We simulate $K = 100$ different and uncorrelated realisations of SN locations and,

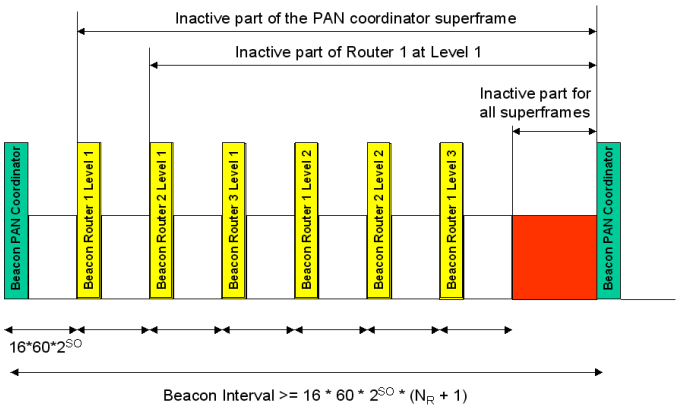

Figure 8.5: The superframe structure used in the tree-based topology.

for each scenario, we simulate $M = 1000$ transmissions for SNs to the PAN coordinator (1000 BI); therefore results reported are based on $K \cdot M = 10^5$ BIs. For each BI we store the instant of arrival at the PAN coordinator (i.e., the time interval between the beginning of the PAN coordinator superframe, set at $t = 0$, and the instant in which the last bit of the packet is received by the PAN coordinator) of a packet coming from a level 2,1 SN. From this result, we can evaluate the probability that a packet arrives at the PAN coordinator in a certain time slot. The time resolution used is the duration of the slot obtained when $SO = 0$, that is $T_{r_{slot}} = 60T_s$ (i.e., the minimum size that a slot can assume). Therefore, we evaluate the number of packets that arrive in each resolution time slot and we compute the frequency of the arrivals for each slot.

Since level 2,1 SNs transmit their packets in the active part of the superframe generated by the PAN coordinator (see Figure 8.5), the traffic will be present only in this part of the superframe, whereas in the inactive part, in which level $2, i$ nodes

(with $i > 1$) transmit to level $2, i-1$ SNs, no traffic toward the PAN coordinator is present.

The statistics of the traffic generated at the PAN coordinator, depends on the values of the following parameters:

- SO, which defines the interval of time in which we can have arrivals at the PAN coordinator;
- BO of the PAN coordinator superframe. It depends on N_R, according to (8.3.3), and defines the BI, that is the periodicity of the arrivals at the PAN coordinator (we have a sequence of arrivals every BI sec);
- the number of SNs at level $2, 1$ hereafter denoted as N_1.

The distribution of the traffic within the active part of the PAN coordinator supeframe depends on the number of GTSs allocated. When no GTSs are allocated, level 2,1 SNs have to access the channel through CSMA/CA; whereas, when a number of GTSs, N_{GTS}, is allocated, only the remaining level 2,1 SNs ($N_1 - N_{GTS}$), use the CAP portion to access the channel.

Moreover, we have evaluated the statistical distribution of the number of packets received by the PAN coordinator per UMTS frame. A UMTS frame has a duration of 10 ms which correspond to 625 T_s. By denoting as n_R the number of packets received per UMTS frame, the probability $P(n_R = x)$, with $x \in [0, N_1]$, is derived. In particular, the number of packets received every 10 ms considering a sequence of 1000 BIs, has been evaluated. Results are averaged over 100 different realisation scenarios. We assume that the beginning of the first UMTS frame is synchronised with the beginning of the first IEEE 802.15.4 superframe.

Finally, we have evaluated the conditioned probability, $P(n_{R_Z} = x|n_{R_p} = y)$, that is the probability that the number of packets received during the Z-th UMTS frame is equal to x, conditioned to the fact that the PAN coordinator has received a total number of y packets in the previous $Z-1$ UMTS frames. In the following, we will denote $P(n_{R_Z} = x|n_{R_p} = y)$ as $P_Z(x|y)$. We suppose, once again, that the first UMTS frame is syncronised with the beginning of the first 802.15.4 frame. The probability $P_Z(x|y)$ is evaluated for Z ranging from 1 to the number of UMTS frames contained in the PAN coordinator superframe. Thus, for example, in case $SO = BO = 0$, we have two UMTS frames in each 802.15.4 superframe and we derive $P_1(n_R)$, which is not conditioned because we are considering the first UMTS frame and $P_2(x|y)$, that is the statistical distribution of the number of packets received in the second UMTS frame, conditioned to the fact that in the first UMTS frame, the sink has received y packets (with $y \in [0, N_1]$).

The knowledge of the conditioned probabilities could be useful for managing data aggregation mechanisms at the PAN coordinator. In general, in fact, the PAN coordinator could perform aggregation of the data received before transmitting it to the infrastructure network. As an example, the PAN coordinator could perform aggregation of the data received in case the probability to have no arrivals in the following frame is high; on the opposite, it could decide to wait for other packets in case the probability to receive data in the following UMTS frames is high.

8.5 Simulation Results

This Section shows numerical results related to the traffic generated by SNs, obtained through our simulator.

We consider a network where nodes are uniformly distributed over a square area, having side $L = 50$ meters and the PAN coordinator is located in the center of the area. We do not simulate the topology formation procedure, but we evaluate performance by varying the number of level 2,1 SNs, N_1, in the network and the number of routers, N_R. Owing to channel model parameters, transmit power and area side selected, all nodes in the network can capture the PAN coordinator queries and could be selected as level $2,1$ nodes. We assume that a maximum number of N_1 children per parent is imposed (capacity constraint) [51], [82], so that the PAN coordinator will select randomly the N_1 level $2,1$ nodes connected to it.

In Figure 8.6 we show the statistical distribution of packet arrival time at the PAN coordinator, as a function of time, normalized with respect to T_s (t/T_s) for different values of SO, BO and N_{GTS}, having fixed $N_1 = 10$. Note that the resolution time chosen in the Figure is equal to $T_{r_{slot}}$. We consider the following cases: (i) $SO = 0$, $BO = 4$ ($N_R = 10$, according to eq. (8.3.3)), $N_{GTS} = 0$; (ii) $SO = 0$, $BO = 4$, $N_{GTS} = 7$; (iii) $SO = 0$, $BO = 5$ ($N_R = 20$), $N_{GTS} = 0$; (iv) $SO = 0$, $BO = 5$, $N_{GTS} = 7$; (v) $SO = 1$, $BO = 5$ ($N_R = 10$), $N_{GTS} = 0$; (vi) $SO = 1$, $BO = 5$, $N_{GTS} = 7$; (vii) $SO = 1$, $BO = 6$ ($N_R = 20$), $N_{GTS} = 0$; (viii) $SO = 1$, $BO = 6$ ($N_R = 20$), $N_{GTS} = 7$. Once we have fixed SO and N_{GTS} the curves do not vary by varying BO, since this parameter affects only the duration of the inactive part of the superframe, where no traffic is present. Therefore, we obtain the same statistic for the cases (i) and (iii); (ii) and (iv), and so on. As we can see, we have no arrivals in the first three resolution slots. The first two slots are devoted to the Beacon transmission (120 T_s) and in the third slot no arrivals are possible, because the minimum delay between the beginning of the CSMA/CA algorithm at the node and the reception of

the packet at the PAN coordinator, is 90 T_s. According to the different SDs (see eq. (8.3.2)) the traffic for $SO = 0$ is distributed between 180 T_s and 960 T_s, whereas for $SO = 1$, it ends at 1920 T_s. Moreover, for $N_{GTS} = 0$ the curves obtained for $SO = 0$ and 1 are approximately the same up to 960 T_s, where the traffic of the case $SO = 0$ finishes. When seven GTSs are allocated, we have an arrival for each GTS (in both cases, $SO = 0$ and 1), because N_1 is larger that 7 and all GTSs are allocated (no losses are possible for packets transmitted in the GTSs). In this case, only the remaining nodes (3 nodes) will use the CAP portion to access the channel.

In Figure 8.7, the distribution of the number of packets received by the PAN coordinator per UMTS frame, $P(n_R = x)$, when $N_1 = 5$ for different values of SO, BO and N_{GTS}, is shown. The probabilities that no packets are received in a UMTS frame, $P(n_R = 0)$, are reported in Table I (to better visualise the distribution for $x > 0$ in the Figure 8.7). As we can see in the Table, these probabilities are very high, with respect to the probabilities $P(n_R = x)$ for $x > 0$. In fact, being $BO = 4$ or 5, the most of the superframe is inactive and no traffic is present. In Figure 8.8 we show the overlapping between the Zigbee and the UMTS frames, in the two cases considered: $SO = 0$, $BO = 4$ (Figure above) and $SO = 1$, $BO = 5$ (Figure below). As stated above, the first UMTS frame is synchronised with the first Zigbee superfarme, but since BI does not contain 625 T_s, the position of the UMTS frames is not always the same in the 1000 BIs simulated. This position is uniformly distributed inside the Zigbee frame. Therefore, the probability $P(n_R = x)$ is larger that zero only when the UMTS frame completely of partially overlaps the active part of the 802.15.4 superframe. Moreover, we can note that by increasing BO, being the duration of the UMTS frame the same, an higher number of UMTS frames is needed to cover all the

Zigbee superframe; therefore, the probability $P(n_R = 0)$ increases (see Table I) and the average number of packets received per UMTS frame decreases too (see Figure 8.7).

In Figure 8.7 we can see that, having fixed $N_{GTS} = 0$, by varying SO and BO the curves trend is approximately the same, but the values are different: by increasing SO and BO, $P(n_R = 0)$ increases and $P(n_R = x)$ for $x > 0$ decreases. When $N_{GTS} = 7$, we have the same probability to receive 1, or 2, or 3, or 4 packets; whereas the probability to receive 5 packets is very high in the case $SO = 0$, $BO = 4$ and very low in the case $SO = 1$, $BO = 5$. The reason is that, in the first case the UMTS superframe is larger (approximately the double) of the duration of the five GTSs were all the traffic of the Zigbee frame is distributed, therefore the probability that the UMTS frame completely overlaps the CFP and that five packets are received is large. Whereas, in the second case, the UMTS duration is approximately the same of the five GTSs and the probability of a complete overlapping is low.

In Figure 8.9 we show the probabilities $P_Z(x|y)$, for $N_1 = 5$ and 10, having fixed $SO = BO = 0$ and $N_{GTS} = 0$ (here no inactive part and CFP are present). Being $SO = 0$, only two UMTS frames are needed to cover the active part of the Zigbee superframe. When $N_1 = 5$ $P_1(x)$ assumes its maximum value for $x = 3$, since the UMTS frame contains a large part of the Zigbee superframe. $P_2(x|2)$ is maximised for $x = 2$, because 2 packets are received in the first frame and there is an high probability that one packet is lost. For the same reason $P_1(x|3)$ is maximum for $x = 1$. We do not report the probability $P_2(x|1)$, since there are too few cases in which only one packet is received in the first UMTS frame. When $N_1 = 10$ in the first UMTS frame the probability is maximum for $x = 4$, whereas, for example, $P_2(x|3)$

is maximum for $x = 3$, since in this case an average number of 3.6 packets are lost. Finally, note that having fixed $SO = 0$, even if BO increases, the curves shown in Figure 8.9 do not change. The only difference is that we will have others $P_Z(x|y)$ for $Z > 2$, that will assume the value 1 for $x = 0$ and zero for $x \neq 0$, whatever y.

Finally, in Figure 8.10 we show the probabilities $P_Z(x|y)$, for $N_1 = 5$, having fixed $SO = BO = 1$ and $N_{GTS} = 0$. Being $SO = 1$, we have 4 UMTS frames in each Zigbee superframe. As we can see, $P_1(x)$ assumes its maximum value once again for $x = 3$; whereas $P_2(x|2)$, $P_2(x|3)$ and $P_2(x|4)$ are maximised, respectively, in $x = 3$, $n_R = 2$ and $x = 1$, since no packets are lost on average. Finally $P_2(x|5)$ is equal to 1 for $x = 0$, since all the packets are arrived in the previous UMTS frames. The same behavior can be observed for $P_3(x|y)$ and $P_4(x|y)$.

8.6 Conclusions

A hybrid hierarchical architecture, where a WSN transmits data to an infrastructure-based network (UMTS) through a gateway, is considered. An IEEE 802.15.4 standard compliant WSN organised in a tree-based topology, is studied: the statistics of the traffic generated by SNs toward the gateway, that is the PAN coordinator, are derived. These results could be useful for the design of the UMTS scheduler. In particular, the statistical distribution of the number of packets received by the PAN coordinator per UMTS frame, has been evaluated for different values of the parameters SO and BO. Results show that by increasing BO the probability that in a UMTS frame no packets are received increases, therefore the interval of time between two successive data bursts increases. Moreover, larger WSNs could be served by increasing BO. On the other hand, however, the larger BO, the larger is the delay with which data are

Table 8.1: $P(n_R = 0)$ for $N_1 = 5$.

SO	BO	N_{GTS}	$P(n_R = 0)$
0	4	0	0.92
1	5	0	0.95
0	4	7	0.94
1	5	7	0.96

delivered to the infrastructure based network increases. Results show also that by increasing SO, the average number of packets received in each UMTS frame decreases; therefore, the load of the UMTS network in each frame decreases. Moreover, by increasing SO the packet losses in the WSN decrease, even if, once again the delay increases. The statistical distribution of the traffic received in the Z-th UMTS frame, conditioned to the fact that y packets were received in the previous $Z - 1$ UMTS frames, is also provided. This probability could be used by the gateway to plan the instant in which performing aggregation of the received data. In fact, in case the probability to have no arrivals in the subsequent frame is high, it is convenient to perform aggregation.

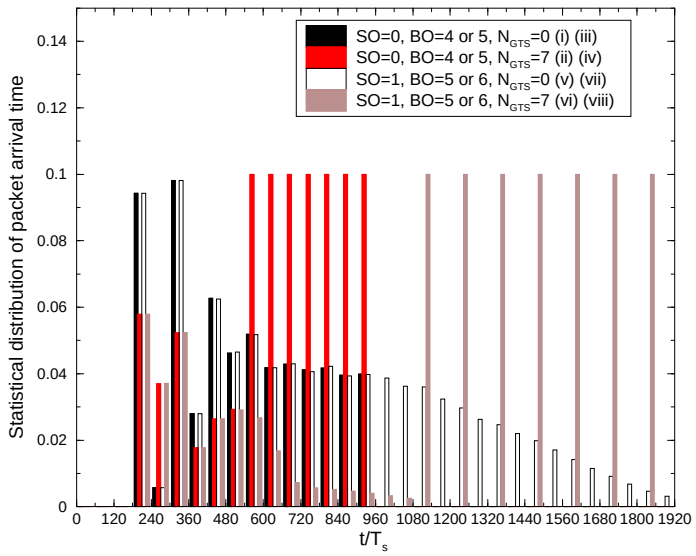

Figure 8.6: Statistical of the packet arrival time for $N_1 = 10$, for different values of SO, BO and N_{GTS}.

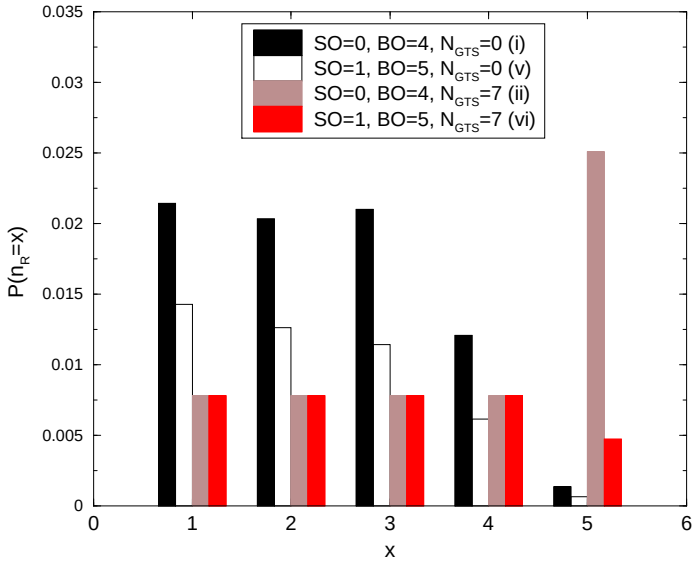

Figure 8.7: The probabilities $P(n_R = x)$ for $N_1 = 5$, for different values of SO, BO and N_{GTS}.

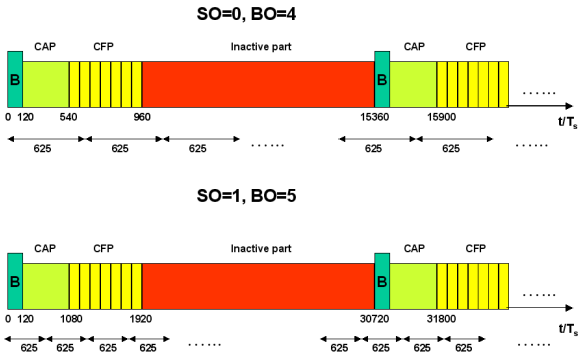

Figure 8.8: The syncronisation between the Zigbee and the UMTS frames, in the cases $SO = 0$ and $BO = 4$ (above Figure) and $SO = 1$ and $BO = 5$ (below Figure).

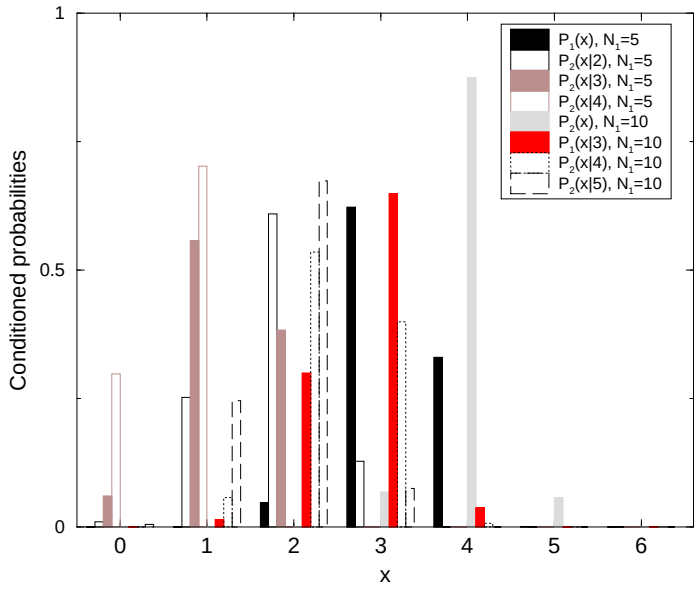

Figure 8.9: The probabilities $P_Z(x|y)$ for $N_1 = 5$ and 10, having fixed $SO = BO = 0$ and $N_{GTS} = 0$.

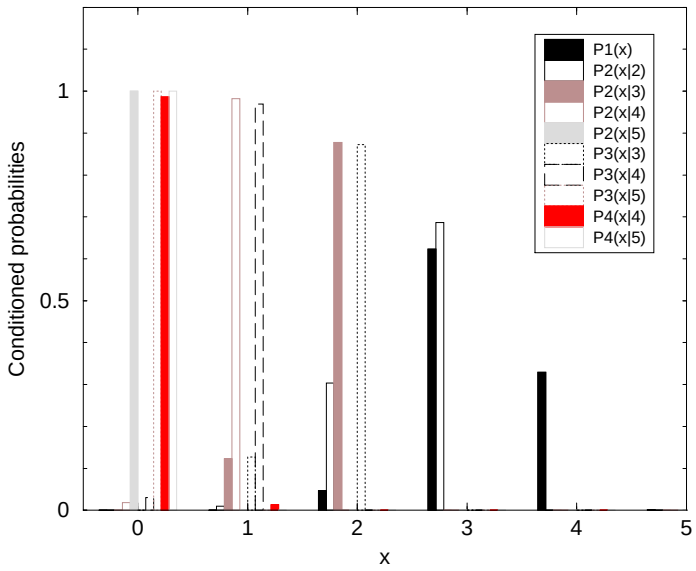

Figure 8.10: The probabilities $P_Z(x|y)$ for $N_1 = 5$, having fixed $SO = BO = 1$ and $N_{GTS} = 0$.

List of acronyms

CH cluster head

MIMO Multiple Input Multiple Output

WAN Wireless Ambient Network

RSSI Received Signal Strength Indication

ED energy detection

r.v. random variable

IF intermediated frequency

ACK acknowledge

DDSP distributed digital signal processing

PPM pulse position modulation

DS-SS direct sequence spread spectrum

BPP Binomial Point Process

RFD reduced function device

PHR Physical Header

LLC Logical Link Control

CRC cyclic redundancy check

IR-UWB impulse radio UWB

OFDM Orthogonal Frequency Division Multiplexing

PAN Personal Area Network

TPP Thomas Point Process

BSN boby sensor network

BPSK binary phase shift keying

CAP Contention Access Period

CH cluster head

CFP Contention Free Period

CSMA carrier sensing multiple access

CSMA/CA carrier sensing multiple access with collision avoidance

CSS chirp spread spectrum

CTR critical transmission range

FFD full function device

GTS Guaranteed Time Slot

HHA Hybrid Hierarchical Architecture

i.i.d. independent,identically distributed

ISM industrial scientific medical

MAC medium access control

MFR MAC Footer

MHR MAC Header

MPDU MAC Payload Data Unit

MSDU MAC Service Data Unit

MSE mean square error

O-QPSK Offset Quadrature Shift Keying

p.d.f. probability distribution function

PHY physical

PPDU Physical Protocol Data Unit

PPP Poisson Point Process

PSDU Physical Service Data Unit

RF radio frequency

r.v. random variable

SHR Synchronization Header

NoE Network of Excellence

EC European Commission

UMTS Universal Mobile Telecommunications System

UWB ultrawide bandwidth

WHN Wireless Hybrid Network

WPAN wireless personal area network

WSN Wireless Sensor Network

Bibliography

[1] T. Basten, M. Geilen, and H. De Groot. *Ambient Intelligence: Impact on Embedded System Design*. Springer, Berlin, Germany, 2003.

[2] W. Weber, J.M. Rabaey, and E. Aarts. *Ambient Intelligence*. Springer, Berlin, Germany, 2003.

[3] L. Benini, E. Farella, and C. Guiducci. Wireless sensor networks: Enabling technology for ambient intelligence. *Microelectronics Journal*, 37(12):1639–1649, 2006.

[4] C. Buratti, A. Giorgetti, and R. Verdone. Simulation of energy efficientcarrier sensing multiple access protocol for clustered wireless sensor network. In *Proc. of IEEE IWWAN 2004*, Oulu, June 2004.

[5] C. Buratti, A. Giorgetti, and R. Verdone. Cross layer design of an energy efficient cluster formation algorithm with carrier sensing multiple access for wireless sensor networks. *Eurasip Journal*, 5:672–685, December 2005.

[6] R. Verdone and C. Buratti. Modelling for wireless sensor network protocol design. In *Proc. of IEEE IWWAN 2005*, London, England, May 2005.

[7] D. Dardari, A.Conti, C. Buratti, and R. Verdone. Mathematical evaluation of environmental monitoring estimation error through energy-efficient wireless sensor networks. *IEEE Trans. Mobile Comput.*, 6:790–803, July 2007.

[8] A. Conti, D. Dardari, C. Buratti, D. Sangiorgi, and R. Verdone. Simulation of energy efficientcarrier sensing multiple access protocol for clustered wireless sensor network. In *Proc. of European Conference on Wireless Sensor Networks, EWSN2005*, Instanbul, Turchy, January 2005.

[9] R. Verdone, C. Buratti, and J. Orriss. On the design of tree-based topologies for wireless sensor networks. In *Proc. IEEE MedHocNet 2006*, Lipari Island, Italy, June 2006.

[10] C. Buratti, J. Orriss, and R. Verdone. On the design of tree-based topologies for multi-sink wireless sensor networks. In *Proc. IEEE NEWCOM/ACORN Workshop 2006*, Vienna, Austria, September 2006.

[11] C. Buratti and R. Verdone. On the number of cluster heads minimizing the error rate for a wireless sensor network using a hierarchical topology over ieee 802.15.4. In *Proc. of IEEE Int. Symp. on Personal, Indoor and MoRadio Communications, PIMRC 2006*, pages 1–6, September 2006.

[12] C. Buratti and R. Verdone. Tree-based topology design for multi-sink wireless sensor networks. In *IEEE Int. Symp. on Personal, Indoor and MoRadio Communications, PIMRC 2007*, Atene, Greece, September 2007.

[13] F. Fabbri, C. Buratti, and R. Verdone. A multi-sink multi hop wireless sensor network over a bounded region: Connectivity and energy consumption issues. In *Proc. of IEEE Wireless Mesh and Sensor Networks, WMSN 08*, New Orleans, LA, USA, November 2008.

[14] C. Buratti. Performance analysis of ieee 802.15.4 beacon-enabled mode. *Submitted to IEEE Trans. on Vehicular Technologies.*

[15] C. Buratti and R. Verdone. A mathematical model for performance analysis of ieee 802.15.4 non-beacon enabled mode. In *Proc. IEEE European Wireless, EW2008*, Prague, Czech Republic, June 2008.

[16] C. Buratti and R. Verdone. Performance analysis of ieee 802.15.4 non-beacon enabled mode. *IEEE Trans. Veh. Technol.*, 2009.

[17] C. Buratti. A mathematical model for performance of ieee 802.15.4 beacon-enabled mode. In *Submitted to IEEE IWCMC 2009*, 2009.

[18] R. Verdone, F. Fabbri, and C. Buratti. Area throughput for csma based wireless sensor networks. In *Proc. of IEEE Int. Symp. on Personal, Indoor and MoRadio Communications, PIMRC 2008*, Cannes, France, September 2008.

[19] C. Buratti, F. Fabbri, and R. Verdone. Area throughput of an ieee 802.15.4 based wireless sensor network. In *Proc. of Europen Conference on Wireless Sensor Networks, EWSN 2009*, Cork, Ireland, February 2009.

[20] J. Riihijärvi, F. Fabbri, C. Buratti, P. Mähönen, and R. Verdone. Area throughput and energy efficiency for clustered wireless sensor networks deployed in bounded regions. In *Proc. IEEE NEWCOM/ACORN Workshop 2009*, Barcelona, Spain, March 2009.

[21] F. Fabbri, C. Buratti, R. Verdone, J. Riihijärvi, and P. Mähönen. Area throughput and energy consumption for clustered wireless sensor networks. In *Proc. of IEEE WCNC 2009*, Budapest, Hungary, April 2009.

[22] C. Buratti and Alberto Zanella. Capacity analysis of two-hop virtual mimo systems in a poisson field of nodes. In *Proc. of IEEE Vehicular Technologies, VTC fall 2009*, Barcelona, Spain, April 2009.

[23] C. Buratti, I. Korpeoglu, E. Karasan, and R. Verdone. Bluetooth or 802.15.4 technologies to optimise lifetime of wireless sensor networks: Numerical comparison under a common framework. In *WNC3, Wireless Networks: Communication, Cooperation and Competition Workshop, WiOpt 2008*, Berlin, Germany, March 2008.

[24] C. Buratti, F. Cuomo, S.D. Luna, U. Monaco, J. Orriss, and R. Verdone. Optimum tree-based topologies for multi-sink wireless sensor networks using ieee 802.15.4. In *Proc. IEEE 65th Vehicular Technology Conference (VTC'07)*, pages 130–134, April 2007.

[25] C. Buratti and R. Verdone. A hybrid hierarchical multi-hop wireless network: From wireless sensors to the fixed infrastructure. In *Proc. of LOCAN 2007*, Pisa, Italy, October 2007.

[26] C. Buratti and R. Verdone. A hybrid hierarchical architecture: From a wireless sensor network to the fixed infrastructure. In *Proc. of IEEE European Wireless, EW2008*, Prague, Czech Republic, June 2008.

[27] Ian F. Akyildiz, Yogesh Sankarasubramaniam Weilian Su, and Erdal Cayirci. A survey on sensor networks. *IEEE Commun. Mag.*, 40(8):102–114, August 2002.

[28] M. Tubaishat and S. Madria. Sensor networks: an overview. *IEEE Potentials*, 22:20–30, April 2003.

[29] Anna Hac. *Wireless Sensor Network Designs*. John Wiley & Sons Ltd, 2003.

[30] C.S. Raghavendra, Krishna M. Sivalingam, and Taieb Znati. *Wireless Sensor Networks*. Kluwer Academic Publishers, 2004.

[31] K. Sohrabi, J. Gao, V. Ailawadhi, and G.J. Pottie. Protocols for self-organization of a wireless sensor network. *IEEE Personal Communications*, 7:16–27, October 2000.

[32] David Culler, Deborah Estrin, and Mani Srivastava. Overview of sensor networks. *IEEE Computer*, 37(8):41–49, August 2004.

[33] V. Rajaravivarma, Yi Yang, and Teng Yang. An overview of wireless sensor network and applications. In *Proc. of 35th Southeastern Symposium on System Theory, 2003*, pages 432–436, March 2003.

[34] R. Verdone. *Wireless sensor networks. Proc. of the 5th European Conference, EWSN 2008, Bologna, Italy.* Springer-Verlang, January 2008.

[35] R. Verdone, D. Dardari, G. Mazzini, and A. Conti. *Wireless sensor and actuator networks.* Elsevier, 2008.

[36] C. Y. Lin, Y. C. Tseng, and T. H. Lai. Message-efficient in-network location management in a multi-sink wireless sensor network. In *IEEE Int. Conf. on Sensor Networks, Ubiquitous, and Trustworthy Computing, 2006.*, pages 1–8, June 2006.

[37] Y. Chen and Q. Zhao. On the lifetime of wireless sensor networks. *IEEE Commun. Lett.*, 9(11):976–978, 2005.

[38] M. Esseghir, N. Bouabdallah, and G. Pujolle. A novel approach for improving wireles sensor network lifetime. In *IEEE Int. Symp. on Personal, Indoor and MoRadio Communications, 2005. PIMRC 2005*, volume 4, pages 11–14, Berlin, Germany, September 2005.

[39] Texas Instruments. *Chipcon Products.*

[40] G. Lu, B. Krishnamachari, and C. S. Raghavendra. An adaptive energy efficient and low-latency mac for data gathering in wireless sensor networks. In *Proc. of 18th International Parallel and Distributed Processing Symposium, 2004*, 2004.

[41] C. Schurgers and M. B. Scrivastava. Energy efficient routing in wireless sensor networks. In *Proc. of IEEE Militaryy Communications Conference, 2001*, volume 1, pages 357–361, 2001.

[42] W. B. Heinzelman, A. P. Chandrakasan, and H. Balakishnan. Energi-efficient communication protocol for wireless microsensor networks. In *Proc. of 33th Hawaii International Conference on System Scuiences, 2000*, volume 2, 2000.

[43] P. J. Marron, D. Minder, and Embeddeed WiseNts Consortium. *Embeddeed WiseNts Reseacrh Roadmap.* Information Society Technologies, Berlin, Germany, 2006.

[44] *EC Project e-SENSE, FP6. See the website: http://www.ist-esense.org.*

[45] *EC Project CRUISE, FP6. See the website: http://www.ist-cruise.eu.*

[46] P. J. Marron. *Cooperating Objects NETwork of Excellence.* University of Bonn, Germany.

[47] M. Lucchi, A. Giorgetti, and M. Chiani. Cooperative diversity in wireless sensor networks. In *WPMC'05*, pages 1738–1742, Aalborg, Denmark, September 2005.

[48] T.Q.S. Quek, D. Dardari, and Moe Z. Win. Energy efficiency of dense wireless sensor networks: To cooperate or not to cooperate. *IEEE J. Sel. Areas Commun.*, 25(2):459–470, February 2007.

[49] S. N. Simić and S. Sastry. Distributed environmental monitoring using random sensor networks. In *Proc. of of Workshop on Information Processing in Sensor Networks*, April 2003.

[50] C. F. Chiasserini, A. Nordio, and E. Viterbo. On data acquisition and field reconstruction in wireless sensor networks. In *Proc. of Tyrrhenian Workshop on Digital Communications, 2005*, July 2005.

[51] Zigbee Aliance. *Zigbee Specifications*. Zigbee Standard Organisation, 2008.

[52] IEEE 802.15.4 Standard. *Part 15.4: Wireless Medium Access Control (MAC) and Physical Layer (PHY) Specifications for Low-Rate Wireless Personal Area Networks (LR-WPANs)*. IEEE, Piscataway, New Jersey, 08855-1331, 2006.

[53] Moe Win and Robert Scholtz. Impulse radio: How it works. *IEEE Commun. Lett.*, 2(2):36–38, February 1998.

[54] IEEE 802.15.4a Standard. *Part 15.4: Wireless MAC and PHY Specifications for Low-Rate Wireless Personal Area Networks (LR-WPANs): Amendment to add alternate PHY (Draft)*. IEEE, Piscataway, New Jersey, 08855-1331, December 2006.

[55] Bluetooth$^{\text{TM}}$. *Specificaton of the Bluetooth System*, volume 0-3. IEEE, 2004.

[56] P. Santi and D. M. Blough. The critical transmitting range for connectivity in sparse wireless ad hoc networks. *IEEE Trans. Mobile Comput.*, 2(1):25–39, 2003.

[57] C. Bettstetter and J. Zangl. How to achieve a connected ad hoc network with homogeneous range assignment: an analytical study with consideration of border effects. In *Proc. of 4th International Workshop on Mobile and Wireless Communications Network 2002*, pages 125–129, September 2002.

[58] C. Bettstetter. On the minimum node degree and connectivity of a wireless multihop network. In *Proc. ACM Symp. on Mobile Ad Hoc Networks and Comp., Mobihoc 2202*, June 2002.

[59] A. Fanimokun and J. Frolik. Effects of natural propagation environments on wireless sensor network coverage area. In *Proc. of 35-th Southeastern Symposium on System Theory, 2003*, pages 16–18, March 2003.

[60] J. Orriss, A.R. Phillips, and S. Barton. A statistical model for the spatial distribution of mobiles and base stations. In *Proc. of IEEE Vehicular Technol. Conference, VTC 1999*, volume 1, pages 19–22, September 1999.

[61] J. Orriss and S. K. Barton. Probability distributions for the number of radio transceivers which can communicate with one another. *IEEE Trans. Commun.*, 51(4):676–681, April 2003.

[62] D. Miorandi and E. Altman. Coverage and connectivity of ad hoc networks in presence of channel randomness. In *Proc. of 24th Annual Joint Conference of the IEEE Computer and Communications Societies, INFOCOM 2005.*, volume 1, pages 491–502, 13-17 March 2005.

[63] E. Salbaroli and A. Zanella. A connectivity model for the analysis of a wireless ad-hoc network of finite area. In *Sensor and Ad Hoc Communications and Networks, 2006 SECON '06 3rd Annual IEEE Communications Society on*, volume 3, pages 756–760, 2006.

[64] F. Zhao, J. Liu, L. Guibas, and J. Reich. Collaborative signal and information processing: an information-directed approach. In *Proc. of IEEE, 2003, to appear.*, volume 91, pages 1199–1209, August 2003.

[65] C.F. Chiasserini and R.R. Rao. On the concept of distributed digital signal processing in wireless sensor networks. In *Proc. of MILCOM 2002*, volume 1, pages 260–264, October 2002.

[66] R. E. Van Dick, L. E. Miller, and M. Gaithersburg. Distributed sensor processing over an ad hoc wireless network: simulation framework and performance criteria. In *Proc. of IEEE Milcom*, October 2001.

[67] D. Miorandi and E. Altman. Coverage and connectivity of ad hoc networks in presence of channel randomness. In *Proc. of IEEE 24th Annual Joint Conference of the IEEE Computer and Communications Societies, INFOCOM 2005*, volume 1, pages 491–502, 13-17 March 2005.

[68] W.A. Gardner. *Introduction to random processes: with applications to signals and systems.* McGraw Hill, second edition, 1989.

[69] E. Masry. Poisson sampling and spectral estimation of continuos-time processes. *IEEE Trans. Inf. Theory*, 24(2):173–183, March 1978.

[70] F.J. Beutler. Alias-free randomly timed sampling of stochastic processes. *IEEE Trans. Inf. Theory*, 16(2):147–152, 1970.

[71] F. Marvasti. Signal recovery from nonuniform samples and spectral analysis on random nonuniform samples. In *Proc. of IEEE International Conference on Acoustics, Speech, and Signal Processing, ICASSP'86*, volume 11, pages 1649–1652, apr 1986.

[72] S. S. Pradhan, J. Kusuma, K. Ramchandran, and F.J. Beutler. Distributed compression in a dense microsensor network. *IEEE Signal Processing Magazine*, pages 51–60, 2002.

[73] W.B. Heinzelman, A.P. Chandrakasan, and H. Balakrishnan. An application-specific protocol architecture for wireless microsensor networks. *IEEE Trans. Wireless Commun.*, 1:660–670, October 2002.

[74] A. De Pedri, A. Zanella, and R. Verdone. An energy efficient protocol for wireless ad hoc sensor networks. In *IEEE Proc. of Int'l Symp. on Autonomous Intelligent Networks and Systems (AINS '03)*, Bologna, Italy, June 2003.

[75] J. Orriss, A. Zanella, R. Verdone, and S. Barton. Probability distributions for the number of radio transceivers in a hot spot with an application to the

evaluation of blocking probabilities. In *IEEE Proc. of Personal, Indoor and Mobile Radio Communications, 2002*, volume 2, September 2002.

[76] R. Verdone, J. Orriss, A. Zanella, and S. Barton. Evaluation of the blocking probability in a cellular environment with hard capacity: a statistical approach. In *IEEE Proc. of Personal, Indoor and Mobile Radio Communications, 2002*, volume 2, September 2002.

[77] W. Ye, J. Heidemann, and D. Estrin. An energy-efficient mac protocol for wireless sensor networks. In *IEEE Proc. of INFOCOM*, volume 3, pages 1567–1576, New York, USA, June 2002.

[78] A. Woo and D. Culler. A transmission control scheme for media access in sensor network. In *Proc. ACM MobiCom 2001*, pages 272–286, Rome, Italy, July 2001.

[79] R. Verdone. An energy-efficient decentralised communication protocol for a network of uniformly distributed sensors polled by a wireless transceiver. In *Proc. of IEEE ICC 2004*, Madison, Wisconsin, May 2004.

[80] P. Santi. *Topology Control in Wireless Ad Hoc and Sensor Networks.* John Wiley and Sons, Chichester, UK, 2005.

[81] C. F. Chiasserini and M. Ajmone Marsan. A distributed self-healing approach to bluetooth scatternet formation. *IEEE Trans. Wireless Commun.*, pages 2649–2654, November 2005.

[82] A. Koubaa, M. Alves, and E. Tovar. Modeling and worst-case dimensioning of cluster-tree wireless sensor networks. In *27th IEEE International Real-Time Systems Symposium, 2006, RTSS 2006*, pages 412–421, December 2006.

[83] J. Orriss, S. K. Barton, and R. Verdone. A hierarchical model for a sensor network. In *Proc. of IWWAN 2005*, London, England, May 2005.

[84] J. Orriss and R. Verdone. Mathematical analysis of tree-based topologies for multi-sink wireless sensor networks. In *Proc. of IWWAN 2006*, 2006.

[85] M. Haenggi. On distances in uniformly random networks. *IEEE Trans. Inf. Theory*, 51(10):3584–3586, oct 2005.

[86] B. Bollobs. *Random Graphs*. Cambridge University Press, second ed., 2001.

[87] R. Meester and R. Roy. *Continuum Percolation*. Cambridge University Press, Cambridge UK, 1996.

[88] M. D. Penrose and A. Pistztora. Large deviations for discrete and continous percolation. *Advances in Applied Probability*, 28:29–52, 1996.

[89] M. D. Penrose. On the spread-out limit for bond and continuum percolation. *Annals of Applied Probability*, 3:253–276, 1993.

[90] M. D. Penrose. On k-connectivity for a geometric random graph. *Random Structures and Algorithms*, 15:145–164, 1999.

[91] Z. Vincze, R. Vid, and A. Vidacs. Deploying multiple sinks in multi-hop wireless sensor networks. In *Proc. of IEEE International Conference on Pervasive Services*, pages 55–63, July 2007.

[92] Pishro-Nik, K.S. Chan, and F. Fekri. On connectivity properties of large-scale sensor networks. In *Proc. of the First Annual IEEE Communications Society Conference on Sensor and Ad Hoc Communications and Networks, 2004, SECON04*, pages 498–507, October 2004.

[93] Freescale. *Freescale Semiconductor's MC13192 Developer's Kit*. Freescale.

[94] S. Vural and E. Ekici. Probability distribution of multi-hop-distance in one-dimensional sensor networks. *ACM Computer Networks: The International*

Journal of Computer and Telecommunications Networking, 51(13):3727–3749, September 2007.

[95] A. Marcucci, M. Nati, C. Petrioli, and A. Vitaletti. Directed diffusion light: low overhead data dissemination in wireless sensor networks. In *IEEE 61st Vehicular Technology Conference*, 30 May - 1 June 2005.

[96] F. Fabbri and R. Verdone. Throughput analysis of an ieee 802.1lb multihop ad hoc network. In *Proc. IEEE European Wireless, EW2008*, Prague, Czech, June 2008.

[97] D. Stoyan, W. S. Kendall, and J. Mecke. *Stochastic Geometry and its Applications*. John Wiley and Sons Ltd, 1995.

[98] G. Lu, B. Krishnamachari, and C. S. Raghavendra. Performance evaluation of the ieee 802.15.4 mac for low-rate low-power wireless networks. In *Workshop on Energy-Efficient Wireless Communications and Networks, 2004. EWCN 2004*, pages 701–706, April 2004.

[99] B. Bougard, F. Catthoor, D. C. Daly, A. Chandrakasan, and W. Dehaene. Energy efficiency of the ieee 802.15.4 standard in dense wireless microsensor networks: Modeling and improvement perspectives. In *Proc. Design Automation and Test in Europe Conference and Exhibition, 2005*, pages 196–201, March 2005.

[100] Anis Koubaa, Mirio Alves, and Eduardo Tovar. A comprehensive simulation study of slotted csma/ca for ieee 802.15.4 wireless sensor networks. In *IEEE International Workshop on Factory Communication Systems, 2006. WFCS 2006*, pages 183–192, June 2006.

[101] T. O. Kim, H. Kim, J. Lee, J. S. Park, and B. D. Choi. Performance analysis of the ieee 802.15.4 with non beacon-enabled csma/ca in non-saturated contition.

In *International Conference on Embedded And Ubiquitous Computing, 2006. EUC 2006*, pages 884–893, August 2006.

[102] J. Misic, V. B. Misic, and S. Shafi. Performance of ieee 802.15.4 beacon-enabled pan with uplink transmissions in non-saturation mode - access delay for finite buffers. In *Proc. First International Conference on Broadband Networks, 2004. BroadNets 2004*, pages 416–425, October 2004.

[103] J. Misic, S. Shafi, and V. B. Misic. The impact of mac parameters on the performance of 802.15.4 pan. *Elsevier Ad hoc Networks Journal*, 3:509–528, September 2005.

[104] J. Misic, S. Shafi, and V. B. Misic. Maintaining reliability through activity management in an 802.15.4 sensor cluster. *IEEE Trans. Veh. Technol.*, 3:779–788, May 2006.

[105] S. Pollin, M. Ergen, S.C. Ergen, B. Bougard, L. Van der Pierre, F. Catthoor, I. Moerman, A. Bahai, and P. Varaiya. Performance analysis of slotted carrier sense ieee 802.15.4 medium access layer. *IEEE Trans. Wireless Commun.*, 7:3359–3371, September 2008.

[106] T.R. Park, T.H. Kim, J.Y. Choi, S. Choi, and W.H. Kwon. Throughput and energy consumption analysis of ieee 802.15.4 slotted csma/ca. *IEEE Electronics Letters*, 41:1017–1019, September 2005.

[107] G. Bianchi. Performance analysis of the ieee 802.11 distributed coordination function. *IEEE J. Sel. Areas Commun.*, 18:535–547, March 2000.

[108] Z. Chen, C. Lin, H. Wen, and H. Yin. An analytical model for evaluating ieee 802.15.4 csma/ca protocol in low rate wireless application. In *Proc. IEEE AINAW 2007*, 2007.

[109] L. Kleinrock. *Queueing Systems*. John Wiley and Sons, 1975.

[110] P. Stuedi, O. Chinellato, and G. Alonso. Connectivity in the presence of shadowing in 802.11 ad hoc networks. In *Proc. IEEE WCNC, 2005*, 2005.

[111] H. Takagi and L. Kleinrock. Throughput analysis for persistent csma systems. *IEEE Trans. Commun.*, 33(7):627–638, July 1985.

[112] K.J. Zdunek, D.R. Ucci, and J.L. Locicero. Throughput of nonpersistent inhibit sense multiple access with capture. *IEEE Electronics Letters*, 25(1):30–31, January 1989.

[113] J. H. Kim and J. K. Lee. Capture effects of wireless csma/ca protocols rayleigh and shadow fading channels. *IEEE Electronics Letters*, 48(4):1277–1286, July 1999.

[114] P. Siripongwutikorn. Throughput analysis of an ieee 802.1lb multihop ad hoc network. In *Proc. IEEE TENCON 2006*, pages 1–4, November 2006.

[115] P. Mahonen, M. Petrova, and J. Riihijarvi. Applications of topology information for cognitive radios and networks. In *Proc. IEEE 2nd International Symposium on New Frontiers in Dynamic Spectrum Access Networks 2007, DySPAN2007*, pages 103–114, 2007.

[116] M. Petrova, P. Mahonen, and J. Riihijarvi. Connectivity analysis of clustered ad hoc and mesh networks. In *Proc. IEEE Global Telecommunications Conference, 2007. GLOBECOM '07*, pages 1139–1143, 2007.

[117] M. Thomas. A generalization of poisson's binomial limit for use in ecology. *Biometrika*, 36:18–25, 1949.

[118] J. Hoydis, M. Petrova, and P. Mahonen. Effects of topology on local throughput-capacity of ad hoc networks. In *IEEE Int. Symp. on Personal, Indoor and MoRadio Communications, 2008. PIMRC 2008*, September 2008.

[119] Y. C. Tay, K. Jamieson, and H. Balakrishnan. Collision-minimizing csma and its applications to wireless sensor networks. *IEEE J. Sel. Areas Commun.*, 22:1048–1057, August 2004.

[120] J. Riihijarvi, P. Mahonen, and M. Rubsamen. Characterizing wireless networks by spatial correlations. *IEEE Commun. Lett.*, 11:37–39, 2007.

[121] M. Dohler, J. Dominguez, and H. Aghvami. Link capacity analysis for virtual antenna arrays. In *Proc. of IEEE Vehicular Technology Conference, VTC 2002-Fall.*, September 2002.

[122] M. Dohler, A. Gkelias, and H. Aghvami. Two-hop distributed mimo communication system. *IEEE Electronics Letters*, 39:1350–1351, September 2007.

[123] M. Dohler et al. Vaa for hot-spots with applied stc. In *M-VCE, Internal Reports I,II, III and IV*, King's College London, University of London, London, 1999-2002.

[124] M. Dohler. Virtual antenna arrays. In *PhD Thesis*, King's College London, University of London, London, 2003.

[125] H. Zhang and H. Dai. On the capacity of distributed mimo systems. In *Proc. of the Conf. on Information Sciences and Systems, CISS 2004*, Princeton, NJ, March 2004.

[126] S. Jayaweera. V-blast virtual mimo for distributed wireless sensor networks. *IEEE Trans. Commun.*, 55:1867–1872, October 2007.

[127] R. H. Y. Louie, I. B. Collings, and M. R. McKay. Analysis of dense ad hoc networks with spatial diversity. In *Proc. of IEEE GLOBECOM 2007*, Washington, DC, November 2007.

[128] K. Stamatiou, J. G. Proakis, and J. R. Zeidler. Evaluation of mimo techniques in fh-ma ad hoc networks. In *Proc. of IEEE GLOBECOM 2007*, Washington, DC, November 2007.

[129] A. Jovicic, P. Viswanath, and S.R. Kulkarni. Upper bounds to transport capacity of wireless networks. *IEEE Trans. Inf. Theory*, 50(11):2555–2565, 2004.

[130] O. Leveque and I.E. Telatar. Information-theoretic upper bounds on the capacity of large extended ad hoc wireless networks. *IEEE Trans. Inf. Theory*, 51(3):858–865, 2005.

[131] H. Bolcskei, R. U. Nabar, O. Oyman, and A. J. Paulraj. Capacity scaling laws in MIMO relay networks. *IEEE Trans. Wireless Commun.*, 5(6):1433–1444, 2006.

[132] H. Jafarkhani, H. Yousefi'zedeh, and J. Kazemitabar. Capacity-based connectivity of MIMO fading ad-hoc networks. In IEEE, editor, *Proceedings of IEEE GLOBECOM 2005*, pages 2827–2831, 2005.

[133] E. Salbaroli and A. Zanella. Achievable rate of wireless sensor networks with multi-antenna sinks. In IEEE, editor, *Proceedings of the Vehicular Technology Conference, 2007. VTC 2007-Spring*, 2007.

[134] A. Zanella, M. Chiani, and M. Z. Win. A general framework for the distribution of the eigenvalues of wishart matrices. In IEEE, editor, *Proc. of IEEE Int. Conf. on Communications, ICC 2008*, Beijing, China, May 2008.

[135] I. S. Gradshteyn and I. M. Ryzhik. *Tables of Integrals, Series, and Products.* Alan Jeffrey, Editor.

[136] Utz Roedig and Cormac J. Sreenan. *Wireless sensor networks. Proc. of the 5th European Conference, EWSN 2009, Cork, Ireland.* Springer-Verlang, February 2009.

[137] N. Abramson. The throughput of packet broadcasting channels. *IEEE Trans. Commun.*, 25:117–128, 1977.

[138] W. Wang Y. Wang and T. A. Dahlberg. Truthful routing for wireless hybrid networks. In IEEE, editor, *Proceedings of IEEE GLOBECOM 2005*, 2005.

[139] Silke Heier and Matthias Malkowski. Umts radio resource management by transport format assignment and selection. In *Proc. of IEEE Wireless Personal Multimedia Communications, 2002*, pages 1187– 1191, October 2002.

[140] Young-June Choi and Saewoong Bahk. Qos scheduling for multimedia traffic in packet data cellular networks. In *Proc. of IEEE Int. Conf. on Communications, ICC 2003*, volume 1, pages 358–362, May 2003.

[141] Patrick Kinney. Zigbee technology: Wireless control that simply works. In *Communications Design Conference*, October 2003.

[142] E. Callaway J. Gutierrez and R. Barret. *Low-Rate Wireless Personal Area Networks - Enabling Wireless Sensors with IEEE 802.15.4*. IEEE, 2006.

Acknowledgements

This work was possible only with the support of many people. In first place, I wish to thank my supervisor, Prof. Roberto Verdone, for his many suggestions and constant support during this research, and the Director of WiLab (the Wireless Communication Laboratory at the University of Bologna, which I belong to), Prof Oreste Andrisano, who set the environment for my work during this PhD.

Then, after Roberto, my guide, I would like to thank the people of WiLab who mainly contributed to this work, and helped me in the different phases: Davide, Alberto, Andrea C., Andrea G. and Flavio. Thank you for the useful discussions and your help in the development of the different models described in this thesis. In different ways and periods they all have contributed to my growth, and taught me different aspects of this job.

I am also thankful to the people I collaborated with in the different Projects, John Orris, Francesca Cuomo and Janne Riihijärvi, and all the Professors and researchers I worked with in the framework of NEWCOM and NEWCOM++.

I would like also to thank my office mates. First of all, Virginia, the person with whom I shared this "travel", the funny and stressed days. And all the (old and new) guys of the laboratory, Daniele, Francesco, Alessandro, Marco, Flavio, Andrea and Cengiz. Finally I would like to thank Silvia, without her support I wouldn't have time for doing research.

Of course I cannot forget the people who make my life fun and complete, Silvia, Federica, Federica and Arianna. Thank you for being so special with me.

Finally, I would like to thank my family, for their patience, love and unconditional support. Without them this work would never have come into existence (literally).

This thesis is dedicated to the person who allowed the realisation of this dream.